AD_____

Award Number: DAMD17-99-1-9571

TITLE: Molecular Mechanisms of Soft Tissue Regeneration and Bone Formation in Mice: Implications in Fracture Repair and Wound Healing in Humans

PRINCIPAL INVESTIGATOR: David J. Baylink, M.D.

CONTRACTING ORGANIZATION: Loma Linda Veterans Association for Research and Education
Loma Linda, California 92357

REPORT DATE: October 2003

TYPE OF REPORT: Annual

PREPARED FOR: U.S. Army Medical Research and Materiel Command
Fort Detrick, Maryland 21702-5012

REPORT DOCUMENTATION PAGE

Form Approved
OMB No. 074-0188

1. AGENCY USE ONLY (Leave blank)	2. REPORT DATE	3. REPORT TYPE AND DATES COVERED
	October 2003	Annual (1 Oct 02-30 Sep 03)

4. TITLE AND SUBTITLE
Molecular Mechanisms of Soft Tissue Regeneration and Bone Formation in Mice: Implications in Fracture Repair and Wound Healing in Humans

5. FUNDING NUMBERS
DAMD17-99-1-9571

6. AUTHOR(S)
David J. Baylink, M.D.

7. PERFORMING ORGANIZATION NAME(S) AND ADDRESS(ES)
Loma Linda Veterans Association for Research and Education
Loma Linda, California 92357

E-Mail: baylid@lom.med.va.gov

8. PERFORMING ORGANIZATION REPORT NUMBER

9. SPONSORING / MONITORING AGENCY NAME(S) AND ADDRESS(ES)
U.S. Army Medical Research and Materiel Command
Fort Detrick, Maryland 21702-5012

10. SPONSORING / MONITORING AGENCY REPORT NUMBER

11. SUPPLEMENTARY NOTES

12a. DISTRIBUTION / AVAILABILITY STATEMENT
Approved for Public Release; Distribution Unlimited

12b. DISTRIBUTION CODE

13. ABSTRACT (Maximum 200 Words)

No abstract provided.

14. SUBJECT TERMS
No subject terms provided.

15. NUMBER OF PAGES
173

16. PRICE CODE

17. SECURITY CLASSIFICATION OF REPORT	18. SECURITY CLASSIFICATION OF THIS PAGE	19. SECURITY CLASSIFICATION OF ABSTRACT	20. LIMITATION OF ABSTRACT
Unclassified	Unclassified	Unclassified	Unlimited

Table of Contents

I. General Introduction

The primary goal of the project funded by the U.S. Army is to identify genes which play an anabolic role in bone tissue and soft tissue function, particularly during regeneration, and to clarify the function of these genes. To accomplish this goal, we have proposed 3 technical objectives during the funding period. These 3 Technical Objectives are as follows:

A. Technical Objective 1:

Studies proposed in the first technical objective are designed to employ state-of-the-art molecular biotechniques to identify the gene located in mouse chromosome 1 that is involved in the regulation of peak bone density.

B. Technical Objective 2:

Our second technical objective has been focused on identifying the key genes that are involved in soft tissue repair/regeneration using inbred strains of mice as model systems.

C. Technical Objective 3:

The goal of our third technical objective is to identify and characterize novel genes, using ENU mutagenesis techniques and to elucidate the function of known genes that play a key role in the metabolism of bone and soft tissue.

Our goals for the last 12-months of the third funding period for each of the technical objectives, as well as our progress for each of the technical objectives, are described below. The progress report for each technical objective is organized according to the outline provided by the office of the U.S. Army Medical Research and Materiel Command.

II. Technical Objectives

A. Technical Objective 1: To clone the gene regulating peak bone density on chromosome 1 in the Cast/B6 congenic mice.

1. Introduction

Our long-term goal in this study is to identify the genes involved in the acquisition of peak bone density and evaluate the functions of those genes. Such genes are particularly relevant in identifying one's risk for and the prevention of stress fractures, as well as identifying the risk for fractures during battlefield injuries and to corresponding gene therapy treatment for such fractures.

In our studies on the identification of candidate genes regulating peak bone density, we focused on a quantitative trait locus (QTL) that contributes significantly to high bone density on mouse chromosome 1 from a cross between C57BL/6J (B6) and CAST/EiJ (CAST) mouse strains (Beamer et al., 1999). We chose the chromosome 1 QTL for our studies based on the following rationale: 1) it contributes to approximately 40% of the total variation of bone density between CAST and B6 mice; 2) it has a LOD (logarithm of the odds) score of 8, which is statistically the strongest QTL identified from the B6 X CAST cross; 3) it is located in a region syntenic with that of human

chromosome 1q21-q23, which has been implicated in peak bone density regulation in humans (Koller et al., 2000); and 4) in order to convincingly demonstrate that the chromosome 1 QTL in Cast mice does, in fact, contribute to higher bone density, we generated congenic strains by transferring CAST chromosome 1 alleles (donor) into the B6 strain (recipient). It was found that the bone density of B6-cast congenic mice containing chromosome 1 QTL from CAST mice was significantly higher that that of B6 mice, thus confirming that CAST chromosome 1 QTL contains gene/s that contribute to high bone density in B6 mice (previous report, Oct. 2002).

In order to further narrow down the size of the chromosome 1 QTL (25cM) to a more manageable size for future studies on the identification of candidate genes, we have produced several subcongenic lines containing smaller pieces of CAST chromosome 1 QTL in B6 mice. Our subcongenic approach not only confirmed the biological activity of the QTL gene in this region, but also further narrowed down the size of the QTL within the chromosome 1 QTL, on chromosome 1 1q21-1q23. It follows that the QTL region could be within 2 cM, a size feasible for proposed studies on identification of candidate genes by various approaches proposed below.

To identify and order genes present within the QTL region, we developed a "sequencing ready" BAC (bacterial chromosome) contig covering the 92-95cM region on mouse chromosome 1 using the RPC1-23 library (Gu et al., 2002). These BAC clones are currently being sequenced by our collaborator at the University of Oklahoma and are deposited into the NCBI database. The availability of the genomic sequence for the QTL region in mouse chromosome 1 from public (NCBI) as well as private (CELERA) databases will provide valuable resources for our proposed studies on the identification of candidate gene in chromosome 1 QTL.

To achieve the goal of identifying the candidate gene in chromosome 1 (Chr.1) involved in bone density regulation, we have designed state-of-art molecular techniques which include differences in gene expression, sequence polymorphism, presence of functional motif consistent with bone formation or resorption action in candidate genes, and *in vitro* functional testing. For *in vitro* testing of candidate genes, we proposed to develop a functional assay in which the candidate gene (sense or antisense orientation) will be inserted into a viral expression vector and used for evaluating the effect of over-expression of a candidate gene in osteoblast line cells on bone formation parameters, as well as the production of factors regulating formation and activity of osteoblasts. We are familiar with all of the proposed techniques and are therefore confident that we will be successful in our efforts to identify the candidate gene in the Chr.1 QTL that contributes to high bone density.

Our Specific Objectives for the first 12 months of this continuation grant period were as follows:

a) Specific Obejective 1: To identify all of the genes present in the 2 cM region of the mouse chromosome 1 QTL and determine candidate genes for regulation of bone density. To accomplish this goal, we planned to:

(1) Identify coding and regulatory regions for each of the genes present in mouse Chr.1 QTL region using private and public genomic databases.

(2) Identify those genes which are also present in the corresponding syntenic region in human Chr.1q21-1q23, which has been implicated in regulating high bone density in humans.

(3) Determine those genes that show significant homology to genes known to be involved in regulating osteoblast and/or osteoclast cell functions.

(4) Prioritize candidate genes for further testing based on several criteria including: (a) known expression pattern in bone cells, (b) function, (c) location in the QTL region and (d) presence or absence of human homolog.

b) Specific Objective 2: To evaluate expression levels of selected candidate genes in the bones of the Chr.1 subcongenic line with high bone density and corresponding age-matched control mice. To accomplish this goal, we planned to:

(1) Breed the Chr.1 subcongenic line containing the smallest QTL region to homozygosity.

(2) Isolate bones and other tissues* (muscle, kidney and liver) from congenic and B6 mice at selected age (4, 8 and 16 weeks) groups (* Because Chr.1 QTL influences bone but not other tissues, we anticipate changes in the expression of a candidate gene in bone, but not in other tissues. Alternatively, if the candidate gene is a systemic hormone produced in liver or other non-bone tissues, we would then anticipate a corresponding change in expression of a candidate gene in other tissues, but not in bone)

(3) Isolate RNA and perform in house microarray using PCR amplified products of selected candidate genes as probes

(4) Identify those genes that are differentially expressed in a manner consistent with the bone density difference between congenic and B6 mice at 16 weeks, but not at 8 weeks.

c) Specific Objective 3: To identify polymorphism in the regulatory region of select candidate genes which show differential expression in the bones of congenic and B6 mice. To accomplish this goal, we planned the following:

(1) Design oligos to amplify the appropriate regulatory regions.

(2) PCR amplify and purify the DNA fragments of regulatory regions from congenic and B6 mice.

(3) Sequence the DNA fragments of regulatory regions.

(4) Compare the sequences between congenic and B6 mice.

(5) Determine if sequence polymorphism between congenic and B6 mice is unique by sequencing regulatory regions from two other.

(6) Identify if polymorphism for congenic and B6 mice is located in a region where a binding motif for a potential transcription factors resides.

2. Body

Our progress during the first 12 months of this continuation grant period for each specific objective is given below

a) Specific Objective 1: To identify all of the genes present in the 2 cM region of the mouse chromosome 1 QTL and determine candidate genes for regulation of bone density.

(1) Identify coding and regulatory region for each of the genes present in mouse chromosome 1 BMD QTL region.

We have used the Celera database to find the sequence of the genes located in the BMD QTL region. The QTL region has been delimited using the different subcongenic lines we prepared (Fig. 1). The Celera web-site gives both the sequence of the transcript (mcT.) and the DNA sequence, including the coding and non-coding regions (mCG.). A list of the genes in the chromosome 1 BMD QTL region is provided in Table 1

(2) Identify those genes which are also present in corresponding syntenic region in human chromosome 1q21-1q23, which has been implicated in regulating high bone density in humans.

Using the Celera database, we checked the genes located in the region 1q21-1q23 which contained a human BMD QTL. Koller et al. (2000) conducted an autosomal genome screen in 595 sister pairs (464 Caucasians and 131 African-Americans) and found a BMD QTL at 1q21-1q23, which showed the highest LOD score of 3.86. Most of the genes in this region have been conserved both in mouse and human BMD QTL. The list of the genes conserved in the mouse and human BMD QTL in Chr.1 is provided in Table 2.

(3) Determine those genes that show significant homology to genes known to be involved in regulating osteoblast and/or osteoclast cell functions.

We made a search using the Celara database to obtain information about the identity of the genes. We then used this information to search in various databases, including NCBI, PubMed and Online Mendelian Inheritance in Men (OMIM), to identify whether any of the genes located in the BMD QTL could be involved in bone metabolism. Table 3 shows the genes selected to be candidates to regulate bone cell function.

(4) Prioritize candidate genes for further testing based on several criteria, including: (a) known expression pattern in bone cells, (b) function, (c) location in the QTL region and (d) presence or absence of human homolog.

We consider the 5 genes reported in Table 3 as candidate genes based on the following: 1) they are conserved in mouse and in human BMD QTL region 1q21-1q23; and 2) they are involved on regulating cell growth and/or cell differentiation, processes which are known to be involved in regulating bone formation.

b) Specific Objective 2: To evaluate expression levels of selected candidate genes in the bones of chromosome 1 sub-congenic line with high bone density.

(1) Breed chromosome 1 subcongenic line containing smallest QTL region to homozygosity.

In our Annual progress report of last year (Oct. 2002), we provided the genotyping data and BMD data from some of the sub-congenic lines prepared from the cross B6-cast. During the last 12 months, we have fine mapped the sub-congenic lines that cover the BMD QTL region in Chr.1 using more markers. The markers used are shown in Table 4. We generated homozygous mice for the subcongenics and we compared the pQCT data between all the sub-congenic lines and the B6 wild type mice at 16 weeks. Our efforts to fine map the subcongenics and analyze their phenotype are summarized below.

In order to fine map the QTL region, we used 24 markers. Since some of the markers used were of less than a 1Mb interval, we blast-searched the markers using the Celera database to find their position in Mb (Table 4 and Fig-1), which allowed us to determine, with accuracy, the length of the cast segment transferred into the B6 background for every congenic line.

Genetic analyses: Genomic DNA was prepared by digestion of 3-4mm tail tips in RBC lysis solution from PURGENE DNA isolation kit (Gentra Systems Inc.) and following the protocol provided by Gentra Systems Inc. Genotyping of individual mouse DNA was accomplished by polymerase chain reaction (PCR) using oligonucleotide primer pairs (Mit markers) from Integrated DNA Technology. These primer pairs amplify simple dinucleotide repeated sequences of anonymous genomic DNA that are of different sizes, and through gel electrophoresis or ABI 3100 Genetic Analyzer, can uniquely discriminate between B6 and Cast alleles. The position of cast alleles in Chr.1 for different subcongenic lines are presented in Fig.-1. Each congenic strain was given an abbreviated designation; "Cong." Means congenic line, the number "1" means that the cast alleles transferred are from chromosome 1.

BMD measurements by peripheral quantitative computed tomography: Female mice were necropsied at 16 weeks of age. Femora isolated and used for peripheral quantitative computed tomography (pQCT). The results of the pQCT measurements are presented in Tables-5 and -6. Total mineral content (26%), total area (10.5%) and volumetric bone mineral density (11.3%) were significantly increased in the congenic Cong.1-14. Total mineral content and volumetric total density, but not the total area, were significantly higher in both Cong.1-16 and Cong.1-17 (Table 5). Cortical thickness was significantly higher in Cong.1-14, Cong.1-15, Cong.1-16 and Cong.1-17 (Table 6).

(2) Isolate bones and other tissues from congenic and B6 mice at selected age groups.

14-old female B6 mice and congenic mice were euthanized, femurs flashed with syringes in order to extract bone morrow, and bones without bone morrow kept in liquid nitrogen for RNA extraction. Liver was also extracted and kept in liquid nitrogen for RNA extraction.

(3) Isolate RNA and perform in house microarray using PCR amplified products of select candidate genes as probes.

The RNA was extracted from femur and liver of 14 week-old congenic and B6 female mice using Trizol (Life Technology) protocol.

Preparation of labeled cDNA from 200-250ng RNA then cDNA hybridization to printed PCR products was done following the protocol described by MICROMAX TSA labeling and Detection kit (PerkinElmer Life Sciences, Inc.)

(4) Identify those genes that are differentially expressed in a manner consistent with the bone density difference between congenic and B6 mice at 16 weeks but not at 8 weeks.

In order to identify candidate genes for BMD, we combined the microarray technique and real time PCR to compare the gene expression pattern between B6 and the congenic mice. Since bone density was significantly different between congenic and B6 mice at 16 weeks of age, we evaluated gene expression difference between congenic and B6 mice at 14 weeks of age. We predicted that gene expression changes that contribute to phenotypic differences between congenic and B6 should occur prior to 16 weeks of age and, as a consequence, we used 14 week-old mice for gene expression studies.

For gene expression studies, we chose genes located in the chromosome 1 congenic region that contributed to increased BMD in congenic mice. We used the following approach to evaluate gene expression changes between congenic and B6 mice by microarray and real time PCR.

- The primers were designated for the genes located in the region between 172-185Mb in chromosome 1.
- The primers were blast searched with private (Celera) and public (NCBI) databases to make sure that there was no homology with other sequences in other regions of the mouse genome.
- The PCR conditions were optimized for every pair of primer. For microarray, the primers were selected in order to amplify a product of 350-600bp to give a detectable signal after hybridization (Table 7 represents the genes used in microarray). However, for Real Time PCR (RT-PCR), the primers were designated using PrimerExpress Software (from Applied Biosystems) to amplify a product of 100-150bp. The primers for RT-PCR have all the same melting temperature. The list of the genes used in RT-PCR are in Table 8.
- For microarray: segments from the genes were amplified, then the PCR products were filtered using 96-well multiscreen filter plates (Millipore) to remove unincorporated nucleotides and primers from the reaction products. Microarray slides were prepared by printing purified PCR products suspended in 50% Dimethylsulfoximide (DMSO) to CMT-GAPS aminosilane-coated glass microscope slides using GMS 417 Arrayer. Labeled cDNA was prepared from 200-250ng femur RNA and then cDNA was hybridized to printed PCR products following the protocol described by MICROMAX TSA labeling and Detection kit (PerkinElmer Life Sciences, Inc.). After hybridization, the slides were scanned with ScanArray from PerkinElmer Inc. and the data were extracted using Imagene 4.0 software.
- For real time PCR: cDNA has been prepared from 500ng RNA using M-MLV Reverse Transcriptase from Promega. Then for the amplifications, we used SYBR Green QPCR Master Mix from Stratagen.

- We prepared cDNA from liver RNA and we are currently in the process of performing real time PCR for all the genes that we could not make PCR products for micorarray and real time PCR using the selected primers and RNA from bone.

Microarray Results: We have used femurs without bone marrow from 14 week-old female mice to evaluate the expression pattern of the genes located in the QTL region. The wild type B6 were used as a control and the 2 congenic 1-14 and 1-17 were used to identify the candidate genes for bone mineral density. Since both lines 1-14 and 1-17 showed high BMD when compared to the wild type B6 mice, we used those genes showing a significant differential expression in both lines compared to B6 mice as the criteria for the selection of candidate genes.

From the 156 genes printed on CMT-GAPS slides, only 4 genes showed differential expression between 14 week-old female B6 mice and Cong.1-14 and between B6 and congenic 1-17 mice (Table 9).

In order to confirm the microarray data, we are in process of performing real time PCR for the 4 genes that are up-regulated in congenic mice.

Results from Real Time PCR: Some of the genes in the QTL region couldn't be amplified for microarray, however, since we need only a small segment of 100-150bp for RT-PCR, we were able to measure the expression levels of 32 more genes. We used beta-actin as internal control to adjust for differences in RNA concentration in different samples. Table 11 shows the expression levels of the 32 genes in femur without bone marrow from 2 different lines of congenic mice and in B6 mice. For every strain, we used at least 2 replicates.

The expression levels of 2 genes shown in bold were significantly different between the B6 and the 2 lines of congenic mice (Tables –11 and -12)

The expression levels of 180 genes located in the BMD QTL region were evaluated, representing 89% of the total number of the sequenced genes located in this region. 6 genes were found to be up-regulated in the 2 high BMD congenic mice:

- The C-reactive protein (previous report) and serum amyloid are known as inflammatory genes, which are up-regulated in femur from the high BMD congenic. C-reactive protein is turned-on by Il-1 and Il-6, previously known genes linked to bone metabolism. However, the role of C-reactive or serum amyloid in bone is yet to be determined. We are planning to check the role of these 2 genes in regulating bone density. To this end, we plan to knock-out the genes by SiRNA technique and determine the effect on osteoblast proliferation and differentiation.
- The transcription factors ELYS might be involved in regulating the bone related genes.
- The 3 other genes found using microarray analyses have never been reported to be expressed in bone. Therefore, we plan to confirm the difference in the expression by real time PCR.
- As for the Duffy blood group gene, we as yet do not have a clear explanation of how this gene could be responsible of high bone density. We need to identify its role in bone formation and/or bone resorption by knocking it down and evaluating the consequence of reduced expression on osteoblast and osteoclast phenotype.

c) Specific Objective 3: To identify polymorphism in the regulatory region of select candidate genes which show differential expression in the bones of congenic and B6 mice.

For sequence polymorphism studies, we choose C-reactive protein (CRP) based on its importance, location in the BMD QTL region, and differential expression between B6 and congenic mice.

CRP belongs to a family of proteins which, under electron microscopy, show a discoid arrangement of five noncovalently bound subunits. Proteins of the pentaxin family are involved in acute immunological responses. Three of the principal members of the pentaxin family are serum proteins: namely, CRP, serum amyloid P component protein (SAP), which was found to be also up-regulated in our high BMD congenic mice, and the female protein (FP). CRP is expressed during acute phase response to tissue injury or inflammation in mammals. The protein resembles antibody and performs several functions associated with host defense: it promotes agglutination, bacterial capsular swelling and phagocytosis, and activates the classical complement pathway through its calcium-dependent binding to phosphocholine. CRP and SAP have been very stably conserved throughout vertebrate evolution and homologous proteins are apparently present even in invertebrates. This strongly suggests that they have important functions, although these have not yet been precisely delineated. The gene coding for CRP is located at 172.548,249-172,550,422 within the BMD QTL region (Fig.-1). The gene contains 2 exons and one intron.

In our previous reports, we stated that the CRP was the only known gene in the mouse BMD QTL region that showed differential expression between B6 and the congenic mice from commerce microarray data. These data were confirmed by semi-quantitative PCR. The human syntenic gene was also present in the corresponding syntenic region of chromosome 1 so we wanted to check if the difference in the expression is due a polymorphism between B6 and cast sequences. To accomplish this goal, we undertook the following approach.

(1) Designed oligos to amplify the appropriate regulatory regions.

We designed primers that over-lap with each other in order to cover the whole gene. We then blast-searched every pair of primers with NCBI database to make sure there was no homology with any other sequence than the CRP gene.

The following are the primers used for sequencing:

CRP1-F: 34GAT TCA GGG GTC ACA GGA GTT 54
CRP1-r: 513TTG GGA TCA AGG GTC ATCTGG493

CRP2-F: 202AAA TCT GAG GAT GGG CTG GGC222
CRP2-R: 624GAC TCC TTG GGA AAT ACA AAG604

CRP3-F: 610ATT TCC CAA GGA GTC AGA TAC630
CRP3-R: 1023GCA TCA AAG TCA CCG CCA TAC1003

CRP-F: 582ATG AAG ACA TGT TTA AAA AGG CCT605
CRP-R: 1194CAC AGC TGC GGC TTA ATA AAC ACA1171

CRP4-F: 937AAG TCT GCA CAA GGG CTA CAC957
CRP4-R: 1365CCA TTT AAA TTC CGT GCT CTA1345

CRP5-F: 1304GAA TAT GGC CTT TCA CTT CTC1324
CRP5-R: 1873GGG GCC CTC CTG ATA GAT TAT1853

CRP6-F: 1345TAG AGC ACG GAA TTT AAA TGG1365
CRP6-R: 2133TCA AAT TCA TTC AAG CCA AAG2113

(2) PCR amplify and purify the DNA fragments of regulatory regions from congenic and B6 mice.

After optimizing the PCR condition for every pair of primers, we prepared 5X100ul PCR product from every segment and every strain (we used B6 and Cast DNA, in addition of Balb and C3H DNA). Then the PCR products were purified using QIAquik PCR purification kit from Qiagen.

(3) Sequence the DNA fragments of regulatory regions.

60-120ng from purified PCR products were sequenced using the ABI machine.

(4) Compare the sequence between congenic and B6 mice.

We compared the CRP sequences between the B6 and Cast because the congenic mice carry cast segment, which contains C-reactive from Cast mice, and we found the polymorphisms shown in Table 13.

(5) Determine if sequence polymorphism between congenic and B6 mice is unique by sequencing regulatory regions.

We sequenced the gene for 2 other mice strains: Balb mice have low bone density and C3H mice have a high bone density. Table 14 shows the polymorphic sequences for the 4 mice strains. We have found that the sequence of the polymorphic region is similar in Balb, C3H and Cast but different in B6. The B6 has its unique sequence, which is different than the sequences from the 3 other mice strains. Future studies are needed to evaluate if these polymorphic changes have any functional relevance in osteoblast.

(6) Identify if polymorphism for congenic and B6 mice is located in a region where a binding motif for a potential transcription factor resides.

One way to evaluate if the polymorphism in a given gene is biologically significant is to determine if the polymorphism is in a conserved region. In order to identify if CRP gene polymorphism resides in a conserved region, we compared CRP sequences from different species (Fig.-3)

The "A" at position 1095 is highly conserved among different vertebrates. The codon "AAC" encodes for the amino acid asparagines, which has a terminal amid and no hydroxyl group. With "G" instead of "A", the codon change to "AGC," which encodes for serine. Serine contains an aliphatic hydroxylated group. Future studies are needed to address if the change from asparagine to serine leads to alteration in protein function.

Because CRP expression was different between the bones of congenic and B6 mice, we expected polymorphic differences in the regulatory region of CRP. In this

regard, it is possible that the observed polymorphism at positions 111, 231 or 417 could be involved in regulating change in CRP expression. Accordingly, Ohnishi et al. (1988) reported that the position 111 is located between the glucocorticoid and cytokine responsive elements which are required for Il-6 expression and a heat-shock site. Il-6 and Il-1 turn-on the CRP. It is possible that the change of thymine into cytosine may affect the expression of the CRP.

3. Additional work:

In addition of fine mapping the B6-cast sub-congenic, we also did fine mapping of the BMD QTL for the F2 population generated from the cross B6-cast. We did the fine mapping with 24 pair of primers (Table 4), then we performed linkage analyses for the data from genotyping and the data from pQCT. Our approach to fine map BMD locus is as follows:

(1)-Selected primers that flank the polymorphic sequences in the BMD QTL region.

(2)- Performed blast-search to make sure that the primers selected exhibit no homology with any other sequence

(3)- 24 pair of primers covering the QTL region at 0.5-5Mb interval were selected, we optimized conditions to use these primers for genotyping using ABI 3100.

(4)- Female F2 mice were necropsied at 16 weeks of age and spleens were saved for genotyping and femurs used for BMD measurement (pQCT).

(5)- DNA extracted from spleen: 453 animals

(6)- 10 872 PCR were performed then were ran on electrophoreses gels and ABI3100 machine.

The data from pQCT from the genotyping were analyzed using interval mapping with MapQTL software. We checked for the presence of QTL for: total femur bone mineral density (Femur vBMD), total femur mineral content (Femur BMC), total femur volume, cortical femur bone mineral density (Cortical vBMD), cortical femur bone mineral content (Crotical BMC) and femur cortical volume. We did not find any QTL for femur total volume, however, we did find one QTL that is in common for all the other parameters (Fig.-4). This QTL has the highest LOD score 5-12 for various phenotypes and is located between 172-178Mb in Chr.1. Another QTL was found for Femur vBMD and cortical vBMD with LOD scores of 5.5 and 8.5, respectively (Fig.-4.) and was found in the region 180-185 Mb.

In conclusion, the results of fine mapping the F2 mice, from the cross between B6 and Cast mice, confirmed the position of the bone mineral density QTL found using B6-cast congenic mice (Fig.s-4 and -5)

4. Key Research Accomplishments

- We have Fine mapped the B6-cast congenic mice using more markers.
- We have made microarray chips for 156 genes with 3 replicates from every gene.

- We performed real time PCR for 32 genes located in the region of the BMD QTL with the highest LOD score, which revealed candidate genes that show differences in the expression between B6 and the congenic mice.
- We have fine mapped the F2 population generated from the cross between B6 and cast, which confirmed the data from the congenic fine mapping and indicated the existence of not only one BMD QTL but two BMD QTL in the region 172-185Mb.

5. Reportable Outcomes

None.

6. Conclusions

a) We have determined with accuracy the size of the cast segment transferred from Cast into B6 background in every congenic line by fine mapping.

b) Microarray slides of 156 genes were prepared and microarray was done to compare their expression pattern between B6 mice and B6-cast conegnic mice. Four genes were found to be differentially expressed between B6 and two high BMD congenic strains, one of them is ESTs and needs to be studied further.

c) Using real time PCR, we analyzed the gene expression of 32 genes located in the region 172-179 Mb. We found 2 genes that were more than 3-fold up-regulated in the two congenic strains. The two genes are conserved both in mouse BMD QTL and human BMD QTL, which makes them a good candidate genes for future studies.

d) We identified polymorphisms in the C-reactive gene, which is up-regulated in the femur of congenic mice. One polymorphism in the coding region was found to be highly conserved in vertebrates. These data suggest that the change of this sequence may contribute to functional difference in C-reactive protein between B6 and Cast mice.

e) Fine mapping of F2 mice with additional markers revealed that the original BMD QTL may in fact contains, 2 BMD loci.

7. References

1. Beamer WG, Shultz KL, Churchill GA, Frankel WN, Baylink DJ, Rosen CJ, Donahue LR. (1999) Quantitative trait loci for bone density in C57BL/6J and CAST/EiJ inbred mice. *Mamm Genome,* Nov;10(11):1043-9.

2. Koller DL, Econs MJ, Morin PA, Christian JC, Hui SL, Parry P, Curran ME, Rodriguez LA, Conneally PM, Joslyn G, Peacock M, Johnston CC, Foroud T. (2000) Genome screen for QTLs contributing to normal variation in bone mineral density and osteoporosis. *J Clin Endocrinol Metab.* Sep;85(9):3116-20.

3. Gu WK, Li XM, Edderkaoui B, Strong DD, Lau KH, Beamer WG, Donahue LR, Mohan S, Baylink DJ. (2002) Construction of a BAC contig for a 3 cM biologically significant region of mouse chromosome 1. *Genetica*;114(1):1-9.

4. Frank KF, Mesnard-Rouiller L, Chu G, Young KB, Zhao W, Haghighi K, Sato Y, Kranias EG. (2201) Structure and expression of the mouse cardiac calsequestrin gene. *Basic Res Cardiol.* Nov;96(6):636-44.

5. Hao C, Beguinot F, Condorelli G, Trencia A, Van Meir EG, Yong VW, Parney IF, Roa WH, Petruk KC. (2001) Induction and intracellular regulation of tumor necrosis factor-related apoptosis-inducing ligand (TRAIL) mediated apotosis in human malignant glioma cells. *Cancer Res.* Feb 1;61(3):1162-70.

6. Sattler AM, Schoppet M, Schaefer JR, Hofbauer LC. (2003) Novel Aspects on RANK Ligand and Osteoprotegerin in Osteoporosis and Vascular Disease. *Calcif Tissue Int.* Oct 6.

7. Sarkar SN, Das HK. (2003) Regulatory roles of presenilin-1 and nicastrin in neuronal differentiation during in vitro neurogenesis. *J Neurochem.* Oct;87(2):333-43.

8. James PF, Grupp I L, Grupp G, Woo, AL, Askew GR, Croyle, ML Walsh R A, Lingrel JB. (1999) Identification of a specific role for the Na,K-ATPase alpha 2 isoform as a regulator of calcium in the heart. *Molec. Cell* 3: 555-563.

FIGURES AND TABLES FOR TECHNICAL OBJECTIVE 1

Table 1. List of the genes present in mouse Chr.1 QTL region

Celera ID (mouse transcripts)	*Celera ID. (mouse genes)*	*Position (Mb)*	*Gene Description*
mcT164955	mCG1047251	168,871,580 - 168,872,216	similar to suppressor of initiator codon mutations, related sequence 1 (S. cerevisiae) [Mus musculus]
mcT123544	mCG122327	168,916,936 - 168,956,539	Cell division cycle associated 1 (Kinesin related)
mcT178120	mCG10644	169,079,007 - 169,119,249	regulator of G-protein signaling 5
mcT52400	mCG52217	169,167,699 - 169,173,651	regulator of G-protein signaling 4
mcT164995	mCG1047291	169,370,885 - 169,376,701	EST
mcT178119	mCG10642	169,391,593 - 169,411,287	17-beta-hydroxysteroid dehydrogenase type 7 [Mus gb|AAM21211.1|AF367475_1 17-beta-hydroxysteroid dehydrogenase type 7 [Mus musculus]musculus]
mvT10785	mCG10642	169,391,593 - 169,411,287	hydroxysteroid (17-beta) dehydrogenase 7
mcT10781	mCG10638	169,419,397 - 169,553,257	discoidin domain receptor family, member 2
mcT17821	mCG10645	169,578,600 - 169,611,386	EST AA437972 (UDP-N-Acetylglucosaminepyrophosphorylase)
mcT10784	mCG10641	169,635,831 - 169,694,875	kinase interacting with leukemia-associated gene (stathmin)
mcT123551	mCG122334	169,687,526 - 169,691,034	ref|XP_193957.1| similar to EWS/FLI1 activated transcript 2 [Mus musculus]
mcT178118	mCG10639	169,710,204 - 169,717,677	EWS/FLI1 activated transcript 2
mcT10786	mCG10643	169,741,684 - 169,745,024	EST
mcT10789	mCG10646	169,759,615 - 170,028,224	gb|AAC40065.1| carboxyl-terminal PDZligand of neuronal nitric oxide synthase [Rattus norvegicus]
mcT179662	mCG142266	170,070,905 - 170,071,413	gb|AAH03896.2| similar to 60S RIBOSOMAL PROTEIN L17 [Mus musculus]
mcT179663	mCG142265	170,071,437 - 170,072,017	gb|AAH03896.2| similar to 60S RIBOSOMAL PROTEIN L17 [Mus musculus]
mcT164994	mCG1047290	170,075,913 - 170,076,545	gb|AAH03896.2| similar to 60S RIBOSOMAL PROTEIN L17 [Mus musculus]
mcT7070	mCG8644	170,088,705 - 170,127,040	RIKEN cDNA 4832415H08 gene (calcium independent alpha-latrotoxin receptor-related)
mcT7089	mCG8628	170,151,071 - 170,324,073	ref|XP_129579.1| similar to Cyclic-AMP-dependent transcription factor ATF-6 alpha (Activating transcription factor6 alpha) (ATF6-alpha) [Mus musculus]
mcT7086	mCG8636	70,356,119 - 170,360,533	ref|XP_222875.1| similar to high affinity immunoglobulin gamma Fc receptor I [Mus musculus] [Rattus norvegicus]
mcT7061	mCG8652	170,367,589 - 170,378,911	expressed sequence BB219290

mcT7079	mCG8638	170,376,409 - 170,376,889	Ubiquinol cytochrome c-reductase complex 14KD protein
mcT7087	mCG8637	170,394,414 - 170,394,834	ref|XP_223698.1| similar to cytochrome c oxidase, subunit VIIIa; COX VIII-L [Mus musculus] [Rattus norvegicus]
mcT178163	mCG8634	170,409,879 - 170,426,236	Fc receptor, IgG, low affinity IIb
mcT7080	mCG8631	170,467,117 - 170,477,966	Fc receptor-like 3
mcT178161	mCG8629	170,499,206 - 170,507,751	Fc gamma receptor II [Mus musculus]
mcT178169	mCG8646	170,563,714 - 170,576,544	RIKEN cDNA 1700009P17 gene
mcT178159	mCG8626	170,578,738 - 170,598,850	Succinate dehydrogenase cytochrome B560 subunit
mcT178156	mCG8623	170,600,068 - 170,608,781	myelin protein zero
mcT7062	mCG8653	170,621,386 - 170,644,292	nuclear receptor subfamily 1, group I, member 3
mcT178124	mCG123478	170,662,106 - 170,666,982	nuclear receptor subfamily 1, group I, member 3
mcT178702	mCG8642	170,667,172 - 170,670,592	Mitochondrial import receptor subunit TOM40-related
mcT178167	mCG8635	170,670,047 - 170,674,519	apolipoprotein A-II
mcT7081	mCG8632	170,677,715 - 170,690,515	Fc receptor, IgE, high affinity I, gamma polypeptide
mcT124720	mCG123487	170,691,071 - 170,707,446	NADH dehydrogenase (ubiquinone) Fe-S protein 2
mcT7066	mCG8656	170,706,612 - 170,716,169	a disintegrin-like and metalloprotease (reprolysin type) with thrombospondin type 1 motif, 4
mcT7088	mCG8627	170,726,401 - 170,732,914	UDP-Gal:betaGlcNAc beta 1,4-galactosyltransferase, polypeptide 3
mcT7095	mCG8624	170,733,012 - 170,737,196	protoporphyrinogen oxidase
mcT178154	mCG8621	170,737,979 - 170,743,992	ubiquitin specific protease 21
mcT178172	mCG8647	170,744,592 - 170,751,016	RIKEN cDNA 1110021H02 gene
mcT124257	mCG123031	170,762,082 - 170,762,550	ref|XP_203246.1| similar to ribosomal protein L27 [Rattus norvegicus] [Mus musculus]
mcT178180	mCG8655	170,780,625 - 170,793,170	death effector domain-containing
mcT178158	mCG8625	170,792,065 - 170,797,123	nitrilase 1
mcT178155	mCG8622	170,796,450 - 170,809,856	prefoldin 2
mcT7072	mCG8649	170,809,880 - 170,812,286	EST
mcT165084	mCG1047380	170,814,261 - 170,814,600	ref|XP_136311.1| similar to ribosomal protein L31 [Rattus norvegicus] [Mus musculus]
mcT178703	mCG8650	170,821,770 - 170,839,738	gb|AAL79833.1|AF472510_1 nectin 4 [Mus musculus]
mcT178968	mCG142091	170,840,331 - 170,860,807	ref|XP_170910.2| similar to KIAA1204 protein [imported] - human [Homo sapiens]
mcT177597	mCG8620	170,862,511 - 170,870,112	upstream transcription factor 1
mcT179675	mCG8648	170,870,239 - 170,871,720	ref|XP_129558.2| similar to KAT protein [Homo sapiens] [Mus musculus]
mcT7098	mCG8619	170,945,927 - 170,947,053	RNA and export factor binding protein 2
mcT7076	mCG8641	170,992,840 - 171,011,957	gb|AAF91290.1|AF234831_1 NK cell receptor 2B4 [Mus musculus]

mcT179897	mCG142315	171,039,068 - 171,050,253	ref|NP_034714.1| intelectin [Mus musculus]
mcT124277	mCG123049	171,051,261 - 171,052,947	ref|XP_222891.1| similar to migration inhibitory factor [Rattus norvegicus]
mcT124258	mCG123032	171,091,613 - 171,103,606	ref|NP_034714.1| intelectin [Mus musculus]
mcT124260	mCG123034	171,130,906 - 171,136,521	gb|AAC34859.1| NK cell receptor 2B4 splice variant [Mus musculus]
mcT124266	mCG123039	171,172,083 - 171,175,417	ref|XP_222891.1| similar to migration inhibitory factor [Rattus norvegicus]
mcT124265	mCG123038	171,176,432 - 171,187,029	ref|NP_034714.1| intelectin [Mus musculus]
mcT50094	mCG49911	171,228,246 - 171,229,729	gb|AAA35750.1| DNA-binding protein B /
mcT124264	mCG123037	171,290,249 - 171,300,967	ref|NP_034714.1| intelectin [Mus musculus]
mcT50765	mCG50582	171,322,165 - 171,346,468	gb|AAF91289.1|AF234830_1 NK cell receptor 2B4 [Mus musculus]
mcT124280	mCG123052	171,384,161 - 171,390,324	ref|NP_034714.1| intelectin [Mus musculus]
mcT9902	mCG10012	171,415,060 - 171,441,198	non MHC restricted killing associated
mcT9901	mCG10011	171,446,292 - 171,464,965	lymphocyte antigen 9
mcT177531	mCG10013	171,489,414 - 171,507,845	gb|AAN63158.1|AF467909_1 leukocytecell-surface antigen [Mus musculus]
mcT9900	mCG10010	171,528,344 - 171,529,658	gb|AAA40903.1| cyclin-dependent kinase 4
mcT9903	mCG10014	171,535,397 - 171,536,213	ref|XP_110848.1| similar to ATP-dependent CLP protease ATP-binding subunit ClpX-like, mitochondrial precursor [Musmusculus]
mcT177529	mCG10007	171,538,224 - 171,561,362	CD48 antigen
mcT177530	mCG10009	171,623,296 - 171,657,741	signaling lymphocyte activation molecule
mcT118770	mCG117630	171,696,585 - 171,737,453	CD84 antigen
mcT3574	mCG4493	171,768,999 - 171,795,180	lymphocyte antigen 108
mcT177592	mCG4495	171,856,093 - 171,879,284	loop tail associated protein
mcT3589	mCG4477	171,906,525 - 171,911,824	nescient helix loop helix 1
mcT3587	mCG4479	171,920,062 - 171,936,996	nicastrin
mcT118793	mCG4489	171,937,093 - 171,976,637	coatomer protein complex subunit alpha
mcT177588	mCG4480	171,981,967 - 171,991,040	peroxisomal farnesylated protein
mcT178984	mCG4497	172,002,244 - 172,052,355	expressed sequence AA408877
mcT177589	mCG4482	172,052,694 - 172,062,665	phosphoprotein enriched in astrocytes 15
mcT3588	mCG4481	172,065,863 - 172,075,841	calsequestrin 1
mcT179097	mCG142116	172,079,484 - 172,114,341	ref|NP_074039.1| ATPase, Na+/K+ transporting, alpha 4 polypeptide [Rattus norvegicus]
mcT179096	mCG142115	172,126,613 - 172,151,708	ref|NP_036637.1| ATPase, Na+K+ transporting, alpha 2; ATPase, Na+K+ transporting, alpha 2 polypeptide [Rattus norvegicus]
mcT179668	mCG4496	172,165,492 - 172,173,393	gb|AAN63626.1|AF439263_1 immunoglobulin superfamily member 8 [Mus musculus]
mcT177590	mCG4483	172,175,266 - 172,182,702	potassium inwardly-rectifying channel, subfamily J, member 9
mcT177591	mCG4485	172,194,716 - 172,227,512	potassium inwardly-rectifying channel, subfamily J, member 10
mcT3584	mCG4487	172,229,581 - 172,232,739	phosphatidylinositol glycan, class M
mcT3572	mCG4491	172,328,901 - 172,332,071	CD2 antigen family, member 10

mcT3576	mCG4494	172,335,814 - 172,352,367	immunoglobulin superfamily, member 9
mcT3573	mCG4492	172,353,466 - 172,361,118	gb|AAM54133.1|AF465519_1 SM22beta [Mus musculus] (TRANSGELIN 2)
mcT118799	mCG117653	172,374,884 - 172,400,082	ref|XP_222907.1| similar to Nasopharyngeal epithelium specific protein 1 [Rattus norvegicus]
mcT165228	mCG1047524	172,395,812 - 172,404,902	EST
mcT118794	mCG117647	172,410,065 - 172,418,088	ref|XP_136318.2| similar to coxsackie-adenovirus-receptor homolog [Rattus norvegicus] [Mus musculus]
mcT3575	mCG4488	172,436,185 - 172,444,905	EST
mcT54622	mCG54439	172,454,435 - 172,455,108	ref|XP_223121.1| similar to Cell surface glycoprotein GP42 precursor [Rattus norvegicus]
mcT3579	mCG4486	172,487,229 - 172,489,471	ref|XP_129566.1| similar to hypothetical protein FLJ20442 [Homo sapiens] [Mus musculus]
mcT3586	mCG4478	172,548,249 - 172,550,422	C-reactive protein, petaxin related
mcT164993	mCG1047289	172,624,418 - 172,624,846	ref|XP_136319.1| similar to ribosomal protein L6 [imported] - rat [Mus musculus]
mcT8432	mCG1204	172,741,973 - 172,743,073	serum amyloid P-component
mcT8438	mCG1210	172,804,796 - 172,805,726	olfactory receptor 16
mcT177534	mCG141906	172,981,245 - 172,982,178	olfactory receptor MOR267-4
mcT177535	mCG141907	173,032,724 - 173,033,657	olfactory receptor MOR267-5
mcT53237	mCG53054	173,054,238 - 173,055,107	olfactory receptor MOR267-3
mcT67007	mCG66824	173,067,556 - 173,068,498	olfactory receptor MOR267-2
mcT8437	mCG1209	173,073,176 - 173,079,111	Fc receptor, IgE, high affinity I, alpha polypeptide
mcT53238	mCG53055	173,116,657 - 173,117,590	olfactory receptor MOR267-8
mcT121229	mCG120048	173,122,077 - 173,125,370	ref|XP_136329.2| similar to amyloidP component [Mus musculus]
mcT177538	mCG1208	173,180,865 - 173,182,731	Duffy blood group
mcT177537	mCG1205	173,183,909 - 173,218,087	nectin-like 1
mcT8434	mCG1206	173,275,746 - 173,321,205	ref|XP_136330.1| similar to absent in melanoma 2 [Homo sapiens] [Mus musculus]
mcT8435	mCG1207	173,323,999 - 173,366,534	ref|XP_136331.2| similar to Gamma-interferon-inducible protein Ifi-16 (Interferon-inducible myeloid differentiationtranscriptional activator) (IFI 16) [Mus musculus]
mcT121225	mCG120038	173,450,220 - 173,455,805	ref|XP_129598.1| similar to hypothetical protein MGC23885 [Homo sapiens] [Mus musculus]
mcT121230	mCG120049	173,486,496 - 173,503,074	ref|XP_203732.1| similar to hypothetical protein 4930422C14 [Mus musculus]
mcT179273	mCG62472	173,529,955 - 173,536,634	EST
mcT121218	mCG120093	173,611,292 - 173,630,312	interferon activated gene 204
mcT177536	mCG120042	173,640,511 - 173,662,479	interferon activated gene 203
mcT180034	mCG1047288	173,678,559 - 173,686,776	ref|XP_110818.3| similar to myeloidcell nuclear differentiation antigen [Homo sapiens] [Mus musculus]

mcT130721	mCG129412	173,970,309 - 173,980,061	ref|XP_110285.1| similar to renin (Ren-1-d) [Mus musculus]
mcT154942	mCG1037238	174,984,386 - 174,984,975	ref|XP_223461.1| similar to eukaryotic translation initiation factor 4A1; initiation factor eIF-4A long form [Mus musculus] [Rattus norvegicus]
mcT179032	mCG8643	176,989,294 - 177,000,688	dual specificity phosphatase 12
mcT130265	mCG128960	177,001,906 - 177,003,488	gb|AAK69508.1|AF280810_1 T-DSP4 [Musmusculus]
mcT65150	mCG64967	177,276,981 - 177,278,085	ref|XP_131814.1| RIKEN cDNA D530049N12 [Mus musculus]
mcT129840	mCG128542	177,288,254 - 177,290,609	gb|AAH24348.1| Similar to RIKEN cDNA 1810030J14 gene [Mus musculus] (C-reactive protein)
mcT15793	mCG12318	178,108,805 - 178,114,418	interferon activated gene 205
mcT52708	mCG52525	178,124,281 - 178,125,226	olfactory receptor MOR123-1
mcT175789	mCG141521	178,132,614 - 178,133,553	olfactory receptor MOR123-2
mcT67555	mCG76372	178,148,846 - 178,149,806	olfactory receptor MOR105-5P
mcT55599	mCG55416	178,167,201 - 178,168,140	olfactory receptor MOR105-1
mcT63249	mCG63066	178,181,368 - 178,182,316	ref|XP_136389.1| similar to olfactory receptor MOR105-2 [Mus musculus]
mcT15794	mCG12319	178,193,726 - 178,194,677	ref|XP_222960.1| similar to olfactory receptor MOR105-2 [Mus musculus] [Rattus norvegicus]
mcT55597	mCG55414	178,202,796 - 178,203,677	olfactory receptor MOR105-4
mcT63949	mCG63766	178,232,255 - 178,233,053	olfactory receptor MOR105-2
mcT175790	mCG141522	178,241,890 - 178,242,739	ref|XP_222963.1| similar to seven transmembrane helix receptor [Homo sapiens] [Rattus norvegicus]
mcT60761	mCG60578	178,254,906 - 178,255,871	MOR105-3
mcT175791	mCG141523	178,262,084 - 178,263,050	olfactory receptor MOR105-10
mcT15796	mCG12321	178,281,067 - 178,363,314	spectrin alpha 1
mcT146810	mCG1029106	178,364,847 - 178,365,789	olfactory receptor MOR267-6
mcT115175	mCG114084	178,422,550 - 178,425,800	gb|AAH24348.1| Similar to RIKEN cDNA 1810030J14 gene [Mus musculus] (C-reactive protein)
mcT115176	mCG114085	178,429,580 - 178,430,496	gb|AAL61108.1| olfactory receptor MOR267-8 [Mus musculus]
mcT146809	mCG1029105	178,470,247 - 178,471,177	ref|XP_222916.1| similar to olfactory receptor MOR267-7 [Mus musculus] [Rattus norvegicus]
mcT146808	mCG1029104	178,475,971 - 178,476,882	ref|XP_222917.1| similar to olfactory receptor MOR267-7 [Mus musculus] [Rattus norvegicus]
mcT146807	mCG1029103	178,486,283 - 178,487,084	olfactory receptor MOR267-7
mcT60760	mCG60577	178,507,680 - 178,508,634	olfactory receptor MOR103-10
mcT60762	mCG60579	178,525,553 - 178,526,578	ref|XP_136378.1| similar to olfactory receptor MOR103-10 [Mus musculus]
mcT115172	mCG114081	178,581,387 - 178,911,118	formin 2
mcT52706	mCG52523	178,920,778 - 179,009,726	protein related to DAN and cerberus
mcT171630	mCG140810	179,147,951 - 179,583,016	regulator of G protein signaling 7

mcT2729	mCG4564	179,686,760 - 179,711,278	ref|XP_129612.2| fumarate hydratase1 [Mus musculus]
mcT2728	mCG4562	179,717,835 - 179,746,515	EST
mcT2700	mCG4567	179,748,091 - 179,778,248	opsin (encephalopsin)/g-PROTEIN COUPLED RECEPTOR
mcT2712	mCG4566	179,772,145 - 179,774,011	choroideremia-like
mcT115232	mCG114140	179,811,929 - 179,829,426	EST
mcT2749	mCG4560	179,852,642 - 179,901,660	WD Domain Containing Protein
mcT2746	mCG4561	179,960,224 - 179,990,522	exonuclease 1
mcT61840	mCG61657	180,000,280 - 180,001,310	ref|XP_222933.1| similar to Beclin1 (Coiled-coil myosin-like BCL2-interacting protein) (Protein GT197) [Rattus norvegicus]
mcT61839	mCG61656	180,043,433 - 180,304,499	EST
mcT115489	mCG114397	180,801,893 - 180,875,304	EST
mcT21265	mCG14944	180,882,880 - 181,082,599	gb|AAO27828.1|AF250729_1 centrosomal colon cancer autoantigen protein [Mus musculus]
mcT21270	mCG14949	180,903,494 - 180,906,182	gb|AAC25950.1| non-histone chromosomal architectural protein HMGI-C [Rattus norvegicus]
mcT115487	mCG114395	181,084,102 - 181,309,468	thymoma viral proto-oncogene 3
mcT180384	mCG142401	181,703,593 - 181,704,983	EST
mcT21271	mCG14950	181,784,735 - 181,808,218	EST
mcT21267	mCG14946	181,815,167 - 181,848,460	adenylosuccinate synthetase 2, non muscle
mcT21266	mCG14945	181,838,831 - 181,839,515	ref|XP_127238.1| similar to 40S ribosomal protein S8 [Mus musculus]
mcT115323	mCG114231	181,952,285 - 182,025,817	ref|XP_170953.2| similar to hypothetical protein MGC39581 [Homo sapiens]
mcT147012	mCG1029308	182,054,909 - 182,154,641	ref|XP_170953.2| similar to hypothetical protein MGC39581 [Homo sapiens]
mcT147010	mCG1029306	182,134,449 - 182,134,868	EST
mcT59943	mCG59760	182,162,301 - 182,237,817	ref|XP_170953.2| similar to hypothetical protein MGC39581 [Homo sapiens]
mcT115320	mCG114228	182,208,520 - 182,210,759	gb|AAH04611.1| translin-associated factor X [Mus musculus]
mcT16376	mCG17224	182,247,957 - 182,312,460	EST
mcT55015	mCG54832	182,335,906 - 182,336,502	EST
mcT163771	mCG17219	182,359,010 - 182,360,061	EST
mcT146860	mCG1029156	182,365,218 - 182,365,647	EST
mcT16369	mCG17217	182,378,189 - 182,382,669	EST
mcT170993	mCG17220	182,382,698 - 182,397,397	heterogeneous nuclear ribonucleoprotein U
mcT180739	mCG17221	182,466,053 - 182,542,135	EST
mcT54122	mCG53339	182,880,408 - 182,992,060	EST
mcT16374	mCG17222	183,019,332 - 183,159,290	EST
mcT175473	mCG16788	183,465,565 - 183,588,996	EST
mcT13938	mCG16791	183,591,216 - 183,591,860	ref|XP_129643.1| similar to ribosomal protein L29 [Mus musculus]
mcT117316	mCG116199	183,598,995 - 183,617,641	house-keeping protein 1
mcT117322	mCG116205	183,617,045 - 183,695,923	EST
mcT117321	mCG116204	183,740,226 - 183,750,797	gb|AAD34044.1|AF151807_1 CGI-49 protein [Homo sapiens]

mcT117318	mCG116201	183,792,234 - 183,804,257	gb|AAK21452.1| Kinesin-like protein 6 [Caenorhabditis elegans]
mcT175110	mCG141396	183,809,071 - 183,867,771	embryonic large molecule derived from yolk sac
mcT117313	mCG116196	183,988,893 - 183,989,421	gb|AAD04204.1| 60S ribosomal proteinL21 [Homo sapiens]
mcT5602	mCG6218	184,024,537 - 184,224,552	ref|NP_446109.1| CDC42-binding protein kinase alpha; mytonic dystrophy kinase-related Cdc42-binding kinase [Rattusnorvegicus]
mcT5606	mCG6212	184,227,198 - 184,246,942	chaperone, ABC1 activity of bc1 complex like (S. pombe)
mcT146855	mCG1029151	184,266,961 - 184,277,002	EST
mcT170995	mCG6223	184,291,669 - 184,327,358	presenilin 2
mcT5600	mCG6216	184,390,413 - 184,394,778	ref|XP_203250.1| similar to glyceraldehyde-3-phosphate dehydrogenase [Mus musculus]
mcT5601	mCG6217	184,394,008 - 184,487,598	EST
mcT5607	mCG6213	184,503,606 - 184,550,131	EST
mcT22452	mCG19846	184,634,778 - 184,667,071	ADP-ribosyltransferase (NAD+; poly (ADP-ribose) polymerase) 1
mcT120452	mCG119284	184,709,829 - 184,752,151	ref|XP_222996.1| similar to /prediction=(method:genefinder, version:084, score:147.90)~/match=(desc:LIN-9 PROTEIN,species:CAENORHABDITIS ELEGANS, ranges:(query:19817..20026, target:SWISS-PROT::P30630:205..274, score:162.00), (query:20078..2... [Rattus norvegicus]
mcT22439	mCG19833	184,754,511 - 184,758,471	Mix1 homeobox-like 1 (Xenopus laevis)
mcT22437	mCG19831	184,784,649 - 184,785,195	ref|XP_193159.1| similar to 60S ribosomal protein L21 [Mus musculus]
mcT22444	mCG19838	184,789,162 - 184,816,898	gb|AAB71197.3| peripherial benzodiazepine receptor associated protein; PBR associated protein; PAP7 [Mus musculus]
mcT22451	mCG19845	184,817,905 - 184,822,086	ref|XP_148997.1| RIKEN cDNA 5830405M20 [Mus musculus]
mcT22435	mCg19829	184,865,420 - 184,875,190	gb|EAA01174.1| agCP12107 [Anophelesgambiae str. PEST] (similar to Histone family 3A)
mcT22441	mCG19835	184,914,174 - 184,931,331	EST
mcT22434	mCG19828	184,956,271 - 184,960,818	Transforming Growth Factor Superfamily member
mcT22442	mCG19836	184,967,405 - 184,971,206	left-right determination, factor B
mcT120428	mCG119269	184,999,479 - 185,003,974	Transforming Growth Factor beta related
mcT22458	mCG19852	185,007,992 - 185,040,912	cDNA sequence BC014795

Table 2. List of the genes in the mouse BMD QTL which are also present in the syntenic region in the human BMD QTL region at 1q21-1q23.

Celera ID. Mouse genes)	*Position (Mb)*	*Gene Description*
mCG122327	168,916,936 - 168,956,539	Cell division cycle associated 1 (Kinesin related)
mCG10644	169,079,007 - 169,119,249	regulator of G-protein signaling 5
mCG52217	169,167,699 - 169,173,651	regulator of G-protein signaling 4
mCG10638	169,419,397 - 169,553,257	discoidin domain receptor family, member 2
mCG10645	169,578,600 - 169,611,386	EST AA437972 (UDP-N-Acetylglucosaminepyrophosphorylase)
mCG8628	170,151,071 - 170,324,073	ref|XP_129579.1| similar to Cyclic-AMP-dependent transcription factor ATF-6 alpha (Activating transcription factor6 alpha) (ATF6-alpha) [Mus musculus]
mCG8634	170,409,879 - 170,426,236	Fc receptor, IgG, low affinity IIb
mCG8626	170,578,738 - 170,598,850	Succinate dehydrogenase cytochrome B560 subunit
mCG8623	170,600,068 - 170,608,781	myelin protein zero
mCG123478	170,662,106 - 170,666,982	nuclear receptor subfamily 1, group I, member 3
mCG8642	170,667,172 - 170,670,592	Mitochondrial import receptor subunit TOM40-related
mCG8635	170,670,047 - 170,674,519	apolipoprotein A-II
mCG8632	170,677,715 - 170,690,515	Fc receptor, IgE, high affinity I, gamma polypeptide
mCG123487	170,691,071 - 170,707,446	NADH dehydrogenase (ubiquinone) Fe-S protein 2
mCG8656	170,706,612 - 170,716,169	a disintegrin-like and metalloprotease (reprolysin type) with thrombospondin type 1 motif, 4
mCG8627	170,726,401 - 170,732,914	UDP-Gal:betaGlcNAc beta 1,4-galactosyltransferase, polypeptide 3
mCG8624	170,733,012 - 170,737,196	protoporphyrinogen oxidase
mCG8621	170,737,979 - 170,743,992	ubiquitin specific protease 21
mCG123031	170,762,082 - 170,762,550	ref|XP_203246.1| similar to ribosomal protein L27 [Rattus norvegicus] [Mus musculus]
mCG8655	170,780,625 - 170,793,170	death effector domain-containing
mCG8625	170,792,065 - 170,797,123	nitrilase 1
mCG8620	170,862,511 - 170,870,112	upstream transcription factor 1
mCG8641	170,992,840 - 171,011,957	gb|AAF91290.1|AF234831_1 NK cell receptor 2B4 [Mus musculus]
mCG142315	171,039,068 - 171,050,253	ref|NP_034714.1| intelectin [Mus musculus]
mCG10010	171,528,344 - 171,529,658	gb|AAA40903.1| cyclin-dependent kinase 4
mCG10009	171,623,296 - 171,657,741	signaling lymphocyte activation molecule
mCG117630	171,696,585 - 171,737,453	CD84 antigen
mCG4477	171,906,525 - 171,911,824	nescient helix loop helix 1
mCG4479	171,920,062 - 171,936,996	nicastrin

mCG4480	171,981,967 - 171,991,040	peroxisomal farnesylated protein
mCG4482	172,052,694 - 172,062,665	phosphoprotein enriched in astrocytes 15
mCG4481	172,065,863 - 172,075,841	calsequestrin 1
mCG142115	172,126,613 - 172,151,708	ref|NP_036637.1| ATPase, Na+K+ transporting, alpha 2; ATPase, Na+K+ transporting, alpha 2 polypeptide [Rattus norvegicus]
mCG4496	172,165,492 - 172,173,393	gb|AAN63626.1|AF439263_1 immunoglobulin superfamily member 8 [Mus musculus]
mCG4483	172,175,266 - 172,182,702	potassium inwardly-rectifying channel, subfamily J, member 9
mCG4485	172,194,716 - 172,227,512	potassium inwardly-rectifying channel, subfamily J, member 10
mCG4487	172,229,581 - 172,232,739	phosphatidylinositol glycan, class M
mCG4491	172,328,901 - 172,332,071	CD2 antigen family, member 10
mCG4494	172,335,814 - 172,352,367	immunoglobulin superfamily, member 9
mCG4492	172,353,466 - 172,361,118	gb|AAM54133.1|AF465519_1 SM22beta [Mus musculus] (TRANSGELIN 2)
mCG4478	172,548,249 - 172,550,422	C-reactive protein, petaxin related
mCG1204	172,741,973 - 172,743,073	serum amyloid P-component
mCG1208	173,180,865 - 173,182,731	Duffy blood group
mCG1206	173,275,746 - 173,321,205	ref|XP_136330.1| similar to absentin melanoma 2 [Homo sapiens] [Mus musculus]
mCG1207	173,323,999 - 173,366,534	ref|XP_136331.2| similar to Gamma-interferon-inducible protein Ifi-16 (Interferon-inducible myeloid differentiationtranscriptional activator) (IFI 16) [Mus musculus]
mCG8643	176,989,294 - 177,000,688	dual specificity phosphatase 12
mCG12321	178,281,067 - 178,363,314	spectrin alpha 1
mCG1029105	178,470,247 - 178,471,177	ref|XP_222916.1| similar to olfactory receptor MOR267-7 [Mus musculus] [Rattus norvegicus]
mCG60577	178,507,680 - 178,508,634	olfactory receptor MOR103-10
mCG114081	178,581,387 - 178,911,118	formin 2
mCG52523	178,920,778 - 179,009,726	protein related to DAC and cerberus
mCG140810	179,147,951 - 179,583,016	regulator of G protein signaling 7
mCG4564	179,686,760 - 179,711,278	ref|XP_129612.2| fumarate hydratase1 [Mus musculus]
mCG4567	179,748,091 - 179,778,248	opsin (encephalopsin)/g-PROTEIN COUPLED RECEPTOR
mCG4566	179,772,145 - 179,774,011	choroideremia-like

mCG4560	179,852,642 - 179,901,660	WD Domain Containing Protein
mCG4561	179,960,224 - 179,990,522	exonuclease 1
mCG61656	180,043,433 - 180,304,499	Major Envelope related protein
mCG114395	181,084,102 - 181,309,468	thymoma viral proto-oncogene 3
mCG14946	181,815,167 - 181,848,460	adenylosuccinate synthetase 2, non muscle
mCG116199	183,598,995 - 183,617,641	house-keeping protein 1
mCG6223	184,291,669 - 184,327,358	presenilin 2
mCG19846	184,634,778 - 184,667,071	ADP-ribosyltransferase (NAD+; poly (ADP-ribose) polymerase) 1
mCG19833	184,754,511 - 184,758,471	Mix1 homeobox-like 1 (Xenopus laevis)
mCG19838	184,789,162 - 184,816,898	gb|AAB71197.3| peripherial benzodiazepine receptor associated protein; PBR associated protein; PAP7 [Mus musculus]
mCG19828	184,956,271 - 184,960,818	Transforming Growth Factor Superfamily member
mCG19836	184,967,405 - 184,971,206	left-right determination, factor B
mCG119269	184,999,479 - 185,003,974	Transforming Growth Factor beta related

Table 3. Genes related to bone either by known tissue expression or known function

Gene name (from Celera)	*Position in Chr.1 (Mb)*	*Description (from OMIM and PubMed)*
Nicastrin	171,920,062 -171,936,996	Regulatory role in cell differentiation (Sarkar and Das, 2003)
phosphoprotein enriched in astrocytes 15	172,052,694 -172,062,665	Regulate the caspase-8 which activates NF-KappaB (RANKL) and RANKL is an important cytokine for bone resorption (Hao & al., 2001 and Sattler & al., 2003)
calsequestrin 1	172,065,863 -172,075,841	Calsequestrin is a sarcoplasmic reticulum protein, which plays a predominant role in diastolic Ca2+-storage in the mammalian heart. (Frank & al., 2001)
similar to absent in melanoma 2 (AIM2)	173,275,746 -173,321,205	Overexpression of AIM2 reversed the tumorigenic phenotype in a melanoma cell line
Gamma-interferon-inducible protein Ifi-16	173,323,999 -173,366,534	The interferons are a family of vertebrate cytokines with pleiotropic activities including the regulation of cell growth and differentiation
ATPase, Na+K+ transporting, alpha 2 polypeptide	172,126,613 -172,151,708	specific role for the ATP1A2 protein in calcium signaling (James & al., 1999)

Table 4. Molecular markers along the QTL region used to fine map the congenic sub-lines

Marker Name	*Approximate Position (Mb)*
D1MIT453	164.6
D1Mit57	166.12
D1Mit145	166.70
D1MIT110	167.189
D1Mit370	167.42
D1MIT112	168.40
D1MIT113	171.66
D1MIT149	172.50
D1Mit354	172.70
D1Mit206	172.85
D1Mit150	178.70
D1MIT403	179.70
D1mit166	180.5
D1Mit359	181.30
D1mit207	181.59
D1Mit358	181.61
D1MIT115	181.73
D1Mit315	183.00
D1Mit509	184.86
D1Mit152	188.9
D1Mit221	189.18
D1MIT407	190.11
D1MIT459	191.58
D1MIT17	196.00

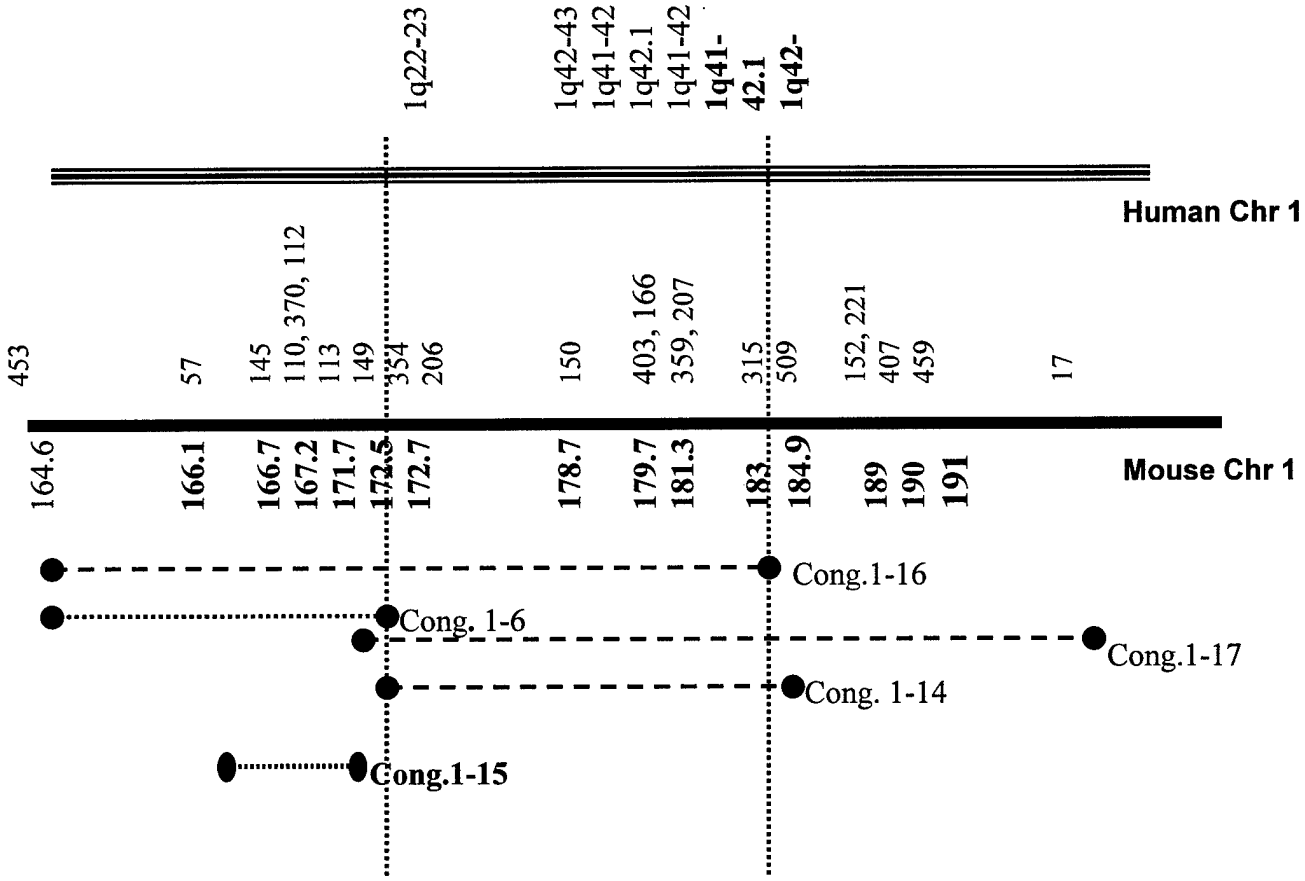

Fig. 1. Subcongenic Lines of the QTL Region.

1) On the top is human chromosome 1. The triple line represents the homologous regions on human Chr 1 to mouse chromosome 1. 2) In the middle is the map of mouse chromosome 1. The solid bar represents the original region of Chr 1 from CAST within the congenic strain B6.CAST-1. Numbers above the solid bar represent the position and names of D1 MIT microsatellite markers, while the number under the solid bar represents the Mb. distance on mouse Chr 1. 3) At the bottom are the subcongenic strains for the QTL locus of bone density on mouse chromosome 1that have been fine mapped with additional markers. The dashed lines represent the chromosomal regions covered by the five subcongenic strains that contain the QTL gene. The dotted lines represent the region covered by each of the five subcongenic strains that did not contain the QTL gene. The region indicated by the solid two-headed arrow between the two vertical lines is the proposed QTL region, based on information of BMD of subcongenic strains. The region indicated by a dotted two-headed arrow indicate a possible QTL region based on chromosomal location of BMD QTLs in mice and humans.

Table 5. Mid-diaphyseal data

Strain	*Tot.Cont.(%)*	*Tot.A.(%)*	*Tot.Dens.Read(%)*
Cong.1-16	120.6[b]	**102.1**	**113.7**[b]
Cong.1-17	119.6[a]	**105.8**	**108.7**[a]
Cong.1-14	126.1[a]	**110.5**[d]	**111.3**[a]
Cong.1-6	103.2	95.9[d]	106.1
Cong.1-15	103.2	99.7	104.0
B6 wild type	100	100	100

Values are represented as % of B6, N=6, except for Cong.1-16, N=3
[a]: p<0.001, [b]: 0.001>P<0.002, [c]: 0.004>P<0.009, [d]: 0.01>P<0.05
Tot. Con. Means: total content, Tot. A. means: Total area, Tot. Dens. Read: Total density read.

Table 6. Size data

Strain	*Cort.Thick*	*Endo.C*	*Perio_C2.(%)*
Cong.1-16	**117.8**[a]	95.6	99.9
Cong.1-17	**110.9**[a]	99.9	102.7
Cong.1-14	**115.5**[a]	101.2	104.9
Cong.1-6	104.8	95.5[d]	97.8
Cong.1-15	106.9[b]	98.0	99.3
B6 wild type	100	100	100

Values are represented as % of B6, N=6, except for Cong.1-16, N=3
[a]: p<0.001, [b]: 0.001>P<0.002, [c]: 0.004>P<0.009, [d]: 0.01>P<0.05
Cort.Thick means: cortical thickness, Endo. C means: endosteal circumference, Perio.C. means: Periosteal circumference.

Table 7. List of the genes used in microarray

Gene Symbol	*Gene description*
Tlr5	Toll-like receptor 5
Fmn2	formin 2/ref|NP_062318.1| (NM_019445) formin2 [Mus musculus]
BEbpnt	bisphosphate 3'-nucleotidase 1(Bpnt1)
DUSP12	dual specificity phosphatase 12/protein tyrosine phsophatase realted
TGFb2	Transforming growth factor-beta2
Esrrg2	ESTROGEN-RELATED RECEPTOR GAMMA
Zfp238	zinc finger protein 238
Rgs7	regulator of G protein signaling 7
Chm1	RAB PROTEINS GERANYLGERANYLTRANSFERASE (CF11787:SF10)
	EST
	Nuclear VCP like protein
	ADP-ribosyltransferase (NAD+; poly (ADP-ribose) polymerase) 1
	peripherial benzodiazepine receptor associated protein; PBR associated protein; PAP7 [Mus musculus]

	EST
	ref|XP_150989.1| hypothetical protein XP_150989 [Mus musculus]
	EST
	EST
	ref|XP_223042.1| similar to hypothetical protein FLJ14146 [Homo sapiens] [Rattus norvegicus]
	EST
	EST
	EST
	ref|XP_136525.1| similar to 60S ribosomal protein L21 [Mus musculus]
	ref|XP_135705.1| similar to SET translocation [Mus musculus]
	EST
	EST
	ref|NP_659045.1| expressed sequence AI848994; expressed sequence N28096 [Mus musculus]
	EST
	calpain 2
	EST
	gb|AAN64660.1| dispatched [Mus musculus]
	EST
	EST
	EST
	gb|AAH14683.1| Similar to kynurenine 3-hydroxylase/3-monooxygenase [Mus musculus] (kmo)
	ref|XP_129612.2| fumarate hydratase 1 [Mus musculus]
	opsin (encephalopsin) (opn3)
	ref|XP_222933.1| similar to Beclin 1 (Coiled-coil myosin-like BCL2-interacting protein) (Protein GT197) [Rattus norvegicus]
	exonuclease 1
	EST
	EST
	gb|AAO27828.1|AF250729_1 centrosomal colon cancer autoantigen protein [Mus musculus]
	EST
	EST
	ref|XP_129606.1| RIKEN cDNA 1700016C15 [Mus musculus]
	EST
	EST
	EST

	ref|XP_222930.1| similar to hypothetical protein [Macaca fascicularis] [Rattus norvegicus]
	EST
	EST
	gb|AAH04611.1| translin-associated factor X [Mus musculus]
	EST
	EST
	signal recognition particle
	EST
	ref|NP_081464.1| RIKEN cDNA 2410008A19 [Mus musculus](HSKM-B-Related)
	gb|AAH10403.1| presenilin 2 [Mus musculus]
	EST
	calpain 8
	gb|EAA01174.1| agCP12107 [Anopheles gambiae str. PEST]
	EST
	EST
	EST
	EST
	EST
	ref|NP_081464.1| RIKEN cDNA 2410008A19 [Mus musculus](HSKM-B-Related)
	ref|XP_136486.1| similar to Hypothetical protein Y97E10AL.1 [Caenorhabditis elegans] [Mus musculus]
	house-keeping protein 1
	EST
	ref|XP_129647.1| glutamyl-prolyl-tRNA synthetase [Mus musculus]
	EST
	Zinc-transporter-SLC30A1
	Isoleucyl tRNA-synthetase
	ref|XP_282886.1| similar to hypothetical protein YR-29; TGF beta inducible nuclear protein 1; hairy cell leukemia protein 1 [Homo sapiens] [Mus musculus]
	hypothetical protein MGC28394
	EST
	EST
	EST
	EST
	EST
	EST
	EST
	EST

	EST
	ref|XP_219750.1| similar to glyceraldehyde-3-phosphate dehydrogenase [Mus musculus] [Rattus norvegicus]
	tumor protein p53 binding protein, 2
	EST
	EST
	degenerative spermatocyte homolog (Drosophila)
	gb|AAD04204.1| 60S ribosomal protein L21 [Homo sapiens]
	EST
	EST
	Mix1 homeobox-like 1 (Xenopus laevis)
	EST
	ref|XP_129630.1| expressed sequence AA545216 [Mus musculus]
	ref|XP_193159.1| similar to 60S ribosomal protein L21 [Mus musculus]
	EST
	EST
	ref|XP_203250.1| similar to glyceraldehyde-3-phosphate dehydrogenase [Mus musculus]
	EST
	EST/Cell proliferation antigene KI67 (transcription factor, ELYS pending)
	ref|NP_446109.1| CDC42-binding protein kinase alpha; mytonic dystrophy kinase-related Cdc42-binding kinase [Rattus norvegicus]
	EST
	EST
	EST
	ref|XP_222971.1| similar to hypothetical protein FLJ10157 [Homo sapiens] [Rattus norvegicus]
	gb|AAH04485.1|AAH04485 Unknown (protein for MGC:10665) [Homo sapiens]
	ref|XP_127238.1| similar to 40S ribosomal protein S8 [Mus musculus]
	EST
	Cell proliferating antigen KI-67-related
	EST
	EST
	EST
	ref|XP_222999.1| similar to Transforming growth factor beta 4 precursor (TGF-beta 4) (Endometrial bleeding-associated factor) (Left-right determination factor A) (Lefty-A protein) [Rattus norvegicus]
	ref|XP_223000.1| similar to endometrial bleeding associated factor [Mus musculus] [Rattus norvegicus]
	EST
	epoxide hydrolase 1, microsomal

	gb|EAA01174.1| agCP12107 [Anopheles gambiae str. PEST] (Histone H3)
	ref|NP_659043.1| hypothetical protein MGC11687 [Mus musculus]
	EST
	ref|XP_136489.1| similar to sphingolipid delta 4 desaturase; membrane fatty acid (lipid) desaturase; dihydroceramide desaturase [Homo sapiens] [Mus musculus]
	ref|NP_445881.1| fibroblast growth factor receptor 3 [Rattus norvegicus]
	EST
	ref|XP_223698.1| similar to cytochrome c oxidase, subunit VIIIa; COX VIII-L [Mus musculus] [Rattus norvegicus]
	EST
	EST
	EST
	ref|NP_598576.1| lamin B receptor; ichthyosis [Mus musculus]
	ref|NP_598466.1| RIKEN cDNA 1810018M05 [Mus musculus](Pyrroline-5-carboxylate reductase=Panter best hit)
	EST
	ref|XP_133324.1| RIKEN cDNA 2310022K01 [Mus musculus]
	ref|XP_145024.2| similar to 40S ribosomal protein S2 [Mus musculus]
	EST
	EST
	gb|AAH20044.2| similar to WD40 repeat protein [Mus musculus]
	EST
	dual specificity phosphatase 10
	ref|NP_663601.1| similar to hypothetical protein FLJ12806 [Mus musculus]
	ref|XP_046126.4| similar to Meningioma-expressed antigen 6/11 (MEA6) (MEA11) [Homo sapiens]
	EST
	gb|AAH30340.1| Unknown (protein for MGC:40682) [Mus musculus](Rhophilin related=Panter best hit)
	EST
	TATA box binding protein (Tbp)-associated factor, RNA polymerase I, A
	RIKEN cDNA 4930507C10 gene
	ref|XP_156065.1| similar to ribosomal protein L35a [Rattus norvegicus] [Mus musculus]
	gb|AAH05357.1|AAH05357 Similar to RIKEN cDNA 1700073K01 gene [Homo sapiens]
	heterogeneous nuclear ribonucleoprotein U(gb|AAH18353.1| Similar to transporter protein; system N1 Na+ and H+-coupled glutamine transporter [Mus musculus])
	EST
	EST

	ref|NP_666217.1| RIKEN cDNA 9630058J23; hypothetical protein MGC31547 [Mus musculus]
	EST
	thymoma viral proto-oncogene 3(Akt3) (RAC serine/threonine kinase)
	adenylosuccinate synthetase 2, non muscle
	ref|XP_129643.1| similar to ribosomal protein L29 [Mus musculus]
	EST
	EST

Table 8. List of the genes used for Real Time PCR.

Celera ID	*Gene Description*
mcT178984	EST
mcT177589	phosphoprotein enriched in astrocytes 15
mcT3588	calsequestrin 1
mcT179097	ref|NP_074039.1| ATPase, Na+/K+ transporting, alpha 4 polypeptide [Rattus norvegicus]
mcT179096	ref|NP_036637.1| ATPase, Na+K+ transporting, alpha 2; ATPase, Na+K+ transporting, alpha 2 polypeptide [Rattus norvegicus]
mcT179668	gb|AAN63626.1|AF439263_1 immunoglobulin superfamily member 8 [Mus musculus]
mcT177590	potassium inwardly-rectifying channel, subfamily J, member 9
mcT177591	potassium inwardly-rectifying channel, subfamily J, member 10
mcT3584	phosphatidylinositol glycan, class M
mcT3572	CD2 antigen family, member 10
mcT3576	immunoglobulin superfamily, member 9
mcT3573	gb|AAM54133.1|AF465519_1 SM22beta [Mus musculus] (TRANSGELIN 2)
mcT118799	ref|XP_222907.1| similar to Nasopharyngeal epithelium specific protein 1 [Rattus norvegicus]
mcT165228	EST
mcT118794	ref|XP_136318.2| similar to coxsackie-adenovirus-receptor homolog [Rattus norvegicus] [Mus musculus]
mcT3575	EST
mcT54622	ref|XP_223121.1| similar to Cell surface glycoprotein GP42 precursor [Rattus norvegicus]
mcT3579	ref|XP_129566.1| similar to hypothetical protein FLJ20442 [Homo sapiens] [Mus musculus]
mcT3586	C-reactive protein, petaxin related

mcT164993	ref|XP_136319.1| similar to ribosomal protein L6 [imported] - rat [Mus musculus]
mcT8432	serum amyloid P-component
mcT8438	olfactory receptor 16
mcT177534	olfactory receptor MOR267-4
mcT177535	olfactory receptor MOR267-5
mcT8437	Fc receptor, IgE, high affinity I, alpha polypeptide
mcT177538	Duffy blood group
mcT177537	nectin-like 1
mcT8434	ref|XP_136330.1| similar to absentin melanoma 2 [Homo sapiens] [Mus musculus]
mcT8435	ref|XP_136331.2| similar to Gamma-interferon-inducible protein Ifi-16 (Interferon-inducible myeloid differentiationtranscriptional activator) (IFI 16) [Mus musculus]
mcT121225	ref|XP_129598.1| similar to hypothetical protein MGC23885 [Homo sapiens] [Mus musculus]
mcT121230	ref|XP_203732.1| similar to hypothetical protein 4930422C14 [Mus musculus]
mcT179273	EST
mcT121218	interferon activated gene 204
mcT177536	interferon activated gene 203
mcT180034	ref|XP_110818.3| similar to myeloidcell nuclear differentiation antigen [Homo sapiens] [Mus musculus]
mcT130721	renin 2 tandem duplication of Ren1
mcT154942	dual specificity phosphatase 12
mcT130265	EST

Table 9. Genes up-regulated in 14 week-old Congenic female mice

Microarray #	*Position in Chr.1 (bases)*	*Gene description*
90	179,686,760 - 179,711,278	fumarate hydratase 1
91	179,717,835 - 179,746,515	Similar to kynurenine 3-hydroxylase/3-monooxygenase
174	183,809,071 - 183,867,771	Similar to transcription factor, ELYS pending
188	184,503,606 - 184,550,131	ESTs similar to Hypothetical protein Y97E10AL.1

Fig. 2. Expression pattern of the genes that show differences in the expression in both congenic lines when compared to the wild type B6 mice: 96-F was used for the cong.1-17 and 13-F was used for the cong.1-14

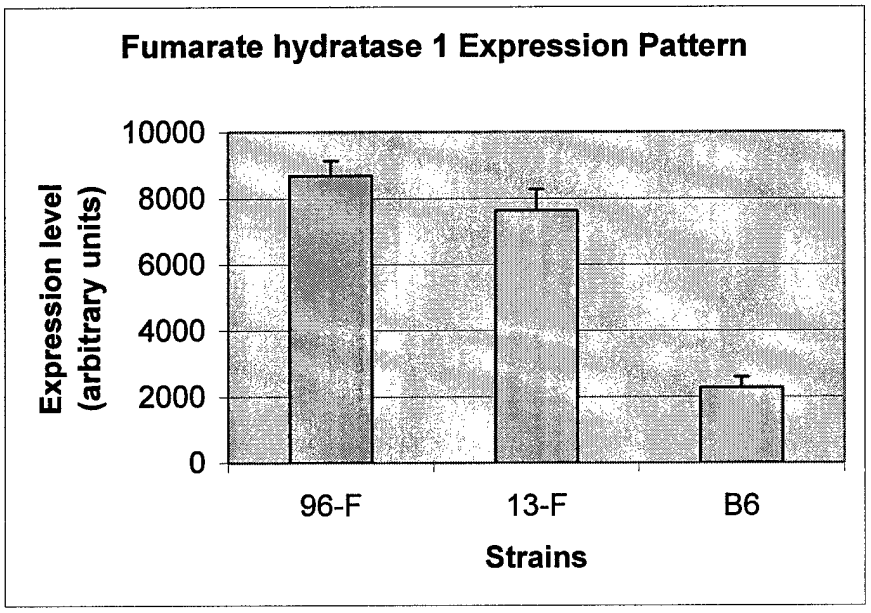

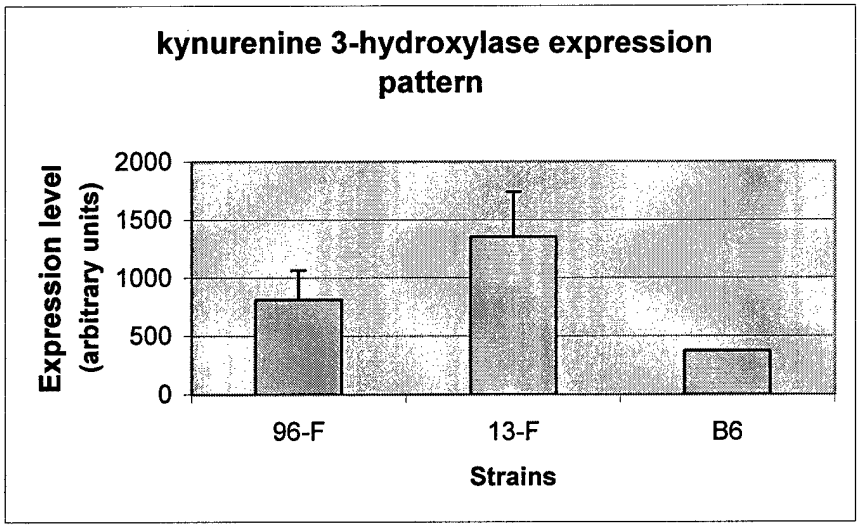

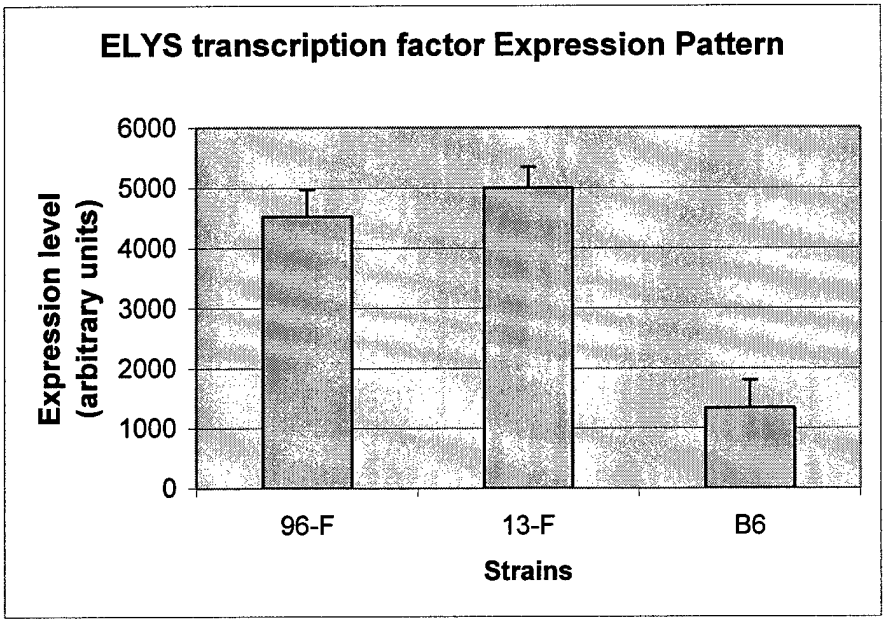
ELYS transcription factor Expression Pattern
Expression level (arbitrary units)
6000
5000
4000
3000
2000
1000
0
96-F
13-F
B6
Strains

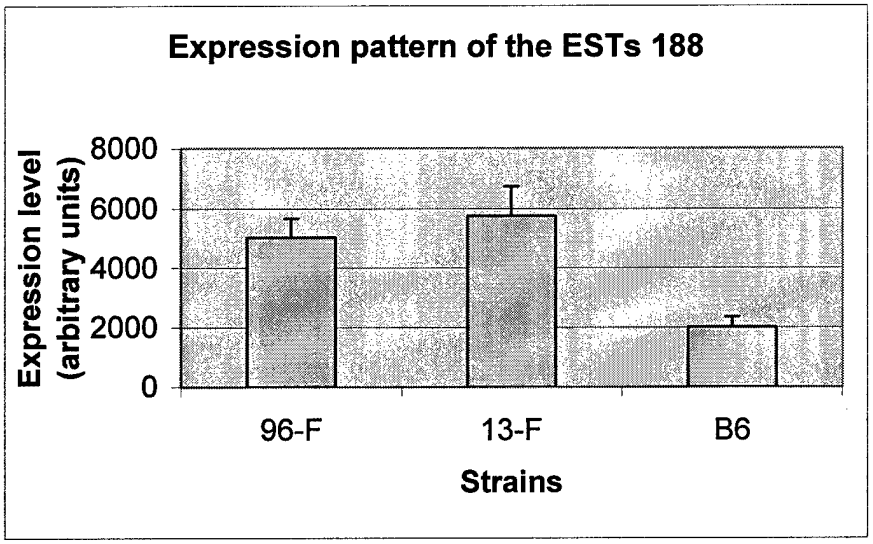
Expression pattern of the ESTs 188
Expression level (arbitrary units)
8000
6000
4000
2000
0
96-F
13-F
B6
Strains

Table 10. Fold difference in gene expression between Congenic mice and B6 wild type mice

Microarray ID	*Gene description*	*Ratio [a]Cong.1-17/B6*	*Ratio [a]Cong.1-14/B6**
90F1#6	fumarate hydratase 1	3.8	3.3
91F1#6	Similar to kynurenine 3-hydroxylase/3-monooxygenase	2.2	3.6
174F1#1	Transcription factor, ELYS pending	3.4	3.7
188F2#1	ref|XP_136486.1| similar to Hypothetical protein Y97E10AL.1 [Caenorhabditis elegans] [Mus musculus]	2.5	2.9

**the ratio is the average of 2 replicates (2 congenic mice and 2 B6 mice)*

[a] P≤0.01

Table 11. Expression level of genes present in the BMD QTL region by real time PCR in B6 and B6-Cast subcongenic mice

Celera ID	*B6*[a]	*Cong.1-14*[a]	*Cong.1-17*[a]	*Fold change B6-Cong.1-14*	*Fold change B6-Cong.1-17*
mct3587	21.1	21.08	-	-0.42	-
mct118793	23.5	22.1	24.43	2.35	-1.06
mct177588	23.4	23.9	25.25	-1	-3.9
mct178984	21.6	21.2	22.65	1	-0.9
mct121218	23.2	23.0	-	0.56	-
mct8432	**35.9**	**30.7**	**26.4**	**10.28***	**19.08***
mct3588	21.3	21.9	24.3	-1.12	-6.22
mct179096	21.1	21.6	25.26	-0.98	-7.12
mct179097	27.2	27.4	-	-0.61	-
mct3584	25.1	25.03	-	0.09	-
mct177536	22.4	23.01	23.2	-1.4	-1.0
mct12130	22.7	23.48	23.4	-1.84	-1.7
mct3575	27.5	27.2	-	0.4	
mct177590	28.45	29.24	29.2	-1.21	-1.69
mct3572	27.7	28.2	25.75	-1.3	5.42
mct3574	25.2	24.8	24.75	0.9	2.4
mct8434	23.7	24.5	26	-1.8	-3.2
mct177538	**25.2**	**23.1**	**23.9**	**3.92***	**3.96***
mct8437	23.8	24.54	24.05	-1.5	0.97
mct177534	28.4	29.2	29.2	-1.21	-1.6
mct118794	28.5	28.8	28.7	-0.5	-0.47
mct179668	26.57778	26.06333	26.75	0.908889	-0.26444
mct179273	28.18444	28.66	22.98333	-1.07111	10.48222
mct177537	25.6	27.54133	26.01667	-4.00267	-0.75333
B-actin	15.5	15.6	16.1	1	0.9

**P≤0.01 between B6 and the subcongenic mice, [a]: Values shown represent the threshold cycle (Ct.) when the amplified product starts to be detected by the ABI. PCR machine. "-": Real time PCR has not been done.*

Table 12. Genes that show significant difference between B6 and the high BMD congenic mice

Celera ID	*Position in chr1. (Megabases)*	*Gene description*	*Cong1-14/B6*[a]	*Cong1-17/B6*[a]
mct8432	172.7	Serum Amyloid P-component	**10.28**	**19.08**
mct177538	173.18	Duffy blood group	**3.92**	**3.96**

[a]: *Fold difference in the expression of the gene between the congenic and B6 mice*

Table 13. Polymorphism found between B6 sequence and Cast sequences.

Position (base)	*Polymorphism*	*Region*	*Position-Function*
111	T/C	5'UTR	Between the glucocorticoid and cytokine responsive elements, required for Il-6 expression and a heat-shock site
231	A/G	5'UTR	Promoter region after the TATAbox
417	C/T	1st intron	Intervening sequence
1069	C/T	Exon 2, no amino acid change	Coding region
1095	G/A	Exon 2, serine/asparagine	Coding region
1715	C/T	3'UTR	3' non-coding region
1988	T/G	3'UTR	3' non-coding region

Table 14. Comparison of the polymorphic sequences between B6, Balb, Cast and C3H mice

Position	*B6 (amino acid)*	*Balb (amino acid)*	*Cast (amino acid)*	*C3H (amino acid)*
111	T	C	C	C
231	A	G	G	G
417	C	T	T	T
923proline	C* (117alanine)	G (117alanine)*	G (117proline)*	C (117alanine)*
1069	C (no aa change)	C	C	T
1095	G (191serine)	A	A	A(191asparagine)

* PCR done once

Fig. 3. Results of the CRP blast-search using NCBI database

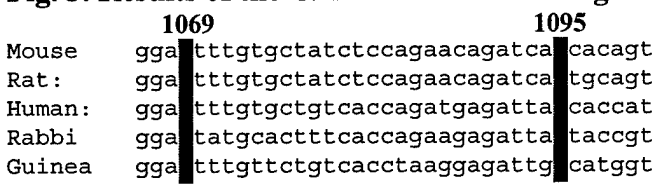

Fig. 4. Interval maps for chromosome 1.

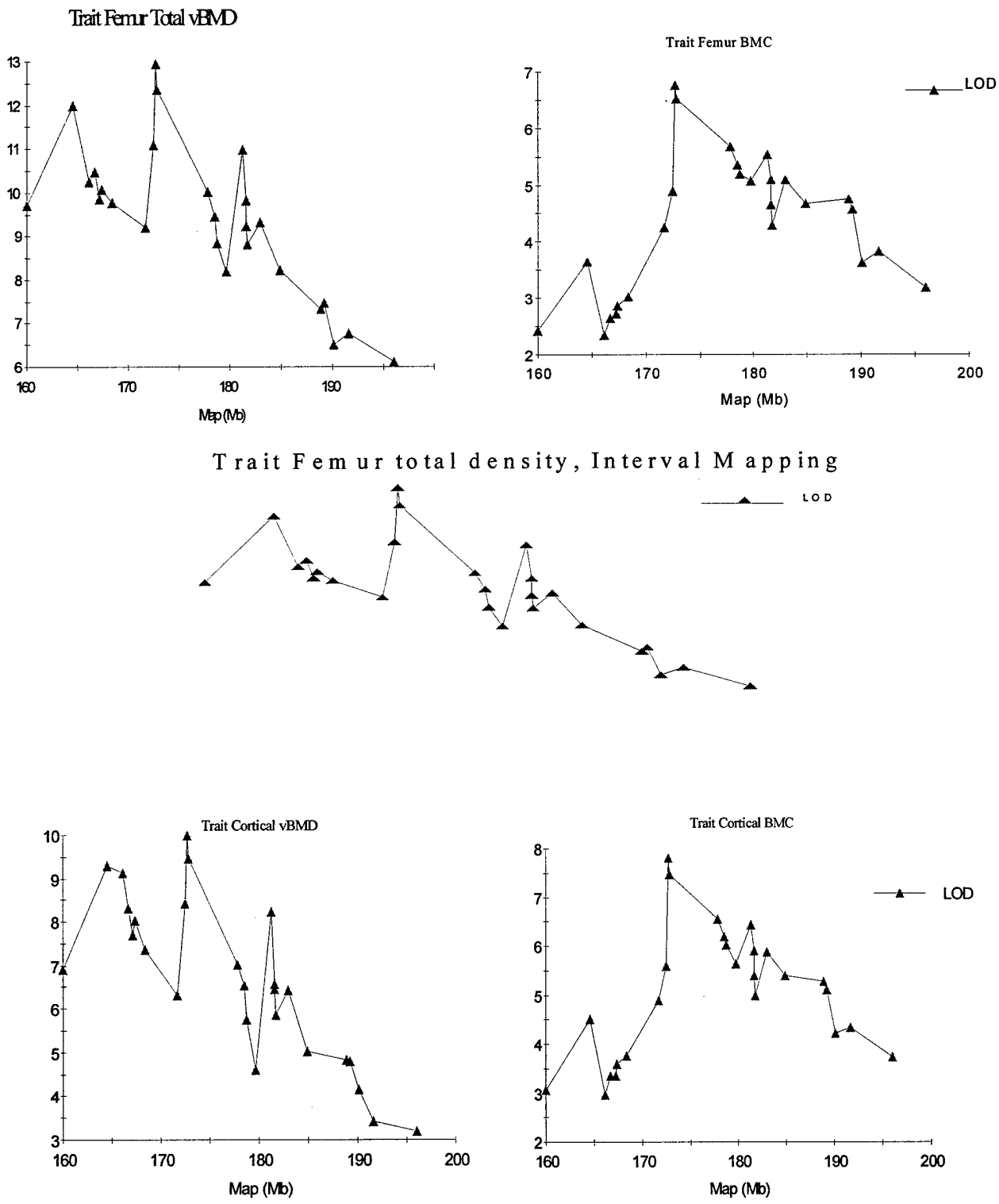

Fig. 5. Combining the results from congenic fine mapping and F2 population fine mapping.

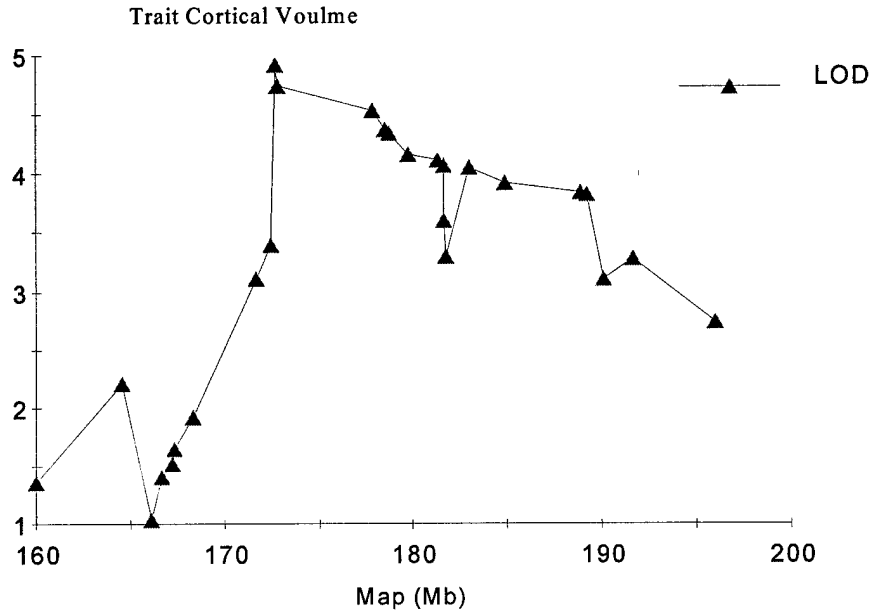

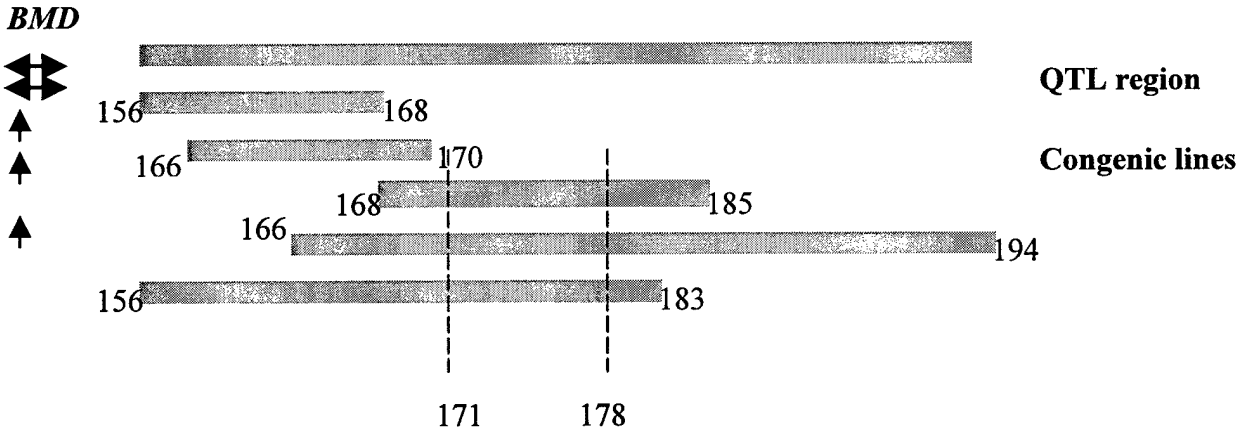

B. TECHNICAL OBJECTIVE 2: To identify the key genes that are involved in the soft-tissue repair/regeneration in MRL/MpJ and SJL/J mice.

1. Introduction

The primary goal of wound treatment is rapid wound closure with minimal scar formation, an important determinant for cosmetic appearance (1-2). Wound healing involves two major clinical issues: 1) the rate of healing; and 2) the quality of healing. However, the success of using therapeutic approaches to treat wounds depends heavily on understanding the molecular mechanisms underlying the process of wound healing. The aim of this project is to identify the key genes and their cellular function that regulate soft tissue repair and regeneration in a mouse model.

Our studies are designed to employ state-of-the-art molecular biotechniques to identify the genes located in chromosomes 1 and 9 involved in the regulation of wound healing/regeneration.

Our Specific Objectives during the first 12 months of this grant period were as follows:

a) Specific Objective 1: To confirm the QTL effects for soft tissue heal 1 (sth1) and soft tissue heal 9 (sth9) by developing congenic strains that contain the QTL region on chromosomes 1 and 9, respectively.

b) Specific Objective 2: To identify all of the genes present with in the sth1 and sth9 loci and determine candidate genes for the regulation of wound healing/ regeneration.

c) Specific Objective 3: To examine the differential expression of the majority of the genes identified within the sth1 and sth9 loci between MRL and SJL mice using in-house microarray at the 7 day time point (other time points will be examined in the future).

d) Specific Objective 4: To identify sequence polymorphism in the regulatory region of selected candidate gene/s which show differential expression and are located in the sth1 or sth9 loci

Our progress in each of the specific objectives is given below.

To achieve our objective of identifying key genes involved in soft-tissue regeneration, we proposed to use an integrated strategy involving: 1) development of congenic strains to confirm the phenotype; 2) utility of genomic resources to identify genes present in the QTL region; 3) sequencing of regulatory and coding regions of key candidate genes located in the QTL region to identify sequence variation/s; and 4) utilization of existing and development of new technologies for studying the function of candidate genes in wound healing/regeneration (e.g. microarray, knockout and *in vivo* functional assay). We believe that a combination of traditional genetic approaches along with genomic resources and technologies for testing the functions of candidate genes would allow us to make faster progress on the identification of QTL genes regulating wound healing compared to using any one of the above approaches alone.

2. Body

Our progress during the first 12 months of this continuation grant period for each specific objective is given below.

a) Specific Objective 1: To confirm the QTL effects for sth1 and sth9 by developing congenic strains that contain the QTL region on chromosomes 1 and 9, respectively.

Our initial focus is on two of the 10 QTL, namely soft tissue healing (sth) 1 and 9, which are located in chromosomes 1 and 9, respectively. We chose these QTL for the following reasons. Sth1 QTL represents the sharpest QTL (i.e. narrow chromosomal region) among all QTL identified and represents the second largest QTL in terms of relative contribution (7%) to the phenotypic variance among the F2 population (3). Sth9 represents the largest QTL, contributing to approximately 15% phenotypic variance among the F2 population, but is confined to a much broader region in chromosome 9 compared to sth1. Both sth1 and sth9 exhibit significant interactions with other QTL, thus suggesting that these two QTL play a major role in overall wound healing.

In order to accomplish this objective, we are in the process of developing and characterizing congenic strains for chromosome 9. Chromosome 1 congenic mice could not be developed as proposed because there was no recombination within the region of interest and therefore we are not pursuing it further. To produce new congenic strains for chromosome 9, we crossed the MRL/MPJ female with SJL/J males (parental strains) to get F1 mice. To produce N1 mice, we backcrossed the F1 females with SJL/J males. The N1 were genotyped to identify mice that were heterozygous to sth9 QTL region using 12 microsatelite markers but contain maximum genetic material from SJL mice. The heterozygous N1 females were then backcrossed with SJL males to produce N2, which were then also genotyped. The heterozygous females were backcrossed with SJL to produce N3. The progenies were genotyped in the QTL region. Individuals with a crossover genotype between MRL and SJL in the QTL region were selected for further backcrosses for N4s, N5, N6, and presently, N7 heterozygotes are being crossed (N7 x N7) to allow for characterization of the phenotype (wound healing) (Fig. 1).

Twelve molecular markers were used to characterize the regions of the chromosome from a donor MRL into SJL receipient mice. They are D1Mit336/355/207/208/270/343/196/111/9/308/114/182. Table 1 lists the molecular markers used to genotype the congenic strains, indicating their location on the chromosome in both centiMorgans (cM) and Mega bases (Mb). For genotyping, PCR-based genotyping with microsatellite markers was performed, as described previously (Masinde *et al.* 2001). DNA from the progenies of N1, N2 ..... N7 was extracted from either a piece of tissue from ear punch or a tail tip using the Promega Tissue Kit (Promega, Madison, WI). PCR was conducted on a DNA engine tetrad from MJ Research Inc. (Watertown, MA). PCR products were separated in 6% polyacrylamide gel and visualized with Ethidium Bromide under UV light.

The inbred mouse strains, MRL and SJL, were obtained from The Jackson Laboratory (JAX). Congenic strains are being produced and maintained in the research colony under 14:10 hr. light:dark cycle in the J. L. Pettis Memorial VA Medical Center (JLPMVAMC). An autoclaved diet of NIH-31 with 6% fat and HCl-acidified water (pH 2.8-3.2) was available at all times. The animal protocols were reviewed and approved by the Institutional Animal Care and Use Committee of the Jerry L. Pettis Memorial V.A. Medical Center.

Our congenic approach should confirm the biological activity of the QTL gene in this region when we measure the rate of wound healing in the N7 X N7. After confirmation, we shall further narrow the size of the QTL locus within Chr 9. Fig. 1 shows 12 markers that will help in breaking up the main congenic into sub-congenic of this QTL locus. In the proposal for the first 12 months, specific objective 1, we had proposed to generate up to N3 of the congenic mice but we are ahead of schedule at N7.

b) Specific Objective 2: To identify all of the genes present within the sth1 and sth9 loci and determine candidate genes for regulation of wound healing/ regeneration.

In order to accomplish this objective, we identified all of the genes present in the sth1 and sth9 loci using Celera and/or public databases. Over 174 genes were identified from the two loci and an additional 51 growth factors were blasted for homology with genes previously known to play a role in wound healing. As shown in the Table 2, most of the genes on chromosome 1 had homology with genes known to play a role in wound healing, while most of those genes from chromosome 9 did not have any homology with those genes previously identified for wound healing. We are continuing our search to determine those genes which could be involved in up stream or down stream signaling pathways for candidate genes known to regulate wound healing.

We have identified over 20 genes and ESTs on chromosome 1 using the Celera database that had homology with known genes and these have been shown to play a role in wound healing. None of the chromosome 9 genes that had homology with known genes have been previously linked to wound healing. It is possible that the role of these genes in wound healing was not yet been investigated (Table 2).

The most salient finding is that most of the genes from the loci on chromosomes 1 and 9 were ESTs but, when blasted, they had homology with some genes known to play a role in wound healing. We also found evidence that some genes previously known to play different roles in wound healing exhibited homology with ESTs or genes from wound healing loci on chromosome 1 (Table 2). These genes and ESTs are being further analyzed by microarray to identify those that are upregulated in MRL (good healer) as compared to SJL (poor healer), as shown in Objective 3.

c) Specific Objective 3: To examine the differential expression of a majority of the genes identified within the sth1 and sth9 loci between MRL and SJL mice by in-house microarray at the 7 day time point, a wound healing repair stage (other time points will be examined in the future).

In order to accomplish this objective, we have built a microarray chip using genes from the QTL on chromosome 1 and 9. As was reported in the last annual report of

October 2002, we have built a knowledge-based microarray chip that includes growth factors and other important regulatory genes (e.g. transcription factors) known to be involved in soft tissue repair/regeneration and the genes that are localized in the major soft tissue repair/regeneration QTL regions. We designed primers for polymerase chain reaction (PCR) within the 3' untranslated regions (3' UTRs) and amplified targeted gene fragments using genomic DNA (PCR) or mRNA (RT-PCR) as templates (the average size was about 500 bp). The rationale for choosing 3' UTR for amplification is based on the fact that the hybridization sensitivity and specificity are higher in this region of the gene than in other regions. The PCR fragments were isolated and purified from agarose gel and arrayed in six replicates for each gene fragment on a poly-prep amine slide using a GMS 417 arrayer.

Out of the 146 genes from chromosome 1 and 164 genes from chromosome 9 identified from the Celera database we selected 77 from chromosome 1 and 97 from chromosome 9. 51 growth factors that made our minimum requirements of single strong band and required base pair size were also selected (Table 3). The Celera database is privately owned by the APLERA Corporation, of which we are subscribers. After the selection of genes from the Celera database, we then transferred them to Primer3, a free program from the Internet, for primer design. The probes for these genes were designed using Primer3 and PCR amplifications were completed for 77 genes in chromosome 1 and 97 genes in chromosome 9. In addition, we amplified probes for 51 growth factors and these were then printed on slides. Thus, a total of 225 gene probes were printed on each slide (Table 3). Our decision to make a QTL-based microarray chip was guided by the fact that there is currently no available information on the role of most of the genes/EST within the QTLs for wound healing. To accomplish our goal, we extracted total RNA from 0.4 mm discs of ear punched tissue (4 hrs and 7 days, after injury) and control tissue (QIAGEN). We performed two-color hybridizations; MRL/MpJ control vs. SJL/J punched, and MRL/MpJ punched vs. SJL/J control, and analyzed differential gene expression using the Gene Spring program. Finally, we identified genes that are up-regulated or down-regulated more than two fold after ear punch compared to control and that have more than two fold differential expression between MRL/MpJ and SJL/J mice after ear punch. Based on our previous experience, we diluted the DNA in 50% DMSO at approximately 0.2 μg/μl. The microarrays were printed on the Corning amino-silane coated slides (Corning, NY) using a GMS 417 Arrayer (Genetic MicroSystems). Six replicates of each individual clone were printed on each slide. These replicates substantially increase the reliability of expression data and make it possible to confidently detect real, but small, changes in expression. Commercial controls from Lucidea Universal Score Cards were also included as controls.

We used in-house QTL for chromosomes 1 and 9 genes and growth factor/receptor microarray to determine the temporal gene expression profile of wound healing in the ear-punched tissue of the MRL/MpJ (MRL) mice at 4 hours and 7 days after ear punch (Tables 4 & 5). Our results revealed the dynamic change and diverse patterns of gene expression during wound healing, identified genes shared between the inflammatory and repair wound healing stage that have not been fully recognized to play a role during wound healing, and showed that well-recognized growth factors/receptors during wound healing are most highly and widely expressed at the inflammatory and repair stages of healing.

At the inflammatory stage, 4 hours after ear punch, there are more known growth factors highly expressed than at day 7 during the repair wound healing stage. One of the most interesting findings of this study was that, of about 200 genes studied at inflammatory and repair stages, three genes (connective tissue growth factor, calgranulin A and heparin-binding EGF-like growth factor) were expressed at both inflammatory and repair stages, none of which have an established role in wound healing (Tables 4-5). Also, down-regulated genes were identified as shown in Table 5.

d) Specific Objective 4: To identify sequence polymorphism in the regulatory region of selected candidate gene/s which show differential expression and are located in the sth1 or sth9 loci.

In order to accomplish this objective, we identified regulatory regions of genes that are known to have SNPs in MRL mice that are different from other strains in the Roche database and are located in the sth1 and sth9 loci. Primers were designed to cover the regulatory regions and amplified. The PCR products were purified and then sequenced using ABI 3100. PCR products were purified using EXO Sap It enzyme to remove any non-specific products and sequenced using universal M13 primers.

We identified one gene out of over 10 candidates that had multiple SNPs. Cellular retinol binding protein (CRBPI) was identified on a QTL on chromosome 9 that had a LOD score of over 13 and explained 16 percent of the wound healing phenotype. Some of the identified SNPs in CRBPI were different when compared between MRL (good healer) and SJL (poor healer) mice (Fig. 2 and Table 6). This is evidence that there may be some connection between wound healing and the specific SNPs. The SNPs are within the sequence that is important in regulating stability of mRNA and thus may play a role in wound healing by altering the mRNA levels of CRBPI with the SNP that has the most stable mRNA promoting wound healing. CRBPI also had different SNPs in the 3'UTR region and in the same way this may affect the stability of mRNA and thus affect wound healing (Fig. 4 and Table 7). CRBPI has SNPs within the UUU region of the sequence that is key for binding proteins regulating stability of mRNA.CRBPI has been shown to play a role in liver regeneration and also in the visual pigment regeneration in the eye, making it a potential candidate in wound healing. Functional studies will be done to test the effect of CRBPI in wound healing using MRL mice (4).

3. Additional Progress:

Additional progress was accomplished using data from MRL and SJL mice cross. Four studies were performed to identify Quantitative Trait Loci for: a) femur breaking strength, b) work to failure, c) periosteal circumference (PC) and d) Serum IGF Binding Protein-5 Levels in MRL/SJL mice. These studies were accomplished using 633 (MRL/MpJ X SJL/J) F2 mice, as reported in the last progress report (October, 2002 and Ref. 3) on wound healing.

a) Femur breaking strength and BMD phenotypes in MRL, SJL, F_1 and F_2 female mice: Femur breaking strength (FBS) and femur BMD were examined in 20 MRL, 20 SJL, 36 (MRL X SJL) F_1, and 633 (MRL X SJL)F_2 female mice at 7 weeks of

age. The broad-sense heritability was estimated to be 0.64 for BMD and 0.68 for FBS, similar to previous heritability estimates for mouse BMD (5). The high heritability provides a genetic foundation to search for quantitative trait loci that regulate FBS and BMD, and to distinguish concordant QTLs of two traits from unique QTLs for FBS. A total of 560 primer pairs (410 from the Mouse MapPairs Genome-wide Screening Set) were tested for polymorphism between the two parental strains of mice. One-hundred and fifty-eight markers were identified with distinguishable polymorphisms (28%), of which 119 were used for genotyping of the 633 (MRL X SJL)F_2 female mice. These markers covered all 20 chromosomes, with a spacing of ≤15 cM and an average spacing of 12 cM.

Interval mapping, followed by MQM mapping analysis, identified 6 QTLs for FBS (Table 10) and 9 QTLs for femur BMD (Table 11) that exhibited significant associations between the genotypic markers and phenotypic values (in this report, we proposed to standardize QTL names by using four components. For details, see Table 10). Of the 6 FBS QTLs, five MRL alleles enhance bone strength compared to SJL alleles, with the exception of Fbs8P15.7L4.3 QTL in which an SJL-derived allele contributes more to an increase in bone strength than the MRL allele. Two MRL- and two SJL-derived alleles (Fbs2P54.6L3.6 and Fbs9P47L3.1 for MRL, and Fbs8P15.7L4.3 and Fbs10P47L2.7 for SJL) have a dominant effect, respectively, and the last two loci have an additive effect (Fig. 5).

Loci Fbs1P104L4.7, Fbs17P6.6L8.4 and Fbs9P47L3.1 explained approximately 15% phenotypic variation and appear to be concordant with BMD QTLs, Bmd1P108.8L5.2, Bmd17P6.6L6 and Bmd9P46.5L3.6 (Table 11). An additional three QTLs explained 8% variation in FBS phenotype and seem to specifically influence FBS in this study. After adjustment with periosteal circumference, four out of six QTLs were still significantly associated with FBS and two of them became insignificant (Table 10). Taken together, 6 FBS and 9 BMD QTLs explained 23% and 34% of F_2 variance, respectively. Based on heritability estimate, genetic factors explained 64% phenotypic variation for BMD and 68% for FBS (6).

b) Genome-wide scan revealed five significant QTLs for work to failure: Six hundred and thirty three F_2 mice were genotyped for 119 markers. These markers covered all 20 chromosomes with a spacing of ≤15 cM and an average spacing of 12 cM. Because the distribution of WTF values in F_2 deviated from normal distribution, we performed Kruskal-Wallis analysis (nonparametric mapping) as well as MQM mapping (parametric mapping). As shown in Table 12, five significant QTLs influencing WTF were identified by Kruskal-Wallis analysis, of which two were unique to WTF, two were concordant with FBS QTLs, and only one was concordant with both FBS and BMD QTL. The sixth QTL, Wtf17P6.6L2.1, was below the threshold of $p<0.005$. However, we included this potential QTL in Table 12 in view of the fact that this locus was concordant with FBS and BMD QTLs, and thus could represent a biological QTL with a small effect on WTF. Taken together, six WTF QTLs explained 20.7% of F_2 variance (the percentage was estimated from separate models of each QTL). After adjustment of WTF by periosteal circumference, the five significant WTF QTLs remain significant (7).

c) QTL for Periosteal Circumference: To identify QTL for PC, genotypes from 633 MRL/SJL F2 mice using 137 informative markers that covered all 20 chromosomes with a spacing of ≤15 cM and an average spacing of 12 cM. Because the distribution of PC values in F_2 was normal, we performed interval-mapping analysis (parametric mapping), using unadjusted PC data and adjusted PC data by body weight or femur length. Table 7 shows 7 significant and 5 suggestive QTL for body weight and 11 significant and 1 suggestive QTL for unadjusted PC. While Table 8 shows 4 significant and 2 suggestive QTL for femur length, 6 QTL for PC adjusted by femur length (2 significant and 4 suggestive) and 9 QTL for PC adjusted by body weight (6 significant and 3 suggestive). Five QTL from chromosomes 1 (D1Mit33), 8 (D8Mit125), 15 (D15Mit62), 17 (D17Mit176) and X (DXMit208) were unique for PC, even after adjustment by femur length and body weight, indicating that they are not size QTL but true PC QTL. The PC results were published in 2003 in Journal of Bone (8).

d) QTL for IGFBP-5: In order to isolate QTL for IGFBP-5, as in PC studies above, we used 633 genotypes that were used in wound healing (reported in the last annual report, October 2002). The results of genome-wide scans are presented in Fig. 3. Whole genome scans with marker regression revealed highly significant peaks on Chrs 9, 10, and 11, of which Chrs 9 and 11 contain two QTL while Chr 10 contains one QTL. A suggestive peak was also found in Chr 1. Table 9 provides the list of markers for various QTL that show significant linkage with serum IGFBP-5 levels and the percent of F2 variance explained by individual QTL. Of the six QTL, chromosome 11 QTL (D11Mit36) exhibited the highest LOD score and contributed to 7.5% of the variation in serum IGFBP-5 levels seen in the MRL/SJL F2 mice. The six identified QTL explained 26% of variation in serum IGFBP-5 levels seen in the MRL/SJL F2 mice. These results were published in 2003, in the Endocrinology Journal (9).

4. Key Research Accomplishments

- Developed congenic mice on chromosome 9, covering 35.8 Mb that is ready for phenotype testing.
- Identified genes from the QTL on chromosomes 1 and 9 that have homology with genes previously linked to wound healing.
- Have completed making an in-house micro-array chip for Chromosome 1 and 9 QTL genes.
- Identified differentially expressed genes in chromosomes 1 and 9 during an inflammatory stage (4 hours after wounding) and repair stage (7 days after wounding.
- Identified CRBP1 gene located in chromosome 9 QTL contains SNPs that segregate with good healer (MRL) or poor healer (SJL) phenotype.
- Used MRL/SJL F2 data to study other phenotypes [periosteal circumference (PC), insulin growth factor binding protein 1(IGFBP-5), femur breaking strength and work to failure].

5. Reportable Outcomes

Manuscripts:

1. Masinde, GL, Wergedal, J, Davidson, H., Li, X, Mohan, S, Baylink, DJ (2003). Quantitative trait loci for periosteal circumference (PC): Identification of single loci and epistatic effects in F_2 MRL/SJL mice. *Bone*, 32:554-60.

2. Mohan, S., Masinde G., Li X. and Baylink, DJ. (2003). Mapping Quantitative Trait Loci that Influence Serum IGF Binding Protein-5 levels in F2 Mice (MRL/MPJ X SJL/J). *Endocrinology*,144:3491-6.

3. Li, X., Masinde, G., Gu, W., Wergedal, J., Mohan, S., Baylink, D.J. (2002). Genetic Dissection of Femur Breaking Strength in a large population (MRL-MpJ x SJL/J) of F2 Mice: Single QTL Effects, Epistasis, and Pleiotropy, Genomics, *Genomics* 79: 734-40

6. Conclusions

a) We have developed a congenic strain which contains part of the QTL region on chromosome 9. These congenic are going to be used for production of subcongenic mice to further narrow down the QTL.

b) We have used homology searches with ESTs from Celera data base on chromosomes 1 and 9 to identify those that have homology with genes known to play a role in wound healing and others that do not have a match.

c) We have identified several known genes and ESTs that are differentially expressed using data from in-house micro-array (genes from chromosomes 1 and 9). Because most of these known genes and ESTs are located in the QTL region, they are potential candidate genes.

d) We have identified sequence polymorphism in a gene within the QTL on chromosome 9 that may play a major role in wound healing. Cellular retinol binding protein I (CRBPI) has been implicated in wound healing (Omori *et al.* 1981).

e) We have collected extra data from the MRL-SJL cross for additional progress. We used samples from MRL/SJL F2 cross to identify QTL that regulate, femur breaking strength, femur work to failure Insulin growth factor 1 (IGFBP-5) levels and QTL that regulate Periosteal circumference (PC)

References:

1. Goss, R. J. (1992) The evolution of regeneration. Adaptive or inherent? *J. Theor. Biol.*, 159: 241-260.

2. Singer, A. J. and R. A. F. Clark. (1999) Cutaneous wound healing. *The New England J. Med.* 341: 738-746

3. Masinde G, Li X, Gu W, Heather Davidson, Mohan S and Baylink DJ (2001) Identification of wound healing/regeneration QTLs at multiple time points that

explain seventy percent of variance in (MRL/MpJ X SJL/J) F_2 population. *Genome Res.* 11: 2027-33.

4. Omori M, Muto Y, Nagao T (1981). Cellular retinoid-binding proteins in regenerating rat liver: demonstration of a novel cellular retinoid-binding protein. *J Lipid Res.* 22:899-904.

5. Benes H, Weinstein RS, Zheng W, Thaden JJ, Jilka RL, Manolagas SC, Shmookler Reis RJ (2000) Chromosomal mapping of osteopenia-associated quantitative trait loci using closely related mouse strains. *J Bone Miner Res* 15: 626-633.

6. Li, X., Masinde, G., Gu, W., Wergedal, J., Mohan, S., Baylink, D.J. (2002). Quantitative trait loci for femur breaking strength in a large (MRL-MpJ x SJL/J F2 population: a comparison to femur BMD QTLs. *Genomics* 79: 734-40

7. Li, X., Masinde, G., Gu, W., Wergedal, J., Hamilton-Ulland, M., Mohan, S., Baylink, DJ. (2001). Chromosomal regions harboring genes for the work to femur failure in mice. *Functional Intergrative Genomics*, 1:367-74.

8. Masinde, GL, Wergedal, J, Davidson, H, Li, X, Mohan, S, Baylink, DJ (2003). Quantitative trait loci for periosteal circumference (PC): Identification of single loci and epistatic effects in F_2 MRL/SJL mice. *Bone*, 32:554-60.

9. Mohan, S., Masinde G., Li X. and Baylink, DJ. (2003). Mapping Quantitative Trait Loci that Influence Serum IGF Binding Protein-5 levels in F2 Mice (MRL/MPJ X SJL/J). *Endocrinology*, 44:3491-6.

10. Martin, P. (1997) Wound healing-aiming for perfect skin regeneration. *Science* 276:75-81.

FIGURES AND TABLES FOR TECHNICAL OBJECTIVE 2

Table 1. List of Molecular Markers and their location in chromosome 9 that were used for genotyping of Congenic mice.

Marker	Size (bp)	Size (bp)	Approx. Position(Mb)	Approx. Position(cM)
	MRL	SJL		
D9Mit336	174	144	65.8	33.9
D9Mit355	111	127	98.8	49.2
D9Mit207	167.13	162.95	60.8	31.7
D9Mit208	109.32	88.12	62.5	36
D9Mit270	86.75	82.38	76.3	42
D9Mit343	130.23	113.35	80.8	43
D9Mit196	152.97	163.72	86.8	48
D9Mit111	143.53	165.57	87.5	48.1
D9Mit9	147.29	129.61	88.1	42.6
D9Mit308	128.16	136.59	91.3	49.2
D9Mit114	205.35	160.49	99.3	52
D9Mit182	127.75	121.11	101.6	53.6

a)

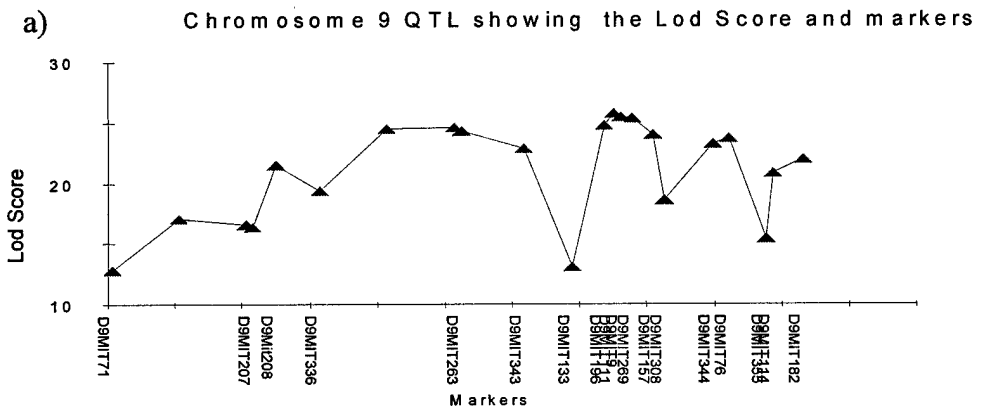

b) Chromosome 9 Congenics

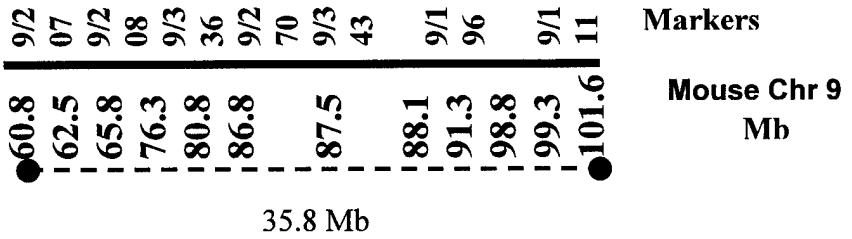

Fig. 1. a) QTL identified on chromosome 9 with a LOD score of over 24, covering the whole chromosome, b) Congenic Line of the Chromosome 9 QTL Region. The solid bar represents chromosome 9 from MRL within the congenic strain MR/SJL. Numbers on the topside of the solid line represent the names of D9mit microsatellite markers, while the numbers on the dotted line represent the Mb distance on mouse Chr 9. On the bottom side of the solid line is the dotted line representing the congenic strain for the QTL locus of wound healing on mouse chromosome 9.

Table 2. The genes that were retrieved from Celera database and blasted to identify those with homology to known wound healing genes. The first column is Gene bank ID and in parenthesis the Celera ID of the original sequence. In order to identify if these genes have previously shown to play a role in wound healing, we searched PubMed database to find out relevant publications on these genes that are related to wound healing. The relevant references that provide evidence for the role of chromosome 1 QTL genes are shown under the heading "wound healing". N/A means no relevant reference identified.

GeneBank ID	GenBank Description	Genomic Position	Wound Healing
NM_175031 (mCT135250)	Mus musculus RIKEN cDNA 1700112N14 gene (1700112N14Rik), mRNA	Chr.1 72.1Mb	N/A
NM_009909 (mCT115902)	Mus musculus interleukin 8 receptor, beta (Il8rb), mRNA.	Chr.1 71.8Mb	Gillitzer R, Goebeler M. (2001) PMID:11310836
NM_178241 (mCT153270)	Mus musculus CXC chemokine receptor 1-like (LOC227288), mRNA.	Chr.1 71.8Mb	Dhawan P, Richmond A. (2002) PMID: 12101257
XP_129773.2 (mCT115907)	Actin related protein 2/3 complex, subunit 2 [Mus musculus]	Chr.1 71.8Mb	Kovacs EM, et al. (2002) PMID: 11882288
NM_146110 (mCT115909)	Mus musculus angio-associated migratory protein (Aamp), mRNA.	Chr.1 71.8Mb	Beckner ME, et al. (2002) PMID: 11969303
NM_009526 (mCT135243)	Mus musculus wingless-related MMTV integration site 6 (Wnt6), mRNA.	Chr.1 72.3Mb	Itaranta P, et al. (2002) PMID: 8268652
NM_009518 (mCT135237)	Mus musculus wingless related MMTV integration site 10a (Wnt10a), mRNA.	Chr.1 72.3Mb	Loureiro JJ. (1999) PMID: 9889131
NM_009872 (mCT135241)	Mus musculus cyclin-dependent kinase 5, regulatory subunit 2 (p39) (Cdk5r2), mRNA.	Chr.1 72.4Mb	Jeong YG, et al. (2003) PMID: 12699769
NM_153111 (mCT135253)	Mus musculus Fev protein (Fev-pending), mRNA.	Chr.1 72.4Mb	Hendricks TJ, et al. (2003) PMID: 12546819
XP_286971.1 (mCT135249)	Hypothetical protein XP_286971 [Mus musculus]	Chr.1 72.5Mb	N/A
NM_010544 (mCT135244)	Mus musculus Indian hedgehog (Ihh), mRNA.	Chr.1 72.5Mb	Wijgerde M, et al. (2002) PMID: 12435628
XP_237311.1 (mCT115905)	Similar to RECS1 [Mus musculus] [Rattus norvegicus]	Chr.1 71.8Mb	N/A
NM_019999 (mCT115904)	Mus musculus brain protein 17 (Brp17), mRNA.	Chr.1 71.8Mb	Whetstone WD, et al. (2003) PMID: 14515352

NM_013612 (mCT115901)	Mus musculus solute carrier family 11 (proton-coupled divalent metal ion transporters), member 1 (Slc11a1), mRNA.	Chr.1 71.9Mb	Wyllie S, et al. (2002) PMID: 12429710
NM_153088 (mCT115908)	Mus musculus nuclear LIM interactor-interacting factor (Nliif-pending), mRNA.	Chr.1 71.9Mb	Satow R, et al.(2002) PMID: 12083771
NM_009509 (mCT115900)	Mus musculus villin (Vil), mRNA.	Chr.1 72Mb	Bement WM, et al.(1993) PMID: 8486737
XP_129889.1 (mCT135264)	Yolk sac permease-like molecule 1 [Mus musculus]	Chr.1 72.6Mb	Guimaraes MJ, et al.(1995) PMID: 7588067
NM_026846 (mCT135257)	Mus musculus RIKEN cDNA 1110060O18 gene (1110060O18Rik), mRNA.	Chr.1 72.7Mb	N/A
NM_023732 (Mct135259)	Mus musculus ATP-binding cassette, sub-family B (MDR/TAP), member 6 (Abcb6), mRNA.	Chr.1 72.7Mb	N/A
NM_026187 (mCT135239)	Mus musculus DNA segment, Chr 1, ERATO Doi 161, expressed (D1Ertd161e), mRNA.	Chr.1 72.7Mb	N/A
XP_129887.1 (mCT135262)	RIKEN cDNA 4833408P15 [Mus musculus]	Chr.1 72.7Mb	N/A
NM_007936 (mCT120686)	Mus musculus Eph receptor A4 (Epha4), mRNA.	Chr.1 74.9Mb	Greferath U, et al. (2002) PMID: 12617813
XP_237290.1 (mCT115903)	Similar to rcd1 (required for cell differentiation) homolog 1; FL10; rcd1 (required for cell differentiation) homolog 1 (S.pombe) [Mus musculus] [Rattus norvegicus]	Chr.1 72.1Mb	Hiroi N, et al. (2002) PMID: 12356739
NM_148937 (mCT135254)	Mus musculus phospholipase C, delta 4 (Plcd4), mRNA.	Chr.1 72.1Mb	N/A
NM_025330 (mCT133876)	Mus musculus RIKEN cDNA 0610039E24 gene (0610039E24Rik), mRNA.	No Match	N/A
NM_025784 (mCT135265)	Mus musculus BCS1-like (yeast) (Bcs1l), mRNA.	Chr.1 72Mb	N/A
NM_021313 (mCT135245)	Mus musculus ring finger protein 25 (Rnf25), mRNA.	Chr.1 72.1Mb	N/A
NM_011494 (Mct135236)	Mus musculus serine/threonine kinase 16 (Stk16), mRNA.	Chr.1 72.7Mb	Ohta S, et al. (2000) PMID: 10947953
NM_009447 (Mct135231)	Mus musculus tubulin, alpha 4 (Tuba4), mRNA.	Chr.1 72.7Mb	N/A

NM_178055 (mCT135232)	Mus musculus DnaJ (Hsp40) homolog, subfamily B, member 10 (Dnajb10), mRNA.	Chr.1 72.7Mb	N/A
NM_008985 (mCT135240)	Mus musculus protein tyrosine phosphatase, receptor type, N (Ptprn), mRNA.	Chr.1 72.7Mb	Magistrelli G, et al. (1995) PMID: 8526904
NM_133708 (mCT135251)	Mus musculus GDP-mannose pyrophosphorylase A (Gmppa-pending), mRNA.	Chr.1 72.9Mb	N/A
NM_008781 (mCT120070)	Mus musculus paired box gene 3 (Pax3), mRNA.	Chr.1 75.6Mb	Mansouri A, et al. (1999) PMID: 10197584
NM_011811 (mCT120072)	Mus musculus phenylalanine-tRNA synthetase-like (Farsl), mRNA.	Chr.1 75.9Mb	Zhou X, et al. (1999) PMID: 10375616
AAH31529.1 (mCT119559)	Fatty acid Coenzyme A ligase, long chain 3 [Mus musculus]	Chr.1 76.1Mb	N/A
XP_129771.2 (mCT135263)	Expressed sequence AI451681 [Mus musculus]	Chr.1 72.2Mb	N/A
NM_024264 (mCT135233)	Mus musculus cytochrome P450, family 27, subfamily a, polypeptide 1 (Cyp27a1), mRNA.	Chr.1 72.3Mb	N/A
NM_153744 (mCT135255)	Mus musculus protein kinase, AMP-activated, gamma 3 non-catatlytic subunit (Prkag3), mRNA.	Chr.1 72.3Mb	N/A
NM_027886 (mCT135258)	Mus musculus RIKEN cDNA 1200014D22 gene (1200014D22Rik), mRNA.	Chr.1 73Mb	N/A
NM_009208 (mCT135242)	Mus musculus solute carrier family 4 (anion exchanger), member 3 (Slc4a3), mRNA.	Chr.1 73Mb	N/A
AAD22981.1 (mCT120597)	AC007204_1 BC273239_1 [Homo sapiens]	Chr.1 73.1Mb	N/A
NM_007734 (mCT119312)	Mus musculus procollagen, type IV, alpha 3 (Col4a3), mRNA.	Chr.1 79.7Mb	N/A
NM_029409 (mCT119317)	Mus musculus RIKEN cDNA 5230400G24 gene (5230400G24Rik), mRNA.	Chr.1 79.8Mb	N/A
NM_025453 (mCT10637)	Mus musculus RIKEN cDNA 1810018L02 gene (1810018L02Rik), mRNA.	Chr.1 79.8Mb	N/A
NM_030006 (mCT10624)	Mus musculus RIKEN cDNA A030005L19 gene (A030005L19Rik), mRNA.	Chr.1 80Mb	N/A
NM_011294 (mCT172847)	Mus musculus RNA polymerase II transcriptional coactivator (Rpo2tc1), mRNA.	No Match	N/A
NM_020513 (mCT15123)	Mus musculus gene for odorant receptor MOR10 (Or10), mRNA.	No Match	N/A

NM_009366 (mCT15543)	Mus musculus transforming growth factor beta 1 induced transcript 4 (Tgfb1i4), mRNA.	No Match	Hurley MM, et al. (1994) PMID: 8132679
NM_010703 (mCT174978)	Mus musculus lymphoid enhancer binding factor 1 (Lef1), mRNA.	No Match	Held W, et al. (2003) PMID: 12731066
NM_007553 (mCT9687)	Mus musculus bone morphogenetic protein 2 (Bmp2), mRNA.	No Match No Match	Valcourt U, et al. (2003) PMID: 12804760
NM_012025 (mCT172009)	Mus musculus Rac GTPase-activating protein 1 (Racgap1), mRNA.	No Match	Kitamura T, et al. (2001) PMID: 11942621
NM_021325 (mCT130006)	Mus musculus antigen identified by monoclonal antibody MRC OX-2 receptor (Mox2r), mRNA.	No Match No Match	Terao A, et al. (2002) PMID: 12399012
NM_010113 (mCT171305)	Mus musculus epidermal growth factor (Egf), mRNA.	No Match	Ramljak D, et al. (2003) PMID: 12837294
NM_010197 (mCT181043)	Mus musculus fibroblast growth factor 1 (Fgf1), mRNA.	No Match	Hashimoto M, et al. (2002) PMID: 12095987
NM_007913 (mCT125153)	Mus musculus early growth response 1 (Egr1), mRNA.	No Match	Jones N, Agani FH. (2003) PMID: 12811826
NM_011577 (mCT6637)	Mus musculus transforming growth factor, beta 1 (Tgfb1), mRNA.	No Match	Valcourt U, et al. (2003) PMID: 12804760
NM_009368 (mCT170443)	Mus musculus transforming growth factor, beta 3 (Tgfb3), mRNA.	No Match	Hosokawa R, et al. (2003) PMID: 12821719
NM_031199 (mCT131835)	Mus musculus transforming growth factor alpha (Tgfa), mRNA.	No Match	Isono M, et al. (2003) PMID: 12866207
NM_010217 (mCT5576)	Mus musculus connective tissue growth factor (Ctgf), mRNA.	No Match	Ivkovic S, et al. (2003) PMID: 12736220
NM_010157 (mCT10556)	Mus musculus estrogen receptor 2 (beta) (Esr2), mRNA.	No Match	N/A
NM_013693 (mCT168333)	Mus musculus tumor necrosis factor (Tnf), mRNA.	No Match	Cai D, et al. (2003) PMID: 12730063
NM_007866 (mCT172917)	Mus musculus delta-like 3 (Drosophila) (Dll3), transcript variant 1, mRNA.	No Match	Dunwoodie, S, et al. (1997) PMID: 9272948

Table 3. Genes that were printed on the microarray slides and used for differential expression.

Accession #	Gene name	Chr.(Mb)
celera mCT115902	interleukin-8 receptor type B (Il8rb) gene	1 (71.8)
celera mCT153270	CXC chemokine receptor 1-like (LOC227288)	1 (71.8)
celera mCT115907	actin related protein 2/3 complex, subunit 2	1 (71.8)
celera mCT115909	angio-associated migratory protein	1 (71.8)
Celera mCT115910		1 (N/A)
Celera mCT115905		1 (71.8)
Celera mCT115904		1 (71.8)
Celera mCT115901		1 (71.9)
Celera mCT115908		1 (71.9)
Celera mCT115900		1 (72.0)
Celera mCT115906		1 (N/A)
Celera mCT115903		1 (72.0)
Celera mCT153426		1 (N/A)
Celera mCT135254		1 (72.1)
Celera mCG133876		1 (38.0)
Celera mCT135265		1 (72.1)
Celera mCT135245		1 (72.1)
Celera mCT135250		1 (72.1)
Celera mCT153427		1 (N/A)
Celera mCT135263		1 (72.2)
Celera mCT135233		1 (72.3)
Celera mCT135255		1 (72.3)
Celera mCT116953		1 (N/A)
Celera mCT50087.1		1 (78.1)
CeleramCT50632.1		1
Celera mCT20284.1		1 (79.3)
Celera mCT119312		1 (79.7)
Celera mCT143551		1 (N/A)
Celera mCT119317		1 (79.8)
Celera mCT10637		1 (79.8)
Celera mCT10624		1 (N/A)
AU022396	EST	(N/A)
TC162113	Rhoip2-pending	13 (N/A)
TC159097	MRC OX-2	16 (N/A)
AA497620	small proline rich protein 2A	3(N/A)
U81541	estrogen receptor beta	12(N/A)
W82549	ESTs similar to STEFIN 3	16(N/A)
AA230451	calgranulin A	3(N/A)
AA073604	Procollagen I	11(N/A)
M14237	MHCII H2-IE-beta cell surface glycoprotein, exon beta-2	17(N/A)

AJ231200	IgVk cu2	6(N/A)
XM_181331	myotubularin related protein 3	11(N/A)
AF068865	delta-like 3 alternative splice products	7(N/A)
CELERA mCT152584		9(N/A)
CELERA mCT152431		9(N/A)
Celera mCT12262.1		9(81.7)
Celera mCT153088		9(N/A)
Celera mCT153089		9(N/A)
Celera mCT152586		9(N/A)
Celera mCT51350.1		9(82.3)
Celera mCT12403.1		9(82.4)
Celera mCT12402.1		9(82.4)
Celera mCT12404		9(82.5)
Celera mCT12401.1		9(82.6)
Celera mCT12916.1		9(82.5)
Celera mCT152433		9(N/A)
Celera mCT2842		9(85.5)
Celera mCT143762		9(N/A)
Celera mCT115341		9(N/A)
Celera mCT149183		9(N/A)
Celera mCT149184		9(N/A)
Celera mCT150516		9(86.3)
Celera mCT150518		9(86.3)
Celera mCT150484		9(N/A)
Celera mCT6967		9(89.0)
Celera mCT150545		9(89.1)
Celera mCT14800.1		9(N/A)
Celera mCT14804.1		9(N/A)
Celera mCT150547		9(89.6)
Celera mCT150548		9(N/A)
Celera mCT150491		9(N/A)
Celera mCT150551		9(91.1)
Celera mCT150552		9(91.2)
Celera mCT19626.1		9(N/A)
Celera mCT10470.1		9(92.0)
Celera mCT150556		9(N/A)
Celera mCT10464.1		9(N/A)
Celera mCT150557		9(N/A)
Celera mCT10469.1		9(N/A)
Celera mCT57040.1		9(N/A)
Celera mCT150471		9(N/A)
Celera mCT150558		9(N/A)
Celera mCT67975		9(92.2)
Celera mCT57359.1		9(72.3)
Celera mCT10467.1		9(72.3)
Celera mCT135243		1(N/A)
Celera mCT135237		1(72.3)

Celera mCT135241		1(72.3)
Celera mCT135253		1(72.4)
Celera mCT135249		1(72.5)
Celera mCT135244		1(72.5)
Celera mCT135264		1(72.6)
Celera mCT135246		1(N/A)
Celera mCT135257		1(72.7)
Celera mCT135259		1(72.7)
Celera mCT135239		1(72.7)
Celera mCT135262		1(72.7)
Celera mCT135236		1(72.7)
Celera mCT135231		1(72.7)
Celera mCT135232		1(72.7)
Celera mCT135240		1(72.7)
Celera mCT135251		1(72.9)
Celera mCT135247		1(N/A)
Celera mCT135258		1(73.0)
Celera mCT135242		1(73.0)
Celera mCT120597		1(73.1)
Celera mCT153241		1(N/A)
Celera mCT153429		1(N/A)
Celera mCT153434		1(N/A)
NM_011294	RNA polymerase II transcriptional coactivator	15
XM_282562	odorant receptor MOR10 (Or10)	14
L36024	heparin-binding EGF-like growth factor	18
NM_009366	transforming growth factor beta 1 induced transcript 4	14
M79301	cell division cycle protein, partial 3' UTR	
NM_010703	lymphoid enhancer binding factor 1	3
D83213	activin beta A subunit, promoter	
NM_010113	epidermal growth factor	3
NM_010197	Fibroblast growth factor 1	18
NM_007913	early growth response 1	18
AF332140	c-fos (Fos) gene, 5' flanking and promoter regions	12
D84196	Tumor necrosis factor alpha, exon 4	17
NM_011577	transforming growth factor, beta 1	7
NM_009368	transforming growth factor, beta 3	12
NM_031199	transforming growth factor alpha	6
NM_010217	connective tissue growth factor	10
X01450	interleukin 1	2
Celera mCT57761.1		9(86.3)
Celera mCT6964.1		9(86.7)
Celera mCT6960.1		9(86.7)
Celera mCT123471		9(N/A)
Celera mCT6969.1		9(86.8)
Celera mCT117339		9(N/A)
Celera mCT150524		9(N/A)
Celera mCT150527		9(87.4)

Celera mCT150529		9(N/A)
Celera 150530		9
Celera mCT3059		9(87.7)
Celera mCT68342.1		9(88.0)
Celera mCT3060.1		9
Celera mCT150534		9(N/A)
Celera mCT150535		9(N/A)
Celera mCT150488		9(88.3)
Celera mCT150539		9(N/A)
Celera mCT150540		9(N/A)
Celera mCT14797		9(88.8)
Celera mCT14803.1		9(88.9)
Celera mCT150541		9(N/A)
Celera mCT150542		9(N/A)
Celera mCT150543		9(N/A)
Celera mCT150544		9(N/A)
Celera mCT10465		9(92.3)
Celera mCT10461.1		9(92.3)
Celera mCT10460.1		9(92.4)
Celera mCT118461		9(92.7)
Celera mCT118463		9(92.8)
Celera mCT118229		9(92.8)
Celera mCT150493		9(N/A)
Celera mCT20299.1		9(92.9)
Celera mCT20286.1		9(93.0)
Celera mCT20290		9(93.1)
Celera mCT20289.1		9(93.1)
Celera mCT20288		9(93.2)
Celera mCT150494		9(N/A)
Celera mCT150472		9(93.2)
Celera mCT150457		9(93.4)
Celera mCT20285.1		9(93.4)
Celera mCT20295		9(93.5)
Celera mCT20291		9(93.5)
Celera mCT153437		1(N/A)
Celera mCT153437		1(N/A)
Celera mCT153439		1(N/A)
Celera mCT153315		1(N/A)
Celera mCT120687		1(N/A)
Celera mCT153273		1(N/A)
Celera mCT120686		1(74.9)
Celera mCT153441		1(N/A)
Celera mCT153442		1(N/A)
Celera mCT153444		1(N/A)
Celera mCT153445		1(N/A)
Celera mCT153317		1(N/A)
Celera mCT120070		1(75.6)

Celera mCT153318		1(N/A)
Celera mCT120072		1(75.9)
Celera mCT153447		1(76.1)
Celera mCT119559		1(76.1)
Celera mCT20320.1		1(76.8)
Celera mCT20313.1		1(76.8)
Celera mCT66207.1		1(N/A)
Celera mCT20315.1		1(77.0)
Celera mCT20311.1		1(77.3)
NM_007553	bone morphogenetic protein 2	2(131.7)
NM_012025	Rac GTPase-activating protein 1	15(98.8)
Celera mCT20292.1		9(93.5)
Celera mCT63996.1		9(N/A)
Celera mCT150569		9
Celera mCT118227		9(93.6)
ARNT 2 F2:590	D63644	7
Celera mCT14765		9(93.7)
Celera mCT49949.1		9(93.8)
Celera mCT14764		9(94.0)
Celera mCT9858.1		9(94.8)
Celera mCT9856		9(94.9)
Celera mCT150574		9(95.1)
Celera mCT9852.1		9(95.1)
Celera mCT9851		9(95.1)
Celera mCT150576		9(N/A)
D63644	ARNT 2 F2:392	7
D63644	ARNT 2 F2:25	7
D63644	ARNT 2 F2:58	7
D63644	ARNT 2 F2:70	7
D63644	ARNT 2 F2:89	7
D63644	ARNT 2 F2:95	7
D63644	ARNT 2 F2:123	7
D63644	ARNT 2 F2:180	7
D63644	ARNT 2 F2:225	7
D63644	ARNT 2 F2:268	7
D63644	ARNT 2 F2:273	7
D63644	ARNT 2 F2:299	7
D63644	ARNT 2 F2:319	7
D63644	ARNT 2 F2:321	7
D63644	ARNT 2 F2:332	7
D63644	ARNT 2 F2:333	7
D63644	ARNT 2 F2:373	7
D63644	ARNT 2 F2:377	7

Table 4. Differentially expressed genes in MRL versus SJL four hours after ear punch.

ACC # (CELERA/NCBI)	Ratio	Gene Name
Celera mCT12402.1	15.91	
NM_010217	7.73	connective tissue growth factor
XM_282562	6.25	odorant receptor MOR10 (Or10)
X01450	5.93	interleukin 1
U81541	5.68	estrogen receptor beta
Celera mCT123471	5.45	
NM_011577	5.15	transforming growth factor, beta 1
Celera mCT12404	4.89	
Celera mCT115903	4.62	
Celera mCT68342.1	4.57	
Celera mCT14803.1	4.55	
ARNT 2 F2:333	4.50	D63644-4
Celera mCT118229	4.19	
Celera mCT20288	4.14	
L36024	4.06	heparin-binding EGF-like growth factor
Celera mCT135265	3.99	
Celera mCT152586	3.96	
Celera mCT12402.1	3.92	
Celera mCT115904	3.80	
Celera mCT116953	3.78	
Celera mCT150491	3.72	
U81541	3.71	estrogen receptor beta
Celera mCT120597	3.69	
XM_181331	3.60	myotubularin related protein 3
ARNT 2 F2:268	3.53	D63644-4
NM_010197	3.49	Fibroblast growth factor 1
NM_031199	3.44	transforming growth factor alpha
AF068865	3.42	delta-like 3 alternative splice products
ARNT 2 F2:180	3.42	D63644-1
U81541	3.34	estrogen receptor beta
Celera mCT135265	3.29	
TC162113	3.21	Rhoip2-pending
Celera mCT118463	3.14	
NM_010113	3.10	epidermal growth factor
ARNT 2 F2:373	3.05	D63644-3
Celera mCT150494-3	3.04	
Celera mCT135236-5	3.01	
Celera mCT10461.1	2.99	
Celera mCT150472	2.91	
Celera mCT123471	2.89	

NM_031199-1	2.82	transforming growth factor alpha
XM_282562	2.78	odorant receptor MOR10 (Or10)
ARNT 2 F2:268-1	2.78	D63644-1
AJ231200-3	2.76	IgVk cu2
CELERA mCT152584-5	2.74	
Ch.1 #104-1	2.71	
Celera mCT118229-3	2.71	
NM_011577-3	2.71	transforming growth factor, beta 1
Celera mCT20288	2.70	
Celera mCT10460.1	2.65	
NM_009366	2.63	transforming growth factor beta 1 induced transcript 4
Celera mCT12401.1	2.63	
Celera mCT119312	2.56	
AA073604	2.55	Procollagen I
Celera mCT115904	2.55	
Celera mCT118227	2.54	
X01450	2.54	interleukin 1
Celera mCT12401.1	2.53	
Celera mCT143551	2.53	
NM_010113	2.51	epidermal growth factor
Celera mCT10465	2.51	
Celera mCT9856	2.48	
Celera mCT10465	2.46	
Celera mCT150544	2.43	
Celera mCT153089	2.41	
Celera mCT150545	2.39	
Celera mCT19626.1	2.36	
Celera mCT119312	2.36	
M79301	2.30	cell division cycle protein, partial 3' UTR
Celera mCG133876	2.27	
Celera mCT119312	2.24	
NM_011577	2.24	transforming growth factor, beta 1
Celera mCT135250	2.22	
Celera mCT20290	2.20	
AA073604	2.19	Procollagen I
AJ231200-5	2.17	IgVk cu2
TC162113	2.15	Rhoip2-pending
Celera mCT150527	2.15	
AF068865	2.14	delta-like 3 alternative splice products
NM_031199	2.07	transforming growth factor alpha
Celera mCT118227	2.07	
Celera mCT10470.1	2.06	
Celera mCT135250	2.06	
Celera mCT57040.1	2.05	
ARNT 2 F2:95	2.01	Arylhydrocarbon nuclear translocator 2
Celera mCT9856	2.01	

Celera mCT153273	2.01	
2 FOLD DOWN	**Ratio**	**Gene Name**
NM_007913	-6.54	early growth response 1
Celera mCT135240	-6.50	
Celera mCT150524	-6.37	
Celera mCT135253	-6.37	
Celera mCT153444	-6.29	
Celera mCT135253	-6.20	
Celera mCT119317	-5.93	
Celera mCT150524	-5.90	
Celera mCT119559	-5.76	
Celera mCT153444	-5.26	
Celera mCT115901	-5.24	
Celera mCT153444	-5.09	
Celera mCT115341	-5.08	
Celera mCT135257	-4.87	
Celera mCT153434	-4.85	
Celera mCT135243	-4.64	
Celera mCT153444	-4.51	
Celera mCT150535	-4.45	
Celera mCT150524	-4.37	
Celera mCT135253	-4.35	
Celera mCT63996.1	-4.22	
Celera mCT150524	-4.13	
Celera mCT119317	-4.04	
Celera mCT153445	-4.03	
Celera mCT119317	-3.96	
Celera mCT150524	-3.88	
Celera mCT153434	-3.81	
Celera mCT135253	-3.80	
D83213	-3.80	activin beta A subunit, promoter
Celera mCT135253	-3.78	
Celera mCT135249	-3.62	
Celera mCT135247	-3.60	
Celera mCT119317	-3.59	
Celera mCT135263	-3.54	
Celera mCT150576	-3.54	
Celera mCT153434	-3.51	
Celera mCT153445	-3.49	
Celera mCT120687	-3.46	
AU022396	-3.41	EST
Celera mCT135244	-3.36	
Celera mCT150541	-3.35	
Celera mCT153445	-3.32	
Celera mCT135231	-3.29	
Celera mCT153427	-3.28	

Celera mCT135241	-3.28	
Celera mCT10624	-3.28	
Celera mCT143762	-3.25	
Celera mCT119317	-3.19	
Celera mCT150535	-3.14	
Celera mCT120687	-3.10	
celera mCT115902	-3.09	interleukin-8 receptor type B (Il8rb) gene
Celera mCT135254	-3.08	
Celera mCT135254	-3.06	
AU022396	-3.05	EST
celera mCT115909	-3.03	angio-associated migratory protein
Celera mCT135247	-3.01	
Celera mCT135257	-3.00	
AU022396	-3.00	EST
CELERA mCT152431	-2.99	
Celera mCT150524	-2.98	
Celera mCT153089	-2.92	
D84196	-2.90	Tumor necrosis factor alpha, exon 4
Celera mCT143762	-2.89	
Celera mCT14765	-2.88	
CELERA mCT152431	-2.86	
Celera mCT153434	-2.83	
Celera mCT10624	-2.82	
Celera mCT150534	-2.74	
Celera mCT150534	-2.74	
Celera mCT135257	-2.70	
Celera mCT115341	-2.68	
Celera mCT153434	-2.67	
Celera mCT153445	-2.66	
Celera mCT150539	-2.64	
Celera mCT115901	-2.62	
Celera mCT153315	-2.62	
Celera mCT153445	-2.56	
Celera mCT150576	-2.55	
Celera mCT63996.1	-2.54	
Celera mCT119317	-2.52	
Celera mCT135253	-2.49	
celera mCT115910	-2.48	
Celera mCT115901	-2.47	
Celera mCT153427	-2.45	
Celera mCT143762	-2.44	
Celera mCT14797	-2.43	
Celera mCT135240	-2.42	
Celera mCT135246	-2.42	
Celera mCT153089	-2.35	
NM_010113	-2.33	epidermal growth factor
Celera mCT115908	-2.33	

Celera mCT150551	-2.31	
Celera mCT150574	-2.30	
Celera mCT63996.1	-2.28	
Celera mCT14803.1	-2.25	
Celera mCT135247	-2.24	
Celera mCT150576	-2.21	
AU022396	-2.16	EST
ARNT 2 F2:225	-2.15	Arylhydrocarbon nuclear translocator 2
Celera mCT9858.1	-2.12	
Celera mCG133876	-2.11	
NM_010197	-2.10	Fibroblast growth factor 1
Celera mCT150541	-2.09	
CELERA mCT152431	-2.08	
Celera mCT20313.1	-2.04	
Celera mCT19626.1	-2.02	

Table 5. Differentially expressed genes in MRL versus SJL at day 7 after ear punch

ACC # (CELERA/NCBI)	RATIO	GENE NAME
2FOLD UP		
AA230451	6.30	calgranulin A
NM_010217	3.87	connective tissue growth factor
Celera Mct143551	3.81	
Celera mCT14804	3.21	
NM_010113	3.17	epidermal growth factor
Celera mCT123471	2.88	
L36024	2.57	heparin-binding EGF-like growth factor
Celera mCT119312	2.40	
Celera mCT149183	2.17	
Celera mCT20286	2.13	
TC162113	2.11	Rhoip2-pending
Celera mCT153273	2.00	
2FLDWN		
Celera mCT153447-2	-24.33	
Celera mCT150524-5	-12.42	
ARNT 2 F2:89-3	-8.82	Arylhydrocarbon nuclear translocator 2
Celera mCT119559-5	-4.32	
Celera mCT115901	-4.10	
ARNT 2 F2:273-3	-3.10	Arylhydrocarbon nuclear translocator 2
Celera mCT150545	-3.08	
Celera mCT14804.1	-3.00	
Celera Mct20288	-2.60	
Celera mCT115900	-2.50	
Celera mCT10464.1	-2.42	
Celera mCT120687	-2.20	

Celera mCT135246	-2.16	
Celera mCT150548	-2.03	

Fig. 2.

Cellular Retinol binding protein 1 (CRBP1F) SNP (Chr 9)

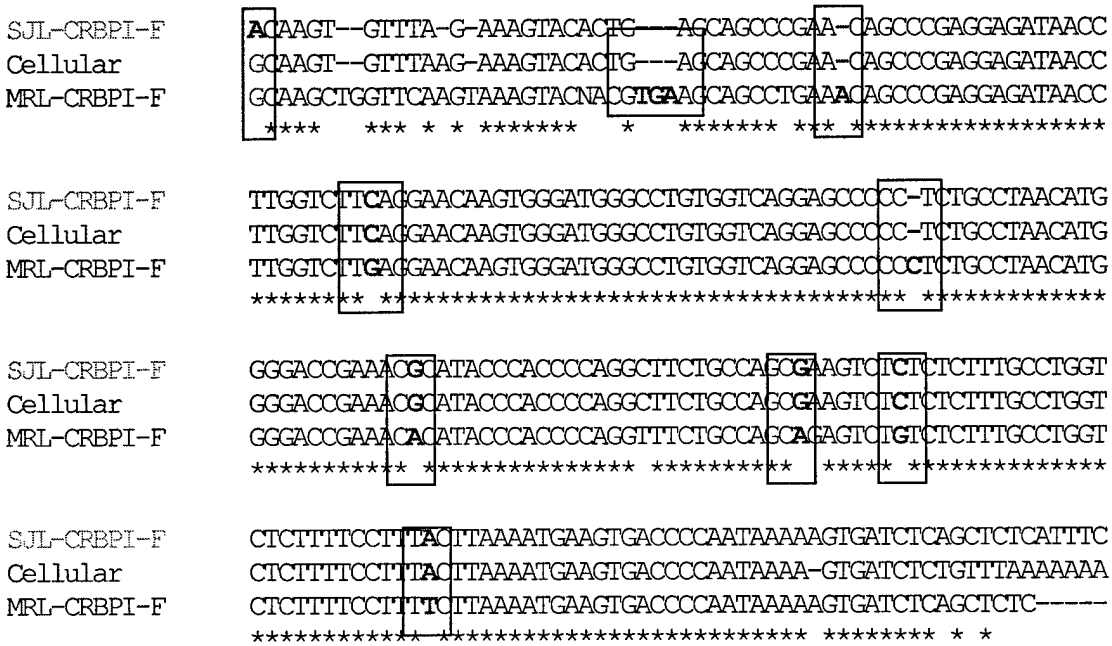

Table 6. CRBP1 3' UTR SNPS (Roche database)

Mouse strain	SNP Type	Healing Rate (Li, *et al*, 2001)
AJ	G	Poor
AKR	G	V. poor healer
C3H/Hej	G	Poor healer
BALB/CbyJ	G	V. poor healer
C57Bl/6J	**G**	**Poor**
BIO.D2.H2/0Suj	G	Poor
MRL/MpJ	**A**	**V. good healer**
DBA/2J	G	Good healer
129/svj	G	Poor healer
NZW/LaC	A	Good healer
SJL/J	**G**	**V. poor healer**

Table 7. Significant and suggestive QTL for body weight and unadjusted PC

		Body Weight		PC	
Marker	Distance (cM)	LOD Score	% explained	LOD score	% explained
D1Mit44	50.3	5.7	4.0	6.8	4.9
D2Mit62	54.6	8.6	6.0	6.8	4.7
D2Mit263	78.7	7.1	5.7	5.4	4.4
D11Mit36	43.7	3.3	2.6	3.6	2.6
D6Mit123	17.5	4.0	3.8	4.9	4.0
D6Mit291	54.2	3.7	3.0	5.8	4.6
D9Mit90	7.7	6.2	5.4	3.8	3.7
D9Mit263	42.0	3.3	2.3	2.8	2.0
D14Mit194	52.5	2.9	2.5	4.1	3.2
D13Mit207	2.2	4.2	3.7	None	None
D17Mit185	35.0	2.7	2.3	None	None
D8Mit125	15.7	None	None	None	None
D1Mit33	82.0	None	None	4.8	3.3
D15Mit62	33.4	None	None	6.7	5.7
D17Mit176	17.0	None	None	4.6	4.6
DXMit208	18.6	None	None	None	None
Total			41.3		47.7

Table 8. Significant and suggestive QTL for Femur Length, adjusted PC with body weight, and adjusted PC with Femur Length.

Marker	Distance (cM)	Femur Length		Adjusted PC with Femur Length[1]		Adjusted PC with Body Weight[1]	
		LOD Score	% explained	LOD score	% explained	LOD score	% explained
D1Mit44	50.3	3.3	2.8	None	None	3.4	2.3
D2Mit32	15.3	5.4	4.7	None	None	5.8	4.2
D2Mit304	59.0	4.9	4.0	None	None	4.2	3.6
D3Mit213	37.2	3.9	3.9	None	None	None	None
D5Mit302	26.2	5.4	5.6	None	None	None	None
D17Mit175	6.6	2.9	4.0	None	None	None	None
D16Mit139	33.9	None	None	3.0	3.9	None	None
D11Mit36	43.7	None	None	3.4	3.2	11.9	9.7
D8Mit125	15.7	None	None	None	None	2.7	2.1
D1Mit33	82.0	None	None	7.7	6.4	5.3	3.9
D15Mit62	33.4	None	None	2.9	3.5	6.2	5.3
D17Mit176	17.0	None	None	2.6	3.4	4.1	4.4
DXMit208	18.6	None	None	5.1	13.1	3.1	3.1
Total			21.0		33.5		38.6

1. The formula used for adjustment of PC for femur length is 3.4889 + .05719 * Femur Length or Body Weigh

Table 9. Significant and suggestive QTL for IGFBP-5 in MRL/SJL F2 mice.

QTL	Marker	Distance (cM)	LOD Score	% explained
BMD-1	**D1Mit33**	**82**	**2.8**	**2.0**
BMD-2	D1mit362	110.4	2.9	2.4
BMD-3	D2Mit62	54.6	4.9	3.5
BMD-4	D2Mit263	78.7	6.6	5.6
BMD-5	D9Mit90	7.7	4.4	4.0
BMD-6	**D11Mit36**	**43.7**	**6.8**	**5.2**
BMD-7	D14Mit194	52.5	4.5	3.9
BMD-8	D15Mit179	7.7	2.7	2.0
Total			**28.6**	

Shared QTL between BMD and IGFBP-5 are shown in bold.

Fig 3. Interval maps for chromosomes 1, 9, 10, and 11 shown to carry QTLs for serum IGFBP-5. Statistical analyses are presented as LOD scores calculated for molecular markers beginning with the centromeric end of each chromosome on the left extending towards telomeric end.

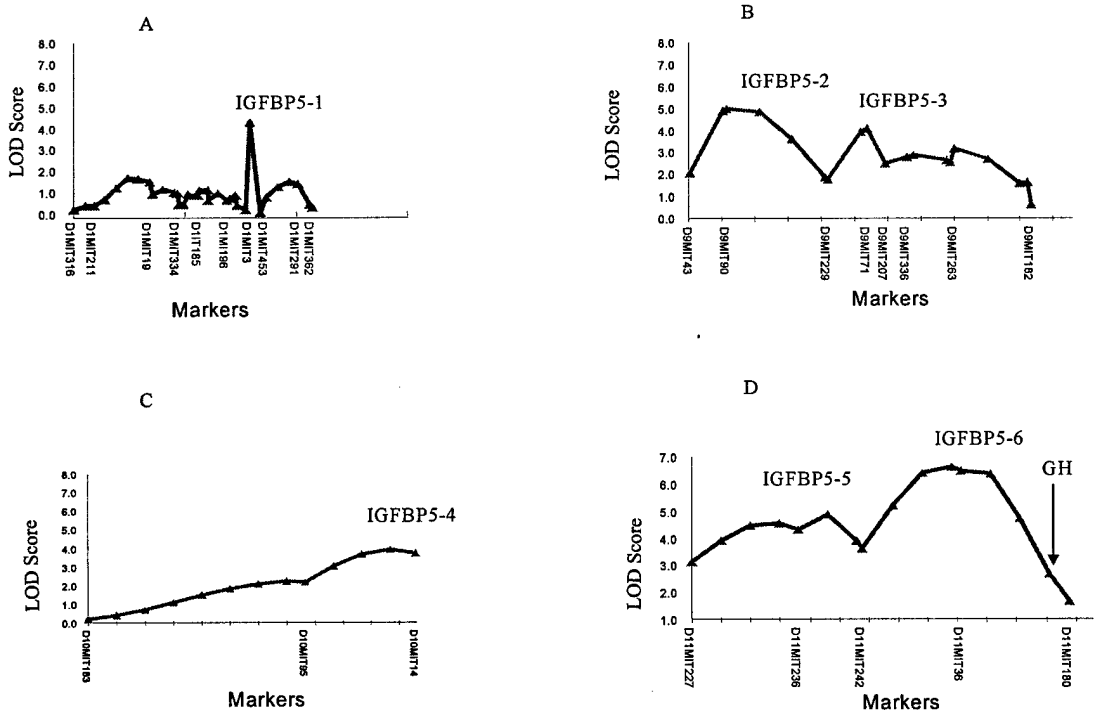

Table 10. Summary of significant QTLs for femur breaking strength[#]

QTL name[*]	Marker close to the peak of QTL (cM)	% Expl	1 LOD interval (cM)	Notes
Fbs17P6.6L8.4	D17Mit175 (6.6)	8.5	6.6	Shared with BMD QTL in this study
Fbs1P104L4.7	D1Mit291 (103.8)	3.4	10.8	Shared with BMD QTL in this study
Fbs8P15.7L4.3	D8Mit125 (15.7)	3.3	11.3	Unique to FBS
Fbs9P47L3.1	D9Mit270 (41.5)	2.9	21.9	Shared with BMD QTL in this study
Fbs2P54.6L3.6	D2Mit62 (54.6)	2.6	10.9	Unique to FBS
Fbs10P47L2.7	D10Mit95 (50.3)	2	8	Unique to FBS
Same QTLs after adjustment with periosteal circumference				
Fbs17P6.6L8.3	D17Mit175 (6.6)	8.5	6.0	
Fbs1P104L6.0	D1Mit291 (103.8)	4.5	10.2	
Fbs8P15.7L3.5	D8Mit125 (15.7)	2.4	12	
Fbs9P47L2.7	D9Mit270 (41.5)	2.1	20	
Fbs2P54.6L1.1	D2Mit62 (54.6)	0.6	32	
Fbs10P47L2.3	D10Mit95 (50.3)	1.6	8	

[*]With the increasing number of QTL mapping papers, QTL name needs to be standardized. In this report, we proposed to use four components to name a QTL: 1) abbreviation of QTL phenotype, 2) chromosome number on which the QTL is located, 3) chromosome position on which the peak of the QTL is corresponding to, 4) LOD score of the QTL. For example, for the QTL "Fbs1P104L5.2", the "Fbs" represents the first component of the name and stands for "femur breaking strength", followed by "1", indicating that this QTL is located on chromosome 1. The "P104" shows that the peak of this QTL corresponds to the position of 104 cM. The "L5.2" indicates that this QTL has a LOD score of 5.2. [#]The LOD threshold is 3.5 for significant linkage and 2.7 for suggestive linkage (equivalent to significant level of 1% and 5%, respectively, for a standard chromosome length of 100 cM).

Table 11. Summary of significant QTLs for femur BMD[*]

QTL name	Marker close to the peak of QTL (cM)	% Expl	1 LOD interval (cM)	Notes
Bmd17P6.6L6	D17Mit175 (6.6)	7.4	6.6	Unique BMD QTL identified in this study
Bmd1P80.4L5.1	D1Mit33 (82)	5.5	6.6	Identified in previous BMD study
Bmd1P108.8L5.2	D1Mit291 (103.8)	4.4	15	Unique BMD QTL identified in this study
Bmd14P10L2.7	D14Mit132 (0)	4.4	17	Identified in previous BMD study
Bmd9P46.5L3.6	D9Mit270 (41.5)	3	14.8	Identified in previous BMD study
Bmd4P55.3L2.8	D4Mit204 (61.2)	2.6	11.1	Identified in previous BMD study
Bmd19P37.8L2.8	D19Mit53 (32.8)	2.6	12.6	Unique BMD QTL identified in this study
Bmd18P25.1L2.7	D18Mit185 (27.3)	2.1	9.6	Identified in previous BMD study
Bmd12P23L2.9	D12Mit156 (28.4)	2	6.1	Unique BMD QTL identified in this study

[*]The LOD threshold is 3.5 for significant linkage and 2.7 for suggestive linkage (equivalent to significant level of 1% and 5%, respectively, for a standard chromosome length of 100 cM).

Table 12. Summary of significant QTLs for the work to failure.

QTL name	Marker close to the peak of QTL (cM)	Nonparametric mapping p value	% Expl	1 LOD interval (cM)	Notes
Wtf2P54.6L8.4	D2Mit62 (54.6)	0.0001	7.1	5.0	Shared with Fbs QTL
WtfXP14.4L3.8	DXMit208 (18.6)	0.0005	3.3	21.0	Unique to Wtf
Wtf8P20.7L3.7	D8Mit125 (15.7)	0.005	2.9	21.3	Shared with Fbs QTL
Wtf7P31.2L2.8	D7Mit232 (26.2)	0.001	2.8	23.3	Unique to Wtf
Wtf9P46.5L2.3	D9Mit270 (41.5)	0.005	1.8	21.9	Shared with Fbs and BMD QTL
Wtf17P6.6L2.1[#]	D17Mit175 (6.6)	0.05	2.8	22.9	Shared with Fbs and BMD QTL
Total % of F_2 variance			**20.7**		
Same QTLs after adjustment with periosteal circumference					
Wtf2P54.6L5.4	D2Mit62 (54.6)	0.0001	5.0	5.0	
WtfXP14.4L3.3	DXMit208 (18.6)	0.0005	3.0	21.0	
Wtf8P20.7L3.3	D8Mit125 (15.7)	0.005	2.7	20.1	
Wtf7P31.2L2.6	D7Mit232 (26.2)	0.005	2.6	24.0	
Wtf9P46.5L2.3	D9Mit270 (41.5)	0.005	1.6	21.9	
Wtf17P6.6L2.0	D17Mit175 (6.6)	0.05	2.5	23.0	
Total % of F_2 variance			**17.4**		

[*]See explanation for QTL term in the methods section. % explained and 1 LOD interval were determined on the basis of MQM mapping. Threshold for nonparametric mapping is $p<0.005$ for significant linkage. [#] This QTL is not significant based on our threshold level, but concordant with FBS and BMD QTLs.

C. Technical Objective 3: To apply the ENU (ethylnitrosourea) mutagenesis to identify new genes that regulates soft- and hard-tissue regeneration in C3H strain of mice.

1. Introduction

The goal of this technical objective is to identify and characterize novel genes or to elucidate the function for known genes that play a key role in the metabolism of bone and soft tissue using the ENU mutagenesis technique.

During the first 11-months of the study period, we proposed the following Specific Objectives:

a) Specific Objective 1: To generate mutations by ENU treatment of C3H male mice and screen mutations by one-generation dominant and two-generation recessive screenings. To accomplish these objectives we will:

(1) Inject three weekly ENU doses of 100 mg/kg to C3H mice to generate founder males.

(2) Breed ENU founder males that regain fertility with wild type C3H females.

(3) Screen 300 F1 mice generated from ENU injected males for dominant mutations affecting: a) body weight; b) muscle size; c) bone density; d) growth markers; and e) serum chemistries.

(4) Breed about 25 randomly selected F1 males with wild type C3H females for recessive screening. All F2 female pups thus generated will be bred back to F1 male. The F3 progeny generated from F2 (female) X ENU founder male will be screened for recessive mutations affecting: a) body weight; b) muscle size; c) bone density; d) growth markers; and e) serum chemistries.

(5) Confirm selected mutations by backcrossing the affected C3H/HeJ mice with wild type C3H/HeJ as well as with other strains of mice.

b) Specific Objective 2: To determine the chromosomal location of the mutant gene responsible for the selected mutant phenotypes. To accomplish this, we will:

(1) Select mouse mutant/s for genotyping based on the importance of phenotype and based on the magnitude of change in phenotype induced by ENU mutation.

(2) Breed mutant C3H mice with another inbred strains of mice (chosen based on the similarity in phenotype with wild type C3H and availability of markers for genotyping) to produce F1 mice.

(3) Intercross F1 mice to produce approximately 50-100 F2 mice

(4) Screen F2 progeny for phenotype and extract genomic DNA from ear punch for genotyping.

(5) Perform a genome-wide scan using appropriate SNPs and/or polymorphic microsatellite informative markers representing all chromosomes with average length of 5-20 cM.

(6) Perform interval mapping using commercially available software and determine the significance level of interval mapping.

2. Body

Our progress during the first 11 months is summarized below.

a) Specific Objective 1: To generate mutations by ENU treatment of C3H male mice and screen mutations by one-generation dominant and two-generation recessive screenings.

The main aim of the Specific Objective-1 was to generate mutations by ENU treatment of C3H male mice, and screen 300 C3H/HeJ (C3H) mice for skeletal phenotypes caused by dominant mutations and 25 lines of C3H mice for recessive mutations.

We have made one change in this specific objective that relates to the inclusion of a low bone density C57BL/6J (B6) mouse strain (in addition to C3H mice) in our dominant, as well as recessive, screening. The rationale for adding an additional strain of mice is as follows: our main aim for using ENU mutagenesis in the mouse model is to identify genes that regulate musculoskeletal phenotypes in mice. We have earlier identified that C3H mice have the highest bone mineral density (BMD), while B6 mice have the lowest BMD among 13 inbred strains. Our experience with ENU mutagenesis in C3H mice indicates that most of the mutations that we have observed so far are loss-of-function mutations resulting in decreased bone density. Based on this observation, it can be assumed that use of a strain with a low BMD is a good candidate for identifying mutations that may result in an increase in bone density. Therefore, we have included B6 mice in our dominant screening. The breeding characteristics of B6 mice are similar to C3H mice and it can tolerate ENU well with a high fertility rate after an initial recovery period. Therefore, use of B6 mice will not affect the number of mice screened from each ENU injected male.

(1) Inject three weekly ENU doses of 100 mg/kg to C3H mice to generate founder males.

We injected one batch of 8-10 week old 20 C3H male mice and two batches of 20 B6 mice with 3x100 mg/kg of ENU. All these batches of ENU injected males were used for generating F1 (for dominant screening) and F3 (for recessive screening) progeny. The C3H mice were injected with a dose of 3x100 mg/kg of ENU, and B6 mice were injected with a dose of 3x110 mg/kg of ENU. In earlier reports, we have shown that B6 mice can tolerate a higher dose of ENU and regain fertility within 12-20 week post ENU injection. We generated three batches of ENU-injected males with an interval of 3-month period, which allowed us a continuous supply of ENU-mutagenized C3H or B6 males for breeding with C3H or B6 wild type females.

(2) Breed ENU founder males that regain fertility with wild type C3H females.

We bred each ENU injected B6 male with two 8-12 week old wild type B6 females 12-14 weeks after the last ENU injections. The B6 ENU injected male mice typically recovered in 14-15 weeks and produced litters with 4-5 pups/litter. However, the fertile period was brief and lasted between 12-16 weeks. About 50% males were fertile and 10-20% males died before recovery of fertility. In general, ENU-injected B6 males produced larger litters as compared to ENU-injected C3H male mice. Females were checked routinely for pregnancy, and the pregnant mice were removed from mating cages and replaced by fresh females. A maximum of 50 progeny were screened from each founder male, with the founder male subsequently euthanized.

(3) Screen 300 F1 mice generated from ENU injected males for dominant mutations affecting: a) body weight; b) muscle size; c) bone density; d) growth markers; and e) serum chemistries.

The generation and screenings of B6 mice were performed as described in Fig. – 1. During the reporting period, we have screened 292 mice for dominant mutations. Mice were screened for: a) visible abnormalities, b) growth or body weight; c) total body bone density determined by DEXA instrument PIXImus; d) volumetric bone density at tibia determined by peripheral quantitative computed tomography, e) bone formation markers; and f) skeletal dysplasia or gross morphological abnormality by x-ray (X-Ray Faxitron). Phenotype screens on F1 offspring were carried out under one episode of anesthesia at 10-weeks of age. An abnormality is recognized if a phenotype differs by three standard deviation (±3SD) as compared to values obtained earlier using age and sex matched non-mutagenized C3H mice. In addition, visible phenotypes were recorded at the time of weaning. Measurements that were found to be abnormal were repeated at 16-weeks to confirm the phenotype. For this purpose, we have obtained additional baseline values for age and sex matched C3H and B6 mice at 16-weeks of age. The bone size parameters, such as BMC, bone area, femur BMD, and endosteal and periosteal circumference are size-dependent and show strong correlation with body weight. Hence, the parameters were normalized with body weight in F1 and F3 progeny for identifying phenodeviant or mutant mice. Those phenotypes confirmed after repeat testing were subjected to inheritance-test (IT) or backcross with wild type mice. Because of the significant efforts involved in progeny testing, we focused on those phenodeviants that had the highest differences in phenotypes. A mutation is considered inheritable if the phenotype is recovered in both B2 and B3 progeny.

Phenodeviants Identified in Dominant Screening: We screened 292 F1 progeny (Table –1) for all phenotypes listed in Specific Objective 1c. We observed 12 phenodeviants in our primary screening performed at 10-weeks and confirmed five quantitative phenodeviants in 16-week repeat testing; these phenodeviants are listed in Table – 2, which includes those that are not yet confirmed in inheritance test crosses. Characteristics of a few phenodeviants confirmed in the repeat testing are discussed below.

a) Phenodeviant with high body weight and high bone density: The phenodeviant was identified in B6 dominant screen and progeny from the phenodeviant (12.13.7) shows approximately 20% high body weight and areal total body bone density (Fig.-2). The affected progeny has 15% higher total body bone density, even after adjustment with body weight (Fig.-2). The average body weight adjusted total body BMC was 15% higher in affected progeny ($p<0.05$).

b) Phenodeviant with hip dysplasia: We observed three phenodeviants with hip dysplasia in B6 dominant screen. X-ray images from two of these phenodeviants are shown in Fig.-3a & b. These mice have a normal gate indicating that dysplasia does not hinder in movement. However, only one of the dysplasia phenodeviants (12.6.4) showed inheritance (Fig.-3c) whereas progeny from crosses between phenodeviant and B6 or C3H have shown some form of hip dysplasia.

c) Phenodeviant with high bone density: The phenodeviant (12.18.4) was identified in B6 dominant screen and progeny from the phenodeviant showed approximately 15% high areal total body bone density (Fig.-4). The affected progeny had 12% higher total body bone density, even after adjustment with body weight. The total area was not significantly affected in affected progeny ($p<0.05$).

Detailed Phenotypic Characterization of Important Phenodeviants:

Mutant Line 917M- *In-vivo Bone Area Phenotype Characterization:* In our previous ENU mutagenesis screen for dominant musculoskeletal phenotypes using a C57BL/6J (B6) strain of mice, a phenodeviant was discovered which exhibited a highly significant decrease in bone size attended by an increase in fat mass. Three main parameters that assess bone size, such as bone area, bone mineral content (BMC), and periosteal circumference, were all significantly lower in affected mice, even after adjustment for decreased body weight as shown in the Table 4. Interestingly, the total body bone area phenotype was consistently expressed in males (92% affected), whereas only 6% of females exhibited partial phenotype (Table 5). The males with decreased bone size also showed 15-20% increase ($p<0.01$ both at 10-weeks and 16-weeks age) in fat mass and 10% decrease in lean mass, as compared to age and sex matched control male mice (Fig.-5). The normal WT B6 males have 10-20% higher bone area ($p<0.0001$) and 6% lower fat mass ($p<0.05$) compared to WT B6 females, whereas mutant males were similar to female littermates in total body bone area (8.79 cm^2 in male Vs 8.96 cm^2 in females, $p>0.05$). These compositional changes in male mutant mice indicate that the mutant gene may regulate gender differences in bone size.

Ex-vivo Bone Area Phenotype Characterization: In addition to the in-vivo measurements of bone size, we also measured bone size in excised bone from the mutant and compared them with wild type. The periosteal circumference and total bone area covering the entire length of femur and tibia are shown in Fig.-6, which indicates that the bone area and periosteal circumference was significantly lower in tibia as well as femur from mutant mice (n=3) as compared to that of age matched WT control mice (n=5).

Characterization of Cellular Mechanism of Low Bone Area Phenotype in Mutant 917: To study the cellular mechanism of decrease in bone area in the 917 mutant, we isolated the periosteal osteoblasts from femur and tibiae of normal and 917 ENU mutant B6 mice and propagated them in culture for in vitro phenotypic characterization. In brief, the mice were euthanized with CO2 and decapitated. Soft tissue was removed from femur and tibia without scraping off the bones so that periosteal cells were not lost at this point. Femur and tibia were placed separately in 50 ml falcon tubes containing sterile PBS, and subsequently in culture dish containing 10 ml of DMEM/antibiotics and the left over muscles were removed from the bones. The periosteal cells were extracted from bone by collagenase digestion for 90 minutes at 37°C. Cells were counted and plated at a density of 10^6 cells per dish and grown with 10% FBS/DMEM/antibiotics. Periosteal osteoblasts at passage 2-3 were used to study cell proliferation, differentiation, and apoptosis. These characteristics cells from mutant mice were compared with cells isolated in identical manner from age and sex matched wild type mice. Cell proliferation was studied using (3H)-thymidine incorporation and results were confirmed by using Cyquant-GR cell proliferation assay from Molecular Probes. Cell differentiation was measured by observing changes in the alkaline phosphatase activities using PNPP as substrate. For apoptosis

studies, the Homogeneous Caspases Assay from Roche Biochemicals was used which is a fluorimetric assay for the quantitative *in vitro* determination of caspases activity in microplates. Periosteal cells were incubated with DEVD-Rhodamine 110 for 2 h. Upon cleavage of the substrate by activated caspases, fluorescence of the released Rhodamine 110 was measured. Apoptosis results were further confirmed using FACS analysis of isolated cells in presence/absence of 10%FCS.

Cell Proliferation: Fig.-7 shows the basal proliferation rates of periosteal osteoblasts isolated from femur and tibiae of 16-week-old normal and ENU mutant B6 male mice. A significant decrease ($p<0.001$) in the basal rate of cell proliferation was observed in cells from mutant mice as compared to the normal WT mice. When the cells were grown in absence of 10% FCS, there was a significant increase ($p<0.001$) in proliferation rates of cells from mutant mice (Fig.-8).

Cell Differentiation: The specific activity of alkaline phosphatase (a marker of osteoblasts differentiation) was estimated in periosteal cells derived from normal and ENU mutant mice (Fig.-9). No significant changes were observed in ALP activities of cells from different mutant mice as compared to those from wild type mice.

Apoptosis (Caspase activity): Fig.s-10 & 11 show the rate of apoptosis, as measured by the caspase activities in periosteal osteoblasts isolated from 16 week old B6 normal and ENU mutant mice. The caspase activities increased significantly ($p<0.001$) in the cells from mutant mice indicating an increased apoptosis in these cells.

Flow Cytometric analysis: The results of caspase activity measurements were confirmed by studying the apoptosis rates in cells by FACS analysis using annexin V conjugated with Alexa Fluor 488 to stain the apoptotic cell population. FACS analysis also showed a significant increase in apoptosis in cells from mutant mice as compared to those from normal mice (Fig.-12).

Effect of shear stress on cell proliferation: Since the mutation affects periosteal bone cells, which are involved in bone adaptive response to mechanical loading, we studied effect of shear stress on the proliferation rate of cells isolated from mutant mice bones. We used physiologically relevant flow shear strains of 20 dynes/cm^2 and measured the effect on [^{3}H]-thymidine incorporation (an index of cell proliferation) in periosteal osteoblasts derived from normal and ENU mutant mice (Fig.-13 & 14). We found that application of steady fluid flow shear strain of 20 dynes/cm^2 for 30 minutes on normal cells caused a significant ($p<0.001$) increase (50-100%) in the [^{3}H]-thymidine incorporation (after 24-hours) as compared to control cells that were without the shear strain. The pattern of increased proliferation due to application of stress seen in the case of cells from normal mice was absent or significantly decreased in cells from mutant mice.

In conclusion, our preliminary data on the bone area and cellular characterization of the osteoblasts cells from mutant 917 indicates that the decreased bone area in mutants may in part be due to decreased osteoblast cell numbers.

(4) Breed about 25 randomly selected F1 males with wild type C3H females for recessive screening. All F2 female pups thus generated will be bred back to F1 male. The F3 progeny generated from F2 (female) X ENU founder male will be screened for recessive mutations affecting: a) body weight; b) muscle size; c) bone density; d) growth markers; and e) serum chemistries.

The aim of this specific objective was to identify phenodeviants that have recessive mode of inheritance. Therefore, a three-generation breeding strategy (shown in Fig.-1) was used to recover recessive mutations in F3 progeny. To generate F3 mice for recessive screening, we randomly selected 32 F1 males generated in our dominant screening and bred them with 110 wild type B6 females (Fig.-1). Each F1 male was mated with 1-2 normal wild type female mice. Once the mating was successful, pregnant mice were separated and placed separately to give birth to F2 littermates. If F2 litter had 3-4 female mice, they were used to generate F3 progeny. Otherwise, a new WT B6 female was bred until 3-4 F2 females were obtained. Each F2 female was reintroduced for mating with a F1 male to produce at least one litter with a minimum of 4 pups. The aim was to screen a minimum of 20 F3 progeny from each line.

During the current reporting period, we bred approximately 260 female F2 pups with 30 F1 males (founder male), 2 F1 males were not efficient in mating and hence discontinued. From 28 lines, so far we have screened approximately 339 F3 progeny for recessive mutations affecting: a) visible abnormalities, b) growth or body weight; c) total body bone density determined by DEXA instrument PIXImus; d) volumetric bone density at tibia determined by peripheral quantitative computed tomography (pQCT), e) x-ray imaging using X-Ray Faxitron, f) bone formation markers; and g) blood chemistry, which included calcium, magnesium, blood urea nitrogen, cholesterol, high density lipids, triglyceride, and Creatinine Kinase. Our screening strategy involved repeat testing at 16-weeks of all phenodeviants identified in a 10-week screening. Those phenotypes that were confirmed after repeat testing were subjected to inheritance-test (IT) or backcross with wild type mice.

Phenodeviants Identified in Recessive Screening: We observed 20 phenodeviants in our primary screening performed at 10-weeks and have so far confirmed 7 quantitative phenodeviants at 16-week repeat testing; these phenodeviants are listed in Table – 2. Several of the phenodeviants identified in primary screening have not yet reached the16-week screen age and hence are not yet confirmed in repeat testing (Fig.s 15-21). Characteristics of a few phenodeviants confirmed in the repeat testing are discussed below.

Phenodeviant with low bone area and high bone density: The phenodeviant (12.14.5M) was identified in a C3H recessive screen as a 20% lower bone area whereas the BMC was largely unaffected. The body weight was about 10% lower in the phenodeviant mice, however, the body weight adjusted BMD was 23% higher. These data indicate that mutation causes reduced bone size without significant reduction in BMC leading to higher density. This phenodeviant is currently under inheritance testing.

Phenodeviant with high volumetric bone density: The phenodeviant (B7.2M) was identified in a B6 recessive screen as a 10-12% higher bone density measured by pQCT whereas the bone area and BMC were not significantly affected. The areal bone density was higher but the difference was less than 3SD units from wild type mean. The phenotype is confirmed in at least two F3 litters from the same F1 founder male (Fig.-15). The body weights of the phenodeviant mice were normal.

Phenodeviant with blood chemistry phenotypes: In the current screen, we incorporated measurements of several blood chemistry analytes to screen for mutations affecting skeletal metabolism (alkaline phosphatase and calcium), lipid metabolism (total cholesterol, high density cholesterol, and triglycerides), muscle metabolism (creatinine kinase and creatinine kinase-MB isoform), and kidney function (serum creatinine and

blood urea nitrogen). We have identified several phenodeviants in blood chemistry phenotypes, which are shown in Fig.s 18-21. Several of these phenodeviants are currently repeat tested at 16-weeks to confirm the phenotype. So far, we have confirmed one phenodeviant with 6-10 folds higher levels of creatinine kinase (Line B5.1) in the 16-week repeat testing and this phenodeviant is currently undergoing inheritance testing.

(5) Confirm selected mutations by backcrossing the affected C3H/HeJ mice with wild type C3H/HeJ as well as with other strains of mice.

In the current reporting period, we introduced 11 phenodeviant mice (including both C3H & B6) into inheritance testing by mating affected male and female with wild type C3H or B6 mice. Each phenodeviant was mated with 1-2 normal wild type male or female mice. Once the mating was successful, pregnant mice were separated and placed separately to give birth to B2 littermates. If the F1 affected mouse was female, it was reintroduced for mating to produce 3-5 litters, totaling about 20-25 F2 pups. If the affected mouse was male, 3-5 female mice were mated simultaneously. The inheritance testing (IT) F2 offspring were screened at 10-and 16-weeks of age. A mutation was considered inheritable if the phenotype was recovered in both B2 and B3 progeny. The animals were not genotyped at this stage in order to differentiate mutant from non-mutant genotypes; thus, phenotype distribution was the only means for separating the mutants from their unaffected littermates. To avoid potential breeding of an un-affected progeny, we bred only extreme scoring mice for generating affected progeny. All phenodeviant mice that underwent inheritance testing and produced some progeny are listed in Table 1 & 3. In addition to new phenodeviants identified in the current reporting period, we also progeny tested phenodeviants from the previous years' screens; these phenodeviants are listed in Table 3.

We have confirmed three phenodeviants from previous screens as inheritable; these are 9.1.7B (low bone area), Line 5.27.7 (low total body bone density), and Line 2.8.6 (binary phenotype of greasy fur and low BMD). Of these three mice, the 917 F1 male was bred extensively because of its interesting phenotype. The original F1 male mouse produced 30 1st generation progeny, and selected breeding of 1st generation affected mice with WT B6 females produced about 160 2nd and 3rd generation mice (Table 5). Thus, this mutant phenotype was confirmed in two generations of inheritance-test crosses with wild type B6 females.

In the current screen, we have confirmed one phenodeviant 12.13.7 that has high body weight, BMC, and BMD. In addition, we observed three phenodeviants 12.18.4 (high BMD), 12.6.4 (hip dysplasia), and B7.2 (high volumetric BMD) as probably inheritable from the current screen because 1-2 litters from these mice show expected phenotype. The ratio of affected and non-affected mice corresponds to 40-50% for dominant phenodeviants and 20-25% for recessive mutation, which was close to expected ration for dominant (50% affected) or recessive mutation (25% affected). Characteristics of five mutants confirmed in the inheritance testing are shown in Fig.s 2-6. Additionally, inheritance testing is currently underway to test other phenodeviants.

In addition to inheritance testing in same strains of mice, we also carried out breeding of phenodeviant mice with different strains of mice as indicated in Table 3. This was done because skeletal phenotype in each strain of mice depends on the genetic background of that strain and it is possible that, in certain backgrounds, the mutant phenotype is not expressed. Breeding with different strains of mice and subsequent

evaluation of IT progeny allowed us to evaluate the genetic background effect before we started genotyping. To achieve this, we bred each B6 phenodeviant mice with C3H and CAST/i mice and each C3H phenodeviant mice with 129SvEv and B6. The results from these breeding are showed that three phenodeviants 9.1.7B (low bone area), Line 2.8.6 (binary phenotype and low BMD), 12.13.7 (high body weight, BMC, and BMD) expressed expected phenotype in different genetic background (Table 3).

b) Specific Objective 2: To determine the chromosomal location of the mutant gene responsible for the selected mutant phenotypes.

The aim of this Specific Objective was to determine the chromosomal location of the mutant gene, which is responsible for the phenotypes in the selected mutant. Our progress on this specific objective is discussed below.

(1) Select mouse mutant/s for genotyping based on the importance of phenotype and based on the magnitude of change in phenotype induced by ENU mutation.

We selected two mutant lines of mice for genotyping based on phenotype characterization discussed in 'Specific Objective-1c' and magnitude of change obtained in the phenodeviant upon inheritance testing. One of the phenodeviants was a dominant mutation (917, B6 strain) and other was a recessive mutation (Line286, C3H strain). In both these mutant strains of mice, phenotype was observed at two different ages (10-and 16-weeks) and inheritance confirmed in large number of inheritance test progeny (Table 3). In addition, these mice also showed a phenotype in at least one different background strain of mice than that used for inheritance testing. These data revealed that the mutant gene would show expected the phenotype in a different genetic background during genotyping.

When a different strain of mice is used for interval mapping of a mutant strain, the mapping will reveal several quantitative traits loci (QTL) associated with the background strains, which is irrespective of mutation. Therefore, it is prudent to study normal QTLs occurring in non-mutagenized F2 population, which is generated from same strains of mice that is used for generating mutant F2 population. To achieve this, we selected three wild type strains to perform two intercrosses, C3H-B6 and C3H-129SvEv. We selected these crosses because we are currently using the C3H, B6, and 129SvEv strains for generating F2 mice from mutant C3H or B6 mice in our QTL mapping. We believed genotyping the wild type F2 mice would be helpful in identifying a unique QTL that could be attributed to ENU induced mutation.

(2) Breed mutant C3H mice with another inbred strains of mice (chosen based on the similarity in phenotype with wild type C3H and availability of markers for genotyping) to produce F1 mice.

We bred a 917B6 phenodeviant with C3H and 286C3H phenodeviants and B6 to generate 15-30 F1 mice. These strains were selected because of the availability of large numbers of informative polymorphic markers between these trains; we identified 46-50 polymorphic markers (Tables-6 & 7) based on the location of each marker and differences in size of alleles. To generate F1 mice, the mutant male was mated with 3-4 normal wild type female mice. Once the mating was successful, pregnant mice were separated and

placed separately to give birth to F1 littermates. Each F1 female was then bred with each F1 male to produce at least one litter, with minimum of 4 pups. To generate F1 mice from wild type, the male wild type mice from the same strain, as in case of mutant male, was mated with 3-4 normal wild type female mice of different strain. Therefore, the breeding pattern is identical in mutant and wild type intercross.

(3) Intercross F1 mice to produce approximately 50-100 F2 mice.

To generate F2 mice we intercrossed 15-30 F1 mice from three different crosses to produce 90 F2 mice for 917Mutant-C3H, 204 F2 mice for wild type B6-C3H, and 125 F2 mice for wild type C3H-129SvEv crosses. We generated at least one litter from each female and male in the F1 Male x F1 Female crosses.

(4) Screen F2 progeny for phenotype and extract genomic DNA from ear punch for genotyping.

We have screened 420 F2 progeny for bone density and size phenotypes at 10- and 16-weeks of age as described in our dominant and recessive screen protocol. In addition, we collected blood from 10-week old mice for biochemical analysis. The bone area phenotype data, which is the main phenotype in the 917Mutant, is shown in Fig.-22. Comparison of bone area data in 917Mutant F2 mice with wild type F2 mice shows significantly lower bone area in 917Mutant male mice (Fig.-22), which indicates that mutation is causing the shift in bone area in males but not in females (the phenotype is only expressed in males). Fig.s-23 & 24 show bone density data from 286Mutant F2 mice and wild type C3H-B6 F2 mice. The 286Mutant mice show a visible abnormality (greasy fur) and a low bone density. Consequently the bone density comparison between mutant and wild type F2 mice shows a significant decrease in both total body BMD and body weight adjusted BMD (Fig.s-23 & 24).

The tail clips were collected from 420 F2 mice from three different intercrosses and genomic DNA was extracted from 420 F2 mice for genotyping. Genomic DNA was isolated from tail clips using DNAeasy kits (Qiagen) for mouse tissue. DNA samples were quantified and quality determined by measuring their absorbance at 260 nm and 280 nm. If a DNA sample was not satisfactory, we extracted genomic DNA from back-up tissue (ear punch) for genotyping.

(5) Perform a genome-wide scan using appropriate SNPs and/or polymorphic microsatellite informative markers representing all chromosomes with average length of 5-20 cM.

A genome-wide genotyping scan was undertaken in the 420 F2 mice using the 50 informative polymorphic markers (shown in Tables-6 & 7). In the current reporting period, we have completed genotyping of 242 F2 mice. A whole genome screen was implemented and completed for 917Mutant F2 mice (n=90) and wild type C3H-B6 F2 mice (n=152). 50 Fluorescently labeled [labeled with FAM (blue), VIC (green), and NED (yellow)] informative markers were PCR amplified from 242 F2 DNA. Markers were spaced at either end of each chromosome, and in some cases in the middle (for larger chromosomes).

We performed about 12,000 PCR reactions to achieve genotyping in these two intercrosses. PCR reactions and running conditions allowed from 4 to 6 microsatellite

markers to be multiplexed in a single electrophoretic lane. All 6 reactions were run in a single capillary on the ABI 3100 DNA analyzer. Following electrophoresis on the ABI 3100 DNA Analyzer, Genotyper software macros were used to semi-automatically score the allele calls for all the multiplex pools of every single F2 mice. The pooled products were analyzed for fragment size on ABI Model 3100 DNA Analyzer and Genescan software was used to size alleles (Applied Biosystems). After initial scoring by these macros, allele calls were visually checked and edited if necessary. Allele calls and edits were done using Genotyper software (Applied Biosystems) and exported as tab-delimited tables. A table of the calls was generated and the allele sizes converted into respective allele bins for entering into software program MapQTL 4.0 (CPRO-DLO, Wageningen, Netherlands).

(6) Perform interval mapping using commercially available software and determine the significance level of interval mapping.

Interval mapping was performed using commercially available software, MapQTL 4.0. Phenotype data and genotype data were imported into the software in text file format; mice with missing phenotypic and genotypic data were coded as phenotype unknown. During the current reporting period we have completed QTL mapping of 917Mutant mice. Although we genotyped all 917Mutant F2 mice including females, we report QTL mapping data only for male because mainly male mice show the mutant phenotype.

Two main regions of the genome were found to give suggestive linkage with LOD>2.0. A LOD score is the logarithm of odds score, i.e. the logarithm of the likelihood that two loci are linked/likelihood that loci are unlinked. Thus, a LOD score of 2 indicates that there are 100:1 odds that a respective genetic region shows linkage to that trait. Fig.s 25 to 28 show LOD plots for chromosomes 1, 2, 4 and 5 for the affected/unaffected MapQTL linkage analysis of the F2 mice from mutant as well as wild type mice. Chromosomes 1, 2, 4, and 5 were the regions of the genome that gave LOD scores above 2.0, other regions (not shown) produced only weak linkage with LOD score<2.0. We compared LOD scores of all QTLs on 19 autosomes and x-chromosome between 197Mutant F2 population and wild type F2 population. Two regions, chromosome–1 (Fig.-25) and chromosome-4 (Fig.-27) indicated the presence of unique QTL in 917Mutant F2 mice as compared to wild type. These two QTLs explain about 71% of the phenotypic variance in mutant B6 strain and C3H strain of mice. Two other regions, chromosome-2 (Fig.-26) and chromosome-5 (Fig.-28) showed presence of QTLs that is common between mutant and wild type F2 mice. After the first round of quantitative trait screens, we have added additional markers within the suggestive QTL regions to confirm and increase the accuracy the QTL position. These additional markers are currently genotyped for linkage analysis.

3. Key Research Accomplishments

- We have screened 292 F1 mice in dominant screen and 339 F3 offspring from recessive screen for bone and growth related phenotypes.
- We identified 32 phenodeviants in dominant and recessive screens.
- We confirmed 13 phenodeviants in repeat testing.
- We progeny tested 11 C3H and B6 phenodeviants.
- We have confirmed six C3H and B6 phenodeviants in inheritance testing.
- We have initiated crosses between mutant strain and a mapping strain for genotyping ENU mutation.
- We have generated 420 F2 mice from intercrosses between mutant and wild type strains.
- We have genotyped 242 F2 mice using approximately 50 informative markers.
- We have performed interval mapping and compared QTLs for mutant crosses with that of wild type mice.
- We have identified some suggestive QTLs (loci) that may harbor mutant gene(s) for one of the ENU mutant strain.

4. Reportable Outcomes

Abstract

Paper presentation at 25th Annual Meeting of American Society for Bone and Mineral Research, 19-23 September 2003.

Srivastava AK, Mohan S, Wergedal JE, & Baylink DJ. An ENU Mutant Mouse Characterized by the Combination of a Decrease in Bone Size and Increase in Fat Mass with Evidence of Gender Difference. 25th Annual Meeting of American Society for Bone and Mineral Research, Program and Abstracts, Vol 18(1), pS176, September 2003.

Manuscript

Srivastava A K, Mohan S, Wergedal J E & Baylink DJ. A Genome-wide Screening of N-Ethyl-N-nitrosourea Mutagenized Mice for Musculoskeletal Phenotypes. Manuscript In press BONE, 2003 (preprint included).

5. Conclusions

a) We injected three batches of C3H/HeJ and C57BL/6J males with an ENU dose of 3x110 mg/kg to generate ENU founder males.

b) We bred the ENU injected males in a breeding scheme to generate about 300 F1 mice for dominant screening and 30 lines of recessive screening F3 progeny.

c) We screened 292 mice for dominant mutation and 339 mice for recessive mutation.

d) In addition, we have screened 60 mice to generate normative data.

e) Thus, total number of mice screened was 691, and therefore, we have acceded our goals for first fourth objectives of the 'Specific Objective-1.'

f) We have tested the inheritability of 11 phenodeviants and confirmed 6 phenodeviants as inheritable mutations.

g) We have screened 523 mice generated in inheritance testing crosses.

h) Therefore, we have achieved the fifth objective of 'Specific Objective-1' of repeat testing and confirming the inheritance of observed mutations. Furthermore, from the mice generated in inheritance-test crosses, we have done extensive characterization of mutant phenotype to explore cellular mechanism responsible for mutant phenotype; this was an additional progress from the proposed work.

i) We have tested expression of phenotype in a different strain of mice than the parent strain and then bred two ENU mutant mice to generate 90 F2 mice for genotyping. In addition, we bred wild type non-mutagenized mice to generate 330 F2 mice for genotyping. We have genotyped 242 F2 mice using 50 genome wide informative markers to find out QTLs harboring mutant gene (s). Therefore, we have completed the first four objectives of 'Specific Objective-2.' We are in the process of genotyping remaining 178 F2 mice using 50 genome wide markers.

j) Finally, we have performed a genome wide interval mapping of one ENU mutant (917) and identified two suggestive QTL regions that may harbor mutant gene (s). We Thus, we have achieved the final objective of 'Specific Objective-2' during this study period.

Figures and Tables for Technical Objective 3

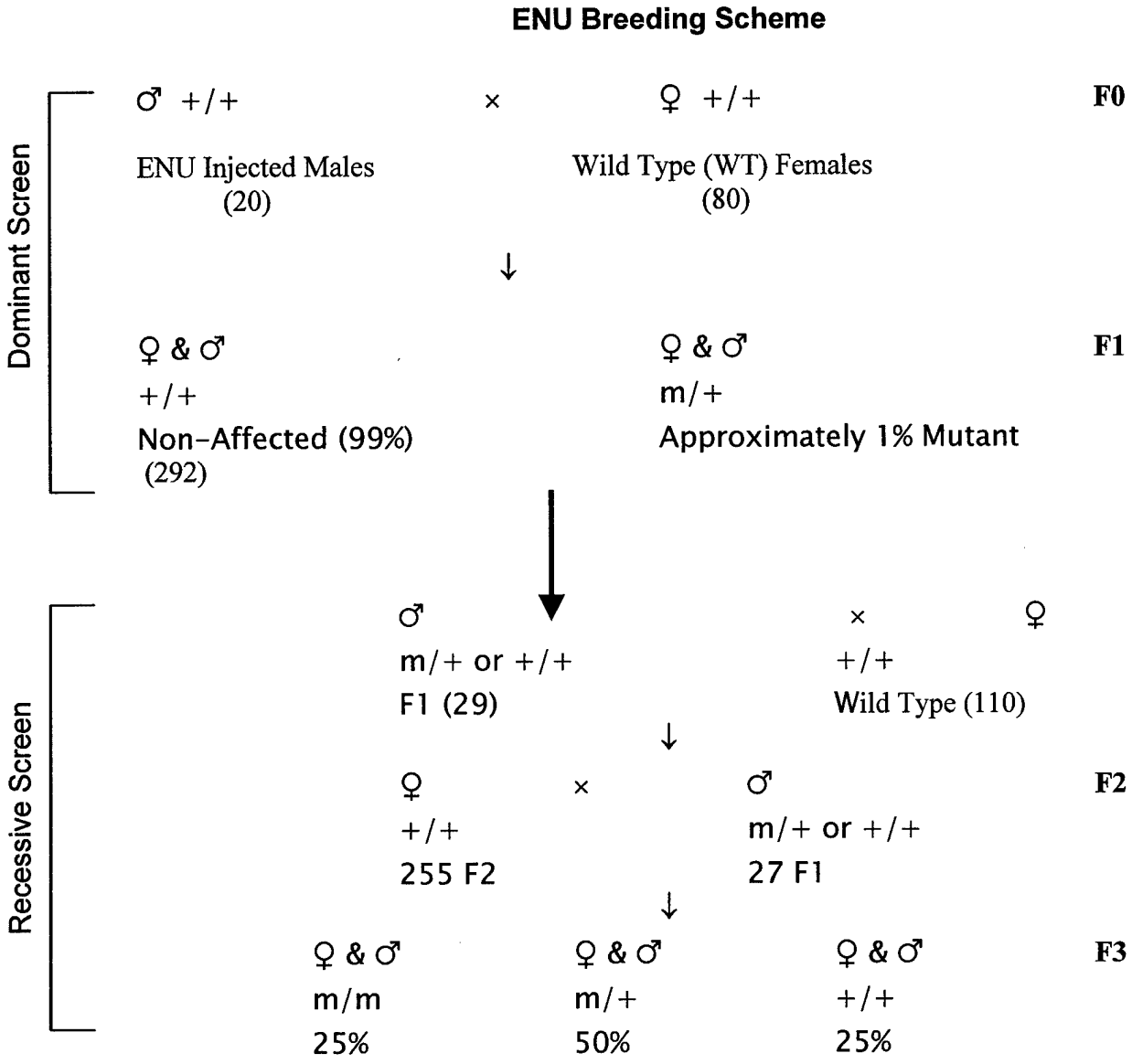

Fig. 1. ENU Breeding Scheme. The breeding scheme incorporates both dominant and recessive screens. We have screened 292 C3H or B6 mice for dominant screen and about 339 mice in recessive screen.

Table 1. Number of mice tested, phenotypes scored (including visible and musculoskeletal), and inherited mutations identified.

Procedure	Number of C3H/HeJ Mice	Number of C57BL/6J Mice
Screened for Dominant Mode of Inheritance	148	144
Screened for Recessive Mode of Inheritance	40	299
Abnormal Phenotypes Identified in Primary Screen (dominant as well as recessive screening)	4	28
Abnormal Phenotypes Confirmed in Secondary Screen	2	11
Phenotypes Introduced to Progeny Testing	2	11
Phenotypes Confirmed in Progeny Testing	-	3
Phenotypes Not-inherited in Progeny Testing (including those died or could not mate)	-	2
Outlier Mice Currently Under Progeny Testing	2	6

*Total number of mice screened was 292 in dominant screening and 339 in recessive screening.

Table 2. List of phenodeviants identified in dominant and recessive screening.

Phenotype (Mice ID)	Description of Phenotype	Mice Strain	ENU Screen
12.13.7.D.M	20% High body weight and 15% high body weight adjusted BMD	B6	Dominant
12.18.4.D.F	15% High BMD	B6	Dominant
12.15.1.C.F	Hip Dysplasia, See Fig.-4	B6	Dominant
12.6.4.D.F	Hip Dysplasia, See Fig.-4	B6	Dominant
12.13.9.I.F	Hip Dysplasia, See Fig.-4	B6	Dominant
14.7.3.B.M	25% Low bone area and BMC	B6	Dominant
11.16.6.B.M	12% High volumetric BMD	C3H	Recessive
12.14.5.E.A.M	20% Low Area and 15% high total body BMD	C3H	Recessive
B2.4.C.M	20% High total body BMD	B6	Recessive
B7.2.B.M	10% High volumetric BMD	B6	Recessive
B13.2.A.M	10% High volumetric BMD	B6	Recessive
B5.1.c	6-10 Folds high Creatinine Kinase	B6	Recessive
B3.2.F	High blood cholesterol, HDL and triglyceride	B6	Recessive

Table 3. List of phenodeviants put to inheritance testing (IT) to confirm heritability of mutation.

Mice ID	Description of Phenotype	IT Mice Produced	Inheritance Test Result
Phenodeviants from Previous Screens (2001-2002)			
9.1.7.B	10-15% Low Total Body Bone Area	**180**	Confirmed in B6 and C3H background. Testing in Cast/i background.
9.18.7.B	5-7% High BMD at mid-shaft of tibia	**28**	Not confirmed in B6 background
Line 5.27.7	10% low total body BMD	**56**	Confirmed in 129SvEv Background
Line 2.8.6	10-12% Low total body BMD, BMC, 10-20% low body weight, fur has greasy appearance	**62**	Confirmed in C3H and B6 background
9.16.8.C	4-6% Low Total Body BMD, and 5-7% Low BMD at mid-shaft tibia	**26**	Not confirmed in B6 background
9.14.6.C	40-50% Lower serum osteocalcin concentration	**48**	Not confirmed in B6 background
New Phenodeviants (2002-2003)			
12.13.7.D.M	20% High body weight and 15% high body weight adjusted BMD	**30**	Confirmed in B6 and C3H background
12.18.4.D.F	15% High BMD	**33**	Probably Inheritable, Testing
12.1.5.C.F	Hip Dysplasia, See Fig.-4	**13**	Testing
12.6.4.D.F	Hip Dysplasia, See Fig.-4	**12**	Probably Inheritable, Testing
12.13.9.I.F	Hip Dysplasia, See Fig.-4	**15**	Testing
12.7.3.B.M	25% Low bone area and BMC	**5**	Testing
11.16.6.B.M	12% High volumetric BMD	**6**	Testing
12.14.5.E.A.M	12% Low Area and 15% high total body BMD	**3**	Testing
B7.2.B.M	10% High volumetric BMD	**6**	Probably Inheritable, Testing

Table 4. Mean percent difference in body weight adjusted bone area parameters in 16-week old phenodeviant mice as compared to non-mutagenized control mice

	Total Body Bone Area (Excluding skull)	Tibia Middiaphysis		
		Bone Area	BMC	Periosteal Circum.
Male (n=21)	-10.4**	-16.9**	-11.7**	-8.8**
Female (n=36)	-2.6*	-5.1*	-1.4#	-2.4*
#p=NS, *p<0.05, **p<0.001 Vs normal non-mutagenized control mice (n=40)				

Table 5. Summary of bone size phenodeviant observed in 10-week old progeny from inheritance test (917 Mutant with dominant mode of inheritance).

Progeny	Low bone area phenotype	
	Affected Female	Unaffected female
1st Generation	6	12
2nd Generation	3	58
3rd Generation	0	31

*The mice from 1st or 2nd generation may have multiple mutations resulting in phenotype appearance, which was diluted in 3rd generation and hence these mice do not show phenotype.

Table 6. List of informative markers used for C3H-B6 genotyping.

Chromosome	Marker	Distance (Cm)	Chromosome	Marker	Distance (Cm)
1	D1Mit132	1	10	D10Mit213	11
1	D1Mit64	5	10	D10Mit233	62
1	D1Mit159	81.6	11	D11Mit2	2.4
1	D1Mit155	112	11	D11Mit214	70
2	D2Mit1	1	12	D12Mit60	16
2	D2Mit66	47.8	12	D12Mit133	56
2	D2Mit285	86	13	D13Mit275	16
2	D2Mit145	98.5	13	D13Mit151	71
3	D3Mit203	11.2	14	D14Mit98	3
3	D3Mit311	45.2	14	D14Mit75	54
3	D3Mit19	87.6	15	D15Mit6	13.7
4	D4Mit193	7.5	15	D15Mit161	69.2
4	D4Mit308	57.4	16	D16Mit131	4.3
4	D4Mit42	81	16	D16Mit139	43.1
5	D5Mit387	15	17	D17Mit51	22.9
5	D5Mit309	44	17	D17Mit39	45.3
5	D5Mit95	68	18	D18Mit64	2
6	D6Mit138	0.7	18	D18Mit48	50
6	D6Mit14	71.3	19	D19Mit68	6
7	D7Mit294	8	19	D19Mit103	52
7	D7Mit98	53.3	X	D20Mit68	17.2
8	D8Mit289	11	X	D20Mit64	45
8	D8Mit178	33	X	D20Mit223	73.3
8	D8Mit88	58			
9	D9Mit285	21			
9	D9Mit336	35			
9	D9Mit16	61			

Table 7. List of informative markers used for C3H-129SvEv genotyping.

Chromosome	Marker	Distance (Cm)	Chromosome	Marker	Distance (Cm)
1	D1Mit64	5	10	D10Mit38	26.8
1	D1Mit380	36.9	10	D10Mit96	56
1	D1Mit440	54	11	D11Mit2	2.4
1	D1Mit426	101	11	D11Mit214	70
1	D1Mit155	112	12	D12Mit182	2
2	D2Mit61	34	12	D12Mit7	50
2	D2Mit395	66.9	13	D13Mit16	10
2	D2Mit145	98.5	13	D13Mit260	65
2	D2Mit148	105	14	D14Mit126	5
3	D3Mit203	11.2	14	D14Mit170	63
3	D3Mit51	35.2	15	D15Mit13	6.7
4	D4Mit18	5.2	15	D15Mit161	69.2
4	D4Mit9	44.5	16	D16Mit160	23.4
4	D4Mit170	66.6	16	D16Mit52	66.8
5	D5Mit348	8.0	17	D17Mit245	3
5	D5Mit352	20	17	D17Mit93	44.5
5	D5Mit277	58	18	D18Mit222	6.0
5	D5Mit247	80	18	D18Mit48	50
6	D6Mit138	0.70	19	D19Mit68	6
6	D6Mit373	74.3	19	D19Mit17	43
7	D7Mit267	11	X	D20Mit68	17.2
7	D7Mit259	72	X	D20Mit216	63
8	D8Mit155	1.0			
8	D8Mit88	58			
9	D9Mit250	5			
9	D9Mit151	72			

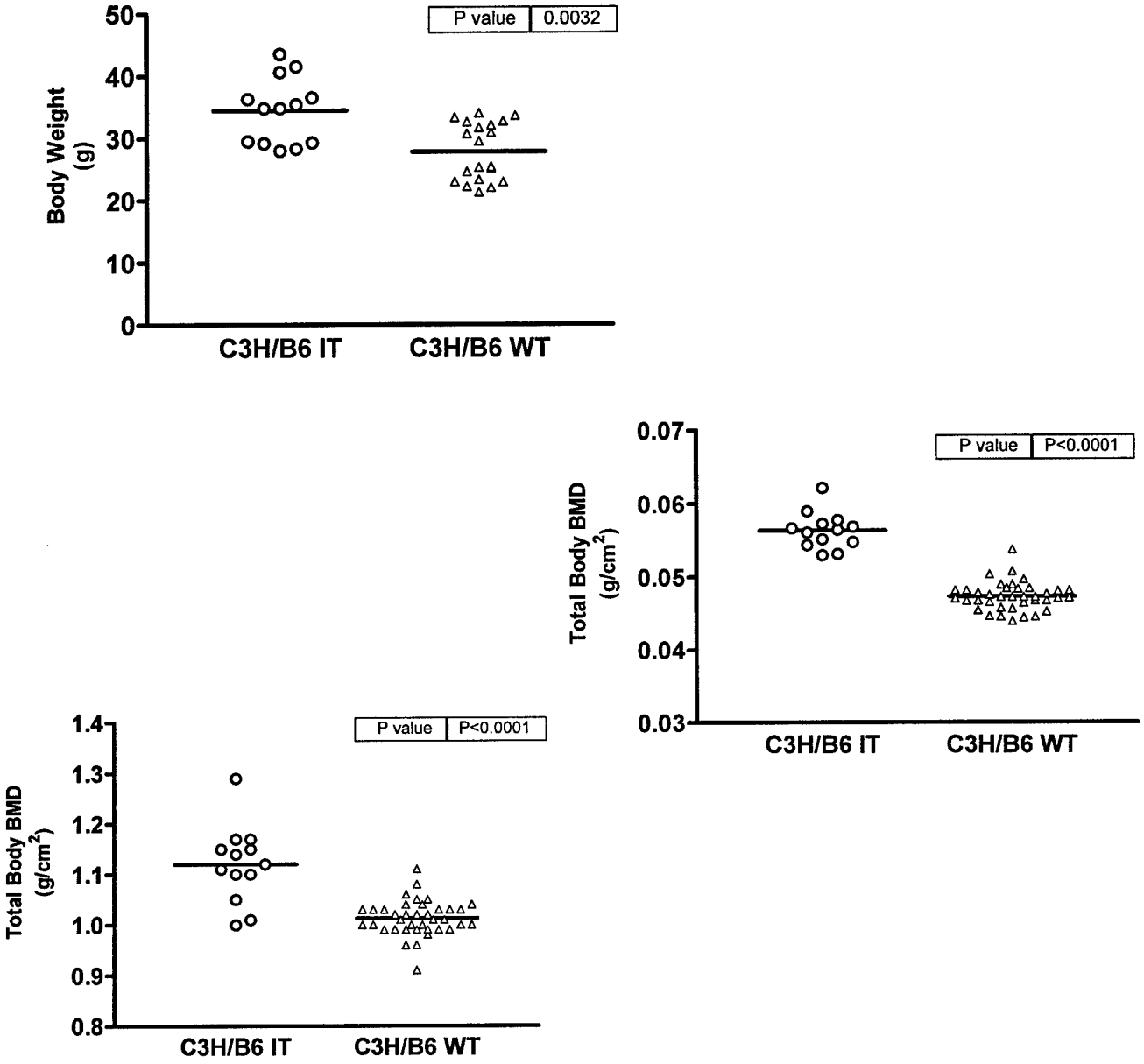

Fig. 2. Body weight, total body bone density (excluding skull), and body weight adjusted bone density in 16-week old progeny from IT crosses (between the 12.13.7 ENU outlier mice and wild type C3H mice). The body weight and bone densities of affected mice are shown along with wild type (WT) male and female mice. The body weight adjusted total body bone density were 14% ($p<0.0001$) higher in affected progeny as compared to WT B6/C3H mice.

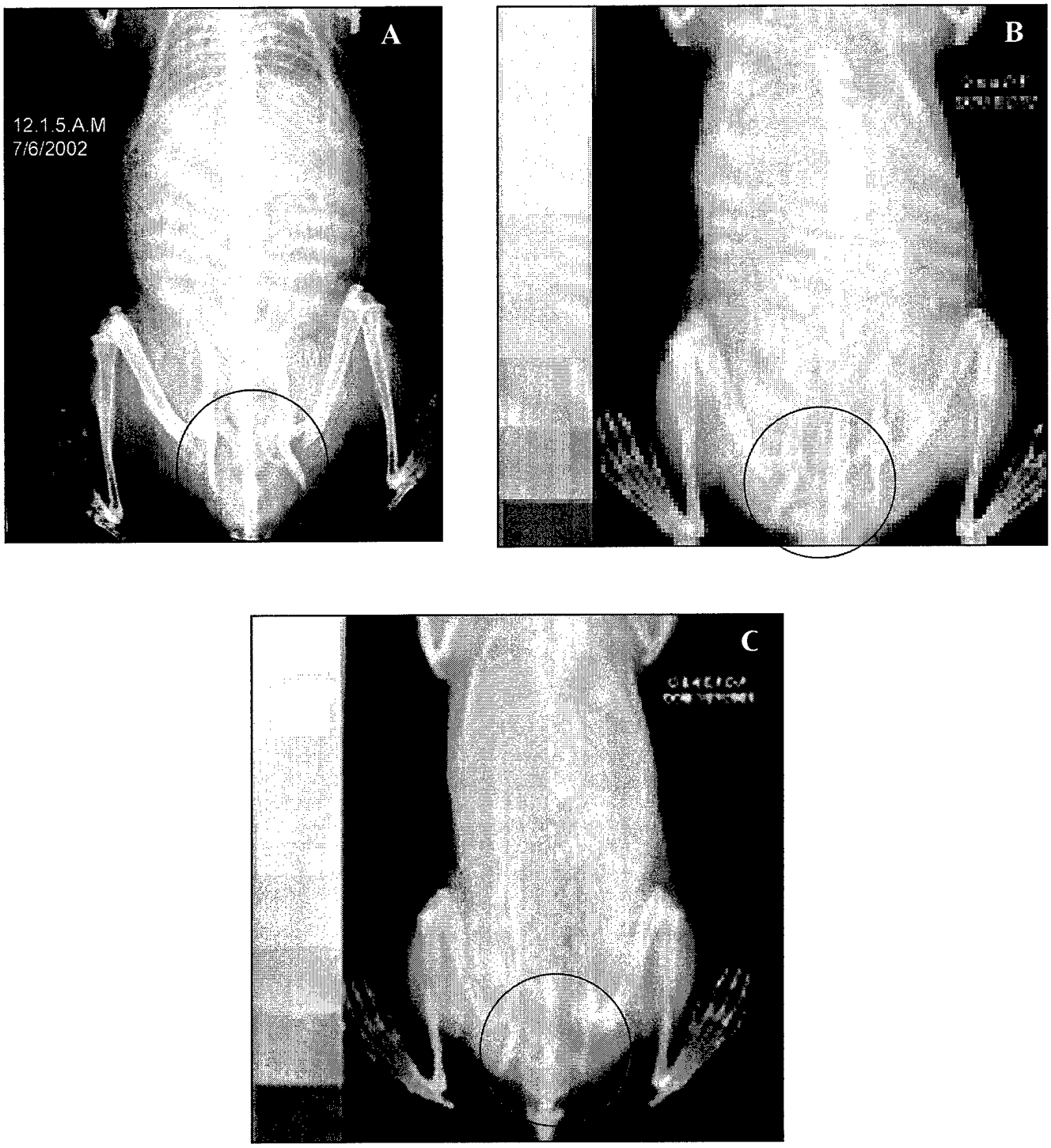

Fig. 3. A & B – Hip dysplasia observed in F1 progeny from dominant screen (B6). C – One of the phenodeviant with hip dysplasia (12.6.4) produced progeny that showed that the phenotype was inheritable.

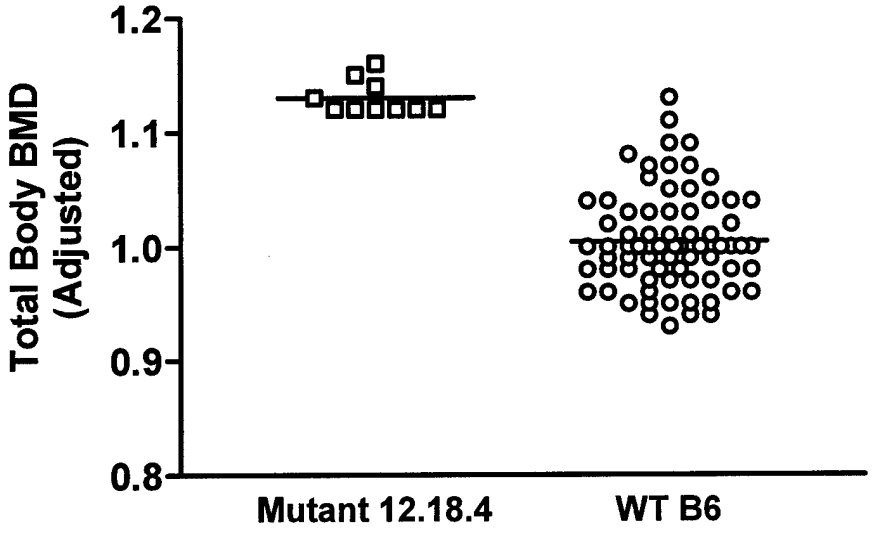

Fig. 4. Body weight adjusted total body bone density of 16-week old progeny from a B6 dominant screen mutant (12.18.4) and wild type B6 mice. The body weight adjusted bone densities of affected mice are shown along with wild type (WT) male and female mice. The bone densities were 13% ($p<0.0001$) higher in affected progeny as compared to WT B6 mice or unaffected littermates.

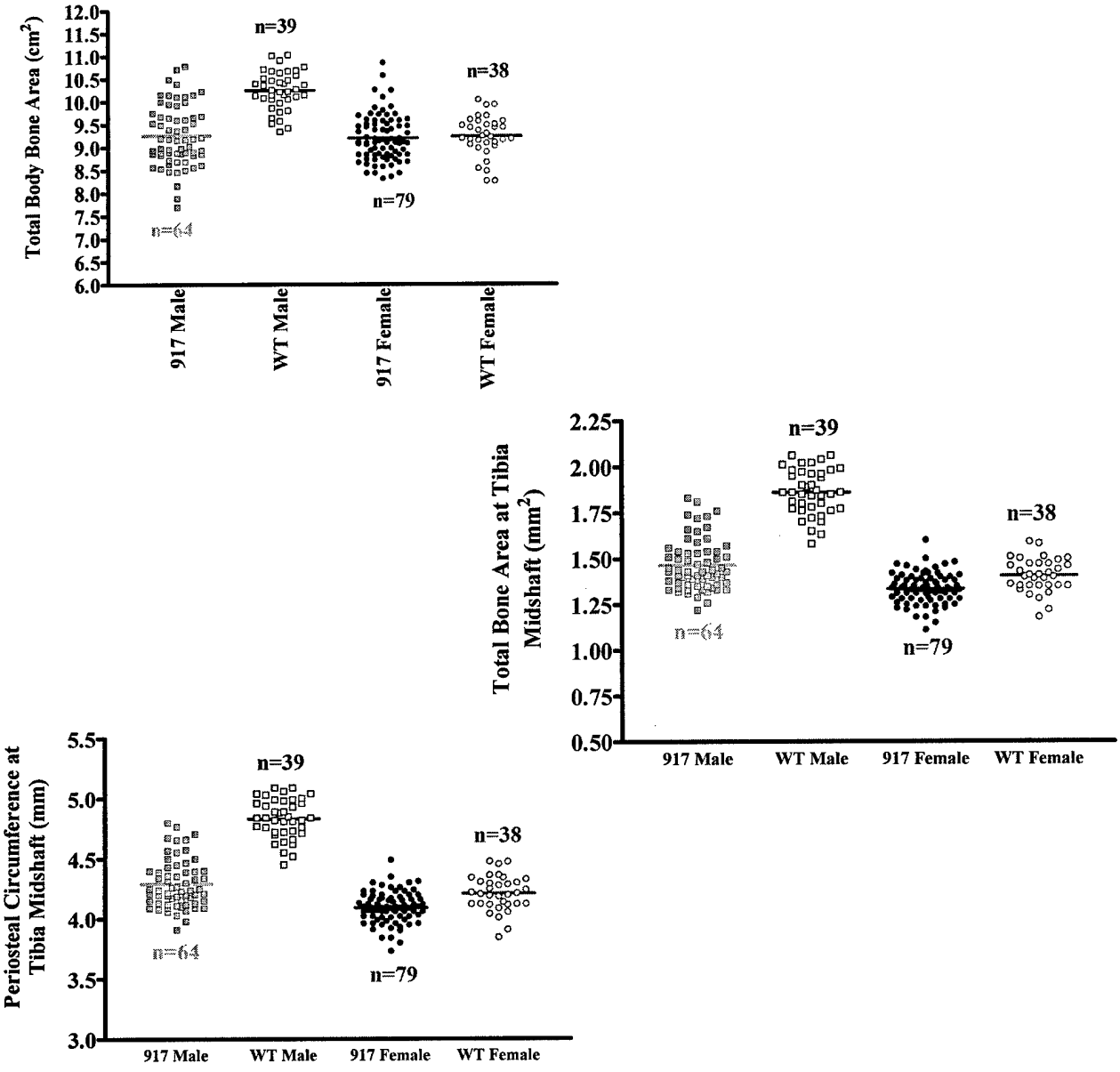

Fig. 5. Phenotype data of a bone size mutant identified in dominant screen (917M). Total bone area (excluding skull) measured by PIXImus, and tibial bone area and periosteal circumference measured by pQCT in 16-week old progeny from IT crosses (between the 917AM ENU outlier mice and wild type B6 mice). Bone areas of affected 917 male mice are shown along with female littermates and wild type (WT) male and female mice. The mean total bone area of the affected male progeny (n=37) was 14.3% lower ($p<0.0001$) whereas female progeny were largely un-affected (96%). The body weight adjusted total body bone area (A) were 10% ($p<0.0001$) lower in affected progeny as compared to littermate and WT male B6 mice.

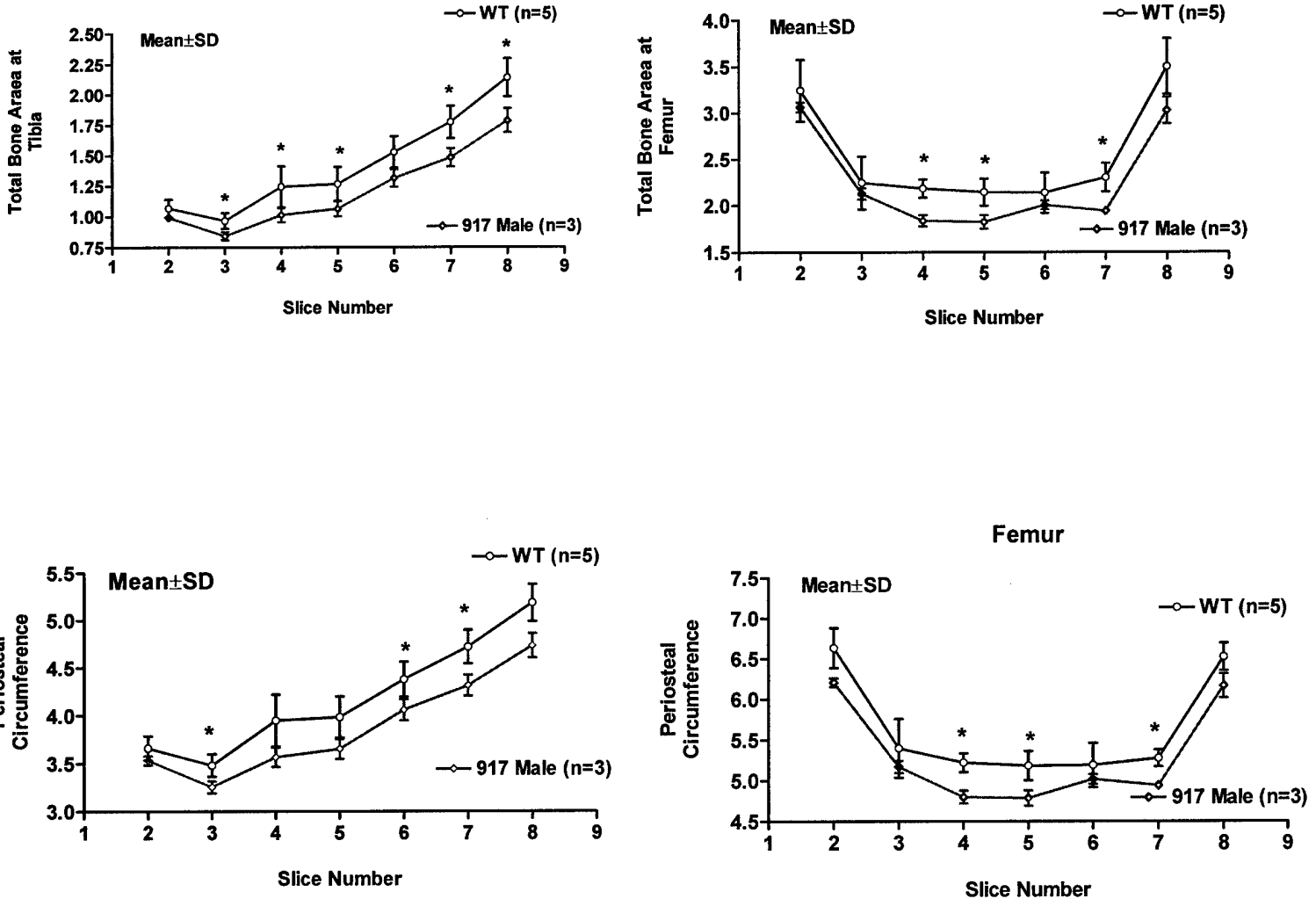

Fig. 6. Ex-vivo bone area measurements in tibia and femur from bone size mutant identified in dominant screen (917M). Bone area and periosteal circumference measured by pQCT in 16-week old progeny from IT crosses. Nine slices covering entire length of the bone (slices 1 & 9 were excluded due to large variation) were scanned. Bone areas of affected 917 male mice were consistently lower over the entire length of tibia and femur as shown with age and sex matched type (WT) mice. *$p<0.05$

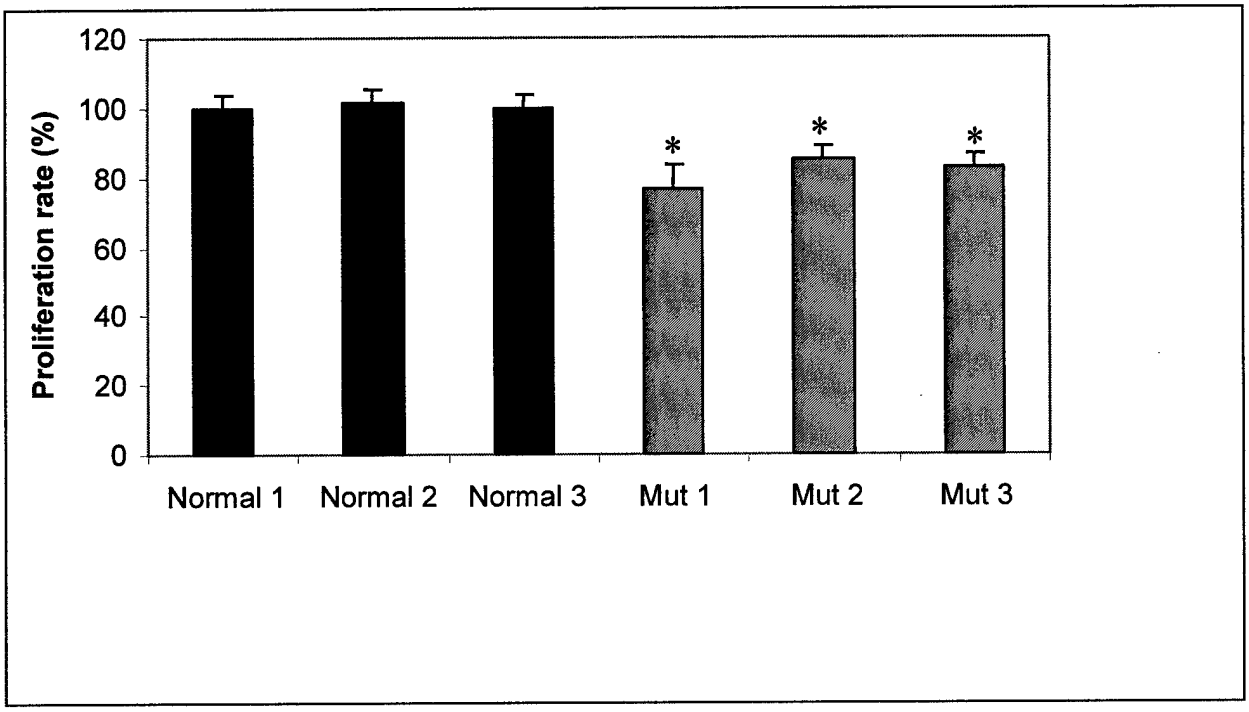

Fig. 7. Basal proliferation rate of periosteal osteoblasts isolated from femur and tibia of 16 week old B6 normal and 917ENU mutant male mice. Periosteal osteoblasts from mutant mice show decreased basal proliferation rate as compared to those from wild type mice. Each bar represent cells from one mouse, the error bars represents mean±SD of 8 measurements (wells), *$p<0.001$.

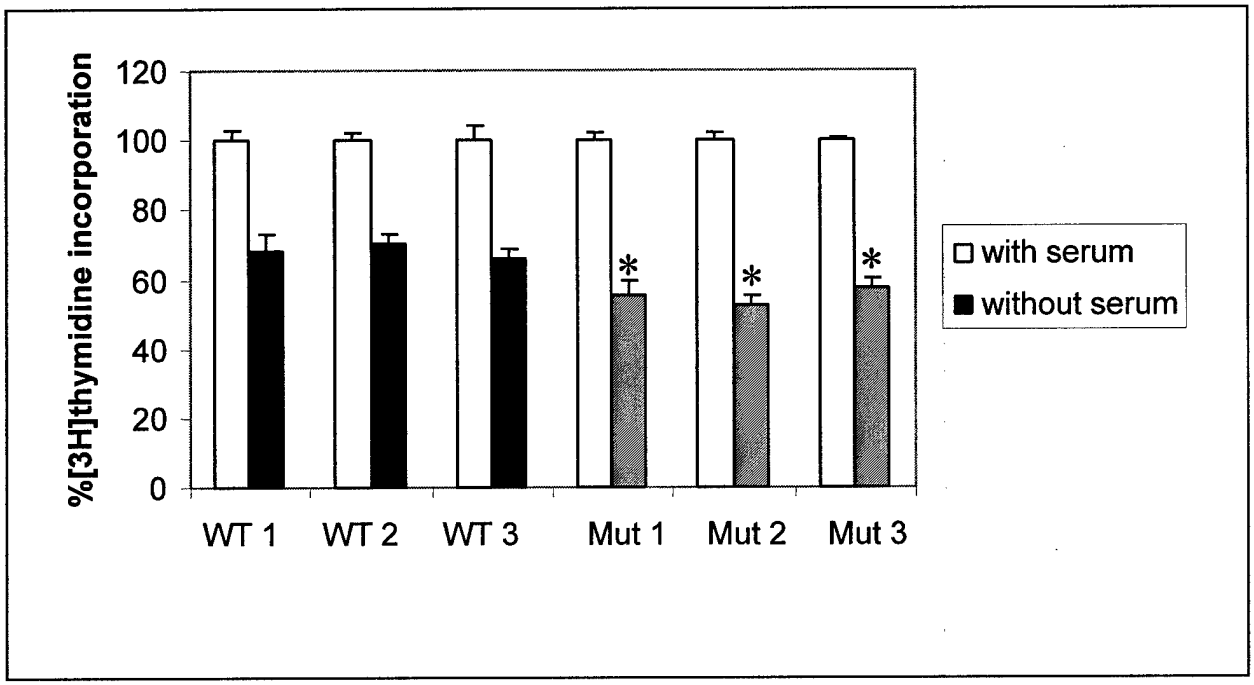

Fig. 8. [^{3}H]-Thymidine incorporation in periosteal osteoblasts from 16 week old normal and 917ENU mutant B6 male mice in presence and absence of 10% FCS. Cells were grown in presence/absence of 10%FCS and [^{3}H]-thymidine incorporation was measured after 48 hours. Periosteal osteoblasts from mutant mice show decreased proliferation in absence of serum as compared to those from wild type mice. Each bar represent cells from one mouse, the error bars represents mean±SD of 8 measurements (wells), *$p<0.01$.

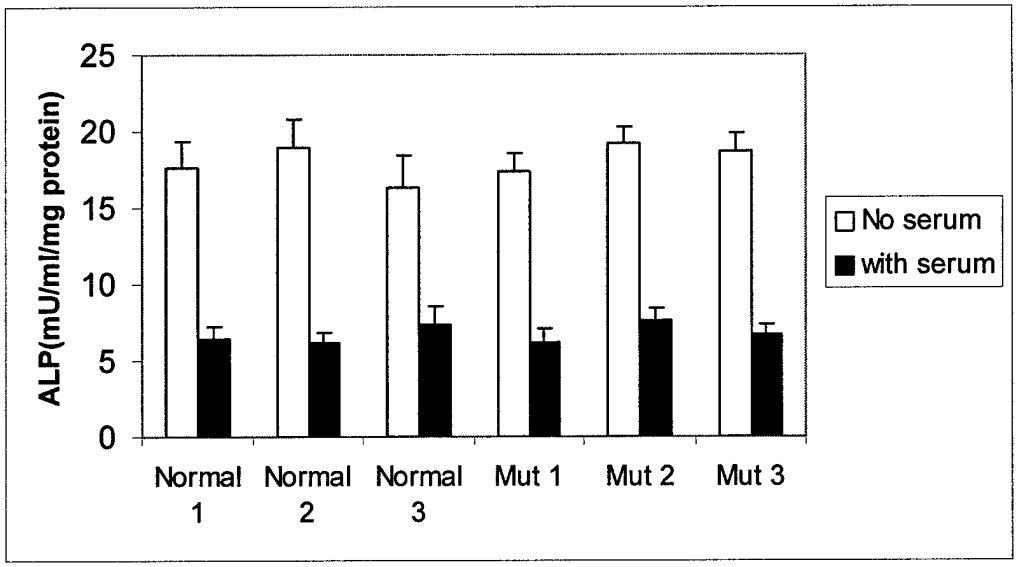

Fig. 9. ALP specific activity in periosteal osteoblasts isolated from femur and tibiae of 16 week old B6 normal and 917ENU mutant male mice. ALP measurements were performed in cells grown with or without 10%FCS. Rate of differentiation was not significantly different in periosteal osteoblasts from mutant mice as compared to those from wild type mice. (Each bar represent cells from one mouse, the error bars represents mean±SD of 12 measurements).

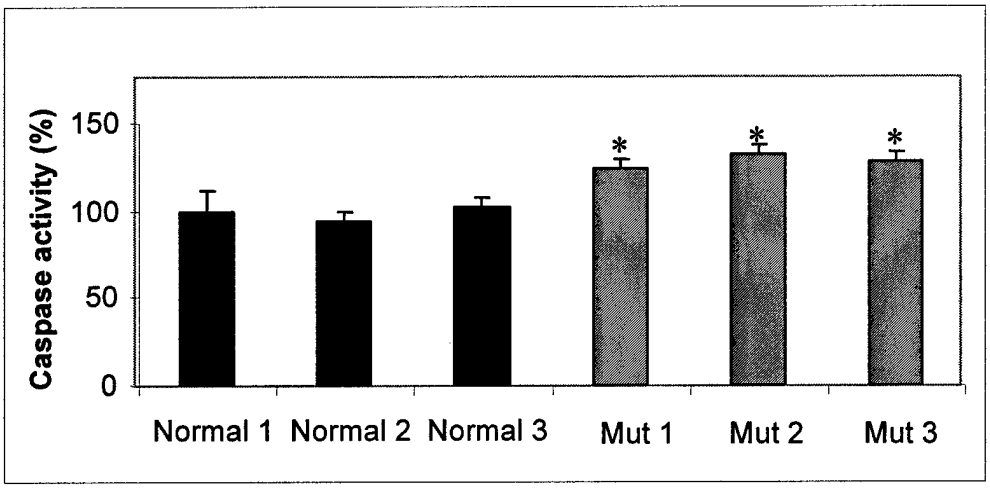

Fig. 10. Caspase activity in periosteal osteoblasts from femur and tibiae of 16-week-old B6 normal and 917ENU mutant male mice. Periosteal cells were incubated (2000 cells/well in 96 well microplates) in presence of 10%FCS for 24 hrs and DEVD-Rhodamine 110 added and further incubated for 2 h. Upon cleavage of the substrate by activated caspases, fluorescence of the released Rhodamine 110 was measured. These data suggest increased rate of apoptosis in cells from mutant mice as compared to cells from wild type mice. Each bar represent cells from one mouse, the error bars represents mean±SD of 8 measurements (wells), *$p<0.01$.

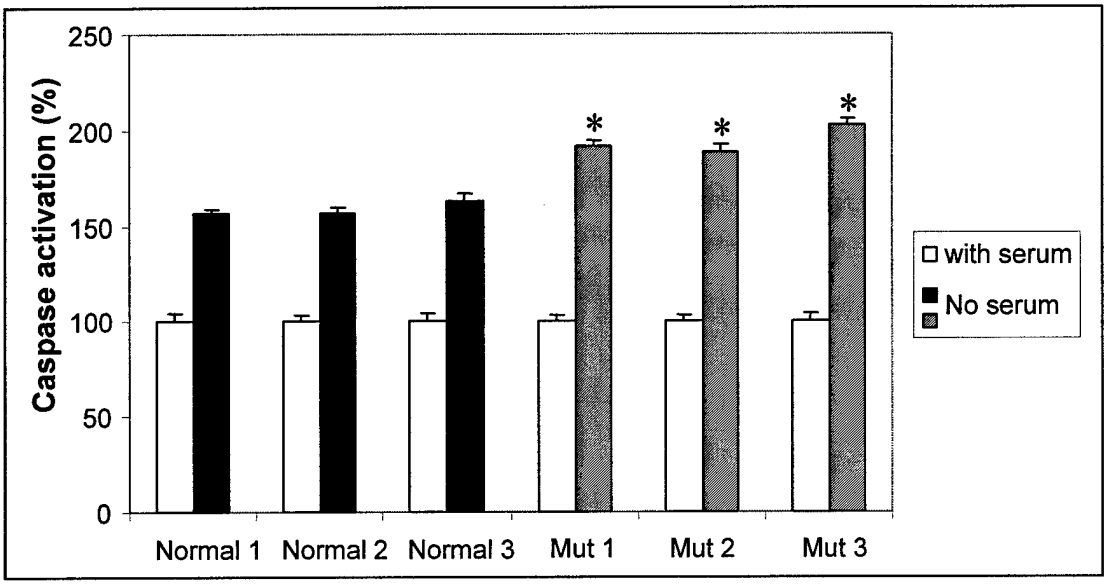

Fig. 11. Caspase activity in 'serum depleted' periosteal osteoblasts isolated from femur and tibiae of 16-week-old B6 normal and ENU mutant male mice. Periosteal cells were incubated (2000 cells/well in 96 well microplates) in presence/ absence of 10%FCS for 14 hrs and DEVD-Rhodamine 110 added and further incubated for 2 h. Upon cleavage of the substrate by activated caspases, fluorescence of the released Rhodamine 110 was measured. These data suggest increased rate of apoptosis in cells from mutant mice as compared to cells from wild type mice. Each bar represent cells from one mouse, the error bars represents mean±SD of 8 measurements (wells), *$p<0.001$)

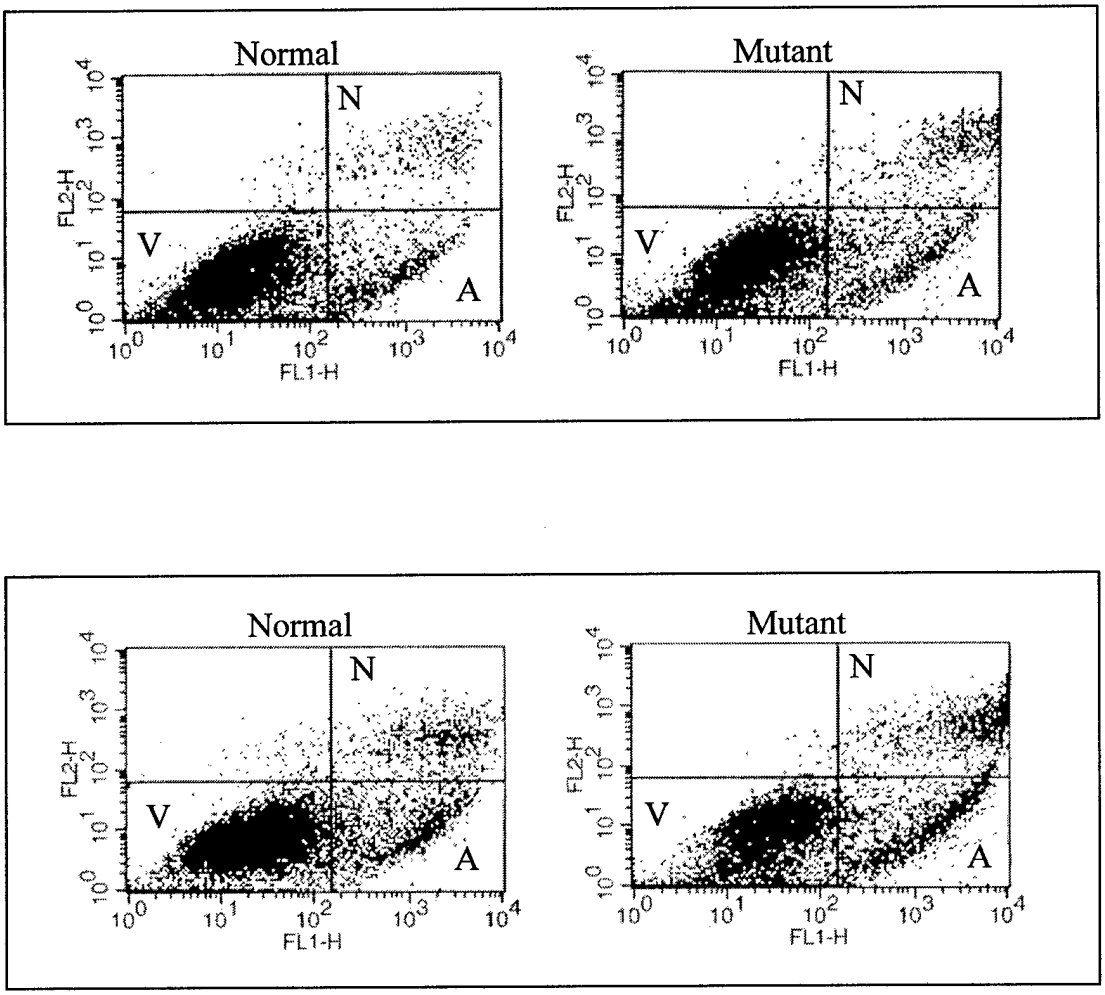

Fig. 12. FACS analysis of periosteal osteoblasts isolated from femur and tibia of 16-week-old normal and 917ENU mutant B6 male mice. Periosteal cells from normal and mutant mice were grown with (upper panel) or without 10% FCS (bottom panel) for 24 hours. Cells were then treated with Annexin V conjugated to Alexa Fluor 488 dye and Propidium Iodide for 15 minutes, followed by flow cytometric analysis. In presence of 10%FCS (upper panel) the 917 mutant cells have a higher percentage (10.38%) of apoptotic cells (indicated by an "A") as compared to normal cells (8.85%). When the apoptosis was induced by serum depletion (bottom panel), the 917 mutant cells were found to have 18.67% apoptotic cells as compared to 13.33% apoptotic cells in normal cell population. V=viable cells, N=necrotic cells.

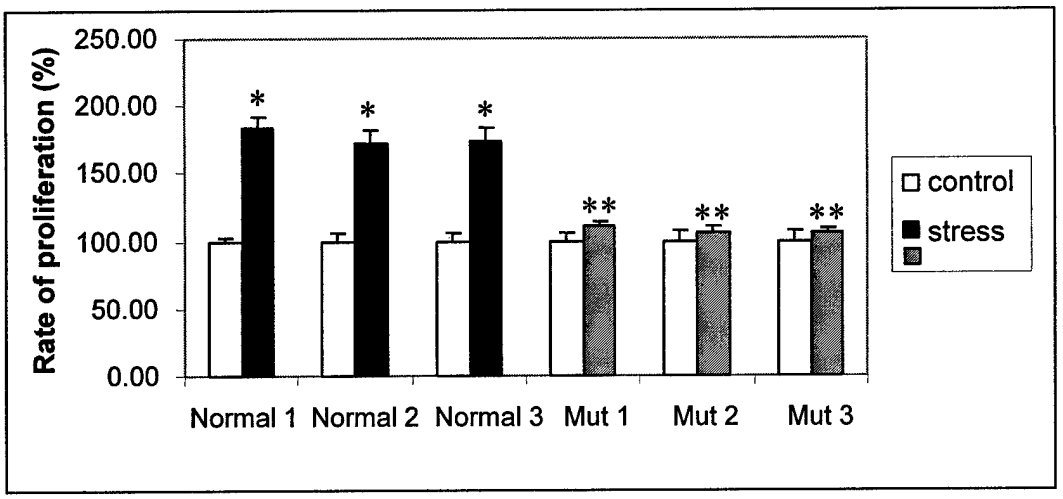

Fig. 13. [^{3}H]-Thymidine incorporation in periosteal osteoblasts from normal and ENU mutant male mice subjected to 30 minute steady fluid flow shear strain. Cells were subject to fluid flow of 20 dynes/cm^2 for 30min. [^{3}H]-Thymidine incorporation was measured after 24-hours. Each bar represent cells from one mouse, the error bars represents mean±SD of 4 measurements (wells), *p<0.001, **p<0.001

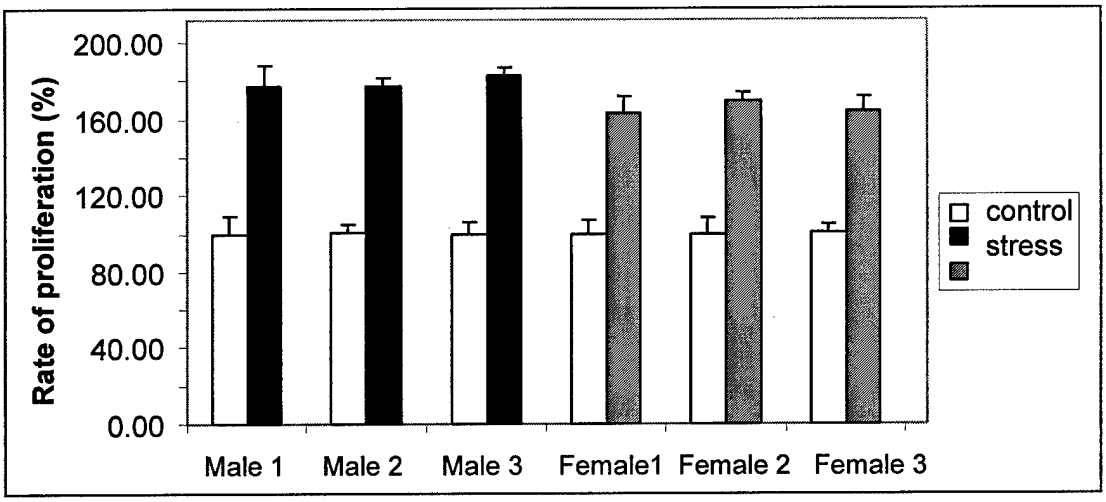

Fig. 14. [3H]-Thymidine incorporation in periosteal osteoblasts from 16 week old normal male and female B6 mice subjected to 30 minute steady fluid flow shear strain. Cells were subjected to fluid flow of 20 dynes/cm^2 for 30min. [3H]-thymidine incorporation was measured after 24hours. Each bar represent cells from one mouse, the error bars represents mean±SD of 4 measurements (wells).

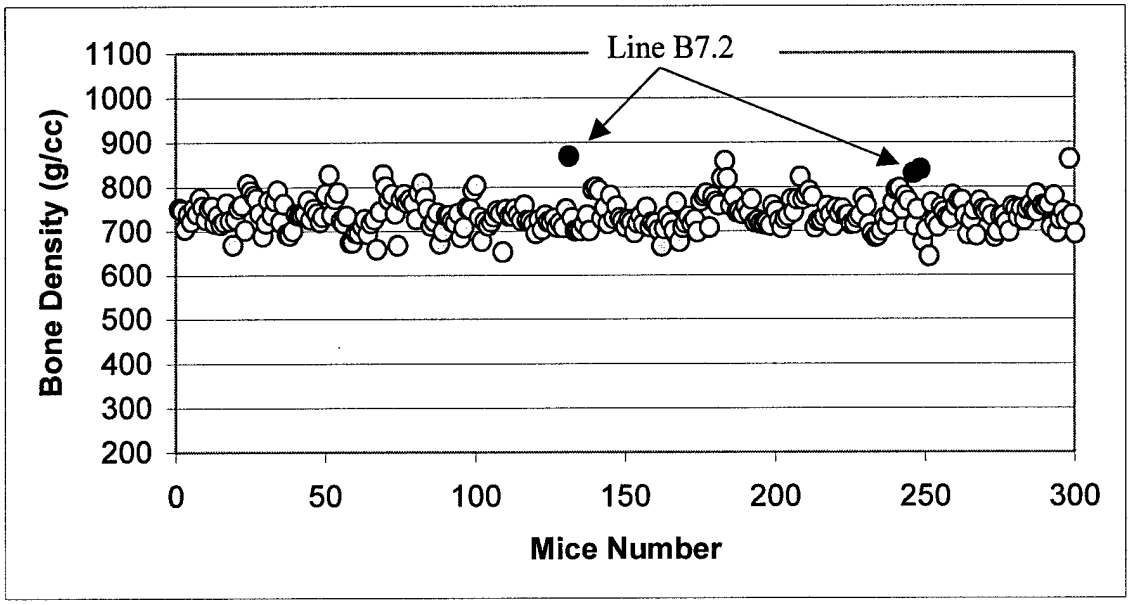

Fig. 15. Representative data on volumetric bone density (measured by pQCT) from 300 B6 mice screened for recessive mutation. Mice indicated by arrow were with high bone density from one founder male (line B7.2).

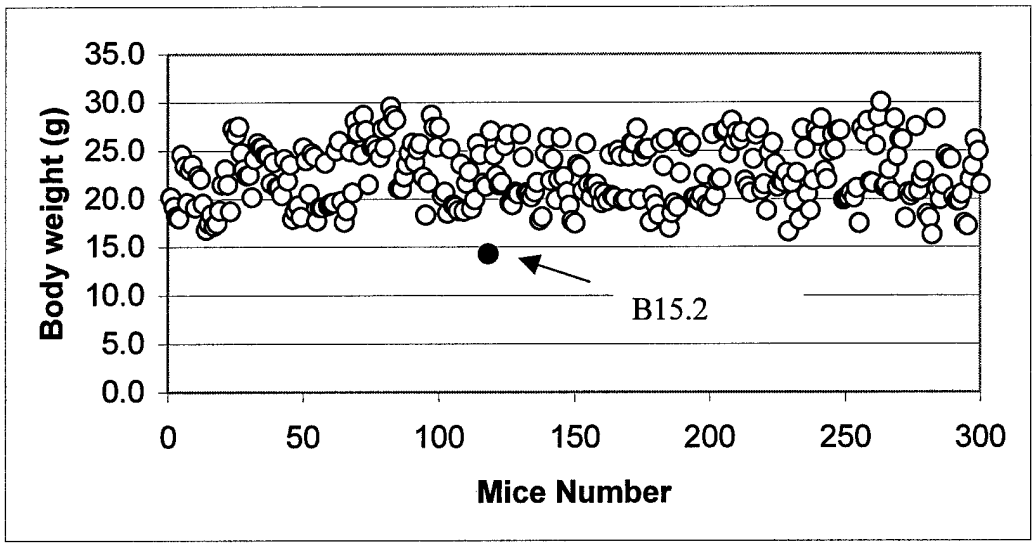

Fig. 16. Representative data on body weight from 300 B6 mice screened for recessive mutation. A mouse indicated by arrow was identified as low body weight and low bone area (line B15.2).

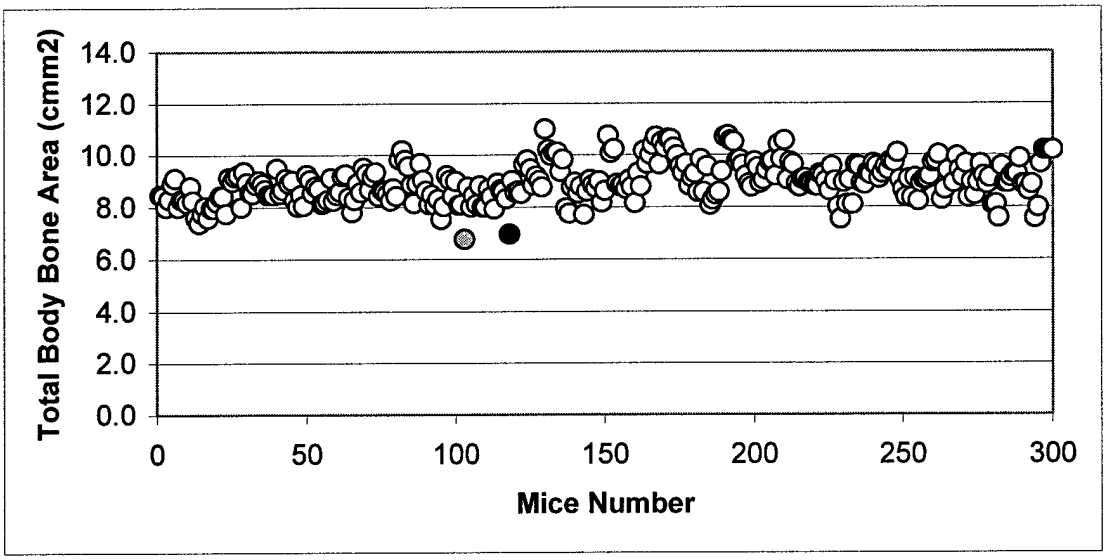

Fig. 17. Representative data on total body bone area (measured by PIXImus) from 300 B6 mice screened for recessive mutation. Two mouse indicated by solid spheres were identified as low bone area; one of the low area mouse was also associated with low body weight (line B15.2) indicated by black sphere.

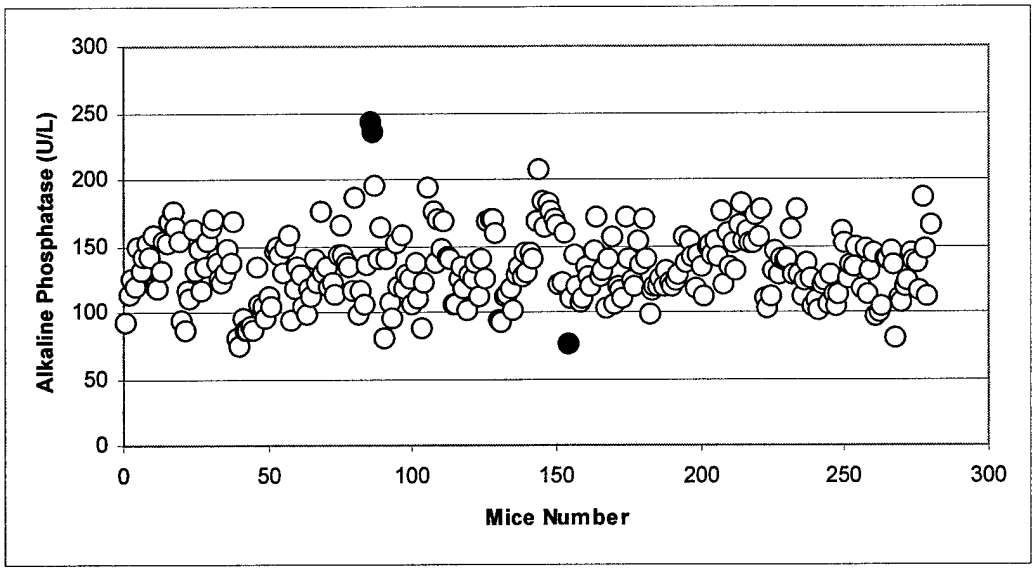

Fig. 18. Representative data on alkaline phosphatase activity (measured by Clinical Chemistry analyzer Hitachi 912) from 300 B6 mice screened for recessive mutation. Two mouse indicated by solid spheres were identified as high alkaline phosphatase activity (Line B5.3), and one with low alkaline phosphates activity (Line B14.2).

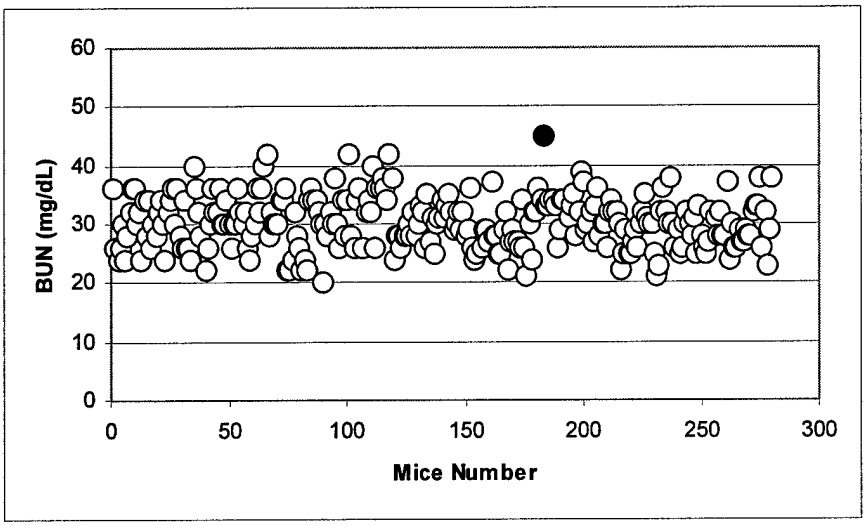

Fig. 19. Representative data on blood urea nitrogen (BUN) (measured by Clinical Chemistry analyzer Hitachi 912) from 300 B6 mice screened for recessive mutation. A mouse indicated by solid sphere was identified as high BUN (Line B7.2).

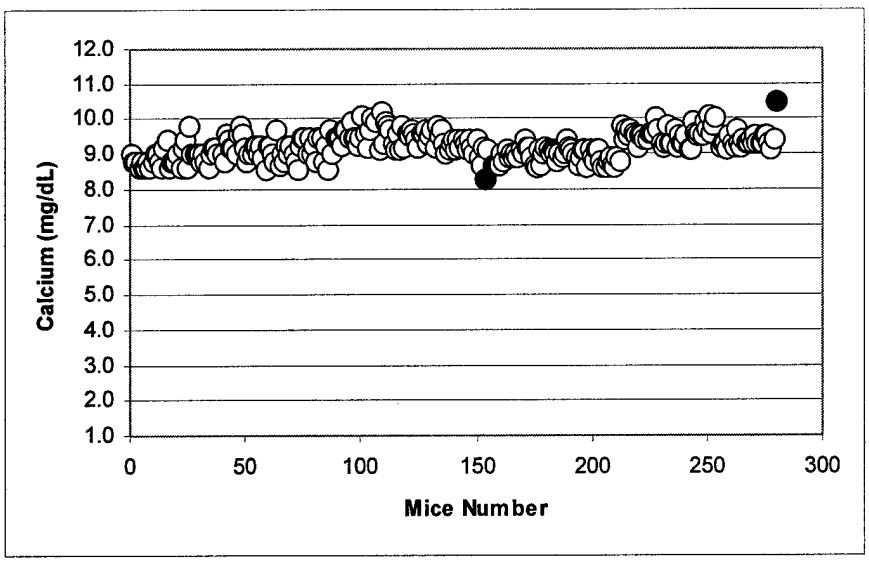

Fig. 20. Representative data on serum calcium levels (measured by Clinical Chemistry analyzer Hitachi 912) from 300 B6 mice screened for recessive mutation. Mice indicated by solid sphere were identified as low (Line 14.4) or high calcium levels (Line B3.5).

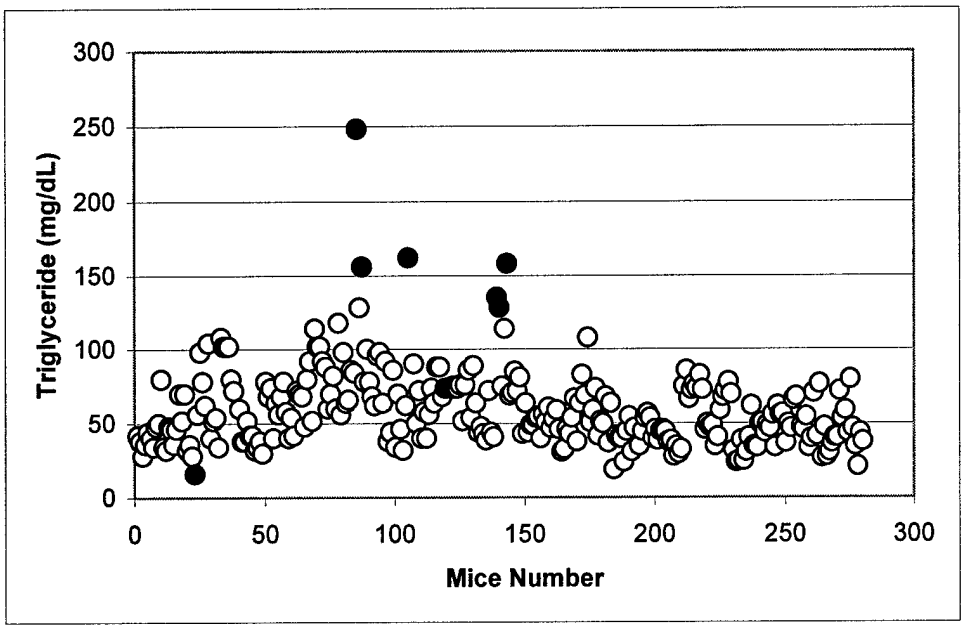

Fig. 21. Representative data on serum triglyceride levels (measured by Clinical Chemistry analyzer Hitachi 912) from 300 B6 mice screened for recessive mutation. . Mice indicated by solid sphere were identified as abnormal triglyceride (Line 5.1 and 5.2 with high) levels. These mice also showed similar lipid profile for total cholesterol and high-density lipid (HDL).

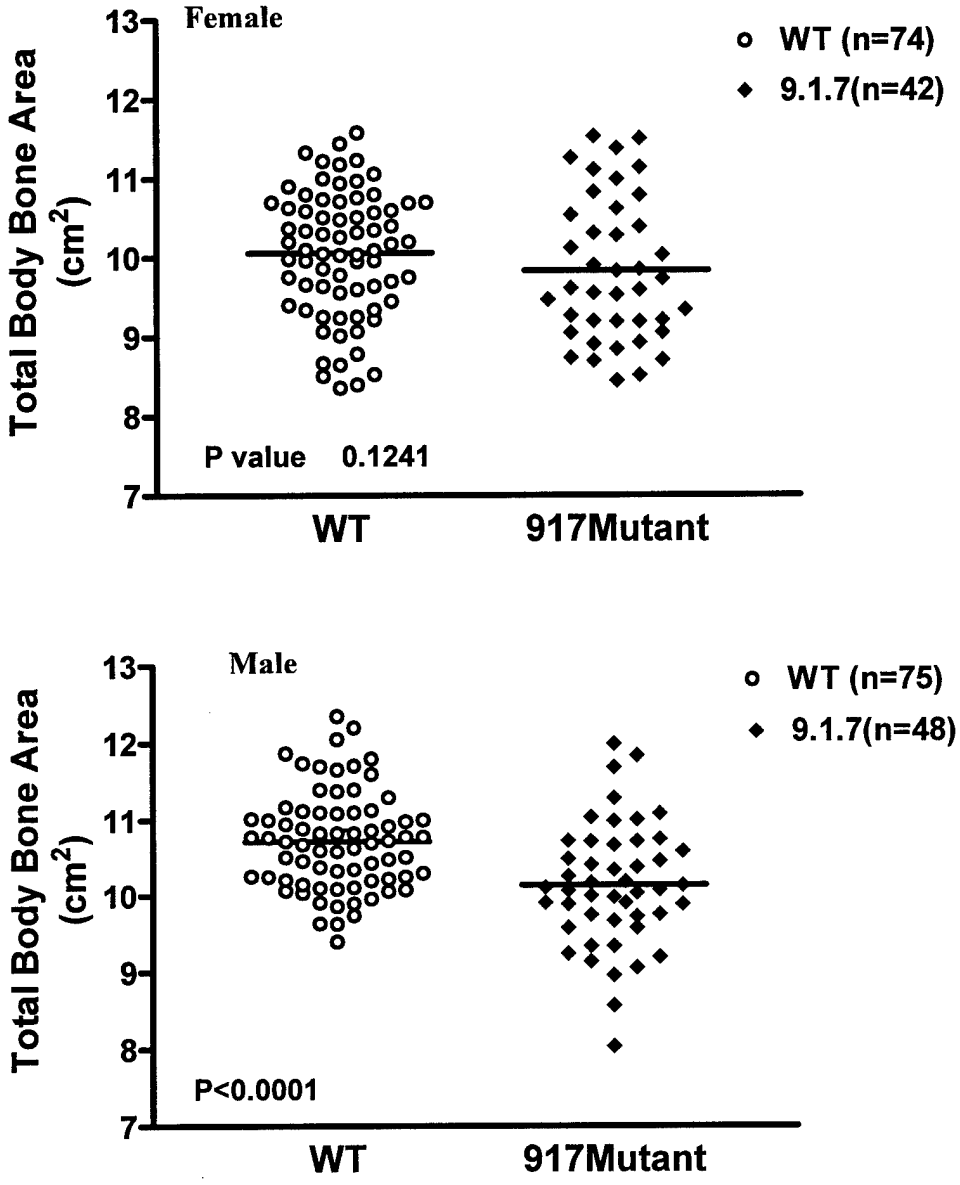

Fig. 22. Phenotype distribution of 917Mutant and wild type F2 population (genotyping). The figure shows total body bone area of 16-week old 917MutantxC3H F2 mice and wild type B6xC3H F2 mice. The 917 B6 mutant, which exhibits low bone area phenotype, was bred with C3H to generate C3H/B6 F1 hybrids, which were then bred (siblings) to generate about 90 F2 male and female mice. The wild type animals are non-mutagenized normal C3H-B6 F2 progeny generated in similar fashion as described for 917mutant F2s. The top graph shows bone area from female F2 mice and bottom graph shows bone area distribution of male mice. Since the mutant phenotype is mainly expressed in males, only male F2 mice show significant different bone area from wild type F2 mice.

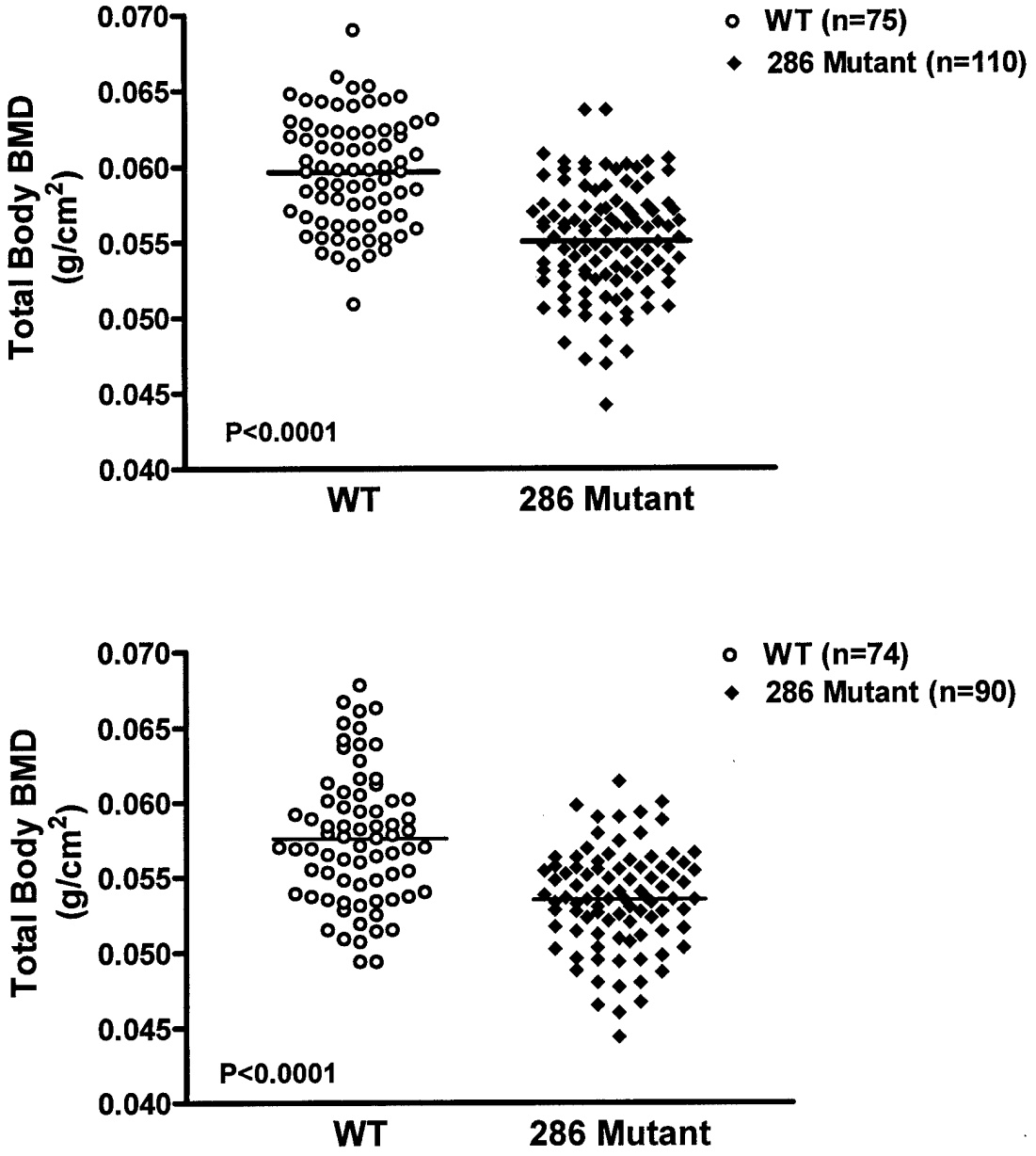

Fig. 23. Phenotype distribution of 286 Mutant F2 population. Total body bone density of 16-week old 286mutantxC3H F2 mice and wild type B6xC3H F2 mice. The 286Mutant (C3H), which exhibits visible and low bone density phenotype, was bred with B6 to generate C3H/B6 F1 hybrids; the littermates were then bred to generate about 204 F2 male and female mice. The wild type animals are non-mutagenized normal C3H-B6 F2 progeny generated in same way as described for 917mutant F2s. The top graph shows bone area from male F2 mice and bottom graph shows bone area distribution of female mice. Similar differences in volumetric BMD density were seen in mutant and wild type F2 population.

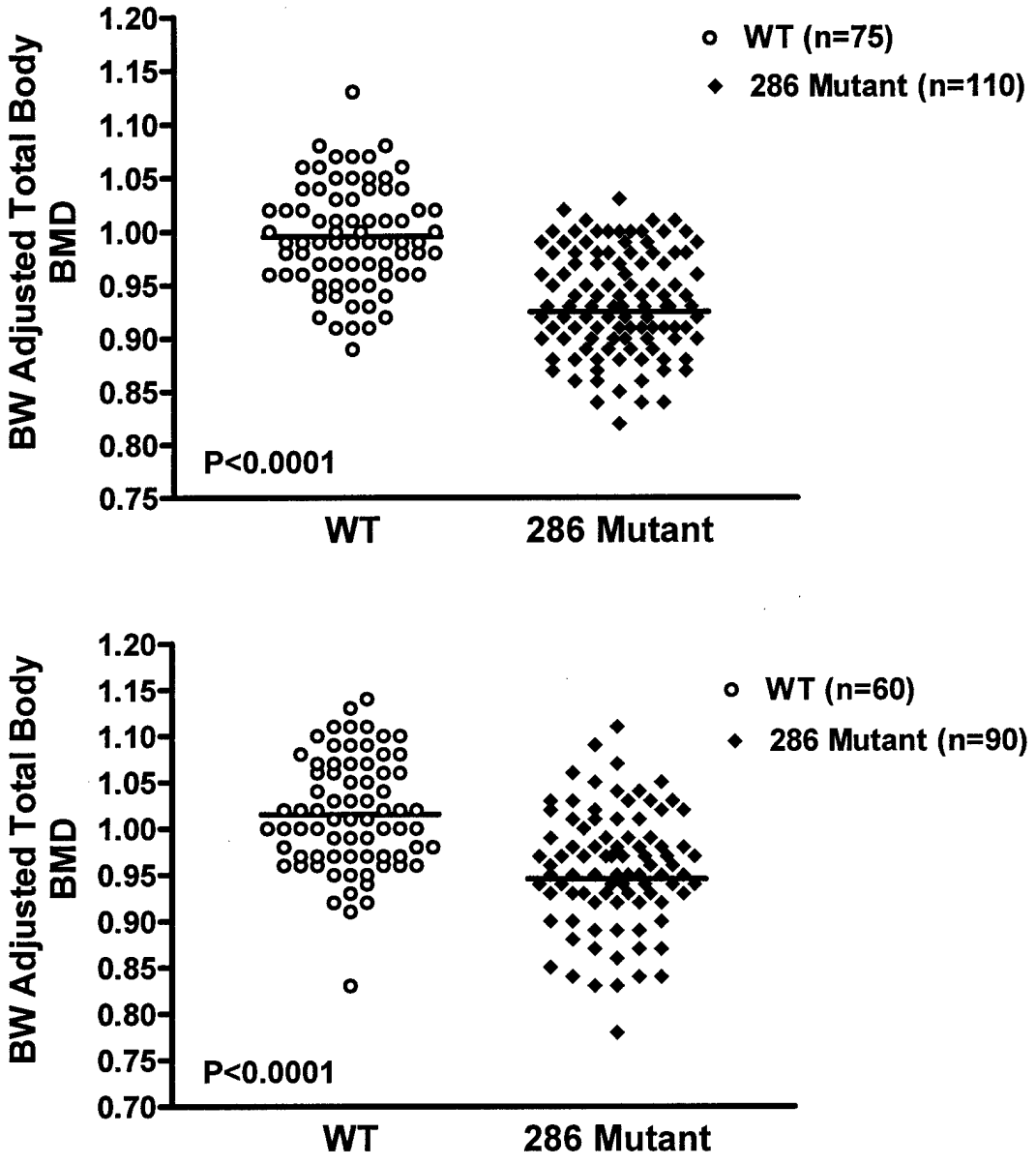

Fig. 24. Phenotype distribution of 286 Mutant F2 population. Body weight adjusted total body bone density of 16-week old 286mutantxC3H F2 mice and wild type B6xC3H F2 mice. The 286Mutant (C3H), which exhibits visible and low bone density phenotype, was bred with B6 to generate C3H/B6 F1 hybrids; the littermates were then bred to generate about 204 F2 male and female mice. The wild type animals are non-mutagenized normal C3H-B6 F2 progeny generated in same way as described for 917mutant F2s. The top graph shows bone area from male F2 mice and bottom graph shows bone area distribution of female mice.

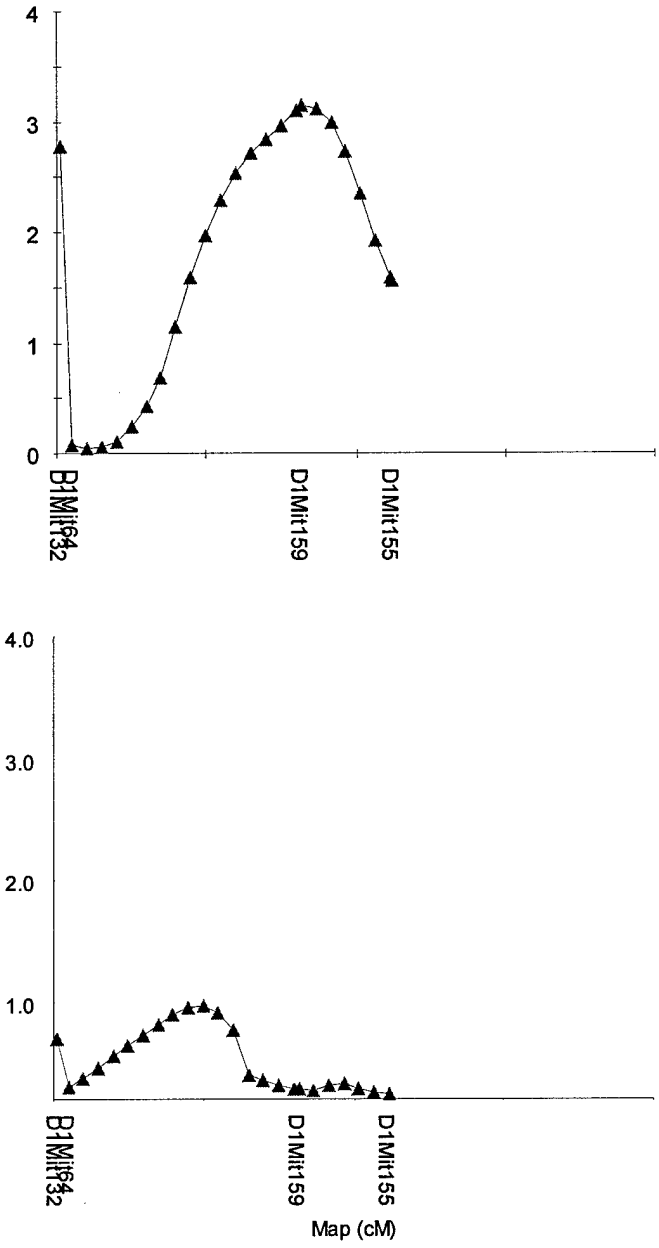

Fig. 25. Interval mapping of low bone area trait at 16-week age showing QTL(s) on chromosome 1. The LOD score is on the Y-axis and location of marker name and distribution in centiMorgans (cM) on the X-axis. The top graph shows QTL from 917Mutant (n=48) and bottom graph shows QTL from wild type population (n=75). Since phenotype is expressed in mainly male mice only males were used for interval mapping. Two suggestive QTLs were observed that associated with marker D1Mit132 (LOD score 2.78, that explained 23% phenotypic variance) and D1Mit159 (LOD score 3.15, that explained 26% phenotypic variance). Both these QTLs were not observed in interval mapping of wild type population.

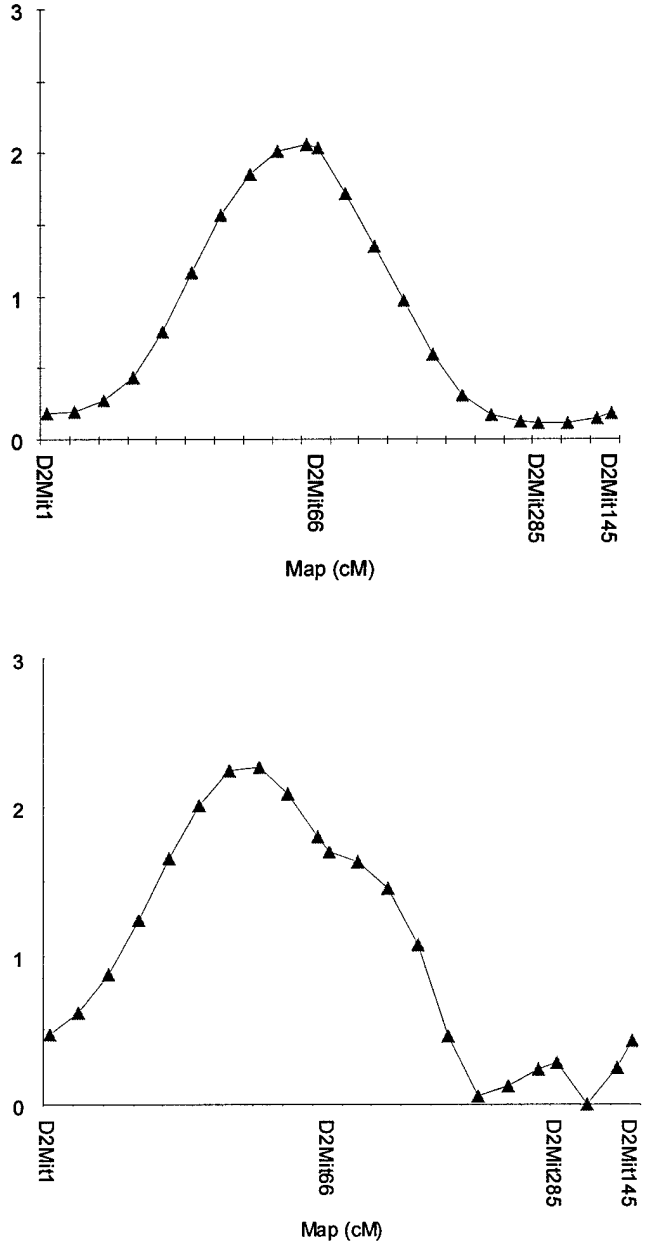

Fig. 26. Interval mapping of low bone area trait at 16-week age showing QTL(s) on chromosome 2. The LOD score is on the Y-axis and location of marker name and distribution in centiMorgans (cM) on the X-axis. The top graph shows QTL from 917Mutant (n=48) and bottom graph shows QTL from wild type population (n=75). Since phenotype is expressed in mainly male mice only males were used for interval mapping. One suggestive QTL was observed that was associated with marker D2Mit66 with LOD score of 2.04 (explained 18% phenotypic variance) in 917 Mutant and LOD score of 1.7 (explained 10% phenotypic variance) in wild type population.

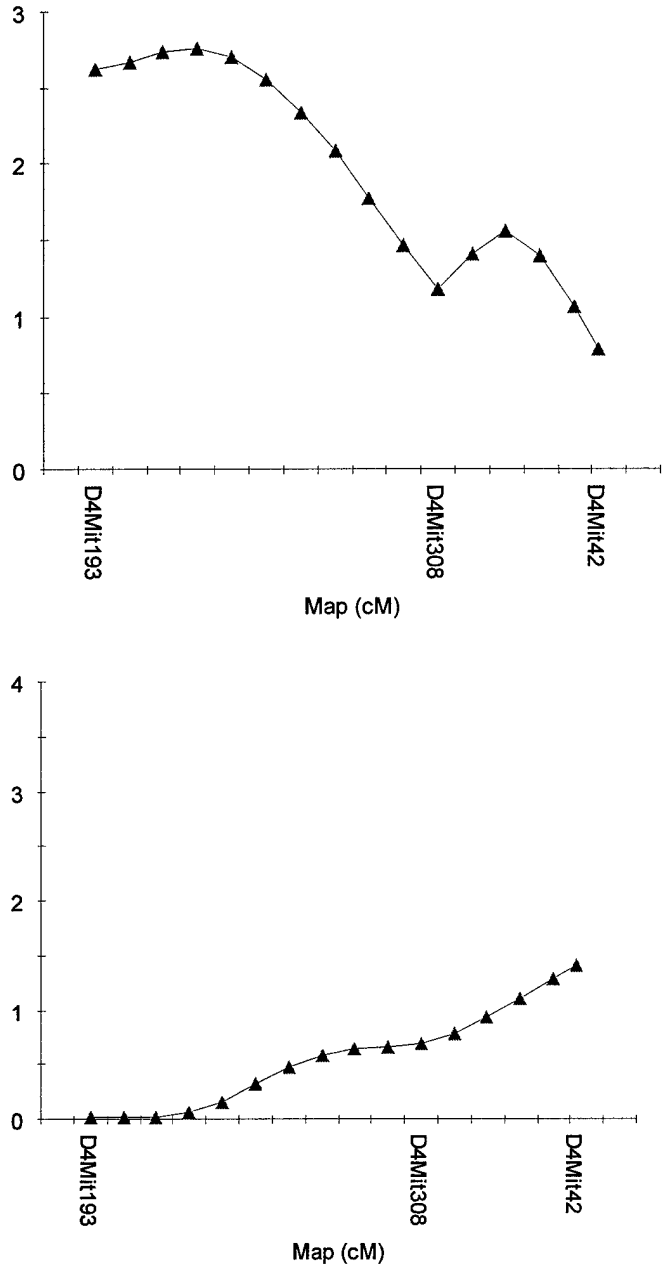

Fig. 27. Interval mapping of low bone area phenotype at 16-week age showing QTL(s) on chromosome 4. The LOD score is on the Y-axis and location of marker name and distribution in centiMorgans (cM) on the X-axis. The top graph shows QTL from 917Mutant (n=48) and bottom graph shows QTL from wild type population (n=75). Since phenotype is expressed in mainly male mice only males were used for interval mapping. One suggestive QTL was observed that was associated with marker D4Mit193 with LOD score of 2.62 (explained 22% phenotypic variance) in 917 Mutant, this QTL was not observed in wild type population.

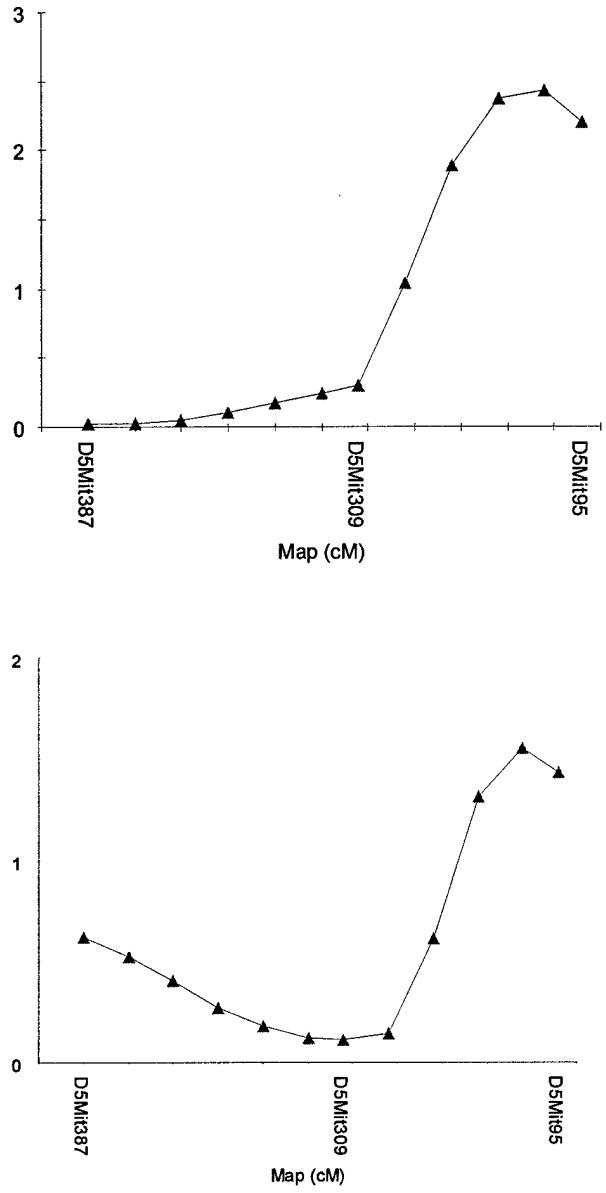

Fig. 28. Interval mapping of low bone area phenotype at 16-week age showing QTL(s) on chromosome 5. The LOD score is on the Y-axis and location of marker name and distribution in centiMorgans (cM) on the X-axis. The top graph shows QTL from 917Mutant (n=48) and bottom graph shows QTL from wild type population (n=75). Since phenotype is expressed in mainly male mice only males were used for interval mapping. One suggestive QTL was observed that was associated with marker D5Mit95 with LOD score of 2.2 (explained 19% phenotypic variance) in 917 Mutant and LOD score of 1.4 (explained 9% phenotypic variance) in wild type population.

Appendices

Abstracts

1. Paper presentation at 25th Annual Meeting of American Society for Bone and Mineral Research, 19-23 September 2003.
Srivastava AK, Mohan S, Wergedal JE, & Baylink DJ. An ENU Mutant Mouse Characterized by the Combination of a Decrease in Bone Size and Increase in Fat Mass with Evidence of Gender Difference. 25th Annual Meeting of American Society for Bone and Mineral Research, Program and Abstracts, Vol 18(1), pS176, September 2003.

Manuscripts

1. Masinde, GL, Wergedal, J, Davidson, H., Li, X, Mohan, S, Baylink, DJ (2003). Quantitative trait loci for periosteal circumference (PC): Identification of single loci and epistatic effects in F_2 MRL/SJL mice. Bone, 32:554-60.

2. Mohan, S., Masinde G., Li X. and Baylink, DJ. (2003). Mapping Quantitative Trait Loci that Influence Serum IGF Binding Protein-5 levels in F2 Mice (MRL/MPJ X SJL/J). Endocrinology,144:3491-6.

3. Li, X., Masinde, G., Gu, W., Wergedal, J., Mohan, S., Baylink, D.J. (2002). Genetic Dissection of Femur Breaking Strength in a large population (MRL-MpJ x SJL/J) of F2 Mice: Single QTL Effects, Epistasis, and Pleiotropy, Genomics 79: 734-40

4. Srivastava A K, Mohan S, Wergedal J E & Baylink DJ. A Genome-wide Screening of N-Ethyl-N-nitrosourea Mutagenized Mice for Musculoskeletal Phenotypes. Manuscript In press BONE, 2003

Print this Page for Your Records Close Window

An ENU Mutant Mouse Characterized by the Combination of a Dcerease in Bone Size and Increase in Fat Mass with Evidence of Gender Differences

A. K. Srivastava, S. Mohan, J. Wergedal, D. J. Baylink. Musculoskeletal Disease Center, J. L. Pettis VAMC, Loma Linda, CA, USA.

Presentation Number: SA111

The N-ethyl-N-nitrosourea (ENU) mouse mutagenesis provides a powerful platform for gene function studies. In our ENU mutagenesis screen for dominant musculoskeletal phenotypes using a C57BL/6J (B6) strain of mice, a phenodeviant was discovered which exhibited a highly significant decrease in bone size attended by an increase in fat mass. This mutant phenotype was confirmed in two generations of inheritance-test crosses with wild type B6 females. The affected progeny from inheritance-tests have 8-9% lower body weight. However, three main parameters that assess bone size such as bone area, bone mineral content (BMC), and periosteal circumference were all significantly lower in affected mice even after adjustment for decreased body weight as shown in the table. Interestingly, the total body bone area phenotype was consistently expressed in males (92% affected), whereas only 6% of females exhibited the phenotype (partial). The males with decreased bone size also showed a 15-20% increase ($p<0.01$ both at 10-weeks and 16-weeks age) in fat mass and a 10% decrease in lean mass, as compared to age and sex matched control male mice. The normal WT B6 males have 10-20% higher bone area ($p<0.0001$) and 6% lower fat mass ($p<0.05$) compared to WT B6 females, whereas mutant males were similar to females littermates in total body bone area (8.79 cm^2 in male Vs 8.96 cm^2 in females, $p>0.05$) and a similar (slightly higher) percent fat mass (15.4% in male Vs 14.0% in female, $p<0.05$). These compositional changes in male mutant mice indicate that the mutant gene may regulate gender differences in bone size and fat mass. In conclusion: 1) a germ line mutant mouse with reduced bone size and increased fat content has been identified using genome wide ENU mutagenesis screen for musculoskeletal disorders; 2) gender specific differences in bone size and fat mass were observed in progeny from a mutant mouse; and 3) based on the past findings, we speculate that mutation may involve the gene(s) pathway accounting for male/female differences in bone size and fat mass.

Mean difference in BW adjusted bone area parameters in 16-week old phenodeviant mice compared to WT

	Total Body Bone Area (Excluding skull area)	Total Bone Area (Tibia Midshaft)	BMC (Tibia Midshaft)	Periosteal Circumference (Tibia Midshaft)
Male (n=21)	-10.4%*	-16.9%**	-11.7%**	-8.8%**
Female (n=36)	-2.6%*	-5.1%*	-1.4%#	-2.4*

#p>0.05, *p<0.05, **p<0.001

ELSEVIER

Bone 32 (2003) 554–560

BONE

www.elsevier.com/locate/bone

Quantitative trait loci for periosteal circumference (PC): identification of single loci and epistatic effects in F_2 MRL/SJL mice

G.L. Masinde, J. Wergedal, H. Davidson, S. Mohan, R. Li, X. Li, and D.J. Baylink*

Molecular Genetics Division, Musculoskeletal Disease Center, J.L. Pettis VA Medical Center and Loma Linda University, Loma Linda, CA 92357, USA

Received 20 August 2002; revised 6 November 2002; accepted 16 January 2003

Abstract

To test the hypothesis that periosteal circumference (PC), which is associated with bone size through cross-sectional moment of inertia (CMI), has heritable components, we performed a linkage analysis using 633 MRL/SJL F_2 mice that have 14% difference in mean PC. PC was determined in femurs by use of peripheral quantitative computerized tomography (pQCT). The genome-wide scan identified nine QTL for PC adjusted by body weight on chromosomes 1 (2 QTL), 2 (2 QTL), 8, 11, 15, 17, and X, which accounted for 38.6% of phenotype variance. QTL on chromosomes 1 (D1Mit33), 8 (D8Mit125), 15 (D15Mit 62), 17 (D17Mit176), and X (DXMit208) were unique for PC adjusted by body weight and femur length, while the remaining PC QTL were shared with body weight but not femur length. Four epistatic interactions were identified which accounted for 37.6% of phenotype variance. There was also evidence of pleiotropic effects on chromosome 11 among four size phenotypes (PC, body length, body weight, bone mineral density, and muscle size), which may represent a common genetic mechanism that may regulate bone size and body size.

Keywords: Periosteal circumference; pQCT (peripheral quantitative computed tomography); Quantitative trait loci (QTL)

Introduction

The ultimate measure of resistance to fracture is bone strength. Recent studies in mice and humans indicated that bone size, shape, architecture, and tissue quality influence bone fragility [1–8]. Cortical stiffness and strength of the bone are essential for preventing a fracture trace from starting [5,9,30,33]. Cortical bone architecture can be analyzed in peripheral quantitative computed tomography (pQCT) scans from which not only the cortical area but also periosteal and endosteal circumference can be derived. Periosteal circumference (PC) is an important indicator of bone size and is closely correlated with bone strength and work to femur failure [10,11,34]. PC as a key measure of bone size can be determined directly using pQCT with high precision. Bone strength is measured by work to femur failure but the precision of measurement for PC is superior to bone strength measurement using the Instron DynaMight Low-Force Testing system (Instron Corp., Canton, MA) [10,11].

Because the inbred strains of mice have been used as a model of human diseases [32], genetic determinants for PC derived from mice studies could be potentially used to understand bone architecture and help to predict the risk of fracture in humans. Most studies to determine bone strength [12–20,30–31] have concentrated on bone density, which is a major determinant of bone strength, but there is now evidence that other factors, in addition to bone density, can impact bone strength [9–11,21–23].

Recent studies on bone mineral density, work to failure at the femur mid-shaft and bone breaking strength, in the same F_2 cross of MRL/MpJ and SJL/J found that the genetic influence on skeletal density, work to failure, and bone breaking strength are complex traits [10,11,19]. However, the genetic regulations for size parameters (i.e., PC), which influence bone strength, have not been investigated through the linkage analysis method in this model.

In this study, we performed a high-density genome-wide scan for chromosomal regions associated with PC in a large

* Corresponding author. Musculoskeletal Disease Center (151), J.L. Pettis VA Medical Center, 11201 Benton Street, Loma Linda, CA 92357, USA
E-mail address: Baylid@lom.med.va.gov (D.J. Baylink).

8756-3282/03/$ – see front matter
doi:10.1016/S8756-3282(03)00063-2

(633, MRL/MpJ × SJL/J) F_2 population. Based on the fact that body length, body weight, and muscle size are polygenic traits, we hypothesized that PC is a quantitative trait that is regulated by unique genes. In this report, we identified nine significant and suggestive QTL for PC adjusted by body weight and six QTL for PC adjusted by femur length, of which five are unique for PC while the remaining four are shared with body weight.

Experimental methods

Parental F_1 and F_2 mice

Four-week-old MRL/MpJ (MRL) female and SJL/J (SJL) male mice were obtained from the Jackson Laboratory (Bar Harbor, ME) and housed at the Animal Research Facility, J.L. Pettis VA Medical Center (Loma Linda, CA), under the standard condition of 14 h light, 10 h darkness, ambient temperature of 20°C, and relative humidity of 30–60%. These two strains were chosen primarily for their extreme differences in wound healing/regeneration. On the basis of the 80% difference in periosteal circumference between MRL and SJL and distinct genetic origins of these two strains, they are also suitable for the proposed study. The F_2 mice were produced by intercross between the (MRL/MpJ × SJL/J) F_1 mice at the Animal Research Facility. A total of 20 MRL, 20 SJL, 36 F_1, and 633 F_2 female mice were utilized in these genetic analyses. The mice were sacrificed at 7 weeks of age and body weights were recorded at necropsy. Livers from each animal were frozen in liquid N_2 for later DNA extraction. Femurs were isolated and stored in 1× PBS buffer at 4°C for later measurement of periosteal circumference. All experimental protocols were in compliance with the Animal Welfare Act and were approved by the Institutional Animal Care and Use Committee (IACUC) of the J.L. Pettis VA Medical Center.

Periosteal circumference

PC was determined using a pQCT with an XCT Research M (Norland Medical System, Fort Atkinson, WI). The precision of this instrument for PC has been determined to be 0.5% by repeated placement and measurement of a single femur [12]. Analysis of the scans was performed using the manufacturer-supplied software program (STRATEC MEDIZINTECHNIK GMBH Bone Density Software, Version 5.40C). PC was corrected for body weight and femur length using the estimating equation for the regression of PC on body weight (PC = 3.49 + 0.0572 * body weight or femur length).

Genotyping

Genomic DNA was extracted from the liver of each animal using commercial DNA extraction kit according to the manufacturer's instructions (Wizard Genomic DNA Purification Kit, Promega). The Mouse Map Pairs Genome-wide Screening Set (410 primer pairs with 3.5 cM average resolution) and additional markers were purchased from Research Genetics (Huntsville, AL) and used for a genome-wide scan. PCR amplifications were conducted in 96-well plates using PTC-225 DNA Engine Tetrad (MJ Research, Watertown, MA) based on Research Genetics Genome Services Protocol. PCR products were separated on 6% polyacrylamide gel and visualized with ethidium bromide staining.

QTL analysis

Since the distribution of periosteal circumference values in F_2 was normally distributed and the majority of loci appeared to have additive effect, we performed interval mapping, a strategy that requires the assumption of normal distribution for the quantitative trait investigated. The interval mapping was performed using the MapQTL software (Version 4.0; Wageningen, The Netherlands) [24]. The critical threshold values for significance of association were determined, by the permutation test [25,26], to be LOD score of 3.5 for significant linkage and 2.7 for suggestive linkage.

Statistical analysis

Computations were performed with the STATISTICA 5.1 (StatSoft Inc., Tulsa, OK) statistical package. Standard two-way analysis of variance was used to evaluate possible interactions between candidate QTL. The markers closely linked to the QTL were used as independent variables and periosteal circumference was used as the dependent variable. Variance for locus–locus interaction was estimated from $V_{\text{locus} \times \text{locus}}$ = (MS effect − MS error)/average sample size [11].

Results

Periosteal circumference in MRL/MpJ, SJL/J, F_1 and F_2 mice

We measured PC in 20 MRL/MpJ (MRL), 20 SJL/J (SJL), 36 (MRLMpJ × SJL/J) F_1 and 633 (MRL/MpJ × SJL/J) F_2 mice and the individual measurement values are presented as a box plot in Fig. 1. Average PC in F_1 mice was similar to that observed in one of the parental strains, MRL mice, suggesting a directional dominance for PC. The two parental strains had 14% difference in the average PC (Fig. 1). The F_2 mice showed a normal continuous distribution (bell shaped), indicating an effect contributed by more than one gene (Fig. 2).

Table 1 summarizes the correlation coefficients among six related phenotypes. PC was significantly correlated to

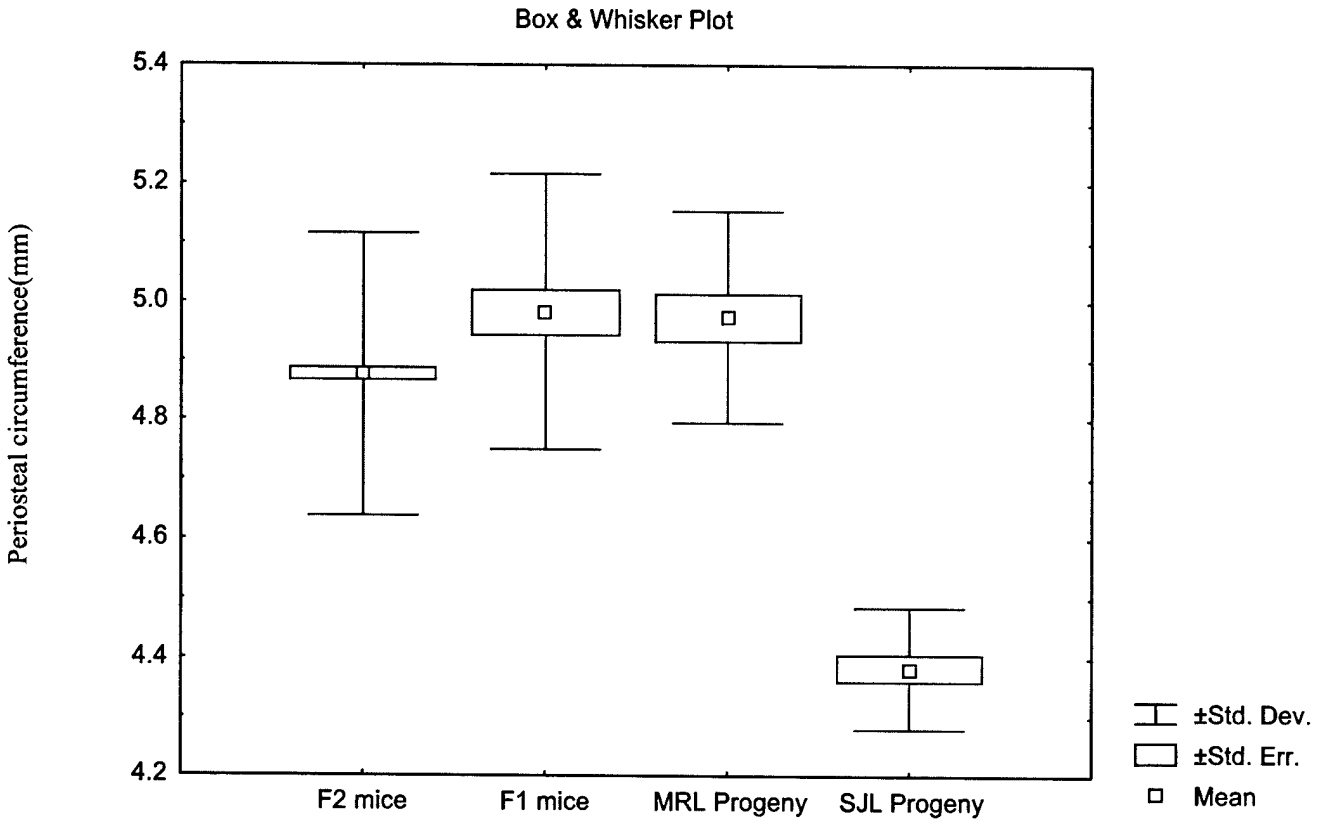

Fig. 1. Box plots of individual PC mean values in parental (MRL and SJL), F_1, and F_2 mice. The mean value for the F_1 and MRL progeny is the same, indicating a directional dominance of PC.

other size phenotypes (femur weight, body weight, body length, femur length, and muscle size).

Genome-wide scan revealed nine significant QTL for PC

Six hundred thirty-three F_2 mice were genotyped for 137 informative markers out of the over 600 screened. These markers covered all 20 chromosomes with a spacing of ≤ 15 cM and an average spacing of 12 cM. Because the distribution of PC values in F_2 was normal, we performed interval-mapping analysis (parametric mapping), using unadjusted PC data and adjusted PC data by body weight or femur length. Table 2a shows 7 significant and 5 suggestive QTL for body weight and 11 significant and 1 suggestive QTL for unadjusted PC, while Table 2b shows 4 significant and 2 suggestive QTL for femur length, 6 QTL for PC adjusted by femur length (2 significant and 4 suggestive), and 9 QTL for PC adjusted by body weight (6 significant and 3 suggestive). Five QTL from chromosomes 1 (D1Mit33), 8 (D8Mit125), 15 (D15Mit62), 17 (D17Mit176), and X (DXMit208) were unique for PC even after adjustment by femur length and body weight, indicating that they are not body or bone size QTL but true PC QTL.

It is clear that many of the loci that affect PC also affect body weight or femur length. These loci may contain genes that affect overall body size or femur length that may influence PC indirectly. To determine the effect of gene loci on bone size that is independent of body weight or femur length we adjusted PC for the effect of body weight and femur length using the estimating equation from the regression of PC on body weight or femur length (equation in methods) prior to QTL analysis. Four of the nine QTL associated with body weight QTL were still significant after adjusting for body weight. These QTL were still significant after adjustment with femur length. These may be due to the genes that have a stronger effect on the bone than on other aspects of body or bone size. Moreover, the adjusted data did identify two additional PC QTL (suggestive) that were not associated with body weight QTL. Thus some PC QTL may be specific for bone size and some may be due to a more generalized effect on body size.

Interaction between loci

We used a two-way ANOVA analysis for evaluating genetic interactions among the loci. The analysis of PC interactions included the test for significant interactions between all markers linked to unadjusted and adjusted PC QTL (Table 3). In addition to analyzing interactions between loci with LOD scores above the level of suggestive

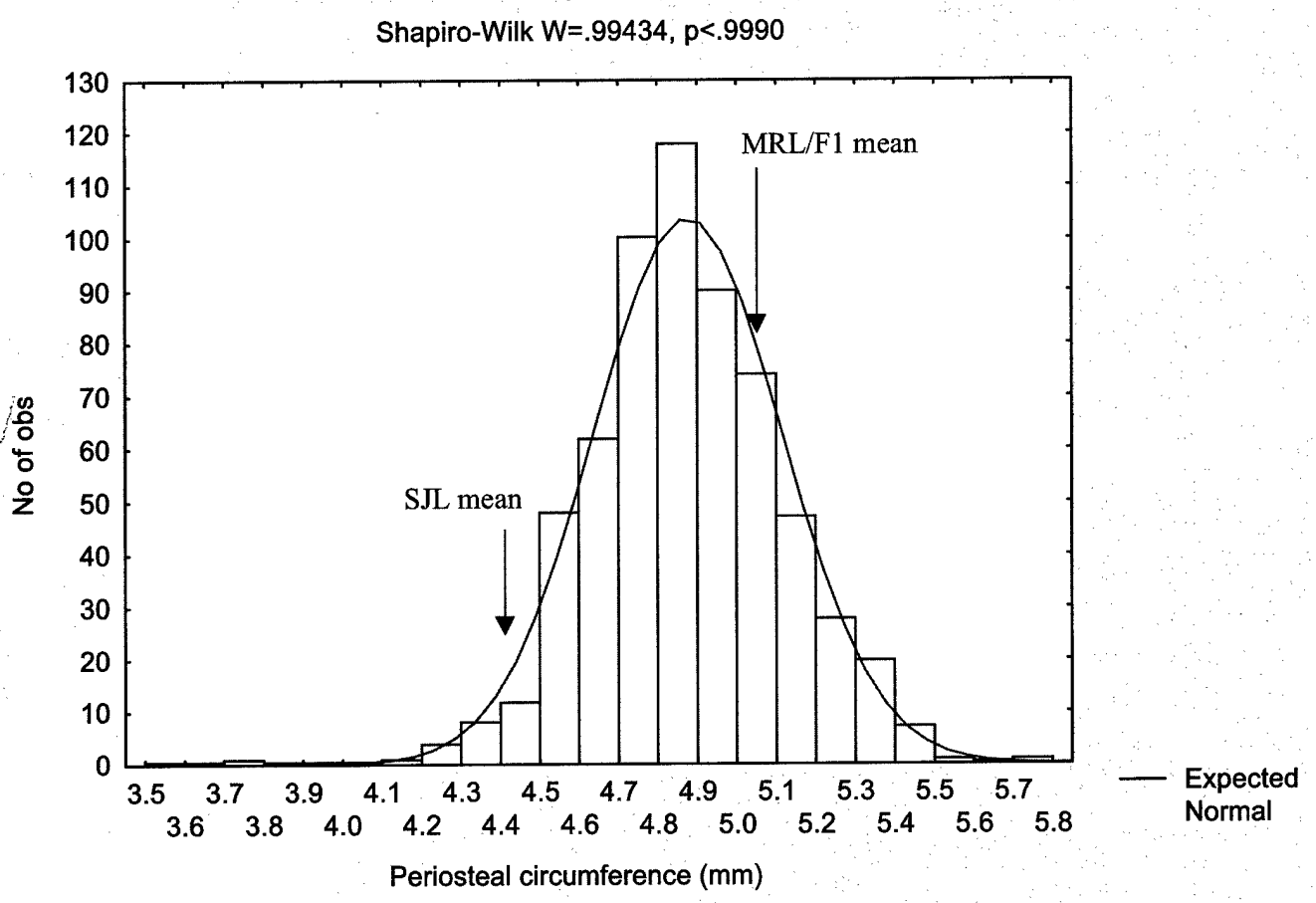

Fig. 2. Distribution of PC values in (MRL/MpJ × SJL/L)F_2 female mice at 7 weeks of age. The bell-shaped line indicates the theoretical normal distribution. The Shapiro–Wilk W test showed that the distribution of PC was not significantly different from normal distribution ($P < 0.9990$). The vertical arrows represent mean values of parental strains.

significance (LOD 2.7), we included all markers with LOD scores greater than or equal to 2.0. From our previous experience, markers with LOD scores of 2.0 and higher could have significant interactions.

Four interactions were significant for PC at $P < 0.003$ (Table 3), which all together explained 37.6% of F_2 variance. Again as for QTL, the two-way ANOVA model does not take into consideration confounding factors and multiple interacting loci so it could be overestimated. One interesting observation for locus–locus interaction worth noting is that one locus (marker) tended to interact with several loci. In this study, DXMit158 interacted with four other loci from chromosomes 1 and 2.

As shown in Table 4, we identified a QTL on chromosome 11 with pleiotropic effects on multiple phenotypes (PC, body weight, femur length, muscle size, and femur weight). This may indicate that there is a common genetic regulation of these phenotypes on chromosome 11 or the genes that regulate them are located in the same QTL.

Table 1
Correlation of periosteal circumference (PC) and other size phenotypes (femur length, body weight, femur weight, body length, and muscle size) with $P < 0.0001$

	Correlation
Femur length	0.33
Body weight	0.60
Femur weight	0.60
Body length	0.53
Muscle size	0.33

Discussion

In this study we analyzed PC phenotype from the F_2 cross of inbred strains of mice, MRL and SJL, that have 14% difference in mean PC. The major findings of this study were: (1) PC is a heritable polygenic trait, (2) PC is regulated by QTL unique to bone as well as those shared QTL with body weight, and (3) epistatic and pleitropic effects are involved in the regulation of PC.

Table 2a
Significant and suggestive QTL for body weight and unadjusted PC

Marker	Distance (cM)	Body weight		Unadjusted PC	
		LOD score	% Explained	LOD score	% Explained
D1Mit44	50.3	5.7	4.0	6.8	4.9
D2Mit62	54.6	8.6	6.0	6.8	4.7
D2Mit263	78.7	7.1	5.7	5.4	4.4
D11Mit36	43.7	3.3	2.6	3.6	2.6
D6Mit123	17.5	4.0	3.8	4.9	4.0
D6Mit291	54.2	3.7	3.0	5.8	4.6
D9Mit90	7.7	6.2	5.4	3.8	3.7
D9Mit263	42.0	3.3	2.3	2.8	2.0
D14Mit194	52.5	2.9	2.5	4.1	3.2
D13Mit207	2.2	4.2	3.7	None	None
D17Mit185	35.0	2.7	2.3	None	None
D8Mit125	15.7	None	None	None	None
D1Mit33	82.0	None	None	4.8	3.3
D15Mit62	33.4	None	None	6.7	5.7
D17Mit176	17.0	None	None	4.6	4.6
DXMit208	18.6	None	None	None	None
Total			41.3		47.7

Single QTL effects

In order to identify QTL that may harbor genes that are involved in the regulation of PC (bone size), a genome-wide scan was performed. Multiple QTL were identified demonstrating that PC is a heritable polygenic trait. To our knowledge, this is the first time that QTL involved in the regulation of PC have been identified. Linkage analysis of the F_2 MRL/SJL mice identified nine chromosomal regions that may harbor genes that influence PC.

The study has identified three different types of PC QTL. First, five QTL were not associated with body weight or femur length QTL. The genes in these sites appear to act uniquely on the bone cross-sectional size. These QTL are of particular interest to the bone field. Second, five QTL disappeared when the PC data were adjusted for body weight. Therefore, these QTL are most likely body size QTL and may contain genes regulating overall body growth. Third four QTL were associated with body weight QTL but did not disappear when the PC data were adjusted for body weight. The genes in these QTL may affect overall growth but in addition have stronger effects on bone. Alternatively, the body weight, femur length, and PC QTL may be due to different genes.

The QTL that were retained but shared with body weight after adjustment of PC by body weight may harbor genes

Table 2b
Significant and suggestive QTL for femur length, adjusted PC with body weight, and adjusted PC with femur length

Marker	Distance (cM)	Femur length		Adjusted PC with femur length[a]		Adjusted PC with body weight[a]	
		LOD score	% Explained	LOD score	% Explained	LOD score	% Explained
D1Mit44	50.3	3.3	2.8	None	None	3.4	2.3
D2Mit32	15.3	5.4	4.7	None	None	5.8	4.2
D2Mit304	59.0	4.9	4.0	None	None	4.2	3.6
D3Mit213	37.2	3.9	3.9	None	None	None	None
D5Mit302	26.2	5.4	5.6	None	None	None	None
D17Mit175	6.6	2.9	4.0	None	None	None	None
D16Mit139	33.9	None	None	3.0	3.9	None	None
D11Mit36	43.7	None	None	3.4	3.2	11.9	9.7
D8Mit125	15.7	None	None	None	None	2.7	2.1
D1Mit33	82.0	None	None	7.7	6.4	5.3	3.9
D15Mit62	33.4	None	None	2.9	3.5	6.2	5.3
D17Mit176	17.0	None	None	2.6	3.4	4.1	4.4
DXMit208	18.6	None	None	5.1	13.1	3.1	3.1
Total			21.0		33.5		38.6

[a] The formula used for adjustment of PC for femur length is 3.4889 + .05719 * Femur Length or Body Weight.

that regulate both bone size (PC) and body size (body weight). It is interesting to note that these shared QTL exhibit different LOD scores for body weight and PC. For example, QTL on chromosomes 11 had a higher LOD score for adjusted PC than body weight. These data suggest that either there are stronger candidate genes for PC than body weight or that epistatic interactions for body weight and bone size QTL may differ.

The phenotypes that have been studied and published using MRL/SJL F_2 mice include work to femur failure [10], femur strength [11] BMD mid-shaft and total body [19] muscle size [27], lean body mass [20] and body weight [20]. The QTL on chromosomes 15 and 16 were unique for PC while the remaining were shared with one or more of the size-related phenotypes (PC, body weight, femur length, muscle size, and femur weight). Also those PC QTL were shared with strength QTL (BMD, work to femur failure, and bone strength) [10,11,19,31,34]. The QTL for PC identified on chromosomes 8, 15, and 17 using MRL/SJL cross have also been identified before in C3H/B6 for CSMI [7,33]. CSMI correlates highly with PC and therefore it is not surprising that they share those QTL [7]. These QTL may be involved generally in the regulation of bone size.

Epistatic effect

In this study, we hypothesized that epistatic interactions might contribute equally in regulating PC. Indeed, a two-way ANOVA test model revealed four significant loci interactions contributing 37.6% phenotypic variance in F_2 mice as compared to 42.5% of PC single QTL effect. This suggests that epistatic interactions play an equally important role as single QTL in the regulation of PC.

Interestingly, loci from chromosome X (DXMit158) interacted with multiple loci from chromosomes 1 and 2. These multiple interactions may suggest that the effect of genes from the X chromosome is manifested when they interact with genes from other chromosomes. Therefore, the male genes (X chromosome) influence bone size (PC) mainly through their interaction with genes from other chromosomes.

Pleiotropic effect

One of the most interesting findings in this study was that the QTL on chromosome 11, with peak marker D11Mit36, is shared by four size phenotypes (PC, muscle size, body length, and body weight). These phenotypes have a pleiotropic effect on each other, suggesting that the genes underlying this QTL may have a general regulatory role on multiple metabolic pathways, which influence growth of bone, muscle, and other tissues. In this regard, nine candidate genes belonging to the same family, the homeobox b (Hoxb1, 2, 3, 4, 5, 6, 7, 8, and 9 genes), are localized on chromosome 11. The Hoxb genes represent one of the important groups of transcription factors that regulate genes that control bone development by regulating osteoblast and chondrocyte differentiation [28]. The Wnt group of genes located on chromosome 11 are known to play a role in the fate of cells in bone and other tissues. Wnt proteins may exert their effects through stromal cells [8,29]. Other candidate genes within the regions identified on chromosome 11 include the genes encoding the signal transduction factors 3, 5a, and 5b (Stat3, Stat5a, and Stat5b).

The two-way ANOVA model used in the identification of loci interactions may have overestimated the interactions because it only took into consideration two but not three or more loci combinations. There is also a possibility of overestimating the interactions, as the two-way ANOVA model does not control for multiple interactions and environmental factors.

Table 3
Periosteal circumference loci that show statistically significant interactions

Loci	*P* value	% Explained by phenotype
D1Mit44 × DXMit158	0.003	8.4
D2Mit62 × DXMit158	0.0005	10.3
D2Mit44 × DXMit158	0.001	9.6
D2Mit304 × DXMit158	0.005	9.3
Total		37.6

Table 4
D11Mit36 marker has a consistent association with PC, body length, body weight, and muscle size, at a LOD score 3.25 and up, suggesting true biological QTL with pleiotropic effect

Phenotype	Peak marker	LOD score	% Explained
Body weight	D11Mit36	3.25	2.6
Body length	D11Mit36	3.28	3.3
PC	D11Mit36	3.53	3.5
Muscle size	D11Mit36	4.24	4.6

Acknowledgments

Assistance Award DAMD17-99-1-9571 supported this work. The U.S. Army Medical Research Acquisition Activity, 820 Chandler Street, Fort Detrick, MD 21702-5014, is the awarding and administering acquisition office. The information contained in this publication does not necessarily reflect the position or policy of the Government and no official endorsement should be inferred. The authors thank the J.L. Pettis VA Medical Center for their support. The authors thank Melanie Hamilton-Ulland for her excellent technical support.

References

[1] Akhter MP, Iwaniec UT, Covey MA, Cullen DM, Kimmel DB, Recker RR. Genetic variations in bone density, histomorphometry, and strength in mice. Calcif Tissue Int 2000;67:337–44.

[2] Deng HW, Deng XT, Conway T, Xu FH, Heaney R, Recker RR. Determination of bone size of hip, spine, and wrist in human pedigrees by genetic and lifestyle factors. J Clin Densitom 2002;5:45–56.
[3] Di Masso RJ, Font MT, Capozza RF, Detarsio G, Sosa F, Ferretti JL. Long bone biomechanics in mice selected for body conformation. Bone 1997;20:539–45.
[4] Duncan CS, Blimkie CJ, Kemp A, Higgs W, Cowell CT, Woodhead H, Briody JN, Howman-Giles R. Mid femur geometry and biomechanical properties in 15- to 18-yr-old female atheletes. Med Sci Sports Exerc 2002;34:673–81.
[5] Jergas M, Gluer CC. Assessment of fracture risk by bone density measurements. Semin Nucl Med 1997;27:261–75.
[6] Nguyen TV, Blangero J, Eisman JA. Genetic epidemiological approaches to the search for osteoporosis genes. J Bone Miner Res 2000;15:392–401.
[7] Turner CH, Hsieh YF, Muller R, Bouxsien ML, Rosen CJ, McCrann ME, Donahue LR, Beamer WG. Variation in bone biomechanical properties, microstructure, and density in BXH recombinant inbred mice. J Bone Miner Res 2001;16:206–13.
[8] Yamane T, Kunisada T, Tsukamoto H, Yamazaki H, Niwa H, Takada S, Hayashi SI. Wnt signaling regulates hemopoeisis through stromal cells. J Immunol 2001;167:764–72.
[9] Ferretti JL. Biomechanical properties of bone. In: Genant HK, Guglielmi G, Jergas M, editors. Bone densitometry. Berlin: Springer-Verlag, 1997. p. 143–161.
[10] Li X, Masinde G, Gu W, Wergedal J, Mohan S, Baylink DJ. Genetic dissection of femur breaking strength in a large population (MRL/MpJxSJL/J) of F2 mice: single QTL effects, epistasis, and pleiotropy. Genomics 2002;79:734–40.
[11] Li X, Masinde G, Gu W, Wergedal J, Hamilton-Ulland M, Xu S, Mohan S, Baylink DJ. Chromosomal regions harboring genes for the work to femur failure in mice. Funct Integr Genom 2002;1:367–74.
[12] Beamer WG, Shultz KL, Churchill GA, Frankel WN, Baylink DJ, Rosen CJ, Donahue LR. Quantitative trait loci for bone density in C57BL/6J and CAST/EiJ inbred mice. Mamm Genome 1999;10:1043–9.
[13] Beamer WG, Shultz KL, Donahue LR, Churchill GA, Sen S, Wergedal JR, Frankel WN, Baylink DJ, Rosen CJ. Quantitative trait loci for femoral and lumbar vertebral bone mineral density in C57BL/6J and C3H/HeJ inbred strains of mice. J Bone Mine Res 2001;16:1195–206.
[14] Benes H, Weinstein RS, Zheng W, Thaden JJ, Jilka RL, Manolagas SC, Reis RJS. Chromosomal mapping of osteopenia-associated quantitative trait loci using closely related mouse strains. J Bone Miner Res 2000;15:626–33.
[15] Drake TA, Schadt E, Hannani K, Kabo JM, Krass K, Colinayo V, Greaser LE, Golden J, Lusis AJ. Genetic loci determining bone density in mice with diet-induced atherosclerosis. Physiol Genom 2001;5:205–15.
[16] Keen RW, Snieder H, Molloy H, Daniels J, Chiano M, Gibson F, Fairbairn L, Smith P, MacGregor AJ, Gewert D, Spector TD. Evidence of association and linkage disequilibrium between a novel polymorphism in the transforming growth factor beta 1 gene and hip bone mineral density: a study of female twins. Rheumatology 2001;40:48–54.
[17] Klein RF, Mitchell SR, Phillips TJ, Belknap JK, Orwoll ES. Quantitative trait loci affecting peak bone mineral density in mice. J Bone Miner Res 1998;13:1657–9.
[18] Koller DL, Liu G, Econs MJ, Hui SL, Morin PA, Joslyn G, Rodriguez LA, Conneally M, Christian JC, Johnstone CC Jr, Foroud T, Peacock M. Genome screen for quantittative trait loci underlying normal variation in femoral structure. J Bone Miner Res 2001;16:985–91.
[19] Masinde GL, Li X, Gu W, Wergadel J, Mohan S, Baylink DJ. Quantitative trait loci for bone density in mice: the genes determining total skeletal density and femur density show little overlap in same F_2 mice. Calcif Tissue Int 2002;71:421–8.
[20] Masinde GL, Li X, Gu W, Davidson H, Hamilton-Ulland M, Mohan S, Baylink DJ. Quantitative trait loci (QTL) for lean body mass: four QTLs and seven epistatic interactions determining lean body mass in (MRL/MpJ and SJL/J) F_2 mice. Funct Integr Genom 2002;2:98–104.
[21] Baylink D, Chesnut CH, III. Non-bone mineral density-related factors of fracture risk. Parthenon Med Commun 2003; in press.
[22] Schneider P, Reiners C, Cointry GR, Capozza RF, Ferretti JL. Bone quality parameters of the distal radius as assessed by pQCT in normal and fractured women. Osteopros Int 2001;12:639–46.
[23] Theodorou DJ, Theodorou SJ, Andre MP, Kubota D, Weigert JM, Sartoris DJ. Quantitative computed tomography of spine: comparison of three-dimensional and two-dimensional imaging approaches in clinical practice. J Clin Densitom 2001;4:57–62.
[24] Van Ooijen JW, Maliepaard C. MapQTL (tm) version 4.0: Software for the calculation of QTL positions on the genetic maps.. The Netherlands: CPRO-DLO, Wageningen, 1996.
[25] Churchill GA, Doerge RW. Empirical threshold values for quantitative trait mapping. Genetics 1994;138:963–71.
[26] Van Ooijen JW. LOD significance thresholds for QTL analysis in experimental populations of diploid species. Heredity 1999;83:613–24.
[27] Masinde GL, Li X, Gu G, Mohan S, Baylink DJ. Quantitative trait loci for muscle size; single QTL and epistatic interactions influencing muscle size in (MRL/MpJ × SJL/J) F_2 mice. Funct Integr Genom 2002;2:120–5.
[28] Horan GS, Kovacs EN, Behringer RR, Featherstone MS. Mutations in paralogous Hox genes result in overlapping homeotic transformations of the axial skeleton: evidence for unique and redundant function. Dev Biol 1995;169:359–72.
[29] Bergwitz C, Wendlandt T, Kispert A, Brabant G. Wnts differentially regulate colony growth and differentiation of chondrogenic rat calvaria cells. Biochim Biophys Acta 2001;1538:129–40.
[30] Seeman E. The structural basis of bone fragility in men. Bone 1999;25:143–7.
[31] Shimizu M, Higuchi K, Bennett B, Xia C, Tsuboyama T, Kasai S, Chiba T, Fujisawa H, Kogishi K, Kitado H, Kimoto M, Takeda N, Matsuchita M, Okumura H, Serikawa T, Nakamura T, Johnson TE, Hosokawa M. Identification of peak bone mass QTL in a spontaneously osteoporotic mouse strain. Mamm Genome 1999;10:81–7.
[32] Smoller JW, Acierno JS Jr, Rosenbaum JF, Biederman J, Pollack MH, Meminger S, Pava JA, Chadwick LH, White C, Bulzacchelli M, Slaugenhaupt SA. Targeted genome screen of panic disorder and anxiety disorder proneness using homology to murine QTL regions. Am J Med Genet 2001;105:195–206.
[33] Turner CH. Biomechanics of bone: determination of skeletal fragility and bone quality. Osteoporos Int 2002;13:97–104.
[34] Yershov Y, Baldini TH, Villagomez S, Young T, Martin ML, Bockman RS, Peterson MG, Blank RD. Bone strength and related traits in HcB/Dem recombinant congenic mice. J Bone Miner Res 2001;16:992–1003.

0013-7227/03/$15.00/0
Printed in U.S.A.

Endocrinology 144(8):3491–3496

doi: 10.1210/en.2003-0042

Mapping Quantitative Trait Loci That Influence Serum Insulin-Like Growth Factor Binding Protein-5 Levels in F2 Mice (MRL/MpJ X SJL/J)

SUBBURAMAN MOHAN, GODFRED MASINDE, XINMIN LI, AND DAVID J. BAYLINK

Musculoskeletal Disease Center (S.M., G.M., X.L., D.J.B.), J. L. Pettis Veterans Administration Medical Center, Loma Linda, California 92357; and Departments of Medicine (S.M., D.J.B.), Biochemistry (S.M.), and Physiology (S.M.), Loma Linda University, Loma Linda, California 92350

Recent studies using twins and inbred strains of mice reveal evidence for genetic mechanisms contributing to variation in circulating levels of IGF-I, IGF-II, and IGF binding protein (IGFBP)-3. To examine the hypothesis that serum IGFBP-5 levels have a strong heritable component, we intercrossed two inbred strains of mice, MRL/MpJ and SJL, which exhibit 79% difference in serum IGFBP-5 levels (554 ± 68 *vs.* 309 ± 51 ng/ml respectively, $P < 0.001$). A genome-wide scan was carried out using 137 polymorphic markers in 633 F2 female mice. Serum IGFBP-5 levels in the F2 progeny showed a normal distribution with an estimated heritability of 74%. Whole genome-wide scans for cosegregation of genetic marker data with high or low serum IGFBP-5 levels revealed six different quantitative trait loci (QTL) in chromosomes 1, 9 (two), 10, and 11 (two), which together explained 24% of F2 variance. Chromosome 11 QTL exhibited the highest LOD score (7.5). Based on the past findings that IGFBP-5 is an important bone formation stimulator, we predicted IGFBP-5 to contribute to bone mineral density variation in F2 mice. Accordingly, we found two of the six IGFBP-5 QTLs (Chrs 1 and 11) identified for serum IGFBP-5 phenotype also showed significant association with total body bone mineral density phenotype (measured by dual energy x-ray absorptiometry) in the F2 mice. (*Endocrinology* 144: 3491–3496, 2003)

IGF-I AND -II ARE GROWTH FACTORS that have both mitogenic and metabolic actions, and participate in the growth, survival, and differentiation of a number of cell types including osteoblasts. The importance of IGFs in regulating bone metabolism is evident from recent studies on skeletal changes using mice with disruption of IGF-I or IGF-II (1–3). The functions of IGFs depend not only on the amount of IGF produced but also on the level of IGF binding proteins (IGFBPs). IGFBPs exert the traditional functions of binding proteins, whereby they modulate the half-life and activity of IGFs. In addition, some of the IGFBPs have been shown to act via mechanisms independent of IGFs (4–6). Of the six high-affinity IGFBPs produced by osteoblasts, IGFBP-5 has several distinct features that suggest it is a key component of the IGF system in bone: 1) IGFBP-5 is the most abundant IGFBP stored in bone, where it is bound to hydroxyapatite and extracellular matrix proteins, binding that provides a mechanism to fix IGFs in bone for subsequent release in a regulatable manner; 2) IGFBP-5 has consistently been shown to stimulate bone formation parameters *in vitro* and *in vivo*; 3) IGFBP-5 shows considerable changes in clinical disease states and correlates with changes in bone formation; and 4) IGFBP-5 can also function as a growth factor in addition to its role as a traditional binding protein as evident from recent studies using IGF-I knockout mice (7–16).

In clinical studies, we found evidence that serum level of IGFBP-5 correlated positively with bone mineral density (BMD) (14, 16, 17). Furthermore, it was found that there was considerable interindividual variation in circulating levels of IGFBP-5 in normal human individuals (14, 16, 17). In terms of potential factors that could contribute to variation in circulating levels of IGFBP-5, a number of possibilities exist, including differences in GH secretion, nutritional uptake, proteolysis, and genetic makeup (5, 16, 18). Of these variables, the genetic component is proposed to exert a significant influence on circulating levels of IGFBP-5 based on several findings. First, Kao *et al.* (19) demonstrated for the first time that the variation in IGF-I levels in healthy twin children is almost completely of genetic origin. Second, Harrela *et al.* (20) showed that, in adults, there is a substantial genetic contribution responsible for interindividual variation of the circulating levels of IGF-I, IGF-II, and IGFBP-3. Third, Rosen *et al.* (21) showed that serum IGF-I levels in C57BL/C3HHeJ F2 mice are inherited as a polygenic trait. Based on these data, we proposed that serum IGFBP-5 level, like IGF-I, has a strong heritable component and is controlled by one or more genes. To evaluate this hypothesis, we performed quantitative trait loci (QTL) studies using two inbred strains of mice that exhibit extreme differences in serum levels of IGFBP-5.

Materials and Methods

Mice

The inbred strains, MRL/MpJ (MRL) and SJL/J (SJL) were purchased from The Jackson Laboratory (Bar Harbor, ME) and maintained under 14-h light, 10-h dark cycles. MRL females were mated to SJL males to produce the F1 progeny, which were then intercrossed to produce F2 progeny. These inbred strains of mice were selected from our study of twenty different strains that were used for ear regeneration studies (22, 23). Parental strains, F1, and F2 mice were killed at 7 wk of age and used for phenotypic and genotypic measurements. GH-deficient *lit/lit* and control *lit/+* mice were generated using breeding pairs of *lit/+* mice

Abbreviations: BMD, Bone mineral density; IGFBP, IGF binding protein; QTL, quantitative trait loci.

kindly provided by Dr. L. R. Donahue (The Jackson Laboratory). Due to a spontaneous mutation in GHRH receptor molecule, the *lit/lit* mice (C57BL/6J) are deficient in GH and are 50% smaller than that of corresponding control *lit/+* mice (24). Serum samples were collected from 8-wk-old *lit/lit* and *lit/+* mice and frozen at −70 C for IGFBP-5 measurements. The experimental protocols were in compliance with animal welfare regulations and approved by the Jerry L. Pettis VA Medical Center.

Serum IGFBP-5 measurements

Serum IGFBP-5 was measured by a RIA that has been validated in our laboratory for measurement of serum IGFBP-5 levels in mice. Recombinant human IGFBP-5 was used as a standard and tracer. Antibodies against recombinant human IGFBP-5 were raised in guinea pigs as described previously (25). IGFBP-5 antiserum that showed cross-reactivity with mouse IGFBP-5 was selected for RIA. Mouse serum samples were diluted 1:10 before assay. The inter- and intraassay coefficient of variation for this assay is less than 10%. The sensitivity of the assay is 10 ng/ml. None of the other IGFBPs showed significant cross-reactivity in this assay.

Serum IGF-I levels. Serum IGF-I levels were measured in MRL and SJL mice by a RIA as previously described (26). IGFs were separated from IGFBPs by an acid gel filtration protocol using BioSpin column as described previously (26).

Bone densitometry

Total body BMD was measured using PIXIMUS densitometer (Lunar Corp., Madison, WI) as described previously (27). The precision of PIXIMUS for measurement of total body BMD is less than 2%.

Genetic analysis

Genomic DNA was extracted from liver using a commercial DNA extraction kit (Promega Corp., Madison, WI). Genotyping of individual mouse DNAs was accomplished by PCR with oligonucleotide primer pairs for microsatellite markers that were purchased from Research Genetics, Inc. (Huntsville, AL). A total of 600 primer pairs were tested for polymorphism between the two inbred strains to identify 137 markers with distinguishable polymorphisms that were used for genotyping. The conditions for PCR cycling were set as described previously (23, 27). PCR products were separated on 6% polyacrylamide gel, stained with ethidium bromide and visualized by the Chemilmager 4400 Low Light Imaging System (α Innotech, San Leandro, CA). Alleles derived from the MRL/MpJ parent were designated "A", SJL/J-derived alleles designated as "B," and MRL/SJL heterozygotes as "H" in data analyses (23, 27).

Statistical analysis

Genotype data were analyzed using a MAPQTL (4.0) program (DLO Center for Plant Breeding and Reproduction Research, Wageningen, The Netherlands). MAPQTL interval mapping was used for QTL mapping and the LOD score significance thresholds were calculated using MAPQTL permutation test (23, 27). The LOD score is a statistical test for measuring the probability that there is a linkage of loci with a given phenotype. QTL with an LOD score of more than 3.5 is considered to be significant while those QTL with a LOD score of more than 2.7 are considered to be suggestive (28). The broad sense of heritability was estimated by using variances obtained from parental strains, F1 and F2 mice as previously described (23, 27).

Results

Validation of IGFBP-5 RIA for measurement of IGFBP-5 in mouse serum samples

To determine whether human IGFBP-5 RIA could be applied for measurement of immunoreactive IGFBP-5 in mouse serum, we tested various IGFBP-5 antisera raised in guinea pigs (25) for competition experiments. We found that one out of the five guinea pig IGFBP-5 antisera tested showed significant cross-reactivity with IGFBP-5 present in mouse serum (data not shown). Figure 1 shows that mouse serum inhibited the binding of [^{125}I]IGFBP-5 to IGFBP-5 antibody raised against human IGFBP-5 in guinea pig in a parallel manner. This antiserum detected IGFBP-5 in human serum as expected. To further validate the IGFBP-5 RIA for measurement of IGFBP-5 in mouse serum, we compared IGFBP-5 levels in GH-deficient *lit/lit* and corresponding control *lit/+* mice. Based on previous findings that GH is a major regulator of serum IGFBP-5 levels, we predicted serum levels of IGFBP-5 to be significantly low in *lit/lit* mice. Figure 2 shows that serum IGFBP-5 level was reduced by 70% in *lit/lit* mice compared with corresponding age-matched control mice.

Serum IGFBP-5 levels are heritable

MRL mice exhibit 79% higher serum levels of IGFBP-5 compared with SJL mice (Fig. 3). Interestingly, serum IGF-I levels were also significantly higher in the MRL mice compared with SJL mice (579 ± 89 *vs.* 425 ± 61 ng/ml, n = 20 per group; $P < 0.001$). F1 mice have a mean serum IGFBP-5 level closer to the MRL parent than to the intermediate level between MRL and SJL parents (Fig. 3). These data suggest that the MRL parent may contain a dominant gene that contributes to high serum IGFBP-5 levels.

Frequency distribution of serum IGFBP-5 in F2 mice is not significantly different from the theoretical normal distribution (Fig. 4). Whereas a majority of the F2 mice exhibit serum IGFBP-5 levels between the two parental strains, few F2 mice exhibit higher or lower serum IGFBP-5 levels than MRL and

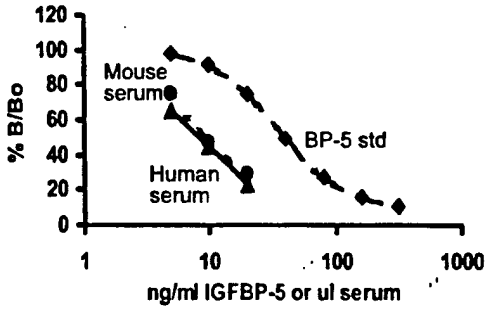

FIG. 1. IGFBP-5 RIA reactivity with human and mouse serum. Displacement of [^{125}I]IGFBP-5 tracer from IGFBP-5 antiserum by the recombinant human IGFBP-5 standard and by human and mouse serum. The y-axis values (B/Bo) ratio are the counts per minute of tracer assayed in the presence of competitor divided by the counts per minute of tracer determined in the absence of competitor.

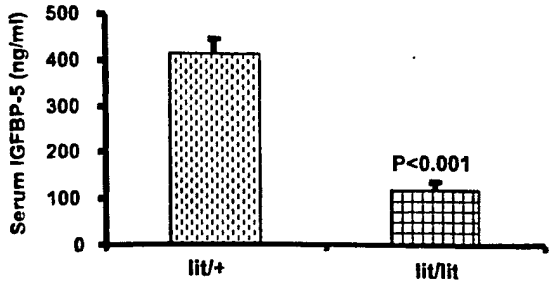

FIG. 2. Serum IGFBP-5 levels in GH-deficient *lit/lit* and control mice. Values are mean ± SD of six mice per group.

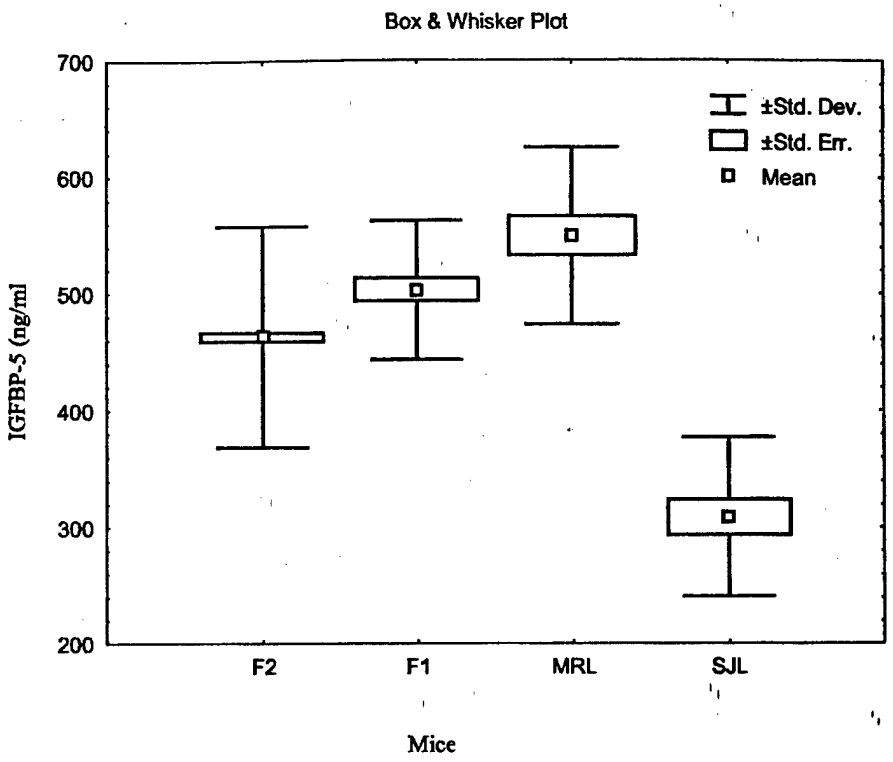

FIG. 3. Serum levels of IGFBP-5 in parental strains, F1 and F2 mice. Twenty MRL, 10 SJL, 36 F1, and 633 F2 mice were used for evaluation. Mean, SD, and SEM of different groups are shown by Box and Whisker plot. Each group is significantly different from other groups by ANOVA.

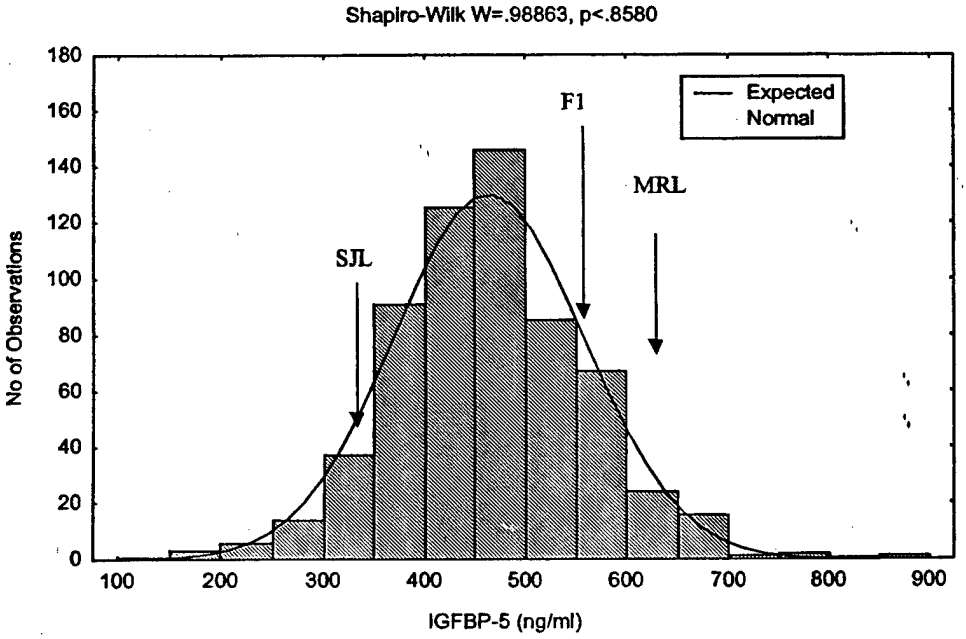

FIG. 4. Normal distribution of serum IGFBP-5 levels in MRL X SJL F2 mice at 7 wk of age. The *bars* show frequency histogram for serum IGFBP-5 levels, whereas the *line* shows theoretical normal distribution. Mean values for MRL, SJL, and F1 mice are shown by *arrows*. Shapiro-Wilk test is used to test the normality of F2 population.

SJL, respectively. These data suggest that serum IGFBP-5 is a quantitative trait and that both MRL and SJL strains contain genetic loci that contribute to variation in serum IGFBP-5 in F2 mice. The estimated broad sense of heritability for serum IGFBP-5 was 74%.

Analyses of QTL effects for serum IGFBP-5 phenotype

The results of genome-wide scans are presented in Fig. 5. Whole-genome scans with marker regression revealed highly significant peaks on Chrs 1, 9, 10, and 11, of which Chrs 9 and 11 contain two QTL, whereas Chrs 1 and 10 contain one QTL. Table 1 provides the list of markers for various QTL that show significant linkage with serum IGFBP-5 levels and the percent of F2 variance explained by individual QTL. Of the six QTL, chromosome 11 QTL (D11Mit36) exhibited the highest LOD score and contributed to 6.7% of the variation in serum IGFBP-5 levels seen in the MRL/SJL F2 mice. The six identified QTL explained 24% of variation in serum IGFBP-5 levels seen in the MRL/SJL F2 mice.

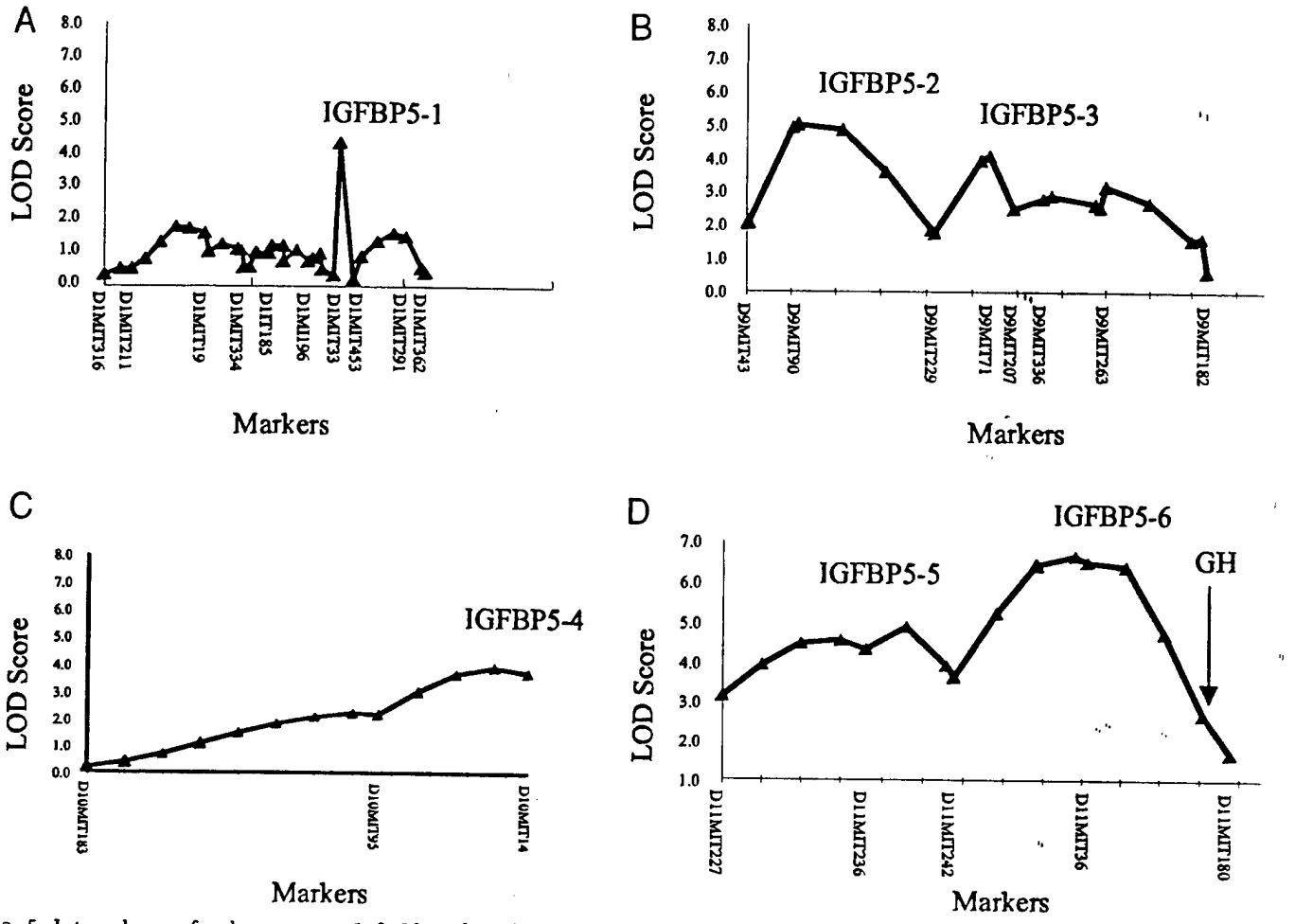

FIG. 5. Interval maps for chromosomes 1, 9, 10, and 11 shown to carry QTLs for serum IGFBP-5. Statistical analyses are presented as LOD scores calculated for molecular markers beginning with the centromeric end of each chromosome on the left extending toward telomeric end. LOD scores between markers were determined using MAPQTL interval mapping program with a default setting of 5 cM between steps. The intermediary data points between the markers represent the intervals used for determination of peak LOD score by MAPQTL interval mapping program. The location of GH gene is shown in chromosome 11. All markers used for genotyping are not shown for chromosomes 1 and 11 for the sake of clarity.

TABLE 1. Significant and suggestive QTL for IGFBP-5 in MRL/SJL F2 mice

QTL	Marker	Distance (cM)	LOD score	% Explained
IGFBP5-1	D1Mit33	82	3.9	2.9
IGFBP5-2	D9Mit90	7.7	4.9	4.2
IGFBP5-3	D9Mit71	29	4.0	2.9
IGFBP5-4	D10Mit14	69.9	3.6	3.3
IGFBP5-5	D11Mit236	19.7	4.9	4.3
IGFBP5-6	D11Mit36	47.6	6.8	6.7
Total				24.3

QTLs with a LOD score of at least 3.5 are considered to be significant, whereas those with a LOD score of at least 2.7 are considered to be suggestive.

TABLE 2. Significant and suggestive QTL for total body BMD in MRL/SJL F2 mice

QTL	Marker	Distance (cM)	LOD score	% Explained
BMD-1	**D1Mit33**	**82**	**2.8**	**2.0**
BMD-2	D1mit362	110.4	2.9	2.4
BMD-3	D2Mit62	54.6	4.9	3.5
BMD-4	D2Mit263	78.7	6.6	5.6
BMD-5	D9Mit90	7.7	4.4	4.0
BMD-6	**D11Mit36**	**47.6**	**6.8**	**5.2**
BMD-7	D14Mit194	52.5	4.5	3.9
BMD-8	D15Mit179	7.7	2.7	2.0
Total				28.6

Shared QTL between BMD and IGFBP-5 are shown in *bold*. QTLs with a LOD score of at least 3.5 are considered to be significant, whereas those with a LOD score of at least 2.7 are considered to be suggestive.

Shared QTL for serum IGFBP-5 and BMD phenotypes

Because IGFBP-5 has been shown to stimulate bone formation in mice in part by an IGF-independent mechanism (13), and because serum IGFBP-5 levels show significant positive correlation with BMD in clinical studies (14, 16, 17), we predicted common genetic mechanisms regulating serum IGFBP-5 and BMD phenotypes. Accordingly, we found that two of the identified QTLs (Chrs 1 and 11) for serum IGFBP-5 also showed significant linkage with total body BMD in the MRL/SJL F2 mice (Table 2).

Discussion

In this study, we found that heritability for serum IGFBP-5 levels was high (74%) and that at least 6 QTLs for serum

IGFBP-5 level had LOD scores greater than 3.5. These loci are distributed in four different chromosomes and accounted for 24% of the variance in serum IGFBP-5 levels among the 633 MRJ/SJL F2 mice. In addition, we have shown that two of the QTLs identified for serum IGFBP-5 also exhibit significant association with total body BMD phenotype.

In previous studies using MRL and SJL inbred strains of mice, we demonstrated significant QTLs for body length, lean body mass, muscle size, femur length, bone density, and wound regeneration (23, 27, 29–31). Because we and others have shown that IGFBP-5 is a stimulator of both osteoblast and myoblast differentiation (10, 32), we predicted IGFBP-5 levels to be different between the two inbred strains of mice. Accordingly, we found serum IGFBP-5 level to be 79% higher in MRL (good healer strain) compared with SJL (poor healer strain). In this study, we have shown that the serum IGFBP-5 variation in MRL/SJL F2 mice has a strong heritable component and that multiple genetic loci contribute to variation in serum IGFBP-5 levels. Although 74% of variation in serum IGFBP-5 levels can be explained on the basis of heredity, the six identified QTL explained only 24% of variation in IGFBP-5 levels seen in F2 mice. There are a number of potential explanations for this low contribution by the QTLs identified in this study: 1) serum IGFBP-5 levels could be under the influence of many genetic loci and we were able to detect only the major QTLs in our study; and 2) there could be significant epistatic interaction between genetic loci that could play an important role in the regulation of serum IGFBP-5 levels. This interaction could occur between the genetic loci that regulate serum IGFBP-5 levels or between IGFBP-5 QTLs and other QTLs (*e.g.* QTLs for other IGF system components). Further studies are needed to determine the other variables that contribute to the remaining two thirds of the observed variation in serum IGFBP-5 levels in the MRL/SJL F2 mice.

IGFBP levels in serum and other biological fluids depend on the rate of synthesis and degradation rate (18). In terms of regulatory molecules involved in regulating IGFBP-5 levels, several lines of evidence demonstrate that GH is a major regulator of serum IGFBP-5 levels. First, serum IGFBP-5 levels were significantly reduced in GH-deficient children as well as in adults (15, 16). Second, GH treatment of GH-deficient children and adults increased serum IGFBP-5 levels to levels similar to those seen in corresponding age-matched normal subjects (15, 16). Third, children with GH receptor insensitivity syndrome exhibited serum IGFBP-5 levels that are 80% less compared with normal children (33). Fourth, serum levels of IGFBP-5 exhibit significant positive correlation with other GH responsive IGF system components (*e.g.* IGF-I, IGFBP-3, and ALS) but not others (*e.g.* IGFBP-4) (34). Finally, GH increased expression of IGFBP-5 in bone (35). To determine if differences in the production and/or actions of GH could contribute, in part, to a variation in serum IGFBP-5 levels, we evaluated if any of the genetic loci identified for the regulation of serum IGFBP-5 levels contain candidate genes known to be involved in the production and actions of GH. In this regard, it is worth noting that GH gene is located in the chromosome 11 QTL (IGFBP5-6) that is linked to serum IGFBP-5 level (Fig. 4D). Because the identified QTL region in chromosome 11 is rather large, further studies using additional microsatellite markers in this region are needed to further define the location of the GH gene in relationship to the chromosomal region that contributes to variation in serum IGFBP-5 levels.

Our findings that serum IGF-I levels are also elevated in MRL mice compared with SJL mice seem to suggest that variations in the production and/or actions of GH could in part contribute to the observed differences in serum IGFBP-5 levels between MRL and SJL mice via increasing the local and endocrine actions of IGF-I (18). We did not measure serum GH levels in this study because GH is secreted in a pulsatile manner and that a single time measurement of GH has not been shown to be a valid measurement of overall GH secretion. In any case, if the prediction involving GH turns out to be true, we would expect the chromosome 11 IGFBP-5 QTL to be a shared QTL with GH, IGF-I, IGFBP-3, and ALS.

It is known that degradation of IGFBP-5 by IGFBP proteases is an important mechanism by which IGFBP-5 levels in serum and other biological fluids are controlled. In this regard, we and others have shown that a number of proteins including ADAM-9, ADAM-12, pregnancy-associated plasma protein-A2, and complement C1s degrade IGFBP-5 specifically (36–39). Of these various IGFBP-5 proteases, the pregnancy-associated plasma protein-A2 gene is found to be located within the chromosome 1 IGFBP-5 QTL region. Based on these and previous findings, it is likely that alterations in both synthesis and degradation of IGFBP-5 could contribute to a variation in serum levels of IGFBP-5 between MRL and SJL mice.

IGFBP-5 is unique in that only IGFBP-5 has been consistently shown to potentiate IGF actions in a variety of cell types including osteoblasts, chondroblasts, and smooth muscle cells. Studies on the mechanisms by which IGFBP-5 stimulates osteoblasts have shown that IGFBP-5 itself is a growth factor capable of stimulating bone formation in the absence of its ligand (13). Accordingly, serum levels of IGFBP-5 have been shown to correlate with BMD in several clinical studies (14, 16, 17). If IGFBP-5 is an important variable regulating BMD, we predicted common genetic determinants for BMD and serum IGFBP-5 phenotypes. In this regard, we found that two of the six IGFBP-5 QTLs are shared QTLs with BMD and serum IGFBP-5 phenotypes. It remains to be established whether the shared QTLs for the BMD and serum IGFBP-5 harbor a single gene that regulates IGFBP-5 levels and, consequently, BMD or if they contain two genes, one that regulates IGFBP-5 levels and consequently BMD and the second that regulates BMD phenotype independently of IGFBP-5.

In conclusion, our study provides the first identification of QTLs regulating serum IGFBP-5 levels and genetic evidence for a binding protein regulating BMD. Future identification of one or more genes regulating extreme differences in serum IGFBP-5 levels between MRL and SJL inbred strains of mice could lead to not only identification of molecular pathways of IGFBP-5 regulation but also of genes regulating BMD differences.

Acknowledgments

All work was performed in the facilities provided by the Department of Veterans Affairs. We would like to thank Alice Kramer for technical assistance and Sean Belcher for secretarial assistance.

Received January 9, 2003. Accepted April 18, 2003.

Address all correspondence and requests for reprints to: Subburaman Mohan, Ph.D., Musculoskeletal Disease Center (151), J. L. Pettis Veterans Administration Medical Center, 11201 Benton Street, Loma Linda, California 92357. E-mail: mohans@lom.med.va.gov.

This work was supported by the National Institutes of Health (AR-31062) and by the Assistance Award No. DAMD17-99-1-9571. The U.S. Army Medical Research Acquisition Activity (Fort Detrick, MD) 21702-5014 is the awarding and administering acquisition office for the DAMD award. The information contained in this publication does not necessarily reflect the position or the policy of the Government, and no official endorsement should be inferred.

References

1. **Mohan S, Richman C, Guo R, Amaar Y, Donahue LR, Wergedal J, Baylink DJ** 2003 IGF regulates peak bone mineral density in mice by both growth hormone-dependent and independent mechanisms. Endocrinology 144: 929–936
2. **Zhang M, Xuan S, Bouxsein ML, von Stechow D, Akeno N, Faugere MC, Malluche H, Zhao G, Rosen CJ, Efstratiadis A, Clemens TL** 2002 Osteoblast-specific knockout of the insulin-like growth factor (IGF) receptor gene reveals an essential role of IGF signaling in bone matrix mineralization. J Biol Chem 277:44005–44012
3. **Yakar S, Rosen CJ, Beamer WG, Ackert-Bicknell CL, Wu Y, Liu JL, Ooi GT, Setser J, Frystyk J, Boisclair YR, LeRoith D** 2002 Circulating levels of IGF-1 directly regulate bone growth and density. J Clin Invest 110:771–781
4. **Mohan S, Baylink DJ** 2002 IGF-binding proteins are multifunctional and act via IGF-dependent and -independent mechanisms. J Endocrinol 175:19–31
5. **Firth SM, Baxter RC** 2002 Cellular actions of the insulin-like growth factor binding proteins. Endocr Rev 23:824–854
6. **Clemmons DR** 1998 Role of insulin-like growth factor binding proteins in controlling IGF actions. Mol Cell Endocrinol 140:19–24
7. **Andress DL, Birnbaum RS** 1992 Human osteoblast-derived insulin-like growth factor (IGF) binding protein-5 stimulates osteoblast mitogenesis and potentiates IGF action. J Biol Chem 267:22467–22472
8. **Mohan S, Nakao Y, Honda Y, Landale E, Leser U, Dony C, Lang K, Baylink DJ** 1995 Studies on the mechanisms by which insulin-like growth factor (IGF) binding protein-4 (IGFBP-4) and IGFBP-5 modulate IGF actions in bone cells. J Biol Chem 270:20424–20431
9. **Schmid C, Schlapfer I, Gosteli-Peter MA, Froesch ER, Zapf J** 1996 Effects and fate of human IGF-binding protein-5 in rat osteoblast cultures. Am J Physiol 271:E1029–E1035
10. **Richman C, Baylink DJ, Lang K, Dony C, Mohan S** 1999 Recombinant human insulin-like growth factor-binding protein-5 stimulates bone formation parameters *in vitro* and *in vivo*. Endocrinology 140:4699–4705
11. **Bauss F, Lang K, Dony C, Kling L** 2001 The complex of recombinant human insulin-like growth factor-I (rhIGF-I) and its binding protein-5 (IGFBP-5) induces local bone formation in murine calvariae and in rat cortical bone after local or systemic administration. Growth Horm IGF Res 11:1–9
12. **Andress DL** 2001 IGF-binding protein-5 stimulates osteoblast activity and bone accretion in ovariectomized mice. Am J Physiol Endocrinol Metab 281: E283–E288
13. **Miyakoshi N, Richman C, Kasukawa Y, Linkhart TA, Baylink DJ, Mohan S** 2001 Evidence that IGF-binding protein-5 functions as a growth factor. J Clin Invest 107:73–81
14. **Boonen S, Mohan S, Dequeker J, Aerssens J, Vanderschueren D, Verbeke G, Broos P, Bouillon R, Baylink DJ** 1999 Down-regulation of the serum stimulatory components of the insulin-like growth factor (IGF) system (IGF-I, IGF-II, IGF binding protein [BP]-3, and IGFBP-5) in age-related (type II) femoral neck osteoporosis. J Bone Miner Res 14:2150–2158
15. **Ono T, Kanzaki S, Seino Y, Baylink DJ, Mohan S** 1996 Growth hormone (GH) treatment of GH-deficient children increases serum levels of insulin-like growth factors (IGFs), IGF-binding protein-3 and -5, and bone alkaline phosphatase isoenzyme. J Clin Endocrinol Metab 81:2111–2116
16. **Thoren M, Hilding A, Brismar T, Magnusson P, Degerblad M, Larsson L, Saaf M, Baylink DJ, Mohan S** 1998 Serum levels of insulin-like growth factor binding proteins (IGFBP)-4 and -5 correlate with bone mineral density in growth hormone (GH)-deficient adults and increase with GH replacement therapy. J Bone Miner Res 13:891–899
17. **Karasik D, Rosen CJ, Hannan MT, Broe KE, Dawson-Hughes B, Gagnon DR, Wilson PW, Visser M, Langlois JA, Mohan S, Kiel DP** 2002 Insulin-like growth factor binding proteins 4 and 5 and bone mineral density in elderly men and women. Calcif Tissue Int 71:323–328
18. **Rajaram S, Baylink DJ, Mohan S** 1997 Insulin-like growth factor-binding proteins in serum and other biological fluids: regulation and functions. Endocr Rev 18:801–831
19. **Kao PC, Matheny Jr AP, Lang CA** 1994 Insulin-like growth factor-I comparisons in healthy twin children. J Clin Endocrinol Metab 78:310–312
20. **Harrela M, Koistinen H, Kaprio J, Lehtovirta M, Tuomilehto J, Eriksson J, Toivanen L, Koskenvuo M, Leinonen P, Koistinen R, Seppala M** 1996 Genetic and environmental components of interindividual variation in circulating levels of IGF-I, IGF-II, IGFBP-1, and IGFBP-3. J Clin Invest 98:2612–2615
21. **Rosen CJ, Churchill GA, Donahue LR, Shultz KL, Burgess JK, Powell DR, Ackert C, Beamer WG** 2000 Mapping quantitative trait loci for serum insulin-like growth factor-1 levels in mice. Bone 27:521–528
22. **Li X, Gu W, Masinde G, Hamilton-Ulland M, Xu S, Mohan S, Baylink DJ** 2001 Genetic control of the rate of wound healing in mice. Heredity 86:668–674
23. **Masinde GL, Li X, Gu W, Davidson H, Mohan S, Baylink DJ** 2001 Identification of wound healing/regeneration quantitative trait loci (QTL) at multiple time points that explain seventy percent of variance in (MRL/MpJ and SJL/J) mice F2 population. Genome Res 11:2027–2033
24. **Donahue LR, Beamer WG** 1993 Growth hormone deficiency in 'little' mice results in aberrant body composition, reduced insulin-like growth factor-I and insulin-like growth factor-binding protein-3 (IGFBP-3), but does not affect IGFBP-2, -1 or -4. J Endocrinol 136:91–104
25. **Mohan S, Libanati C, Dony C, Lang K, Srinivasan N, Baylink DJ** 1995 Development, validation, and application of a radioimmunoassay for insulin-like growth factor binding protein-5 in human serum and other biological fluids. J Clin Endocrinol Metab 80:2638–2645
26. **Mohan S, Baylink DJ** 1995 Development of a simple valid method for the complete removal of insulin-like growth factor (IGF)-binding proteins from IGFs in human serum and other biological fluids: comparison with acid-ethanol treatment and C18 Sep-Pak separation. J Clin Endocrinol Metab 80: 637–647
27. **Masinde G, Li X, Gu W, Wergedal J, Mohan S, Baylink D** 2002 Quantitative trait loci for bone density in mice: the genes determining total skeletal density and femur density show little overlap in same F2 mice. Calcif Tissue Int 71:421–428
28. **Van Ooijen JW** 1999 LOD significance thresholds for QTL analysis in experimental populations of diploid species. Heredity 83:613–624
29. **Masinde GL, Li X, Gu W, Davidson H, Hamilton-Ulland M, Wergedal J, Mohan S, Baylink J** 2002 Quantitative trait loci (QTL) for lean body mass and body length in MRL/MPJ and SJL/J F(2) mice. Funct Integr Genomics 2:98–104
30. **Li X, Masinde G, Gu W, Wergedal J, Mohan S, Baylink DJ** 2002 Genetic dissection of femur breaking strength in a large population (MRL/MpJ x SJL/J) of F2 Mice: single QTL effects, epistasis, and pleiotropy. Genomics 79:734–740
31. **Masinde GL, Li X, Gu W, Hamilton-Ulland M, Mohan S, Baylink DJ** 2002 Quantitative trait loci that harbor genes regulating muscle size in (MRL/MPJ x SJL/J) F(2) mice. Funct Integr Genom 2:120–125
32. **Ewton DZ, Coolican SA, Mohan S, Chernausek SD, Florini JR** 1998 Modulation of insulin-like growth factor actions in L6A1 myoblasts by insulin-like growth factor binding protein (IGFBP)-4 and IGFBP-5: a dual role for IGFBP-5. J Cell Physiol 177:47–57
33. **Burren CP, Wanek D, Mohan S, Cohen P, Guevara-Aguirre J, Rosenfeld RG** 1999 Serum levels of insulin-like growth factor binding proteins in Ecuadorean children with growth hormone insensitivity. Acta Paediatr Suppl 88:185–191; discussion 192
34. **Powell DR, Durham SK, Brewer ED, Frane JW, Watkins SL, Hogg RJ, Mohan S** 1999 Effects of chronic renal failure and growth hormone on serum levels of insulin-like growth factor-binding protein-4 (IGFBP-4) and IGFBP-5 in children: a report of the Southwest Pediatric Nephrology Study Group. J Clin Endocrinol Metab 84:596–601
35. **McCarthy TL, Casinghino S, Centrella M, Canalis E** 1994 Complex pattern of insulin-like growth factor binding protein expression in primary rat osteoblast enriched cultures: regulation by prostaglandin E2, growth hormone, and the insulin-like growth factors. J Cell Physiol 160:163–175
36. **Mohan S, Thompson G, Amaar Y, Hathaway G, Tschesche H, Baylink DJ** 2002 ADAM-9 is an IGFBP-5 protease produced and secreted by human osteoblasts. Biochemistry 41:15394–15403
37. **Loechel F, Fox JW, Murphy G, Albrechtsen R, Wewer UM** 2000 ADAM 12-S cleaves IGFBP-3 and IGFBP-5 and is inhibited by TIMP-3. Biochem Biophys Res Commun 278:511–515
38. **Overgaard MT, Boldt HB, Laursen LS, Sottrup-Jensen L, Conover CA, Oxvig C** 2001 Pregnancy-associated plasma protein-A2 (PAPP-A2), a novel insulin-like growth factor-binding protein-5 proteinase. J Biol Chem 276:21849–21853
39. **Busby Jr WH, Nam TJ, Moralez A, Smith C, Jennings M, Clemmons DR** 2000 The complement component C1s is the protease that accounts for cleavage of insulin-like growth factor-binding protein-5 in fibroblast medium. J Biol Chem 275:37638–37644

doi:10.1006/geno.2002.6760, available online at http://www.idealibrary.com on IDEAL

Genetic Dissection of Femur Breaking Strength in a Large Population (MRL/MpJ × SJL/J) of F2 Mice: Single QTL Effects, Epistasis, and Pleiotropy

Xinmin Li, Godfred Masinde, Weikuan Gu, Jon Wergedal, Subburaman Mohan, and David J. Baylink*

Molecular Genetics Division, Musculoskeletal Disease Center, JL Pettis VA Medical Center and Loma Linda University, Loma Linda, California 92357, USA

To whom correspondence and reprint requests should be addressed. Fax: (909) 796-1680. E-mail: David.Baylink@med.va.gov.

Bone breaking strength is an ultimate measurement of the risk of fracture. For a practical reason, bone mineral density (BMD) has been commonly used for predicting the risk instead. To identify genetic loci influencing femur-breaking strength (FBS), which was measured by three-point bending using an Instron DynaMight Low-Force Testing System, the whole-genome scan was carried out using 119 polymorphic markers in 633 (MRL × SJL) F2 female mice. We identified six significant quantitative trait loci (QTL) affecting bone breaking strength on chromosomes 1, 2, 8, 9, 10, and 17, which together explained 23% of F2 variance. Of those, the QTL on chromosomes 2, 8, and 10 seem to be unique to bone breaking strength, whereas the remaining three QTL are concordant with femur BMD QTL. Genetic analysis suggests that, of these six FBS QTL, three influence BMD, two influence bone quality, and one influences bone size. We detected multiple significant epistatic interactions for FBS, which accounts for half (14.6%) of F2 variance compared with significant single QTL effects. We found evidence that pleiotropic effect might represent a common genetic mechanism to coordinately regulate bone-related phenotypes. Pleiotropic analysis also suggests that our current threshold level for significant QTL may be too high to detect biologically significant QTL with small effect. Together with epistatic interactions, these undetected small QTL could explain 30% of genetic variance that remains unaccounted for in this study (heritability estimate for FBS is 68%). Our findings in single QTL effects, epistasis, and pleiotropy demonstrate that partially overlapped but distinct combinations of genetic loci in MRL/MpJ and SJL/J inbred strains of mice regulate bone strength and bone density. Identification of the genes unique to FBS may have an impact on prediction of osteoporosis in human.

Key Words: bone mineral density, bone strength, epistasis, heritability, and pleiotropy

INTRODUCTION

Bone strength is an ultimate measurement of resistance to fracture. It is mainly determined by bone mineral density (BMD), bone size, and bone quality. Of those, BMD accounts for 60% of the variation in the bone compression strength [1]. As BMD contributes substantially to bone strength and can be practically measured with marked sensitivity and precision, the evaluation of BMD is the most commonly used method for predicting fracture risk in humans. Consequently, determination of the genetic basis of osteoporosis by quantitative trait loci (QTL) analysis [2–6] has been primarily focused on the genetic factors influencing BMD.

However, the sensitivity of BMD as a predictor of fracture risk is limited by the fact that this index does not take into account the geometrical and material characteristics of bone [7] that explain the remaining 40% of the contribution to bone strength. In this context, numerous genetic studies for loci regulating BMD may reveal only a partial description of genetic components determining bone strength (60%). Other important genes contributing to bone strength (40%) remain to be evaluated by alternative approaches.

0888-7543/02 $35.00

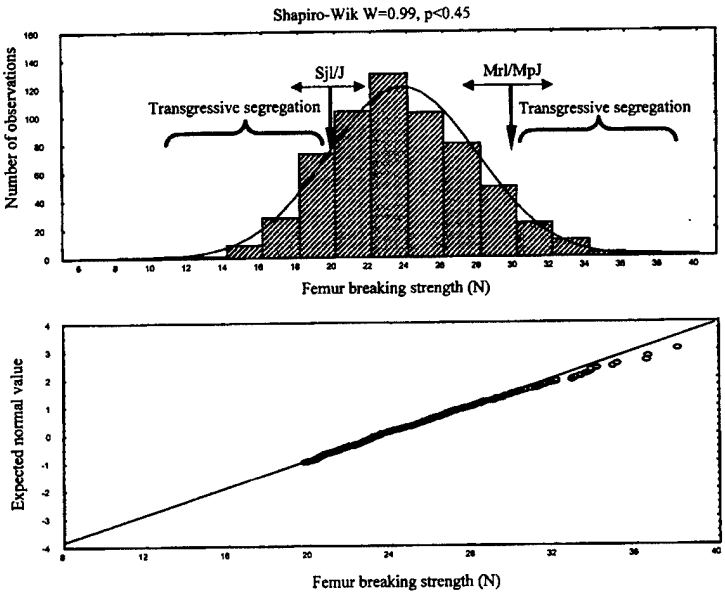

FIG. 1. Normal distributions of FBS and femur BMD in (MRL/MpJ × SJL/L)F2 female mice at 7 weeks of age. (Top) Frequency histogram of F2 mice, which is not significantly different ($P < 0.45$) from the theoretical normal distribution (bell-shaped line). (Bottom) Normal probability plot of FBS, which is consistent with a normal distribution.

The search for the remaining genes can be pursued by directly evaluating bone strength in mouse models. The inbred strains of mice offer genetic homogeneity and differ in bone breaking strength [8–11]. They are therefore amenable to genetic analysis of bone strength via the experimental design of QTL analysis. The availability of a recently developed Instron Mechanical Tester for small animals has made it feasible to measure the bone strength in mice with high precision. Because inbred mice have been for a long time a model of human bone changes leading to osteoporosis [2], bone strength QTL derived from mouse studies could be used to guide osteoporosis research in humans.

Given that BMD accounts for 60% of the variation in the bone compression strength, we hypothesized that some of the bone strength QTL would be the same as BMD QTL and others would be unique to bone strength, and that epistatic interactions played an important role for the regulation of femur breaking strength (FBS), which could be different from those for regulating BMD. We tested these hypotheses by conducting a genome-wide scan for QTL influencing femur BMD and FBS in an F2 intercross of MRL/MpJ and SJL/J mice. We report the identification of six highly significant bone strength QTL, of which three are unique to FBS. Additionally, we present evidence for significant epistatic interactions and pleiotropic effect.

RESULTS

FBS and BMD Phenotypes in MRL, SJL, F1, and F2 Female Mice

FBS and femur BMD were examined in 20 MRL, 20 SJL, 36 (MRL × SJL) F1, and 633 (MRL × SJL) F2 female mice at 7 weeks of age. We used 7-week-old mice because, at this age, the skeleton has already reached 70–80% of its final bone mineral density and bone size, the two major determinants of bone strength, but the mechanisms responsible for determining bone density and bone size are still active. Thus, this age is more amenable for the study of the genetic mechanisms that regulate FBS [12].

Femur BMD and FBS traits in F1 and F2 exhibited mean values between those of the parental strains, and in F2 showed normal distribution (Fig. 1), suggesting polygenic control with an additive mode of inheritance. Some mice have similar body weight, periosteal circumference, and BMD, but markedly different FBS (Fig. 2), which suggests that there are additional genetic factors regulating FBS. The broad-sense heritability was estimated to be 0.64 for BMD and 0.68 for FBS, similar to previous heritability estimates for mouse BMD [2]. The high heritability provides a genetic foundation to search for QTL that regulate FBS and BMD, and to distinguish concordant QTL of two traits from unique QTL for FBS.

Genetic Loci That Influence FBS and Femur BMD

A total of 560 primer pairs (410 from the Mouse Map Pairs Genome-wide Screening Set) were tested for polymorphism between the two parental strains of mice. We identified 158 markers with distinguishable polymorphisms (28%), of which 119 were used for genotyping of the 633 (MRL × SJL) F2 female mice. These markers covered all 20 chromosomes with a spacing of ≤ 15 cM and an average spacing of 12 cM. Interval mapping followed by MQM mapping analysis [13] identified six QTL for FBS (Table 1) and nine QTL for

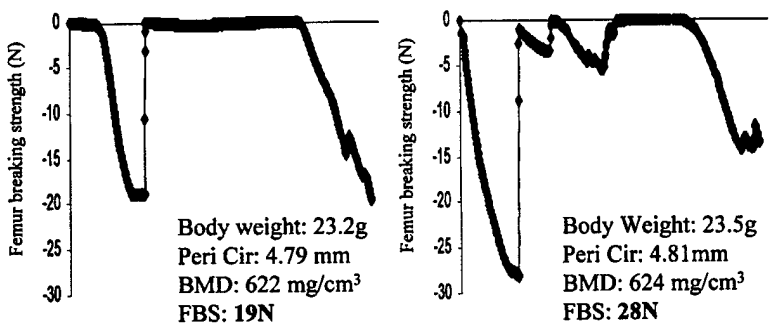

FIG. 2. Difference in FBS between two mice with a similar body weight, periosteal circumference, and BMD. This phenotypic difference suggests that there are other genetic factors unrelated to BMD regulating FBS. The Y axis represents the resistance to break in Newton, and the X axis represents the time point in 0.01-second intervals (time points not shown).

doi:10.1006/geno.2002.6760, available online at http://www.idealibrary.com on IDEAL

TABLE 1: Significant QTL for femur breaking strength

QTL name*	Marker close to the peak of QTL (cM)	% Explained by phenotypic variance	1 Lod interval (cM)	Notes
Fbs17P6.6L8.4	*D17Mit175* (6.6)	8.5	6.6	Shared with BMD QTL in this study
Fbs1P104L4.7	*D1Mit291* (103.8)	3.4	10.8	Shared with BMD QTL in this study
Fbs8P15.7L4.3	*D8Mit125* (15.7)	3.3	11.3	Unique to FBS
Fbs9P47L3.1	*D9Mit270* (41.5)	2.9	21.9	Shared with BMD QTL in this study
Fbs2P54.6L3.6	*D2Mit62* (54.6)	2.6	10.9	Unique to FBS
Fbs10P47L2.7	*D10Mit95* (50.3)	2	8	Unique to FBS
Same QTL after adjustment with periosteal circumference				
Fbs17P6.6L8.3	*D17Mit175* (6.6)	8.5	6.0	
Fbs1P104L6.0	*D1Mit291* (103.8)	4.5	10.2	
Fbs8P15.7L3.5	*D8Mit125* (15.7)	2.4	12	
Fbs9P47L2.7	*D9Mit270* (41.5)	2.1	20	
Fbs2P54.6L1.1	*D2Mit62* (54.6)	0.6	32	
Fbs10P47L2.3	*D10Mit95* (50.3)	1.6	8	

*With the increasing number of QTL mapping papers, QTL name needs to be standardized. In this report, we proposed to use four components to name a QTL: 1) abbreviation of QTL phenotype; 2) chromosome number on which the QTL is located; 3) chromosome position on which the peak of the QTL is corresponding to; and 4) lod score of the QTL. For example, for the QTL "Fbs1P104L5.2," the "Fbs" represents the first component of the name and stands for "femur breaking strength," followed by "1," indicating that this QTL is located on chromosome 1. The "P104" shows that the peak of this QTL corresponds to the position of 104 cM. The "L5.2" indicates that this QTL has a lod score of 5.2. The lod threshold is 3.5 for significant linkage and 2.7 for suggestive linkage (equivalent to significant level of 1% and 5%, respectively, for a standard chromosome length of 100 cM).

femur BMD (Table 2) that exhibited significant associations between the genotypic markers and phenotypic values (we propose to standardize QTL names by using four components; Table 1). Of the six FBS QTL, five MRL alleles enhance bone strength compared with SJL alleles, except Fbs8P15.7L4.3 QTL, in which the SJL-derived allele contributes more to increase bone strength than the MRL allele. Two MRL- and two SJL-derived alleles (Fbs2P54.6L3.6 and Fbs9P47L3.1 for MRL, and Fbs8P15.7L4.3 and Fbs10P47L2.7 for SJL) have a dominant effect, respectively, and the other two loci have an additive effect (Fig. 3).

Fbs1P104L4.7, Fbs17P6.6L8.4, and Fbs9P47L3.1 explained approximately 15% phenotypic variation and seem to be concordant with BMD QTL Bmd1P108.8L5.2, Bmd17P6.6L6, and Bmd9P46.5L3.6 (Table 2). An additional three QTL explained 8% variation in FBS phenotype and seem to specifically influence FBS in this study. After adjustment with periosteal circumference, four of six QTL were still significantly associated with FBS and two of them became insignificant (Table 1). Taken together, six FBS and nine BMD QTL explained 23% and 34% of F2 variance, respectively. Based on heritability estimate, genetic factors explained 64% phenotypic variation for BMD and 68% for FBS. We therefore explored additional genetic contribution to phenotypic variation by quantitative analysis of locus–locus interactions.

Interactions between Loci

The two-way analysis of variance was used for evaluating genetic interactions among the loci. The analysis of FBS interactions included the test for significant interactions between all markers linked to FBS QTL and markers linked to BMD QTL. We chose to look for interaction between FBS and BMD QTL because of the high correlation between FBS and femur BMD ($r = 0.48$, $P < 0.001$) and because of our observation of pleiotropic effects at some QTL. In addition to analyzing interactions between markers with lod scores above the level of suggestive significance (LOD = 2.7), we included all markers with lod scores greater than 2.0. From our previous experience [14], markers with lod scores 2.0 and higher could have significant interactions. Table 3 summarizes significant interactions for FBS and femur BMD and reveals one prominent feature of the locus–locus interactions: all significantly interacting loci are unique for FBS or femur BMD, suggesting that specific genes regulate each phenotype at these loci. The epistatic interactions detected in this study account for half of the percentage of F2 variance compared with significant single QTL effects.

A Novel QTL on Chromosome 17 with Pleiotropic Effects on Multiple Phenotypes

Fbs17P6.6L8.4 is one of the largest QTL for FBS and has not been previously reported to have association with bone-related phenotypes. MQM mapping revealed that this QTL also influenced other bone-related phenotypes and body weight. In addition to having a strong linkage with FBS at a lod score of 8.5, the QTL has a significant association with femur BMD and body weight (Fig. 4), a suggestive association with femur length, and weak association with work required to break the femur. Variation contributed by this QTL varies from 8.5% to 2.5% with an average of 5.6%. Additional loci with pleiotropic effects were also observed (Table 4) when we intentionally included the loci with 2.7 > lod score > 2, as our analysis suggests that loci with lod score smaller than 2 could have biological significance. The *D12mit156* locus had weak association with femur length, body weight, muscle size, and piximus BMD at a lod score of < 2 (Fig. 5). The consistent linkage with multiple traits suggests a true QTL with a small pleiotropic effect.

TABLE 2: Significant QTL for femur BMD

QTL name	Marker close to the peak of QTL (cM)	% Explained by phenotypic variance	1 Lod interval (cM)	Notes
Bmd17P6.6L6	*D17Mit175* (6.6)	7.4	6.6	Unique BMD QTL identified in this study
Bmd1P80.4L5.1	*D1Mit33* (82)	5.5	6.6	Identified in previous BMD study
Bmd1P108.8L5.2	*D1Mit291* (103.8)	4.4	15	Unique BMD QTL identified in this study
Bmd14P10L2.7	*D14Mit132* (0)	4.4	17	Identified in previous BMD study
Bmd9P46.5L3.6	*D9Mit270* (41.5)	3	14.8	Identified in previous BMD study
Bmd4P55.3L2.8	*D4Mit204* (61.2)	2.6	11.1	Identified in previous BMD study
Bmd19P37.8L2.8	*D19Mit53* (32.8)	2.6	12.6	Unique BMD QTL identified in this study
Bmd18P25.1L2.7	*D18Mit185* (27.3)	2.1	9.6	Identified in previous BMD study
Bmd12P23L2.9	*D12Mit156* (28.4)	2	6.1	Unique BMD QTL identified in this study

The lod threshold is 3.5 for significant linkage and 2.7 for suggestive linkage (equivalent to significant level of 1% and 5%, respectively, for a standard chromosome length of 100 cM).

DISCUSSION

A complete genome scan with 119 polymorphic markers was carried out to map the QTL that control FBS in 633 (MRL/MpJ × SJL/J) F2 female mice. Our data revealed several genetic features of this phenotype. First, FBS is a highly inherited polygenic trait in the mouse. Second, there are at least six genetic loci that can contribute to FBS and collectively account for approximately 23% of the phenotypic variance in MRL/MpJ × SJL/J mice. Of those loci, three are concordant with BMD QTL, and the remaining three are unique to FBS. Third, epistatic interactions have an important role in regulating bone strength (explained 14.6% of F2 variance) compared with single QTL effects. Last, pleiotropy, together with epistasis, could be a common genetic mechanism in coordinated regulation of physiologically related traits.

Single QTL Effects

The rationale for such large mapping efforts to identify FBS QTL is based on the fact that FBS is the ultimate test of the risk of fracture, whereas genetic factors regulating BMD can only explain 60% of FBS and the remaining 40% has not been explored through QTL analysis. We therefore hypothesized that some of the QTL identified in this study will be the same as BMD QTL and others will be unique to FBS. The evidence supporting our hypothesis emerged at the characterization of the phenotype stage in which two parental strains have 8% difference in femur BMD but 50% in FBS. These data established the importance of the unique heritable aspect of FBS and provided the impetus of our QTL mapping effort, in which we systematically evaluated the genetic basis of this trait in relation to BMD.

Of the six significant FBS QTL, three shared with BMD QTL, suggesting that these loci influence FBS by regulating BMD. The remaining three QTL could influence FBS by regulating bone size or bone quality (as mentioned earlier, FBS is mainly determined by BMD, bone size, and bone quality). To verify this issue, we adjusted FBS by periosteal circumference. After adjustment, one of the three remaining QTL, Fbs2P54.6L3.6, became insignificant (Table 1), indicating that this QTL influences FBS by regulating bone size (we considered periosteal circumference alone as bone size parameter here because bone length should not affect evaluation of FBS in our three-point bending model). Identification of a major QTL with lod score of 14.4 at the same position for periosteal circumference supports our suggestion. Another remaining QTL,

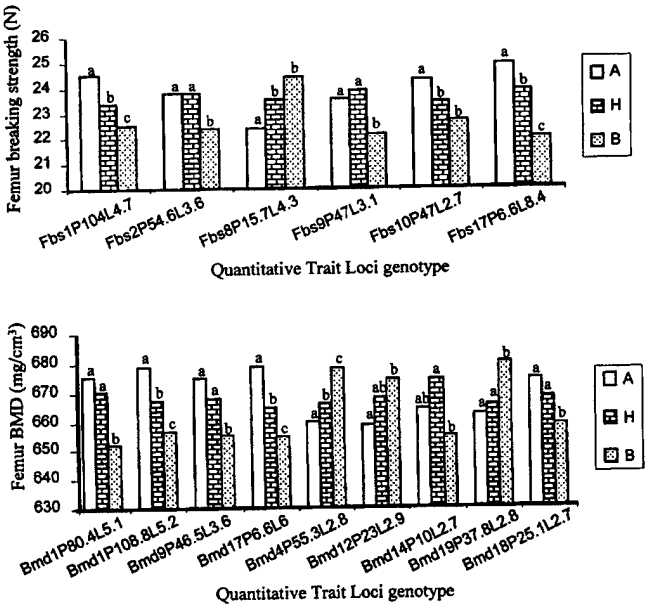

FIG. 3. The effects of genotype on FBS (top) and femur BMD (bottom). The genotypes were derived from the markers near the QTL peaks. The small letters on the top of the bars indicate the level of difference in phenotypic value between genotypes. If the two bars share the same letter, the value between two genotypes will have no statistical difference, otherwise it will be significantly different at $P < 0.05$.

doi:10.1006/geno.2002.6760, available online at http://www.idealibrary.com on IDEAL

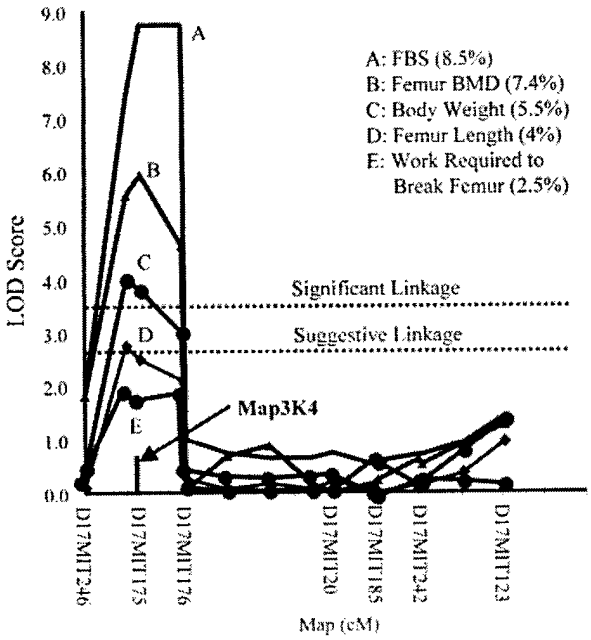

FIG. 4. A novel QTL, Fbs17P6.6L8.4, has pleiotropic effects on multiple bone-related phenotypes and body weight. Dashed horizontal lines represent significant and suggestive lod thresholds determined by permutation test. Numbers in parentheses represent the percentage of F2 variance explained by this QTL.

Fbs10P47L2.7, also became insignificant after adjustment, but it is unlikely due to the bone size effect for the following reasons: 1) there was no periosteal circumference QTL at this position; 2) there was a small change in lod score (from 2.7 to 2.3); and 3) there was no change in one lod interval. Thus, this QTL may regulate FBS by influencing bone quality. The third unique QTL for FBS, Fbs8P15.7L4.3, remained significant after size adjustment. It is likely that this QTL also regulates FBS by influencing bone quality. These analyses suggest that FBS is regulated through three QTL influencing BMD, two QTL influencing bone quality, and one QTL influencing bone size.

Epistatic Effect

QTL analysis showed the involvement of six loci to regulate FBS, which together explained 23% of phenotypic variance, yet 66% of the genetic variance remains unaccounted for (heritability estimate for FBS was 68%). We hypothesized that loci interaction might have an important role in regulating FBS. Indeed, two-way ANOVA revealed three significant loci interactions contributing to 14.6% F2 variance. In consideration of the complex network of gene action in regulating quantitative traits, the observation is more likely to represent a common genetic mechanism than a special case for FBS. Indeed, we also identified substantial epistatic interactions for BMD, which explained 17.4% of F2 variance compared with 34% for single QTL effects.

These multiple interaction loci may contain the genes that encode transcription factors, activation factors, or co-activators that are common to multiple pathways [15]. Perhaps due to the complex interactions, these important loci are often not significant when evaluating single QTL effects (Tables 1, 2, and 3), and therefore could be missed without epistatic analysis or could not be identified by epistatic analysis when there is a limited detection power due to a small F2 population or low marker coverage.

The loci interaction identified here emphasizes the importance of epistasis in regulating complex traits and the need to perform such an analysis in genetic dissection of complex traits. The analysis of these interactions may point to biological relationships among the genes. Identification of the loci involved in multiple interactions is critical during this analysis because they could have a more important role than single QTL.

It is important to point out that the estimates of epistatic effect might be biased due to the simplified model we used for the estimation of interaction effect. Our tests are likely conservative in the estimation of effects contributing to epistasis because loci interaction could occur in a more complicated manner [16].

Pleiotropic Effect

One of the most interesting findings in this study was that the largest FBS QTL, Fbs17P6.6L8.4, has a pleiotropic effect on other bone-related phenotypes including femur BMD, femur length, femur mid-shaft periosteal circumference, and possible work required to break the femur, suggesting that the gene underlying this QTL may have a general regulatory role on multiple bone metabolism pathways. In this regard, one candidate gene localized right under the peak of the QTL (6.5 cM), encoding mitogen activated protein kinase-4 (*MAP3K4*), was brought to our attention. The mitogen activated protein kinases (MAPKs) represent one of the important signaling mechanisms in response to environmental stimuli [17]. MAPKs are phosphorylated and activated by MAPK kinases (MAPKKs), which in turn are phosphorylated and activated by MAPKK kinases. Thus, it is biologically possible for MAP3K4 to affect several bone metabolic pathways through signaling signal transduction pathways. In addition to the Fbs17P6.6L8.4 locus with pleiotropic effect, we provided evidence to suggest that pleiotropy may represent a common genetic mechanism in coordinately regulating development

TABLE 3: Significant locus–locus interaction contributes to F2 variance for FBS and femur BMD

Locus 1 × Locus 2	FBS		Femur BMD	
	P <	% F2 variance	*P* <	% F2 variance
D3mit217 × *D12mit182*	0.001	5.7	ns	ns
D1mit33 × *D11mit36*	ns	ns	0.000	14.4
D10mit95 × *D9mit270*	0.006	4.1	ns	
D1mit291 × *D7mit246*	0.006	4.8	ns	
D11mit36 × *D4mit204*	ns		0.01	3.4
Total % of F2 variance		14.6		17.8

TABLE 4: Pleiotropic effect of same marker loci on different traits

Traits	Lod Score			
	D2mit62	*D9mit270*	*D11mit36*	*D13mit207*
Body Weight	8.3	2.7	3.4	4.2
Bone Strength	3.6	3.1		
BMD by pQCT		3.6	2.2	
BMD by PIXIMUS				3.0
Work to break Femur	8.9	2.3		
Femur Length	5.9			
Lean mass	8.2			4.0
Periosteal circumference	14.4		3.4	
% Fat			11.5	
Ear wound healing		14		

and function of several traits (Table 5), which forms the genetic foundation for high correlation among the traits. It is also possible that pleiotropy may have synergistic effect or negative effect on the phenotype outcome. It is a more complex network than epistasis as it involves different genes interacting to influence the biological outcome in more than one phenotype.

The pleiotropic analysis revealed that one locus could have weak association with multiple traits (Fig. 5). This phenomenon was also observed in several other loci. The consistency in association suggests that the locus may represent true QTL with a small effect. Based on this observation, our current significant threshold level (lod score of 3.5 for significant association and 2.7 for suggestive association) may be too high to detect the QTL with small effect (Fig. 8). This could be one of the reasons that QTL only explained a small percentage of F2 variance in literature. In this report, single FBS QTL explained 23% of F2 variance and locus–locus interaction explained 14.6%. In consideration of the heritability estimate of 68%, there is still 30.4% genetic variance unaccounted for. This part of genetic variance could be due to more complex epistatic interactions, which we could not detect in our analysis, and some small, but true biological QTL, which we did not include because of the high threshold level. In the future, we need to develop more sophisticated bioinformatics software to mimic cellular events and provide the capacity to identify the high level of epistatic interactions. Increasing population size and marker coverage is a costly but effective way to enhance the detection power for small QTL [18]. A practical alternative is to reduce the threshold level to lod score of 2 for those highly inherited traits with considerable measurement error.

MATERIALS AND METHODS

Parental, F1, and F2 mice. Four-week-old MRL/MpJ female and SJL/J male mice were obtained from The Jackson Laboratory (Bar Harbor, ME) and housed at the Animal Research Facility, JL Pettis VA Medical Center, Loma Linda, CA, under the standard condition of 14 hours light, 10 hours darkness, ambient temperature of 20°C, and relative humidity of 30–60%. We produced F2 progeny by intercross between (MRL/MpJ × SJL/J) F1 mice at the Animal Research Facility. A total of 20 MRL/MpJ (MRL), 20 SJL/J (SJL), 36 F1, and 633 F2 female mice were used in these genetic analyses. We sacrificed the mice at 7 weeks of age and body weights were recorded at necropsy. Livers from each animal were frozen in liquid N_2 for later DNA extraction. Femurs were isolated and stored in 1× PBS buffer at 4°C for later measurement of BMD and breaking strength. All experimental protocols were in compliance with the Animal Welfare Act and were approved by the Institutional Animal Care and Use Committee (IACUC) of the JL Pettis VA Medical Center.

Femur BMD and breaking strength. The mid-shaft of femur density was determined using peripheral quantitative computed tomography (pQCT) with an XCT Research M (Norland Medical System, Fort Atkinson, WI). The precision of this instrument for densitometry of mouse bone has been determined to be 1.2% by repeated placement and measurement of a single femur [6]. The measurement of reproducibility was evaluated by comparing right femur versus left femur in five C3H mice and five SJL mice. A CV of 7.7% for maximum load and 8.9% for stiffness was obtained.

Analysis of the scans was performed using the manufacturer-supplied software program (Stratec Medizintechnik GMBH Bone Density Software, version 5.40C). The outer threshold was set at 214 mg/cm^3 and the inner threshold at 300 mg/cm^3 for volumetric bone density estimation.

After measuring BMD, the breaking strength of the same femur was determined by three-point bending using an Instron DynaMight Low-Force Testing System (Instron Corporation, Canton, MA) with a constant span length of 2 mm and a constant speed of 10 mm/minute. The press head, as well as the two support points, was rounded to avoid shear load and cutting. The bone was positioned horizontally with the anterior surface upwards, centered on the supports, and the pressing head was directed vertically to the mid-shaft of the bone. Femur strength was defined as the maximum force (Newton) at failure.

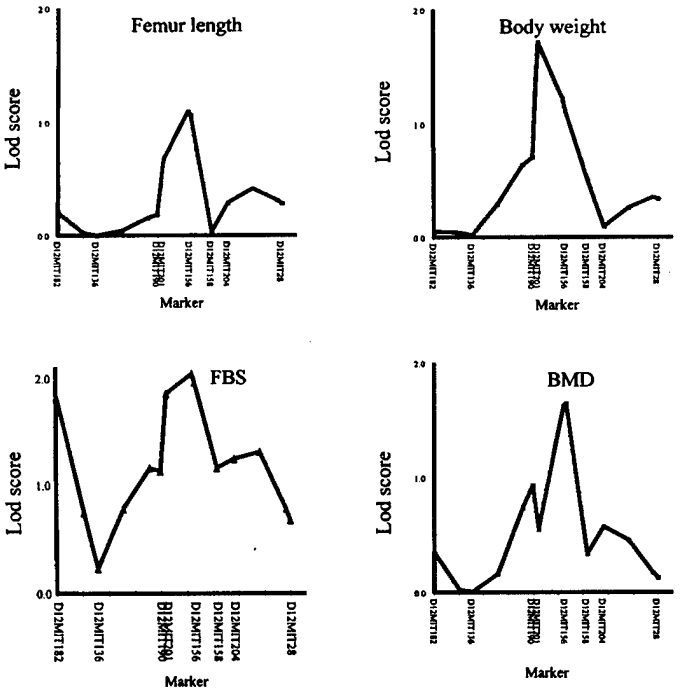

FIG. 5. The *D12mit156* marker has a consistent association with femur length, body weight, muscle size, and piximus BMD at a lod score < 2, suggesting a true biological QTL with a small pleiotropic effect.

A computer automatically recorded the breaking force profile and the maximum force at failure was identified and used for data analysis.

Muscle size measurement. The muscle size in the forearm was measured with a peripheral quantitative computed tomography (pQCT) system from Stratec XCT Research MTM (Norland Medical Systems, Fort Atkinson, WI). The forearm was chosen to measure muscle size because it could be accurately positioned in the instrument. By selecting appropriate density (beam attenuation) thresholds, the muscle area could be separated from areas of fatty tissue or bone. The most important part of the procedure was to determine the scan site where the forearm muscle was the largest. We determined that muscle area was largest at 30% of the forearm length starting from the proximal end. This site is easily accessible and repeat scans were reproducible. An additional two slices (0.5 mm above and below the center scan) were scanned. The forearm muscle size was defined as the average of these three scans. The percentage of measurement error in muscle measurement was 14%.

Genotyping. We extracted genomic DNA from the liver of each animal using a commercial DNA extraction kit according to the manufacturer's instructions (Wizard Genomic DNA Purification Kit, Promega). The Mouse Map Pairs Genome-wide Screening Set (410 primer pairs with 3.5 cM average resolution) and additional markers were purchased from Research Genetics (Huntsville, AL) and used to perform a genome-wide scan. PCR amplifications were conducted in 96-well plates using PTC-225 DNA Engine Tetrad (MJ Research, Watertown, Massachusetts) based on the Research Genetics Genome Services Protocol. PCR products were separated on 6.5% polyacrylamide gel and visualized with ethidium bromide staining. Polymorphism was scored as A for MRL/MpJ allele, B for SJL/J allele, and H for heterozygotes.

QTL analysis. The interval mapping was first performed to detect significant association between femur BMD or FBS and marker loci in F2 progeny using MapQTL software (Version 4.0; Wageningen, The Netherlands). The MQM mapping (multiple-QTL models) was then followed by using the linked QTL markers identified in the interval mapping as cofactors to absorb the effects of nearby QTL, thereby increasing the precision for mapping other segregating QTL [19]. After the first attempt of MQM mapping, if the positions of some QTL were different from those in the interval mapping, new cofactors would be selected on the basis of the revised QTL positions for another round of MQM mapping. This process was repeated until there were no further changes in QTL positions. The critical threshold values for significance of association were determined, by the permutation test [13,20] to be lod score of 3.5 for significant linkage and 2.7 for suggestive linkage.

Statistical analysis. Computations were performed with the STATISTCA 5.1 (Stat Soft Inc., Tulsa, OK) statistical package. Standard two-way analysis-of-variance was used to evaluate possible interactions between candidate QTL. The markers closely linked to the QTL were used as independent variables and FBS or BMD was used as dependent variable. Variance for locus–locus interaction was estimated from Vlocus × locus = (MS effect – MS error) / average sample size. The average sample size was calculated from n = 1 / (9 – 1) × [N – (n2AABB + •••• + n2aabb) / N], where nAABB, ••••, naabb are the sample size for the nine genotypes (combinations of two loci) and N = nAABB + •••• + naabb are the total sample size. Percentage of F2 variance explained was estimated as Vlocus × locus/Vtotal.

The broad-sense heritability was estimated from

$$\hat{H}^2 = \frac{V_{F_2} - (\frac{1}{2}V_{F_1} + \frac{1}{4}V_{P_1} = \frac{1}{4}V_{P_2})}{V_{F_2}}$$

where VF2, VF1, VP1, and VP2 represent F2, F1, MRL/MpJ (MRL), and SJL/J (SJL) variances, respectively. The variances in F1, P1, and P2 were weighted differently, due to the different composition of the F2 population. The F2 population composition is as follows: 25% P1; 25% P2; and 50% F1.

ACKNOWLEDGMENTS

We thank Heather Davidson and Melanie Hamilton-Ulland for their technical support. Assistance Award No DAMD17-99-1-9571 supported this work. The U.S. Army Medical Research Acquisition Activity is the awarding and administering acquisition office.

RECEIVED FOR PUBLICATION OCTOBER 24, 2001; ACCEPTED FEBRUARY 27, 2002.

REFERENCES

1. Weinstein, R. S. (2000). True strength. *J. Bone Miner. Res.* **15:** 621–625.
2. Benes, H., *et al.* (2000). Chromosomal mapping of osteopenia-associated quantitative trait loci using closely related mouse strains. *J. Bone Miner. Res.* **15:** 626–633.
3. Koller, D. L., *et al.* (2000). Genome screen for QTL contributing to normal variation in bone mineral density and osteoporosis. *J. Clin. Endocrinol. Metab.* **85:** 3116–3120.
4. Klein, R. F., Mitchell, S. R., Phillips, T. J., Belknap, J. K., and Orwoll, E. S. (1998). Quantitative trait loci affecting peak bone mineral density in mice. *J. Bone Miner. Res.* **13:** 1648–1656.
5. Shimizu, M., *et al.* (1999). Identification of peak bone mass QTL in a spontaneously osteoporotic mouse strain. *Mamm. Genome* **10:** 81–87.
6. Beamer, W. G., *et al.* (1999). Quantitative trait loci for bone density in C57BL/6J and CAST/EiJ inbred mice. *Mamm. Genome* **10:** 1043–1049.
7. Abbasi-Jahromi, S. H., Matayoshi, A., Kimble, R., Dimarogonas, A., and Pacifici, R. (1996). Bone quality factor analysis: A new noninvasive technique for the measurement of bone density and bone strength. *J. Bone Miner. Res.* **11:** 594–599.
8. Li, X., Mohan, S., Gu, W., Wergedal, J., and Baylink, D. J. (2001). Quantitative assessment of forearm muscle size, forelimb grip strength, forearm bone mineral density and forearm bone size in determining humerus breaking strength in ten inbred strains of mice. *Calcif. Tissue Int.* **68:** 365–369.
9. Akhter, M. P., *et al.* (2000). Genetic variation in bone density, histomorphometry, and strength in mice. *Calcif. Tissue Int.* **67:** 337–344.
10. Turner, C. H., *et al.* (2000). Genetic regulation of cortical and trabecular bone strength and microstructure in inbred strains of mice. *J. Bone Miner. Res.* **15:** 1126–1131.
11. Turner, C. H., *et al.* (2001). Variation in bone biomechanical properties, microstructure, and density in BXH recombinant inbred mice. *J. Bone Miner. Res.* **16:** 206–213.
12. Richman, C., *et al.* (2001). Postnatal and pubertal skeletal changes contribute predominantly to the differences in peak bone density between C3H/Hej and C57BL/6J mice. *J. Bone Miner. Res.* **16:** 386–397.
13. Van Ooijen, J. W. (1999). LOD significance thresholds for QTL analysis in experimental populations of diploid species. *Heredity* **83:** 613–624.
14. Masinde, G. L., *et al.* (2001). Identification of wound healing/regeneration QTLs at multiple time points that explain seventy percent of variance in (MRL/MpJ and SJL/J) F2 population. *Genome Res.* **11:** 2027–2033.
15. Roper, R. J., *et al.* (1999). Interacting quantitative trait loci control phenotypic variation in murine estradiol-regulated responses. *Endocrinology* **140:** 556–561.
16. De Sanctis, G. T., *et al.* (1995). Quantitative locus analysis of airway hyperresponsiveness in A/J and C57BL/6J mice. *Nat. Genet.* **11:** 150–154.
17. Chan-Hui, P. Y., and Weaver, R. (1998). Human mitogen-activated protein kinase mediates the stress-induced activation of mitogen activated protein kinase cascades. *Biochem. J.* **15:** 599–609.
18. Moore, K. J., and Nagle, L. D. (2000). Complex trait analysis in the mouse: The strengths, the limitations and the promise yet to come. *Annu. Rev. Genet.* **34:** 653–686.
19. Jansen, R. C. (1994). Controlling the type I and type II errors in mapping quantitative trait loci. *Genetics* **138:** 871–881.
20. Churchill, G. A., and Doerge, R. W. (1994). Empirical threshold values for quantitative trait mapping. *Genetics* **138:** 963–971.

A Genome-wide Screening of N-Ethyl-N-nitrosourea (ENU) Mutagenized Mice for Musculoskeletal Phenotypes

A. K. Srivastava[1], S. Mohan[1], J. E. Wergedal[1], & D. J. Baylink[1]

[1]Musculoskeletal Disease Center, Jerry L Pettis Veterans Medical Center & Department of Medicine, Loma Linda University, Loma Linda, CA, USA.

Running title: Screening musculoskeletal defects in ENU mutagenized mice

Address for correspondence:

David J Baylink, MD
Musculoskeletal Disease Center
Jerry L Pettis VA Medical Center
11201 Benton Street
Loma Linda, CA 92357
Phone: (909) 825 7084 ext 3101
Fax: (909) 796 1680
E-mail: david.baylink@med.va.gov

ABSTRACT

Chemical mutagenesis followed by screening for abnormal phenotypes in the mouse holds much promise as a method for revealing gene function. We describe a mouse N-ethyl-N-nitrosourea (ENU) mutagenesis program incorporating a genome-wide screen of dominant as well as recessive mutations affecting musculoskeletal disorders in C3H/HeJ mice. In a primary screen, progeny of one-generation dominant mutations (F1) and three generation recessive (F3) mutations were screened at ten weeks of age for musculoskeletal disorders using a dual energy X-ray absorptiometery (DEXA) and biochemical markers affecting bone metabolism, such as osteocalcin, type-I collagen breakdown product, skeletal alkaline phosphatase, and insulin like growth factor-I (IGF-I). Abnormal phenotypes were identified as ±3SD units different from baseline data collected from age and sex matched non-mutagenized control mice. A secondary screen at 16-week of age, which included peripheral quantitative computed tomography (pQCT) in addition to those parameters described in our primary screen, was used to confirm the abnormal phenotypes observed in the primary screen. The phenodeviant or outlier mice were progeny tested to determine whether their abnormality segregates bimodally in their offspring with the expected 1:1 or 1:3 Mendelian ratio, in dominant and recessive screens, respectively. With the above screening strategy, we were able to identify several mice with quantitative abnormalities in BMD, BMC, bone size, and bone metabolism. We have progeny tested and confirmed four outliers with low BMD, low bone size, and growth related abnormality. Our results indicate that the magnitude of change in quantitative phenotypes in the ENU mutagenized progeny was between 10-15%, and hence, the yield of outliers was dependent on the precision of the methods. So far, this ENU mutagenesis program has identified four outliers that can undergo positional cloning.

INTRODUCTION

Osteoporosis is a systemic skeletal disease characterized by low bone mass and micro architectural deterioration of bone tissue. The low bone mass in osteoporotic patients is a result of low amount of bone accrued during the early life, a high rate of bone loss in later life, or a combination of both factors. The factors known to influence bone mass accumulation during growth include heredity, gender, diet, endocrine effectors, and mechanical forces. Quantitatively, the most important determinants appear to be hereditary, which is exemplified in the genetic epidemiological analyses related to recurrence risk [8, 34] and twin studies on bone mineral density (BMD) and bone turnover.[12] Although the precise value of genetic contribution to BMD is subject to discussion, several studies have estimated the heritability for BMD to be as high as 80%,[10, 19, 36] suggesting that the majority of variance in peak BMD values can be explained by genetic factors. This suggests that there are "bone density" genes, variants of which could result in BMD levels that vary from one individual to another. These differences can be seen in differences between individuals how they attaining peak BMD early in life or as differences in the rate of bone loss later in life. An important step in the dissection of the genetic factors in osteoporosis is the identification of models with key inheritable phenotypes contributing to BMD differences in different individuals.

BMD is a polygenetic trait with multiple genes believed to be involved in regulating bone density. Past research towards understanding the genetics of BMD is focused on hypothesis concerning known candidate genes for BMD, several of which were examined using knockout and transgenic mouse models.[22] Genome-wide linkage screens for genes underlying BMD variability, conducted in humans[16, 21, 26] and mice,[2, 3, 35] have highlighted some additional regions that may harbor quantitative trait loci (QTLs) for BMD. So far, these studies have confirmed the influence of some major genes on BMD and related traits; however, the identification of gene(s) has not yet been accomplished. A complementary approach involves screening for particular aberrant phenotypes in

the progeny of chemically mutagenized animals.[11, 13-15, 17-18, 20, 27-29, 31] For this purpose, the chemical mutagen N-ethyl-N-nitrosourea (ENU) has proven to be most effective in generating mutations in mice,[32-33] with a frequency of one mutation per gene every 175-655 gametes,[18] providing a highly efficient screen of mutagenized mice of phenotypes of interest.

In a typical whole genome mutagenesis screen, inbred male mice are treated with ENU and crossed to wild type females, and large number of offspring are screened through a series of tests to identify the individual phenodeviant (a term used for extreme-scoring) mice, which is most likely to bear a large effect Mendelian mutation. The phenodeviant mice, which is often defined as >3SD units from non-mutagenized mean, are each progeny tested to determine whether their abnormality segregates bimodally in their offspring with the expected 1:1 or 1:3 Mendelian ratio. Those that pass this test are subsequently mapped at a moderate resolution in a cross to a different strain using genome-wide markers. With the broad aim of identifying genes regulating musculoskeletal tissue, in this study, we describe: 1) generation of genome-wide mutant by injecting C3H/HeJ mice with ENU; 2) development of a systematic and detailed screening procedure for identifying phenotypes related to bone density and bone mass; 3) issues related to reliability of screening procedures; and 4) our strategy to recover mutations regulating these complex traits. Bone mineral density (BMD) measurement is the most common phenotypic trait used in studies evaluating heritability or polymorphic gene markers of osteoporosis because osteoporosis is defined in individual patients by low bone density. However, several other factors contribute to osteoporosis fracture, including: bone size, shape, architecture, tissue quality, age, body weight, and muscle strength. Therefore, we have used multiple skeletal, and some extra skeletal traits to assess the skeletal status of ENU mutagenized progeny.

Since the genes regulating BMD have been shown to act in both dominant and recessive manner, our strategy for identifying mutants involves both dominant and recessive screening. We have

selected C3H/HeJ (C3H) mice in our ENU mutagenesis program, which we earlier identified[1] to possess the highest bone mineral density (BMD) among 13 inbred strains. Since ENU mutagenesis is most likely to affect gene expression by disruptive mutations, it can be predicted that use of a strain with high BMD mice is ideal for identifying genes that effect bone density. In addition, the C3H strain has been shown[24] to be one of the few mouse strains that tolerated ENU and is most fertile after an initial recovery period. An additional advantage of using this strain is that spermatogonia from the C3H strain can be frozen successfully for the subsequent recovery of mutants.[14, 40, 41]

MATERIALS & METHODS

All animal protocols used in this study had prior approval of the Animal Studies Sub-committee of this research institution.

ENU Mutagenesis

Male (5-6 week-old C3H/HeJ) mice purchased from The Jackson Laboratory (Bar Harbor, ME) were housed on a 12-hour light/dark cycle, fed standard rodent diet and water and allowed to acclimatize for two weeks prior to injection with three different (3X90 mg/kg, 3X100 mg/kg, and 4X85 mg/kg) doses of ENU. ENU concentration was determined by UV spectrometry, details of ENU administration and safety procedures have also been previously described.[17-18] Batches of 20 male mice were injected at 6-8 week interval to insure a weekly supply of about 20-30 mice for phenotype screening. Time to regain fertility and mortality rate were closely monitored and recorded. To insure that enough progeny were produced in the life span of a male, each of the ENU-treated C3H males was mated with two 8-10 week old C3H females. We screened a maximum of 50 progeny per ENU founder male to insure that repeated mutations were not scored.

Generation of F1 mice in one-generation dominant screen: To identify dominant mutations, screening was carried out on the F1 offspring and later descendents of ENU injected C3H male mice crossed with wild type C3H female mice.

Generation of F3 mice in three-generation recessive screen: To identify recessive mutations, selected F1 males from the dominant screen were bred with 2-4 wild type C3H females. The resulting female offspring (about 5-6) were bred back to F1 males (backcross) and later descendents (F3) were screened for mutations. If there is a mutation in F1 male, 0-25% of the F3 offspring from each F2 female will be affected. In a typical case, each F1 male will produce about 30-40 F3 pups for screening.

Baseline Data on Non-mutagenized Control Animals

We used population based reference values for biochemical markers and bone density measurements to identify extreme scoring phenodeviant mice with abnormal bone phenotype. To generate these non-mutagenized normal ranges, male and female C3H/HeJ mice of three different age groups, viz. 3-4-weeks, 7-8-weeks, and 12-14-weeks, were purchased from The Jackson Laboratory (Bar Harbor, ME) and allowed to acclimatize for two-four weeks. In each age group, all animals have the same date of birth. Blood collection, DEXA, and pQCT were performed when animals are 6-week, 10-week, and 16-week of age (age varied by ±2days).

Screening Strategy

General Screening: *At days 1-21*: The following observations were recorded: a) Stillbirths; b) litter size; c) deaths between birth and weaning; and d) visible anomalies.

Primary Screen (Day 70)

Animals were sedated by injecting a mixture of Ketamine (100 mg/kg) and Xylazine (10 mg/kg) and 0.3 – 0.35 ml blood were collected by retro orbital sinus puncture. BMD measurements were performed using dual energy x-ray absorptiometery (DEXA) using the PIXImus instrument (Lunar Corporation, Madison, WI). Sticky-pads were used to maintain the orientation of limbs during the scanning procedure. The validation and utility of *in-vivo* bone density measurements by PIXImus in the mouse model is described earlier.[25] The DEXA measurements and blood collection were performed under one episode of anesthesia. Blood were transferred to small tubes (1.0-ml capacity), stored at 4°C, and plasma was separated within 1-hour of blood collection. Plasma is stored in 2-3 aliquots at –70°C for biochemical analysis.

Biochemical evaluation: To minimize the effect of circadian variation in biochemical markers described earlier[38] we collected all blood samples between 1500 – 1600 hours. The C-telopeptide measurements were performed with a mouse C-telopeptide ELISA,[37] whereas osteocalcin[39] and IGF-I[23] measurements were performed by respective radioimmunoassays. Alkaline phosphatase was measured in serum by a kinetic method using p-nitro phenyl phosphate (PNPP) as substrate and 15 mM L-phenylalanine to inhibit intestinal alkaline phosphatase.[38]

After completion of the primary screening, we euthanized all mice that were normal.

Secondary Screen (Day-112)

If a phenodeviant was identified in the primary screening (10-week), a secondary screening was performed to confirm the phenotype when mice are 16-week old. A second blood sample was collected and DEXA measurements performed as described for primary screening. In addition, we included peripheral quantitative computed tomography[4] (pQCT, XCT Research M, Norland Medical System, Fort Atkinson, WI) in our secondary screen.

pQCT Measurements: Calibration of pQCT was performed daily with a defined standard (cone phantom). The approximate resolution limit of this instrument is 70 μm. Mice were completely sedated as described above; with the right hind limb rested on a plexiglass platform and immobilized with tapes. A two-dimensional scout view was taken first; this permits identification of landmarks and consistent selection of the appropriate site for measurement. Measurements were performed at the mid-diaphysis of tibia. The bones were scanned 3 times, each scan 1 mm apart from the mid-point of the tibia. Slice-2, which is the mid slice, was used for all analysis and comparisons. The complete process of bone density measurement by pQCT was completed in approximately 15-16 minutes. Analyses of the scans were performed by using the manufacturer-supplied program STRATEC MEDIZINTECHNIK GMBH Bone Density Software. Two different thresholds were used for the analysis of scans, a higher threshold of 630 mg/cm^3 gave the most accurate area results and a lower threshold at 214 mg/cm^3 provided the most accurate mineral content values.

Aging phenotypes

Mice with abnormal bone turnover were kept for extended periods (12-18 months), during which time bone density measurements and X-ray scans (Faxitron X-Ray Corporation, Wheeling, IL) were

collected between 26-weeks and 56-weeks of age in order to detect long-term effects of bone turnover on changes in BMD or BMC.

Optimization of Screening Procedure

Selection of appropriate screening age of mutagenized F1or F3 progeny

Ideally, one would like to identify the skeletal phenotypes in an early age group to increase the number of mice screened per unit time. However, rapid changes takes place in the skeleton in young mice, and therefore, variation is larger in young mice. This is illustrated in Figure-1, which shows CVs of three selected parameters (BMD, BMC, and Bone Area) obtained by DEXA in 6-week, 10-week, and 16-week old mice. The high variance, seen in 6-week old mice would lead to classification error and the possibility of a higher rate of false positive or negative outliers. Therefore, we selected the 10-week time point for screening; this minimizes the housing cost with a minimal loss of precision, as compared to the 16-week mice.

Reliability of musculoskeletal screening technique

To identify a phenodeviant with small differences in traits as compared to large background variation, the precision of the screening procedure must be high and repeat testing is necessary to minimize classification errors. Our aim was to optimize a screening procedure in which we can reproducibly detect changes of 5-10%. In this regard, the pQCT technology offers high precision, and has been successfully applied and validated[4, 35] for bone density measurements in a mouse model. However, pQCT measurements are time consuming, a crucial limitation in a large-scale screening, and published data shows that highest precision is achieved in excised bone as compared to *in-vivo* measurements. An alternative to the pQCT is the DEXA, which also has an acceptable precision of 2-4%CV for bone density and body composition parameters. An advantage of the DEXA is that it measures the total body skeletal BMD. We are interested in total body BMD

because we are interested in genes that affect the entire skeleton. While it is known that some genes have specific effects on a given skeletal site, our first priority would be to identify genes that affect the entire skeleton. Therefore, we chose to use DEXA, rather than pQCT, for the screening of live animals where speed, cost effectiveness, and whole body BMD are important issues.

The major shortcoming of DEXA measurements is that BMD is a projected areal density rather than true volumetric density. We observed a significant correlation between BMD and body weight (Table-1), indicating the DEXA BMD is size sensitive. Thus, areal density could result in potential errors in classification particularly if comparison is made between bones of different sizes.[5, 7, 30] Differences in size could arise due to differences in body weight, which could be due to litter size and nursing ability of the mother. Therefore, we compared mutagenized progeny by using unadjusted DEXA BMD data as well as BMD data normalized by body weight. This manipulation provided a BMD independent of bone size (data not shown) as well as reduced population variance. Use of pQCT in secondary screen overcomes the major deficiency in DEXA measurements in the primary screen and provided details on structural abnormalities in bone, particularly differences in size, which are hard to confirm by DEXA measurements alone. We selected the tibia for pQCT measurements because placement of landmarks was more precise in the tibia as compared to femur or other bones. The high *in-vivo* precision achieved by this procedure is evident in a very low population CV of 1.9 – 2.7% in the bone density measurement in the tibia.

Identification of Phenodeviants with Quantitative Bone Size Traits

The densitometric size parameters, such as BMC, bone area, femur BMD, measured by PIXImus and total and cortical BMC, total bone area, endosteal and periosteal circumference, and cortical thickness measured by pQCT techniques, are size-dependent. Hence, it is necessary to normalize the bone mass and bone size data in F1 and F3 progeny with body weight. To derive the body-weight-adjusted bone size traits data, we regressed each of the size traits with body weight using

male (n=60) and female (n=60) non-mutagenized control mice that are 10-week and 16-week old. We analysed this correlation with regression analysis. Since, the regression line showed significant and positive intercept for all size sensitive traits, indicating that the ratio of size parameters and body weight changes over a range of values, we used the estimating regression equation derived from the normal mice population to normalize size traits in the F1 and F3 progeny. For example, the following formula was used for adjusting size sensitive traits in female 10-week C3H mice determined by PXIXImus: [Adjusted Size Trait = Non-Adjusted Size Trait/(Slope × Body Weight + Intercept) where Intercept and Slope are from regression analysis of this Size Trait in 10-week old normal female population (n=60)]. The observed weight-adjusted values for size parameters showed statistically non-significant and negligible correlation with body weight (Table – 1). The body weight adjusted size phenotypes had 10-50% lower variation (population CV) as compared to un-adjusted phenotypes (Table – 1). Since the calculated value was a ratio of observed over body weight normalized non-mutagenized value, this manipulation allowed us to compare all parameters on one scale including male and female data.

Inheritance Testing

The phenodeviant mice were bred with wild type females (as described in the method section earlier) to determine whether the abnormality segregates bimodally in their offspring with the expected 1:1 or 1:3 Mendelian ratio. Those that pass this test are subsequently used for mapping studies. Because it is anticipated that each F1 progeny will have 20-40 mutations, inheritance testing is carried out in at least two-generation of mice by isolating those mice with the phenotype of interest and then selectively breeding them to eliminate about 50% of mutations in each generation. Therefore, after 2-3 generations, each affected mouse will have 5-10 mutations with minimal chances that multiple mutations affecting the same phenotype.

Data Analysis

Differences in phenotype traits between affected, non-affected littermate, and normal mice were assessed by Mann-Whitney t-test because most of the phenotypes were not normally distributed. Correlation between various phenotypes and body weight were performed by Spearman correlation method and correlation is considered significant for p-value<0.05.

RESULTS

ENU Dose: An ENU dose of 3X100 mg/kg was the maximum dose that could be tolerated by the C3H strain with about 20-25% mortality. At this dose, about 40-50% regained fertility after approximately 20-22 week period albeit with a slightly lower litter size of 4.1, as compared to a normal litter size of 6.4.[24] A higher ENU dose of 4 X85 mg/kg resulted in a 95% mortality within 15-week of last ENU injection.

List of Phenotypes and Baseline Data: Table-2 lists all phenotypes measured in the F1 progeny in this study, the *in-vivo* precision of biochemical markers, DEXA and pQCT measurements, and, population variance of various measurements. Data on population variance was collected from non-mutagenized control mice (60 males and 60 females) obtained in three batches with 20 mice in each batch. Table 3 shows the number of mice screened, outliers identified and progeny tested, and those confirmed in this study.

Visible Phenotypes in Dominant and Recessive Screen: Figure 2 shows some of the visible phenotypes observed in this study. We observed several other visible phenotypes such as, syndactyly (fusion of two or more digits in both forepaws and hind-paws, Figure 2A & 2B), dominant spotting, kinky tail, and albino (not shown). Figure 2C (left) shows a phenodeviant mouse (which is identified in recessive mutation and yet to be fully characterized) along with a normal littermate (Figure 2C, right). The affected mice appear weak, have low body weight, splayed gait, and show

fur with a greasy appearance early in development (birth to 5-6 week of age). The affected adults have normal fur but with increased yellow pigmentation at skin surface, and low BMD. We have generated four second-generation affected progeny and all of them show reduced bone density parameters (Figure 2, C1 & C2). The total body BMD was 8% lower ($p<0.0001$) in affected progeny.

Musculoskeletal Phenotypes: Representative data on recessive screen F3 progeny is shown in Figure – 3, including both body weight adjusted and non-adjusted BMD and BMC in approximately 220 male and 180 female F3 progeny. Similar results were obtained from dominant screening of F1 progeny. Mice outside the adjusted as well as non-adjusted reference ranges were retested at 16-weeks; those mice confirmed as extreme scoring outliers subjected to inheritance testing.

Table 4 shows all the abnormal phenotypes identified in the dominant and recessive screen in this study, including those that had yet to be confirmed in inheritance test cross. We observed that several of the outliers identified in the 10-week screen had phenotype values between 1SD - 3SD units when repeat tested at 16-week. However, due to the significant efforts involved in progeny testing, we only pursued outliers (after 16-week screening) with the highest differences, which was independent of body weight (and body size).

Below we present data on three different musculoskeletal phenodeviants. Offspring of three phenodeviant mice that were progeny tested and the results of these tests are displayed in Figures 4-6. The fourth phenodeviant confirmed in inheritance crosses had a decreased body weight of 20% as compared to littermates.

i) Decreased bone size: Figure 4 shows offspring from a phenodeviant mice 5.37.5, the affected progeny identified as <3SD units lower in total BMC compared to normal mean. The first and

second-generation progeny shows an approximate 0.9:1 [affected (n=31): non-affected (n=36)] Mendelian ratio. The average body weight adjusted total body BMC was decreased by 14% ($p<0.00001$), whereas BMC at the mid shaft of tibia decreased by 15%, as compared to littermates. The adjusted total body bone area was lower by 14% ($p<0.00001$), mean periosteal circumference was 9% lower ($p<0.00001$), and average endosteal circumference was 15% lower ($p<0.00001$) (Figure 4), as compared to non-affected progeny. The total BMD (-2%, p=NS) and cortical BMD were not significantly decreased in affected or non-affected progeny. The biochemical markers were not significantly different between affected and non-affected progeny. Summary of all data indicate that mutation causes reduced bone size.

ii) Decreased tibial bone size that exceeds the decrease in total bone size: Figure 5 shows offspring from phenodeviant mouse 6.5.5, which segregated as 0.9:1 [affected (n=11):non-affected (n=12)] in first-generation progeny. The affected mice were identified because of low bone area (<3SD) at the mid-shaft of tibia. The affected progeny had a mean decrease of 12% in bone area at mid-shaft tibia. However, the total body bone area was only 6% ($p<0.05$) lower in affected progeny. In addition, we observed approximately 5% lower periosteal circumference ($p<0.01$), and approximately 15% lower endosteal circumference in affected mice. In summary, the affected offspring showed significantly lower bone size parameters at the tibia, a much smaller decrease in total body bone area, and no significant difference in BMD in affected and non-affected litter mates.

iii) Decrease in bone density: Figure – 6 shows BMD data from a phenodeviant (5.27.7) identified in our recessive screen. Data represents F3 progeny from six litters, which were generated from crosses between heterozygote F2 female and male mouse. The average body weight adjusted data from affected progeny showed 8% lower total body BMD, 9% lower femur BMD, and 18% low total body BMC, as compared to un-affected littermates (Figure 7). The total BMD and total BMC measured by pQCT at the mid-diaphysis of tibia was 3% lower ($p<0.05$) as compared to un-affected

littermates.

Biochemical marker phenotypes: We identified two F1 mice with abnormal biochemical markers level as shown in Table-4. 1) Increased skeletal alkaline phosphatase levels – An F1 female mouse was identified with approximately 70% higher skeletal alkaline phosphate activity in blood as compared to age and sex matched normal mice. The bone density parameters and other biochemical markers of bone metabolism, such as osteocalcin and C-telopeptide were found to be normal. In addition to exhibiting high skeletal alkaline phosphatase activity, this F1 mouse was hyperactive and showed constant circling behavior. This mouse was bred for inheritance testing, however, it has shown difficulties in nursing the pups. Our initial attempts to use a foster mother (FVB mice) to rescue the litters have not been successful. 2) Decreased C-telopeptide (type-I collagen) levels - We observed one F1 male affected by 70% lower levels of C-telopeptide (type-I collagen, alpha-1 chains) in blood as compared to age and sex matched normal mice. The C-telopeptide is a marker of bone degradation and low levels of this marker could be associated with low rate of bone resorption.

DISCUSSION

A systematic phenotype screen using ENU mutagenesis can provide an efficient approach to discover genes and their function relevant to musculoskeletal phenotypes. ENU can create large number of point mutations in vast array of genes and by employing a disease specific screens it is possible to recover mutant strains with any desired phenotypes. Several ENU screens are already employed to uncover a range of mutations incorporating such diverse phenotypes as clinical-chemical,[31] diabetes,[13] visual system,[9] arthritis,[20] dysmorphological,[11] and developmental.[15] The primary focus of our mutagenesis program is to identify mouse mutants that have phenotype abnormalities of bone density, bone mass, bone size, and bone metabolism.

To make the most cost effective use the ENU mutagenesis program, the screening strategy should seek to identify many diverse phenotypes. In this regard, our screen employs a wide-rang of phenotypes including, bone density, bone size, morphological defects, biochemical, and growth related defects. Since ENU mutations are point mutations, we expected mutations generated in this study to be monogenic with phenotypic differences of approximately 5-15% from the normal non-mutagenized controls, and therefore, the other major requirement of our ENU program was an ability to detect deviations of modest magnitude. The high resolution of DEXA and pQCT measurement and a moderate population variation allow us to detect a change of 6-18% in bone density and size phenotypes with 99% confidence limits.

There were two main technical issues affecting our quantitative phenotypes in the ENU mutagenesis screen. The first issue was identification of outliers with bone size phenotypes. As shown in Table-1, the size sensitive parameters are influenced by body size, which means a small mouse will have a lower BMD (by PIXImus), BMC, or bone size than healthy age-matched non-mutagenized control mice, even if their bones (smaller) are otherwise completely normal. Due to this known dependence on bone mass and size parameters, the size sensitive phenotypes in all dominant and recessive progeny have to be normalized in order to distinguish skeletal mutants from growth type mutants. However, there is no established or validated methodology to normalize bone size *in-vivo*. Consequently, we explored several ways to adjust the size sensitive traits, such as use of bone area derived from DEXA measurement, femur length obtained from X-ray images (Faxitron), body length, and body weight measured during screening. Correction formula using bone area resulted in over-adjustment (i.e., adjusted parameters resulted in showing significant negative correlations with body weight). Additionally, measurement of femur length and body length showed large variation suggesting correction with these parameters could increase variance of size parameters. In contrast, the body weight adjusted data showed a negligible correlation with

body weight, and most importantly, a 2-10% (CVs) reduction in population variance compared to non-adjusted data.

Another technical difficulty in the quantitative phenotype-driven mutagenesis is characterizing mice generated from progeny testing. The animals are not genotyped at this stage to differentiate mutant from non-mutant genotypes; thus, phenotype distribution is the only means for separating the mutants from their unaffected littermates. Even after selecting a 3SD unit difference criterion to classify mutants, we still noticed an overlap of mutant and non-mutant phenotype. Thus, the possibility arose that classification errors in distinguishing outliers would have lead to potential breeding of an un-affected progeny mistakenly identified as a phenodeviant. To overcome this possibility, we bred only extreme scoring mice for generating affected progeny and excluded the mice that are on the borderline of 3SD criteria.

We have screened approximately 1000 C3H mice thus far and have identified several outliers, which included BMD, BMC, and bone size (Figure 4 & 5). We report data on progeny of three phenodeviant mice that we have confirmed in the inheritance-test crosses (Figure 4 – 6). Among the three quantitative mutants that we confirmed in the progeny testing crosses, the phenotypes were bone density and bone size. The bone density phenodeviant was a recessive mutation, and our data suggests that this mutation causes decreased bone density at multiple skeletal sites; which is evident from the decreased bone density observed at total body, total femur, and midshaft tibia. The progeny testing shows that phenotype distribution in the F3 population followed an expected Mendelian inheritance ratio of 1:3 (observed ratio was 1:2.9).

We confirmed two outliers as decreased radial bone size mutants in the dominant screen. Both these outliers were identified as low BMC outliers in our primary screening. Our data show that these two bone size phenodeviant were slightly different in their phenotypic parameters. Mutant

5.37.5 was identified as a significantly decreased bone area of the total body as well as the tibia, indicating that mutation causes reduced bone size at multiple skeletal sites. The other bone size phenodeviant (6.5.5) was also identified as low bone size mutant, however, the magnitude of change in total body bone area was approximately half of that observed at mid shaft tibia. Therefore, the affect of this mutation is variable at different skeletal sites. Consequently, our results show differences in two bone-size phenotypes, which support models in which genes responsible for bone size act independently on whole skeleton and selected skeletal sites. However, it remains to be verified if these size outliers were the result of mutation in one gene or multiple genes.

Our data shows that lesser number outliers were with abnormal levels of biochemical markers, and we have not yet confirmed any phenodeviant mice in progeny test. The phenodeviant mouse with increased levels of sALP was also associated with a hyperactive circling behavioral phenotype that affected the nursing ability and could not be progeny tested. A C-telopeptide phenodeviant is currently under progeny testing. In spite of our significant effort to minimize the variability of the biochemical marker measurement[38] the high inter-individual variability limits the utility of markers to identify outliers. The high variability means a 50% or higher difference is required to be classified as a phenodeviant. Since markers are systemic indicators of bone metabolism, it may be possible that genes causing changes in a specific skeletal site will not result in a greater than 50% change in systemic markers.

A brief review of all the outliers observed in this study (Table 4) reveals that most of the mutations were hypomorphic, which could be in part due to our strategy to use the high bone density C3H strain. Studies employing QTL mapping have already reported a number of QTLs responsible for bone density, each differing in magnitude with most QTLs contributing as low as <5% of the variance in parental strains – in contrast, the ENU mutations is presumed to be monogenic traits, and therefore, should be possible to fine map. In addition, our data shows that magnitude of

change in most of the quantitative outliers (which have been already confirmed in progeny testing) was between 10-15%. These phenotypic differences were larger than most of the published QTL deviations,[2-3, 35] which have been shown to explain approximately 2-10% difference in density between progenitor strains. The larger phenotypic differences in the current screen will assist our efforts to disclose the chromosomal location of the mutations because power to detect a QTL contributing to a multigenic phenotype is directly proportional to the magnitude of the specific effects of the loci (assuming that the number of informative markers and recombination rate are constant). Finally, progress in refinement of some phenotypic measurement techniques will improve our low recovery of mutants because several ENU mutants will have smaller phenotypic differences and, as observed in this study, screens with high precision will be more effective in identifying outliers. In the future, additional measurements can be added, for example ability to detect micro-architectural deviations.

In conclusion, we have developed and refined a screening procedure for identifying phenodeviant mice with quantitative abnormalities in BMD, BMC, bone size, and bone markers, in a large scale dominant and recessive screening of ENU-mutagenized progeny. By confirming the phenodeviant mice in progeny tests, we have demonstrated the feasibility of the screen to identify mutations that effect quantitative phenotypes. The preliminary indication from this study is that observed phenotypic differences in ENU mutagenesis were in general larger than those explained by published QTL's. We anticipate that this mutagenesis program would effectively contribute towards the growing information on genes and their functions for the musculoskeletal system.

ACKNOWLEDGEMENTS

This work was supported by Assistance Award No. DAMD17-99-1-9571. The U.S. Army Medical Research Acquisition Activity, 820 Chandler Street, Fort Detrick MD 21702-5014, is the awarding and administering acquisition office. The information contained in this publication does not necessarily reflect the position or the policy of the Government, and no official endorsement should be inferred. All work was performed in facilities provided by the Department of Veterans Affairs.

REFERENCE

1. Beamer WG, Donahue LR, Rosen CJ, and Baylink DJ. Genetic variability in adult bone density among inbred strains of mice. Bone **18**: 397-403; 1996.
2. Beamer WG, Shultz KL, Churchill GA, Frankel WN, Baylink DJ, Rosen CJ, and Donahue LR. Quantitative trait loci for bone density in C57BL/6J and CAST/EiJ inbred mice. Mamm Genome **10**:1043-1049; 1999.
3. Beamer WG, Shultz KL, Donahue LR, Churchill GA, Sen S, Wergedal JR, Baylink DJ, and Rosen CJ. Quantitative trait loci for femoral and lumbar vertebral bone mineral density in C57BL/6J and C3H/HeJ inbred strains of mice. J Bone Miner Res **16**:1195-206; 2001.
4. Breen SA, Loveday BE, Millest AJ, and Waterton JC. Stimulation and inhibition of bone formation: use of peripheral quantitative computed tomography in the mouse in vivo. Lab Anim **32**:467-76; 1998.
5. Carter DR, Bouxsein ML, and Marcus R. New approaches for interpreting projected bone densitometry data. J Bone Miner Res **7**:137-45; 1992.
6. Christian JC, Yu PL, Slemenda CW, and Johnston CC. Heritability of bone mass: a longitudinal study in aging male twins. Am J Hum Genet **44**:429-33; 1989.
7. Compston JE. Bone density: BMC, BMD, or corrected BMD? Bone **16**:5-7; 1995.
8. Cummings SR, Nevitt MC, Browner WS, Stone K, Fox KM, Ensrud KE, Cauley J, Black D, and Vogt TM. Risk factors for hip fracture in white women. Study of Osteoporotic Fractures Research Group. N Engl J Med **332**:767-73; 1995.
9. Favor JN, and Neuhauser Klaus A. Saturation mutagenesis for dominant eye morphological defects in the mouse Mus musculus Mamm Genome **11**:520-525; 2000.
10. Flicker L, Hopper JL, Rodgers L, Kaymakci B, Green RM, and Wark JD. Bone density determinants in elderly women: a twin study. J Bone Miner Res **10**:1607-1613; 1995.
11. Fuchs H, Schughart K, Wolf E, Balling R, and Hrabe_de_Angelis M. Screening for dysmorphological abnormalities – a powerful tool to isolate new mouse mutants. Mamm Genome 11, 528-530; 2000.
12. Garnero P, Arden NK, Grifiths G, Delmas PD, and Spector TD. Genetic influence on bone turnover in postmenopausal twins. J Clin Endocrinol Metab 81**(1)**: 140-146; 1996.

13. Goldsworthy M, Toye A, Eley L, Bentley L, Hough T, Nolan P, Peters J, Vizor L, Moir L, Ritson D, Mcnaughton J, Spurr N, Hunter J, Brown Steve DM, and Cox RD. A new ENU induced type II diabetes mouse mutant IGT1. Diabetes **50(2)**:A238; 2001.

14. Hrabe de Angelis MH, Flaswinkel H, Fuchs H, Rathkolb B, Soewarto D, Marschall S, Heffner S, Pargent W, Wuensch K, Jung M, Reis A, Richter T, Alessandrini F, Jakob T, Fuchs E, Kolb H, Kremmer E, Schaeble K, Rollinski B, Roscher A, Peters C, Meitinger T, Strom T, Steckler T, Holsboer F, Klopstock T, Gekeler F, Schindewolf C, Jung T, Avraham K, Behrendt H, Ring J, Zimmer A, Schughart K, Pfeffer K, Wolf E, and Balling R. Genome-wide, large-scale production of mutant mice by ENU mutagenesis. Nat Genet 25:4 444-7: 2000.

15. Herron BJ, Lu W, Rao C, Liu S, Peters H, Bronson RT, Justice MJ, McDonald JD, and Beier DR. Efficient generation and mapping of recessive developmental mutations using ENU mutagenesis. Nature Genetics **30**:185-189; 2002.

16. Johnson ML, Gong G, Kimberling W, Recker SM, Kimmel DB, and Recker RB. Linkage of a gene causing high bone mass to human chromosome 11(11q12-13). Am J Hum Genet **60**:1326-1332; 1997.

17. Justice MJ, Carpenter DA, Favor J, Neuhauser-Klaus A, Hrabe_de_Angelis M, Soewarto D, Moser A, Cordes S, Miller D, Chapman V, Weber JS, Rinchik EM, Hunsicker PR, Russell WL, and Bode VC. Effects of ENU dosage on mouse strains. Mamm Genome **11**:484-488; 2000.

18. Justice MJ, Zheng B, Woychik RP, and Bradley A. Using targeted large deletions and high-efficiency N-ethyl-N-nitrosourea mutagenesis for functional analyses of the mammalian genome. Methods **13**:423-436; 1997.

19. Kelly PJ, Nguyen T, Hopper J, Pocock N, Sambrook P, and Eisman J. Changes in axial bone density with age: A twin study. J Bone Miner Res **8**:11-17; 1993.

20. Kochiro A, Fuchs H, and Angelis H. Analysis of mutants with arthritis like phenotype in the mouse. 15th International mouse genome conference, Edinburgh, Scotland, Abstract 210; 2001.

21. Koller DL, Rodrigue LA, Christian JC, Slemenda CW, Econs MJ, Hui SL, Morin P, Conneally PM, Joslyn G, Curran ME, Peacock M, Johnson CC, and Foroud T. Linkage of a QTL contributing to

normal variation in bone mineral density to chromosome 11q12-13. J Bone Miner Res **13**:1903-1908; 1998.

22. McCauley Laurie K. Transgenic mouse models of metabolic bone disease. Current Opin Rheumatology **13(4)**:316-325; 2001.

23. Mohan S, and Baylink DJ. Development of a simple valid method for the complete removal of insulin-like growth factor (IGF)-binding proteins from IGFs in human serum and other biological fluids: comparison with acid-ethanol treatment and C18 Sep-Pak separation. J Clin Endocrinol Metab **80**:637-47; 1995.

24. Nagasawa H, Miyamoto M, and Fujimoto M. Reproductivity in inbred strains of mice and project for their efficient production. Exp. Animals (Japan) **22**:119-126; 1973.

25. Nagy TR, and Clair AL. Precision and accuracy of dual-energy X-ray absorptiometry for determining in vivo body composition of mice. Obes Res **8**:392-398; 2000.

26. Niu T, Chen C, Cordell H, Yang J, Wang B, Wang Z, Fang Z, Schork NJ, Rosen CJ, and Xu X. A genome-wide scan for loci linked to forearm bone mineral density. Hum Genet **104**:226-233; 1999.

27. Nolan PM, Peters J, Vizor L, Strivens M, Washbourne R, Hough T, Wells C, Glenister P, Thornton C, Martin J, Fisher E, Rogers D, Hagan J, Reavill C, Gray I, Wood J, Spurr N, Browne M, Rastan S, Hunter J, and Brown SD. Implementation of a large-scale ENU mutagenesis program: towards increasing the mouse mutant resource Mamm Genome **11**:500-506; 2000.

28. Nolan PM, Peters J, Strivens M, Rogers D, Hagan J, Spurr N, Gray IC, Vizor L, Brooker D, Whitehill E, Washbourne R, Hough T, Greenaway S, Hewitt M, Liu X, McCormack S, Pickford K, Selley R, Wells C, and Tymowska_Lalan. A systematic, genome-wide, phenotype-driven mutagenesis program for gene function studies in the mouse. Nat Genet **25**:440-443; 2000.

29. Noveroske, JK, Weber JS, and Justice MJ. The mutagenic action of N-ethyl-N-nitrosourea in the mouse. Mamm Genome 11:478-83; 2000.

30. Ott SM, O_Hanlan M, Lipkin EW, and Newell_Morris L. Evaluation of vertebral volumetric vs. areal bone mineral density during growth. Bone **20**:553-556; 1997.

31. Rathkolb B, Decker T, Fuchs E, Soewarto D, Fella C, Heffner S, Pargent W, Wanke R, Balling R, Hrabe_de_Angelis M, Kolb HJ, and Wolf E. The clinical-chemical screen in the Munich ENU Mouse Mutagenesis Project: screening for clinically relevant phenotypes Mamm Genome **11**:543-546; 2000.

32. Russell WL, Hunsicker PR, Raymer GD, Steele MH, Stelzner KF, and Thompson HM. Dose--response curve for ethylnitrosourea-induced specific-locus mutations in mouse spermatogonia. Proc Natl Acad Sci U S A 79:3589-91; 1982.

33. Russell WL, Kelly EM, Hunsicker PR, Bangham JW, Maddux SC, and Phipps EL. Specific-locus test shows ethylnitrosourea to be the most potent mutagen in the mouse. Proc Natl Acad Sci U S A 76:5818-9; 1979.

34. Seeman E, Hopper JL, Bach LA, Cooper ME, Parkinson E, McKay J, and Jerums G. Reduced bone mass in daughters of women with osteoporosis. N Engl J Med **320**:554-558; 1989.

35. Shimizu M, Higuchi K, Bennett B, Xia C, Tsuboyama T, Kasai S, Chiba T, Fujisawa H, Kogishi K, Kitado H, Kimoto M, Takeda N, Matsushita M, Okumura H, Serikawa T, Nakamura T, Johnson TE, and Hosokawa M. Identification of peak bone mass QTL in a spontaneously osteoporotic mouse strain. Mamm Genome **10**:81-87; 1999.

36. Slemenda CW, Christian JC, Williams CJ, Norton JA, and Johnston CC. Genetic determinants of bone mass in adult women: a reevaluation of the twin model and the potential importance of gene interaction on heritability estimates. J Bone Miner Res **6**:561-567; 1991.

37. Srivastava AK, Bhattacharyya S, Castillo G, Miyakoshi N, Mohan S, and Baylink DJ. Development and evaluation of C-telopeptide enzyme-linked immunoassay for measurement of bone resorption in mouse serum. Bone **27**:529-533; 2000.

38. Srivastava AK, Bhattacharyya S, Li X, Mohan S, and Baylink DJ. Circadian and longitudinal variation in serum C-telopeptide, osteocalcin, and skeletal alkaline phosphatase in C3H/HeJ mice. Bone, **29(4)**:361-367; 2001.

39. Srivastava AK, Castillo G, Wergedal JE, Mohan S, and Baylink DJ. Development and application of a synthetic peptide-based osteocalcin assay for the measurement of bone formation in mouse serum. Calcif Tissue Int **67**:255-259; 2000.

40. Tada N, Sato M, Yamanoi J, Mizorogi T, Kasai K, and Ogawa S. Cryopreservation of mouse spermatozoa in the presence of raffinose and glycerol. J. Reprod. Fertil. 89:511-6; 1990.

41. Thornton CE, Brown SD, and Glenister PH. Large numbers of mice established by in vitro fertilization with cryopreserved spermatozoa: implications and applications for genetic resource banks, mutagenesis screens, and mouse backcrosses. Mamm Genome **10**:987-992; 1999.

Table – 1. Correlation coefficients between size sensitive parameters measured by PIXImus and pQCT, before and after adjustment for body weight (data taken from60 males and 60 females).

Phenotype & Measurement Technique	Non-Adjusted Data		Adjusted Data	
	Spearman Correlation Coefficient (r)	p-Value	Spearman Correlation Coefficient (r)	p-Value
	Male/Female			
BMD (PIXImus)	0.65/0.45	<0.0001	<0.02	NS
BMC (PIXImus)	0.74/0.65	<0.0001	<0.02	NS
Bone Area (PIXImus)	0.58/0.62	<0.0001	<0.02	NS
Femur BMD (PIXImus)	0.58//0.63	<0.0001	<0.02	NS
Total_CNT (pQCT)	0.70/0.63	<0.0001	<0.02	NS
Total_Area (pQCT)	0.65/0.66	<0.0001	<0.02	NS
Periosteal Circumference (pQCT)	0.63/0.63	<0.0001	<0.02	NS
Endosteal Circumference (pQCT)	0.14/0.20	NS		
Cortical_Thickness (pQCT)	0.58/0.50	<0.0001	<0.02	NS

Table – 2. List of phenotypes measured in F1 progeny and methods employed in the phenotype measurements.

Screening Procedure		Phenotype	Method Used for Screening	Population %CV (M/F)	Analytical %CV
Weaning **3-Week**		Weight Visible Defects	E. Balance Eyeball		
Primary Screen **10-Week**	Body Size	Body Weight	E. Balance	6 – 7.2	<1.5
		Body Length	Scale	9 – 10	<1.5
		Lean Body Lean Mass	PIXImus	6.5 – 7.6	<1.5
		Fat Mass*	PIXImus	13 - 18	<1.5
	Bone Size	Total Body BMC	PIXImus	6.3 – 7.5	<1.5
		Total Body Bone Area	PIXImus	4.6 – 4.7	<1.5
		Femur BMC	PIXImus	4.4 – 7.7	<1.5
	Bone Density	Total Body BMD	PIXImus	3.4 – 3.8	<1.5
		Femur BMD	PIXImus	3.9 – 5.4	<1.5
	Bone Markers	Osteocalcin	RIA	10 – 16	<9.0
		C-telopeptide	ELISA	19 – 20	<14.0
		IGF -I	RIA	9.4 – 18	<8.0
		Alkaline Phosphatase	Kinetic Assay	11.1 – 11.3	<3.0
Secondary Screen **16-Week**	Body Size	Body Weight	E. Balance	5.4 – 7.3	<1.0
		Lean Body Mass	PIXImus	5.8 – 7.8	<1.5
		Fat Mass*	PIXImus	10 - 15	<1.5
		Femur BMC	PIXImus	4.4 – 6.5	<1.5
	Bone Size	Total Body BMC	PIXImus	6.5 – 6.7	<1.5
		Total Body Bone Area	PIXImus	4.6 – 4.9	<1.5
		Femur BMC	PIXImus	8.7 – 8.9	<1.5
		Total Tibia Diaphysis BMC	pQCT	5.9 – 7.3	
		Tibia Diaphysis Area	pQCT	5.3 – 6.2	<1.0
		Tibia Diaphysis Periosteal Circumference	pQCT	2.6 – 3.0	<1.0
		Tibia Diaphysis Endosteal Circumference	pQCT	6.3 – 6.5	<1.0
		Cortical Thickness	pQCT	3.9 – 4.3	<1.0
		Cortical Content	pQCT	6.0 – 6.1	<1.0
	Bone Density	Total Body BMD	PIXImus	3.3 – 3.4	<1.5
		Total Tibia Diaphysis BMD	pQCT	1.9 – 2.7	<1.0
		Femur BMD	PIXImus	4.3 – 6.7	<1.5
		Cortical Density	pQCT	1.5 – 1.9	<1.0

*Fat measurements were included here since PIXImus automatically determined fat content.

Table – 3. Number of mice tested, phenotypes scored (including visible and musculoskeletal), and inherited mutations identified

Procedure	Number of Mice
Screened for Dominant Mode of Inheritance (Generated from 40 ENU injected males)	566
Screened for Recessive Mode of Inheritance (Generated from 15 F1 males)	421
Abnormal Phenotypes Identified in Primary Screen (dominant as well as recessive screening)	26
Abnormal Phenotypes Confirmed in Secondary Screen	12
Phenotypes Introduced to Progeny Testing	12
Phenotypes Confirmed in Progeny Testing	4
Phenotypes Not-inherited in Progeny Testing (including those died or could not mate)	2
Phenodeviant Mice Currently Under Progeny Testing	7

Table – 4. List of abnormal phenotypes identified in mutagenized C3H/HeJ progeny by dominant (F1) and recessive (F3) screening.

Trait	Phenotype (Mice ID)	Description of Phenotype	Screening Method
Binary	Syndactyly and /or ploydactyly (2.8.3)	Fusion of two or more digits in both fore-paws and hind-paws	Dominant
	Dominant spotting (6.9.5)	Presence of white spots	Dominant
	Kinky tail	Kink in tail	Dominant
	Albino (Line 2.10.5)	White skin color	Recessive
Quantitative	Uncharacterized (Line 2.8.6)	10-12% Low total body BMD, BMC, bone area, & femur BMD, 10-20% low body weight, fur has greasy appearance and increased yellow pigmentation at skin surface	Recessive
	Size (5.37.5)	16-17% Low BMC, 6-9% low periosteal circumference, 9-20% low endosteal circumference	Dominant
	Growth (6.5.3)	19% Low body weight	Dominant
	Low BMC, Area, Femur BMD (10.17.7)	20% Low femur BMD, BMC and Bone Area	Dominant
	High BMD & Lean Body Weight (6.9.5)	High lean body weight, high bone mineral content, high bone density	Dominant
	Regional Size (6.5.5)	12% Low bone area at tibia, 4-6% low periosteal circumference	Dominant
	BMC (10.6.6)	Low bone mineral content, low body weight, low periosteal circumference	Recessive
	BMC & IGF-I (Line 6.11.6)	20-25% Low body weight, 30% low IGF-I, 10-13% low bone mineral content	Recessive
	Low Femur BMD (Line 6.5.5)	10% Low femur BMD	Recessive
	BMD (Line 5.27.7)	10-14% Low BMD, low femur BMD, low BMC	Recessive
	Skeletal alkaline phosphatase (4.8.4)	75% Higher levels of serum alkaline phosphatase	Dominant
	C-telopeptide (3.8.6)	50-70% Low levels of C-telopeptide, could reflect low bone turnover	Dominant

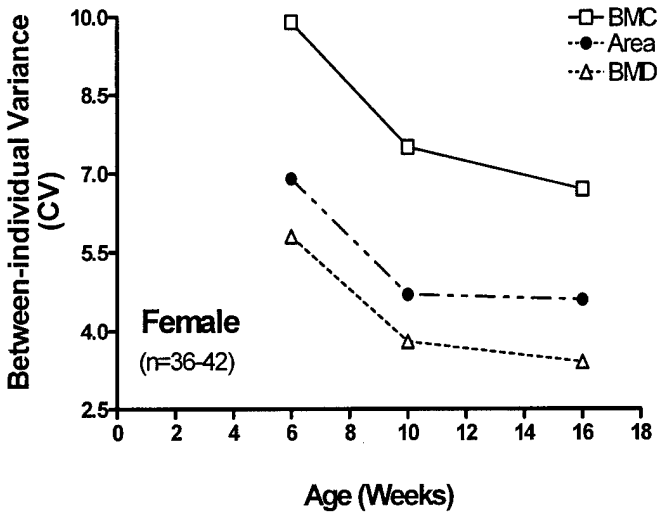
Between-individual Variance (CV)
10.0
8.5
7.0
5.5
4.0
2.5
0
2
4
6
8
10
12
14
16
18
Age (Weeks)
BMC
Area
BMD
Female
(n=36-42)

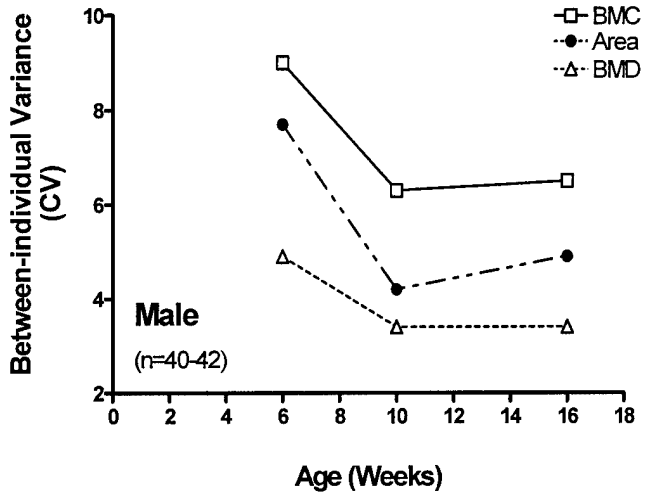
Between-individual Variance (CV)
10
8
6
4
2
0
2
4
6
8
10
12
14
16
18
Age (Weeks)
BMC
Area
BMD
Male
(n=40-42)

Figure – 1

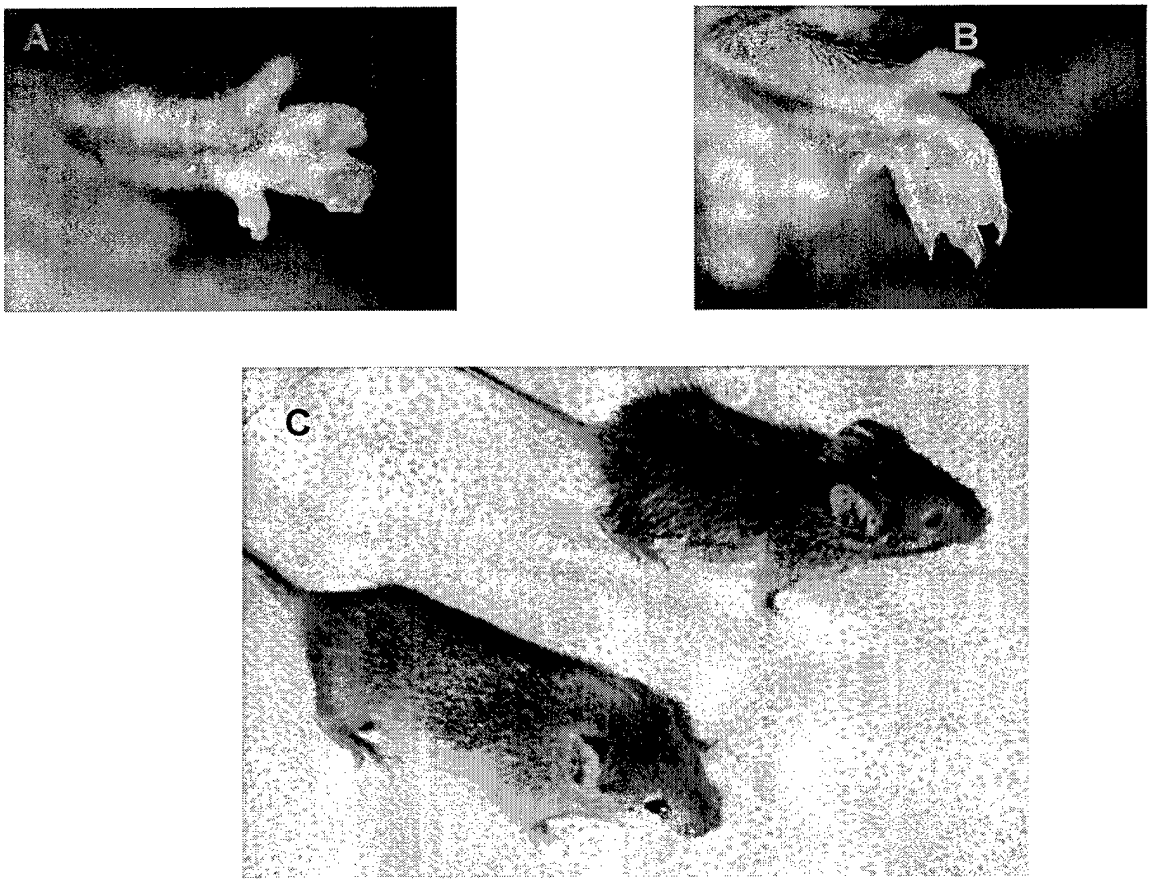
A
B
C
C1
Total Body BMD (g/cm²)
0.0525
0.0500
0.0475
0.0450
0.0425
0.0400
0.0375
Affected
Non-Affected LM
Normal
C2
Body Weight Adjusted Total Body BMD
1.1
1.0
0.9
0.8
0.7
Affected
Non-Affected LM
Normal

Figure – 2

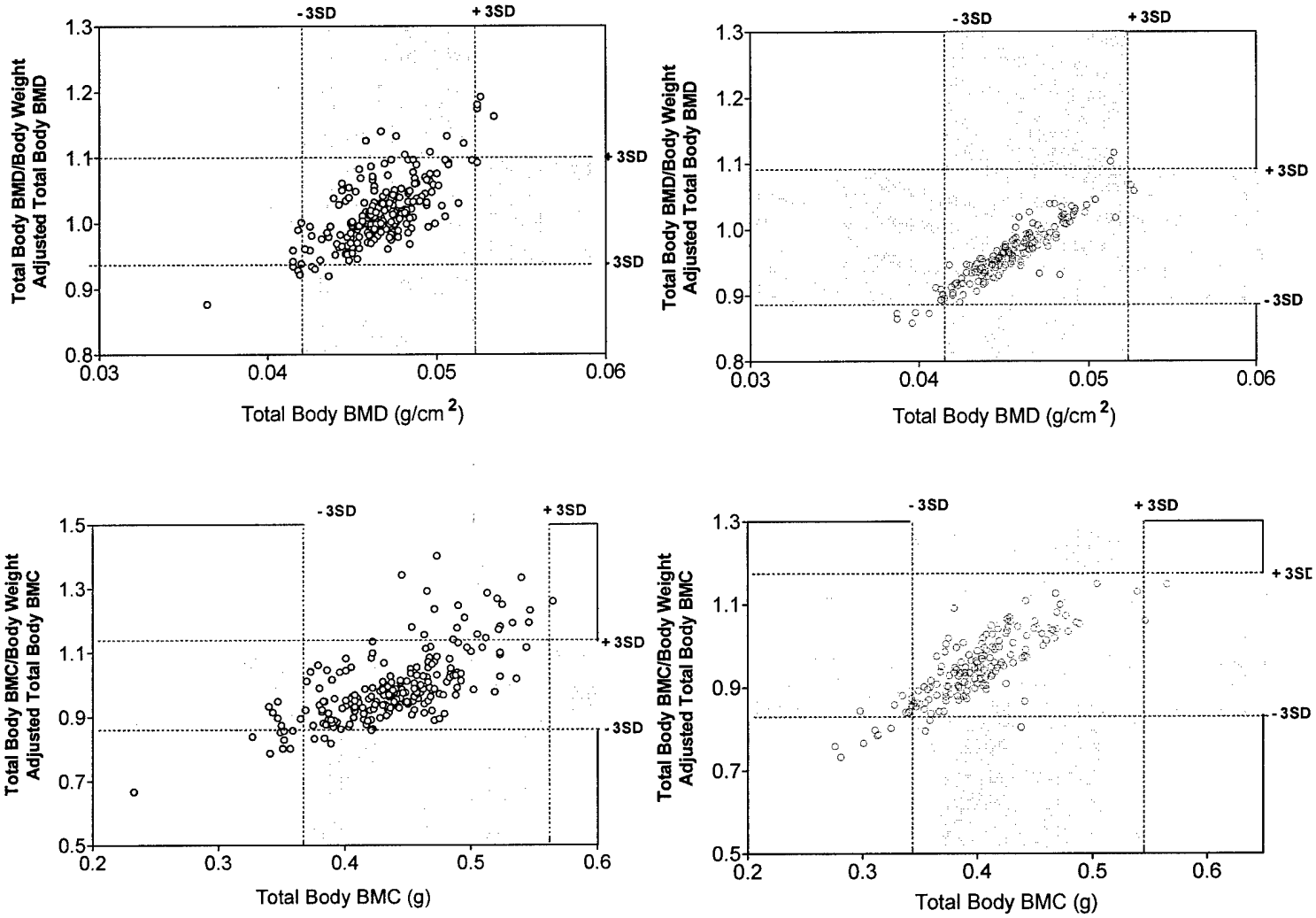
- 3SD
+ 3SD
Total Body BMD/Body Weight Adjusted Total Body BMD
Total Body BMD (g/cm 2)
Total Body BMC/Body Weight Adjusted Total Body BMC
Total Body BMC (g)

Figure – 3

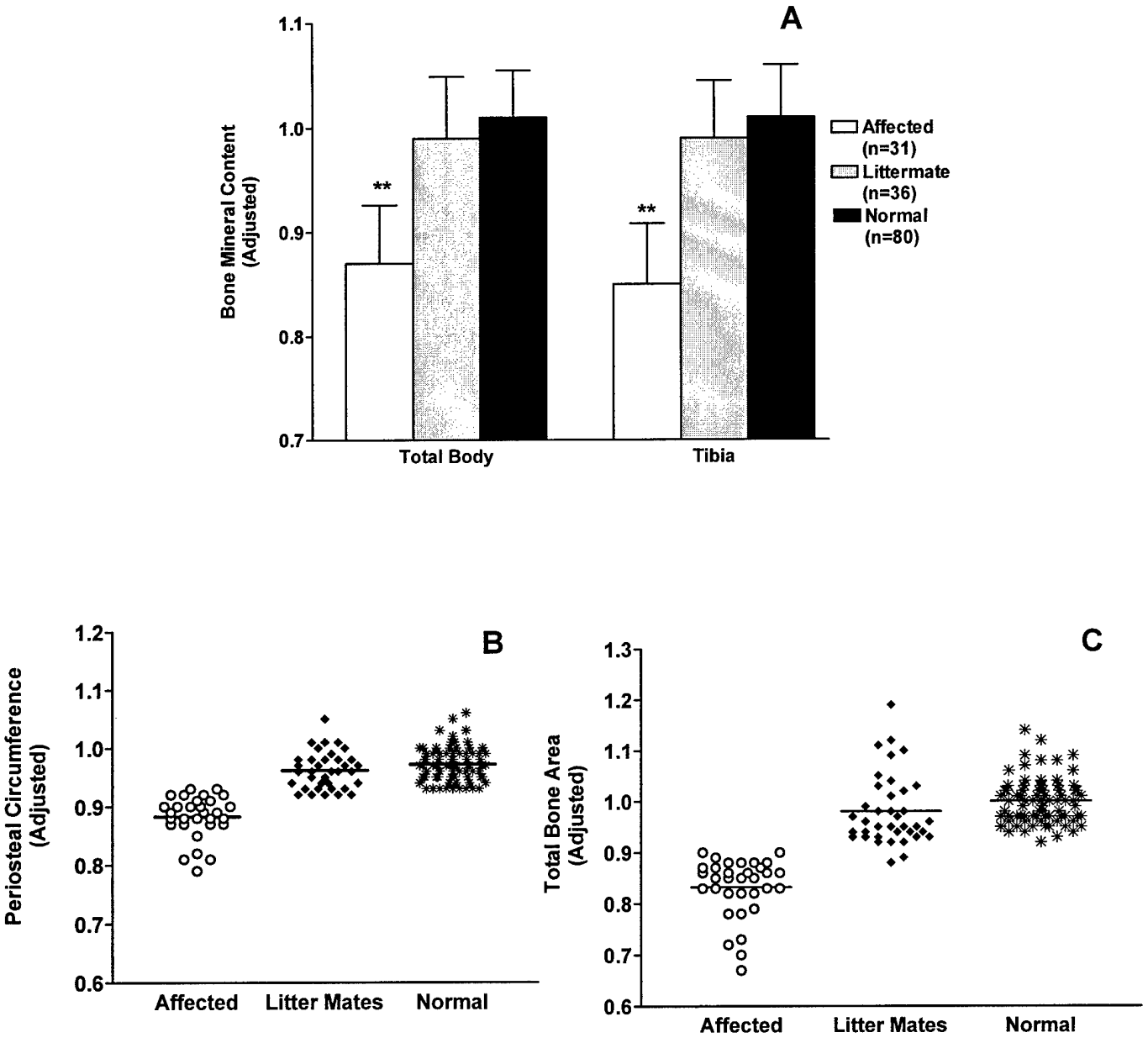
A
Bone Mineral Content (Adjusted)
1.1
1.0
0.9
0.8
0.7
**
**
Total Body
Tibia
Affected (n=31)
Littermate (n=36)
Normal (n=80)
B
Periosteal Circumference (Adjusted)
1.2
1.1
1.0
0.9
0.8
0.7
0.6
Affected
Litter Mates
Normal
C
Total Bone Area (Adjusted)
1.3
1.2
1.1
1.0
0.9
0.8
0.7
0.6
Affected
Litter Mates
Normal

Figure- 4

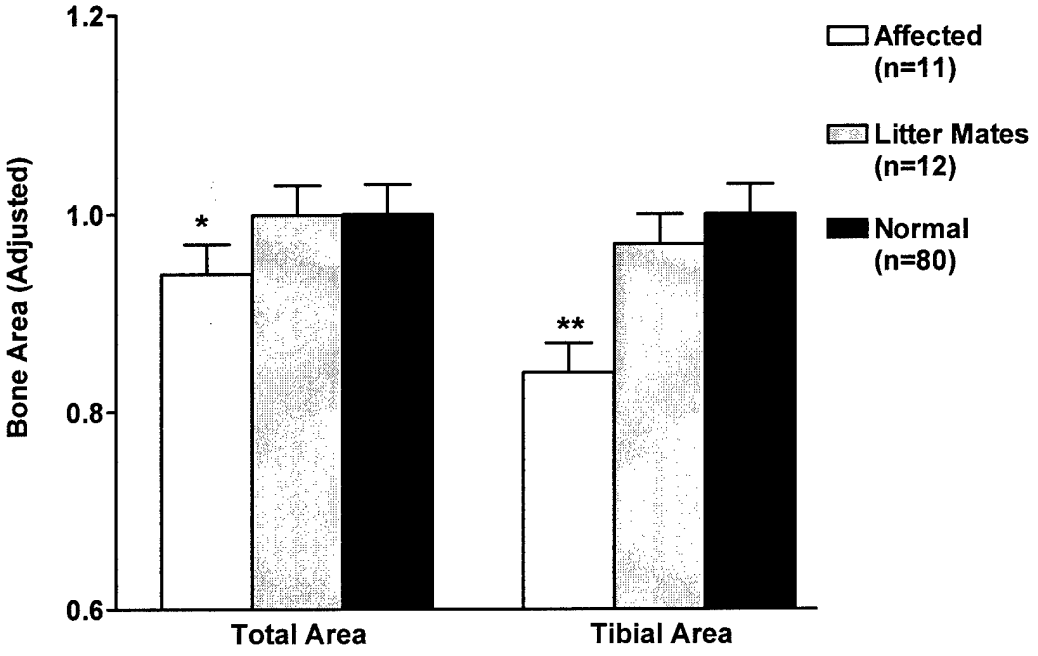
1.2
1.0
0.8
0.6
Bone Area (Adjusted)
*
**
Total Area
Tibial Area
Affected
(n=11)
Litter Mates
(n=12)
Normal
(n=80)

Figure – 5

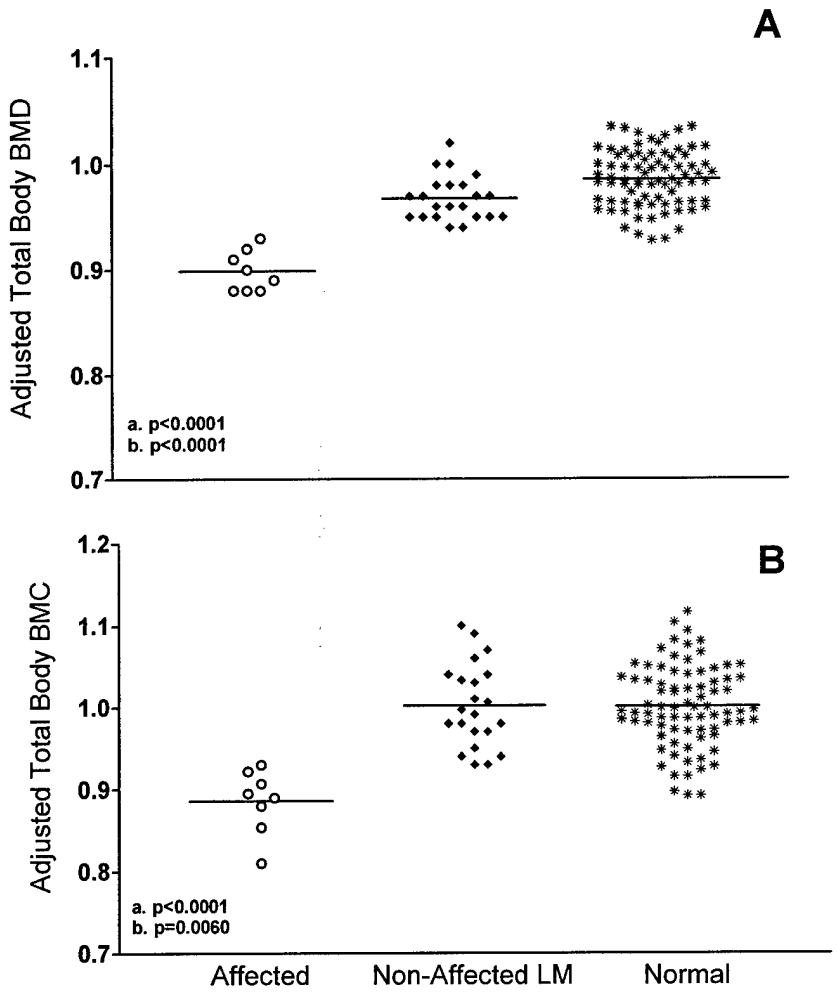
A
Adjusted Total Body BMD
1.1
1.0
0.9
0.8
0.7
a. p<0.0001
b. p<0.0001
B
Adjusted Total Body BMC
1.2
1.1
1.0
0.9
0.8
0.7
a. p<0.0001
b. p=0.0060
Affected
Non-Affected LM
Normal

Figure – 6

LEGENDS

Figure 1. Population variance in the measurements of bone mineral density, bone mineral content, and bone area as determined by Dual Energy X-ray Absorptiometry (DEXA) of female and male C3H/HeJ mice. The higher CVs at 6-week age would result in classification errors in identifying abnormal phenotype using this technique.

Figure 2. Mutant mice with visible phenotypes detected in F1 progeny in dominant screen and F3 progeny in recessive screen. Polydactyly with fusion of digit 2+3 (A) and shows that of digit 2+3+4 (B) (both dominant mutation). (C) A yet to be fully characterized mutant mice (left) shown with normal littermate (right), affected mice appears weak (low body weight) and shows fur with greasy appearance early in development (birth to 6-week age). Adults have hairs with increased yellow pigmentation, and low BMD (recessive mutation).

Figure 3. Representative data on body-weight-adjusted and non-adjusted BMD and BMC from 400 F3 progeny screened for BMD and BMC. The 3SD values were calculated from normal 10-week old male (n=60) and female (n=60) C3H mice (male progeny were shown on left and female on right panels). Phenodeviant were identified as those having both adjusted and non-adjusted values outside the 3SD range.

Figure 4. Phenotype of 16-week old inheritance test progeny from a phenodeviant mice (5.37.5) identified because of low bone mineral content in dominant screening. (A) The body weight adjusted total BMC measured by DEXA was 12% lower and BMC at mid shaft tibia measured by pQCT was 14% lower in the affected (n=31) progeny as compared with non-affected littermates (n=36) or normal non-mutagenized mice (n=80). In addition, the body weight adjusted periosteal circumference (B) and total body bone area (A) were significantly ($p<0.0001$) decreased in affected progeny as compared to littermate. The error bars are Mean±SD. **$p<0.0001$.

Figure 5. Phenotype of 16-week old inheritance test progeny from a phenodeviant mice (6.5.5) identified as low bone size in dominant screening. The affected progeny shows larger decrease in bone area (-12%, $p<0.0001$) at mid shaft tibia as compared to a lower decrease of 6% ($p<0.05$) in total body bone area. The error bars are Mean±SD. *$p<0.05$, **$p<0.0001$

Figure 6. Phenotype of 16-week old progeny from a phenodeviant mice (5.27.7) identified in recessive screen. Body weight adjusted total body bone density was 8-10% lower in affected (n=8) progeny are compared with non-affected littermates (n=23) and normal non-mutagenized control mice (n=80). a = p-value between affected and non-affected litter mates, b = p-value between affected and normal mice.